NATURE VOL 349 nature 28 FEBRUARY 1991

Squaring circle of US energy

The much-awaited US energy strategy, sensible enough in many ways, is a disappointment on the central issue of how oil consumption should be constrained.

How would the world, and the United States in particular, be changed if the cost of a new motor-car were $100 and the price of petrol (gasoline) were double what it is at present, say $4 rather than $2 a gallon? Car-owners would not be impoverished, for the numbers roughly load the cost of owning a medium-sized car onto the cost of buying the petrol required to travel 100,000 miles. But market forces would see to it that car-ownership would increase and that travel (and petrol consumption) would sharply decrease. Of course, there is no obvious way of arranging that new cars should cost $100 each, which would in any case be thoroughly uneconomic; people would buy Cadillacs and park them permanently in the street. But the benefits of reduced petrol consumption could be won more conventionally by increasing the tax on petrol by $2 a gallon and compensating car-users by reducing other taxes.

Such musings will no doubt have crossed the mind of Admiral James Watkins, the able US Secretary of Energy, during his year-long labours on the new Energy Strategy the White House released last week. The document starts from the principle that US dependence on imported oil must be decreased. It makes sensible, if controversial, proposals for increasing the indigenous supply of energy by exploiting environmentally sensitive oil reserves and by removing some impediments to the construction of nuclear plants. But the administration seems to have set its face against increased taxes on petrol, hoping instead to rely on still tougher regulations to improve the efficiency of new cars (and encourage the disposal of older inefficient cars). The trouble is that the policy will not work or, more accurately, will do so only at needless economic cost — that of retiring old cars prematurely, for example.

Endowment

The United States, although better endowed than most other countries with natural resources, is peculiarly placed on energy: a greater proportion of US energy consumption is based on liquid and gaseous hydrocarbons than in other countries except those of the Middle East. The explanation is mostly historical, and owes much to the ingenuity with which various forms of the internal combustion engine have been adapted to the conquest of distance. The question with which Watkins has been wrestling is whether the time has come for an historically perceptible change of direction.

Tradition

Traditionally, the US government has also always been active in moulding the framework of the petroleum business. In the 1920s, the Texas Railroad Commission was a way of subsidizing then-distant oil producers (who also enjoyed substantial tax incentives). More recently, the Inter-State Commerce Commission has shielded natural-gas consumers in the northeast from market prices by regulating the prices gas-pipeline operators charge. Past energy strategy, in other words, has not been to balance supply and demand by the price mechanism, but to help producers with tax incentives and, when seemly, to shield consumers from prices that reflect true costs. These devices stimulated both consumption and fears that supply would be exhausted, whence the designation of important oilfields as strategic reserves and the ban on exports of crude petroleum.

Times have now changed, but the policy has not. Although both Germany and Japan depend entirely on imported oil, that will not do for the United States, which fears the economic disruption caused by fluctuations of the price of oil as well as the secular upward trend of world prices there will be as the more accessible oilfields are worked out. Whence Watkins and his strategy. But the administration has evidently been constrained by its memories of last year's bruising budget compromise, which eventually included a modest federal tax on petrol.

Yet oil consumption would be most simply and surely reduced by increasing its price, either by an import tariff (opposed by the oil companies) or an excise tax (hated by consumers, many of whom are also voters). Specifying improved efficiency by regulation is by contrast an uncertain course: people do not always keep their cars in prime condition (which is in any case expensive), the cost of new cars would be driven up (which would be irremedially deflationary) while there are physical as well as practical limits to the improvement of efficiency. (Has the Department of Energy heard of Carnot's theorem?) On the complaint that higher gasoline taxes would hurt the poor, there are two things to say: first, if the cost of food and other necessities is a component in the calculation of welfare, why not have gasoline stamps as well as food stamps? and, second, why not soak the gas-guzzlers in the cause of social equity? □

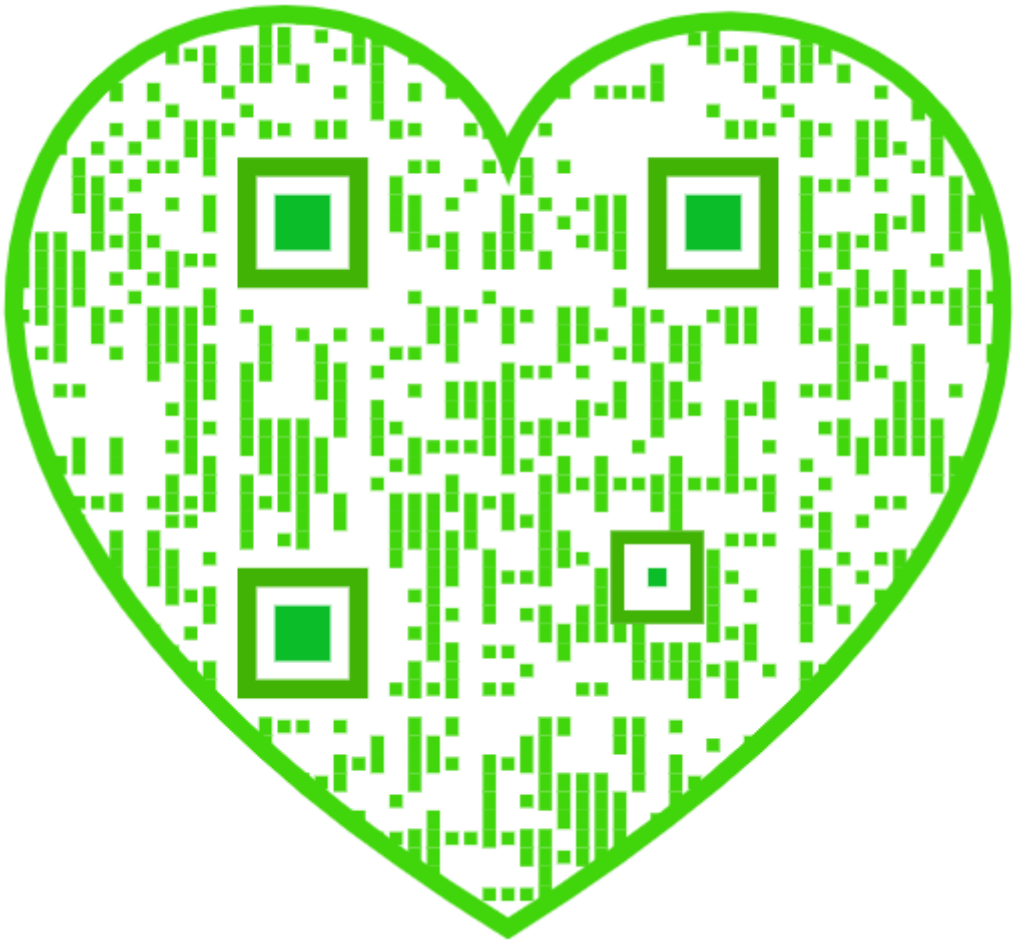

Free trade now free?

Europe's change of heart on agriculture is good for GATT, but US plans on microchips from Japan are not.

THE European Communities (EC) have been thoroughly (and rightly) castigated for causing the breakdown, last December in Brussels, of the negotiations meant to provide for a further bout of trade liberalization in the framework of the General Agreement on Tariffs and Trade (GATT). Can they now expect the indulgence accorded to repentant prodigal sons for having signalled a willingness to be flexible? The sticking-points, last year, were that Europe's offer of a 30 per cent reduction of farm subsidies was calculated with 1986 as the base year (when European subsidies were 10 per cent greater than even now) and that it would not make a separate deal on export subsidies, which are the most direct threat to international trade. Now, the European Commission says that it will, after all, negotiate on the three mechanisms by which it rigs the European market — export subsidies, price supports for farmers and import levies. They are putting out the flags in Geneva, where GATT is based, to signal a resumption of negotiations.

But the cause of trade liberalization, the fastest growing component of the world's economy since the Second World War and the mechanism by which Adam Smith's doctrine that economic wealth rests on the division of labour between efficient producers is literally being made international, is not yet out of the woods. Europe may be willing to negotiate, but may not agree to reduce its protection of agriculture enough to satisfy its chief critics — the United States and the leading agricultural primary producers of the Cairns group (Australia, New Zealand, Argentina and the like).

That is why indulgence will be needed. Europe's critics have consistently failed to appreciate the central role in the Treaty of Rome on which the Economic Communities are founded of the Common Agricultural Policy (CAP), designed to assure 1950s agrarian Europe that farmers would not be impoverished in the intended dash for industrialization. The CAP is now an anachronism and an expensive one, costing Europe perhaps $100 million a year (nearly half in direct costs, the rest in the needlessly high cost of food in Europe). It should be abandoned, but Europe's trading partners should be more patient than they seemed to be last year.

There are, in any case, other issues to be settled. The GATT negotiations themselves embed several other time-bombs, the still incomplete agreement on protection for intellectual property among them. But the whole principle of the GATT negotiation is made a monkey of by a development elsewhere — the declared intention of the United States to renew its five-year price-rigging bilateral agreement with Japan on computer memory chips. The original objective, in 1986, was to protect the US chip-making industry by requiring that Japanese chips should be sold only at inflated prices, and to 'open' the Japanese market to imports from elsewhere.

In the event, the agreement has not functioned as intended. One difficulty is that the government of Japan has been no more able to determine where autonomous manufacturers of computers obtain their components than would have been the government of the United States if the shoe had been on the other foot. The efficient division of labour requires that manufacturers buy their components wherever they can be had most cheaply.

One result is that Japanese chip-makers laugh on the way to their banks. Another is that the cost of memory chips worldwide is greater than it should be. A third is that the pattern of a novel trade is artificially distorted. It is a scandalous agreement, entirely in conflict with the spirit of GATT. On those grounds alone, Japan could (and should) decline to acquiesce, but will probably sign on the dotted line the US Department of Commerce specifies. The question this shabby agreement provokes is whether the United States can be serious about trade liberalization. □

Biotechnology of age

The US administration is seeking a relaxation of regulations — not before time.

BIOTECHNOLOGY has been with us for seventeen years now and, despite scary predictions that genetically engineered organisms would be running rampant across the Earth, there is no record of harm to man or beast. The Bush administration has evidently taken this history of safe research and development into account in formulating its new policy on biotechnology. The report now published (see page 729) from the President's Council on Competitiveness, chaired by Vice-President Dan Quayle, has been prepared by a group whose leader is James B. Wyngaarden, former director of the US National Institutes of Health. It wants to see biotechnology proceed with as little regulation as possible.

The administration's long-awaited policy statement, if implemented, would not only foster biotechnology in the United States, but also have a beneficial effect on collaboration among US scientists and companies and with their colleagues abroad. Meanwhile, the Congress has been given notice that attempts to write new regulations into law will be opposed by the Bush administration.

Scientifically speaking, the new policy is consistent with the recent drift of analyses of risk issues by the National Institutes of Health's Recombinant DNA Advisory Committee (the RAC), which has been pushing for a relaxation of the criteria which determine how many experiments it must oversee. The new policy statement rightly declares that regulators should avoid needless restriction of research and development in this vital technology. Let us hope that people listen. □

GLOBAL WARMING

Third world muscles in on climate treaty

- Negotiations taken out of UNEP
- Climate conference stumbles over details

Washington & London

WHILE 'disappointing' now seems to be the adjective of choice to describe this month's United Nations (UN) meeting on global climate, the gathering did reveal one potentially vital detail: with little fanfare, the balance of power in climate negotiations appears to be shifting towards the world's less-developed countries.

The key move came late last year when, in a little-noticed manoeuvre, a group of developing nations convinced the UN to move the climate treaty process out of the United Nations Environment Programme (UNEP) and into the UN General Assembly, where the developing nations have more influence. As a result, every step of the treaty negotiations, which are aimed at completing a draft treaty by 1992, is now directly subject to General Assembly approval.

The long-term implications of the move are still open to debate, but to judge from the 10-day UN meeting (held 4–14 February in Chantilly, Virginia), it seems clear that the concerns of the developing nations have now risen near the top of the priority list. For instance, negotiations to create a travel fund for the developing nations consumed two full days of the meeting, which at times seemed more like a fund-raiser for developing countries than a climate convention. "It looked like a Jerry Lewis telethon", observed Alan Miller of the University of Maryland Center for Global Climate Change. "Denmark donated $100,000 to the fund and everybody applauded."

With the process now firmly under the wing of the General Assembly, such scenes could become more rule than exception. In UNEP, influence is determined by political might and access to UNEP head Mustafa Tolba. But in the General Assembly, where the rule is one country, one vote, the developing nations believe that they can steer climate negotiations to address many of their own economic and cultural concerns. They argue that the industrialized nations, which are to blame for any global warming because of their unrestricted energy use, should not curtail the energy use of the rest of the world without providing financial aid and incentives to help the developing nations continue their growth.

"The Southern Hemisphere sees this UN move as an opportunity to extract something from the North", says Scott Hajost, an international lawyer with the Environmental Defense Fund. With UNEP no longer in charge, the climate treaty process will now be monitored throughout by the full General Assembly, where the developing world enjoys a 10-to-1 advantage. And that, the developing countries say, means that their voices can no longer be ignored.

If one manic example from the last day of the Chantilly meeting is any sign, they may be right. India led and nearly won a last-minute fight over a proposed fund to help developing countries to cut their carbon dioxide output. Facing off against the United States, India argued that a just-approved fund to encourage developing nations to reduce their use of ozone-destroying chemicals should be a precedent for any future carbon dioxide fund. Finally India gave in, but only so far as to table the point for a future meeting.

Some defend the shift away from UNEP, arguing that the issue of global climate change is bigger than both the UNEP and the World Meteorological Organization (WMO), the two groups that previously shared oversight of climate change. UNEP's past successes have been in such areas as ozone, hazardous waste and chemical exports — important issues, but insignificant compared with global warming. If global warming really is a problem on the order of war and famine, then it belongs on the main floor of the General Assembly with the rest of the world's crises, say the defenders of the shift from UNEP.

But others are concerned that global warming risks clumsy handling by the full UN body. "It's unlikely that the General Assembly is going to be the best place to debate climate diplomacy — as an institution it's too broad", Miller says. "In UNEP, global warming is the highest priority. But in the General Assembly, where does it rank?"

Furthermore, the move appears to be a significant setback for UNEP, which until this decision had been flying high on the success of its recent global ozone accords. And the damage may go even deeper. If the developing countries feel they can go to the General Assembly every time they feel slighted by UNEP, international climate diplomacy is in for a stormy future.

Although UNEP asked the Environmental Defense Fund to help it to lobby to have the climate process returned, the effort made little headway, even with US support. "The United States doesn't have a lot of allies right now", Hajost says. "Even the Europeans basically caved in."

Beyond scuffling over travel funds and the like, the Chantilly meeting resolved only one key issue: delegates agreed to negotiate the treaty with two working groups. One, to focus on "substance", will address the mechanics of global warming, with emphasis on carbon "sources" and "sinks" — automobiles and forests, for example. The second working group, to address "procedures", will write the draft text of the treaty. But, in the spirit of the meeting, no committee chairs were named and no members appointed. That will have to wait for the next meeting, to be held in Nairobi in June.

Christopher Anderson & Peter Aldhous

MANNED SPACEFLIGHT

UK astronaut named

London

THE first Briton in space will be a woman. The food technologist Helen Sharman has been chosen in preference to Tim Mace, a major in the Army Air Corps, to fly on the Juno mission to the Soviet Mir space station in May.

Last summer, the chances of a British astronaut reaching Mir seemed remote,

Mace and Sharman suited for space.

after commercial sponsors failed to come forward with funding for the mission. Juno's original financial backers, the London-based Moscow Narodny Bank, are now paying the Soviets an undisclosed sum to cover the flight, but one casualty has been the roster of British microgravity experiments that were to be included.

Juno's original science director, Heinz Wolff from Brunel University, dissociated himself from the mission in January, after his attempts to revive the British science programme failed.

Sharman will now spend about seven hours on each of the six days she is aboard Mir conducting experiments provided by NPO Energiya, the organization that builds launch vehicles for the Soviet space programme. These include tissue culture, plant growth experiments, and some work on human physiology under weightless conditions. Mace will continue training in the Soviet Union with a backup crew, should Sharman be forced to withdraw for any reason. Peter Aldhous

CANCER EPIDEMIOLOGY

Gold mine in East Germany?

Munich

BY dumping tonnes of pollutants into the country's air, water and soil without investing a penny in cleaning up, the repressive regime of East Germany created some of the worst environmental conditions in the world. At the same time, the regime was nearly paranoid about keeping its citizens under observation and it maintained meticulous health records, including one of the world's most extensive cancer registries.

Now, in a bizarre twist arising from German unification, these two policies may turn out to provide a basis for epidemiological studies of an unprecedented calibre on the effects of environmental pollution on the incidence of cancer. Epidemiologists from the former West Germany say they are eager to get their hands on the data.

But that may not be as easy as it seems — a number of political, scientific and financial hurdles await the scientists who are hoping to study this potentially invaluable cancer registry.

"Unique opportunity"

Earlier this month, a western delegation, including epidemiologists, were given a glimpse into the Berlin-based registry. Although the researchers warn that the registry may not be the treasure trove they were hoping for, they remain excited. To western German legal expert Spiros Simitis, a member of the delegation, the mood among the epidemiologists was reminiscent of "prospectors in San Francisco during the gold rush".

One of Germany's leading epidemiologists, Jürgen Wahrendorf of the German Cancer Research Centre in Heidelberg, calls the chance to assess the East German data "a unique opportunity". And Wilhelm Thiele, head of the cancer registry in the western German *Land* of Hamburg, says "we would be missing an important chance [if we let this drop]". Cancer registries provide just one piece of the puzzle in cancer research and treatment, he notes, but it is an important price.

Between 1953 and 1990, the East German registry collected data on more than 2.1 million cancer cases in a steady population of around 17 million — statistics that make the East German registry the largest in the world in terms of the size of the population it covered.

But if the researchers are to get more than just a glimpse of the East German data, then they must overcome a number of obstacles. The data are now, for instance, recorded on miles of magnetic tape. Simply transferring them to storage accessible to modern computers will certainly be an expensive and labour-intensive task.

Even more daunting will be finding a way to protect the privacy of the subjects of the cancer data, while maintaining free access for researchers. Germany has some of the strictest privacy laws in the world. And it is easy to imagine that eastern Germans, having just been relieved of the secret police called Stasi, may not be eager to have Westerners peering into intimate details of their lives, even if the cause is a good one.

One irony of the registry which increases its allure for Western researchers is that it was hardly ever analysed from the point of view of epidemiology — a medical speciality that was not recognized in East Germany. According to registry employee Wolfhard Staneczek, the registry was created at a time when cancer was even more mysterious than it is now, and doctors wanted to know how big a health problem it was. Later, the data were used to estimate the need for hospital beds in different geographical areas.

Partly because the cancer registry was never intended for epidemiologists, it has several shortcomings that may limit its usefulness. For instance, Thiele points out that cancers in some environmentally sensitive areas, such as the region containing the uranium mines in Saxony, may have been excluded from the registry for political reasons — a fact that may drastically reduce the registry's interest for researchers.

Staneczek admits that there were two groups purposely omitted from the registry: uranium miners and "members of the government". (Both Erich Honecker and Walter Ulbricht, heads of state when East Germany was still under Communist rule, are reported to have had cancer.) But these omissions are not statistically significant, he claims.

Erasure is an option

Epidemiologists may also face legal barriers to the data. Simitis, a professor of law at the University of Frankfurt, says that unless a legal basis can be found for using the registry, the only option will be to "erase all the data". He points out that it would be illegal under German law to grant access to the registry to researchers because the patients whose data are stored there did not give their consent.

Creating a legal framework for using the data will be tricky and difficult, not least because of the understandable reluctance of the population to give up privacy in any form to the government.

The reorganization of eastern Germany from its original 229 districts into six *Länder* (states), including a single *Land* of Berlin (east and west) will increase the size of the challenge. The transition to a structure based on *Länder* will also make it more difficult to continue the registry in eastern Germany.

Keeping the registry going, however, would be very desirable, Wahrendorf says, because of the opportunity that it would provide for observing the incidence of cancer in this population in those cases where it may take 10 or 15 more years to emerge.

Legal expert Simitis says that all six *Länder* must reach an agreement in the form of a treaty to delegate authority over collecting and administering data to one central body. But given the chaotic political conditions that now prevail in eastern Germany, it is unlikely that this will be achieved, says Thiele.

Who will pay

Under the unification treaty signed last year, Bonn agreed to keep open until the end of 1991 all institutions formerly affiliated with the East German Academy of Sciences. But the Bonn Research and Technology Ministry, which has jurisdiction over the Academy, has said that the eastern German *Länder* must take over after that.

It is clear that the registry will not be a high enough priority to be maintained by the eastern *Länder*, all of which are close to bankruptcy. There is a consensus among members of the delegation that the costs for maintaining the registry, or even just for analysing the data already collected, will at least initially have to come from Bonn.

Members of the delegation, which was organized by the science advisory council Wissenschaftsrat, suggested that the campaign to save the registry would gain momentum later this year, when other issues concerning science in eastern Germany have been addressed. The council plans to make a recommendation about the future of the registry by midsummer.

If western German epidemiologists ever do get a good look at the cancer registry, they may be in for a few surprises. Just after unification, the East German registry reported to the Federal Statistics Office in Wiesbaden an unexpected result: despite the obvious additional risk suffered by citizens of East Germany because of environmental pollution, the rate of cancer deaths in 1989 in the east (209 per 100,000 population) was actually lower than that in the west (274.5 per 100,000). Staneczek warns that the data must be looked at "extremely sceptically" as the cause of death was determined in a different way in the two German states.

Nevertheless, even these incomplete figures are enough to make western researchers hungry for more.

Steven Dickman

BIOTECHNOLOGY

Staying in competition

Washington

IF the United States is to retain its competitive edge in the international biotechnology arena, federal regulators must reduce the burden of regulations that hamper companies trying to bring products to market. That is the conclusion of a *Report on National Biotechnology Policy* released last week by the President's Council on Competitiveness.

The report also played down the risks of bioengineered organisms, stating that "products developed through biotechnology processes do not *per se* pose risks to human health and the environment".

Thus the council continues to oppose efforts to introduce new legislation to regulate biotechnology — a position that is in concurrence with the 1986 *Coordinated Framework for the Regulation of Biotechnology*, which was a guide for federal agencies with overview for biotechnology to follow. When evaluating an organism, the report says, federal regulators should disregard whether it has been produced by traditional breeding methods or recombinant DNA techniques and instead focus on the individual characteristics of the organism and its intended use.

Although most scientists would probably find this a reasonable position, it does bother some critics. Margaret Mellon, director of the National Wildlife Federation, called the report the administration's "most extreme statement yet" of its "unwillingness to regulate the technology". Mellon's organization supports the introduction of new legislation to establish a comprehensive regulatory framework for environmental release. She argues that neither the interests of the public nor of industry are best served by issuing a "blanket reassurance" that the technology is safe and by attempting "to force the whole technology" upon the consumer — which she says is happening with recombinant bovine somatotropin.

Among the report's 15 recommendations, the administration continues to oppose any legislative changes to the Orphan Drug Act that would undermine the economic incentives — tax incentives and marketing advantages — provided to companies that develop drugs to treat rare diseases (defined as those affecting fewer than 200,000 people). Although most agree that the act has worked well for the most part, critics argue that in a few cases the market monopoly has had the unintended effect of allowing companies to reap huge profits for drugs that would probably have been developed without the incentives of the act. Last year, Congress attempted to amend the act to allow limited competition in cases where a drug is expected to be so profitable that two or more companies are in a race to market it, but the effort was thwarted when President George Bush would not sign the amendments into law.

The Council on Competitiveness also recommended that the US should pay attention to safeguarding intellectual property rights in biotechnology, in particular by bringing US patent law more in line with that of Europe and Japan. The administration says it would back legislation authorizing the US Patent Office to grant patent protection for the production process, so long as the starting material is novel; this would close what many believe to be a loophole in US patent law. It is expected that legislation addressing these problems, introduced last year by Representative Rick Boucher (Democrat, Virginia), will be reintroduced this year.

Pamela Bridgen, executive director of the Association of Biotechnology Companies, says that the council's intention to re-examine tax issues could have a beneficial effect on small biotechnology companies, particularly those that are not yet profitable. As the tax rules stand at present, "the research and experimentation tax credit is of no value to small companies", says Bridgen.

Almost five years have lapsed since the *Coordinated Framework* was published, and both the Environmental Protection Agency and the US Department of Agriculture have still to put in place the regulations that will be necessary to guide products through to commercialization.

Diane Gershon

ENERGY POLICY

More free market, less regulation, Bush asks

Washington

WITH the unveiling of his National Energy Strategy last week, President George Bush threw his weight firmly behind a free market approach to energy policy. He called for decreasing the country's demand for oil, increasing US production of oil and expanding the use of alternative fuels — all with as little direct government intervention as possible.

Prominent in the proposal was an appeal for research and development aimed at fostering new sources of energy, including safer atomic power and nuclear fusion. "Investing in American ingenuity and know-how is a far better way of achieving our energy objectives than relying on command and control measures, such as increased government regulations and taxes", said the Department of Energy in a prepared statement.

To reverse the US trend away from nuclear power, Bush is urging regulatory reform to make it easier to license nuclear reactors, and is pushing for the establishment of a nuclear waste repository — an act that so far has been delayed by squabbling over where the waste storage site will be located. And to guarantee that nuclear energy can continue to supply at least 20 per cent of US energy needs over the next several decades, the president's strategy asks for accelerated development of advanced reactors.

As part of a long-term plan to achieve a stable energy supply, the policy points to fusion power and sets the goals of an operating demonstration plant by 2025 and commercial fusion power by 2040. This emphasis heartened fusion enthusiasts, who have often seen their funding cut and their timetables delayed. But the energy document has one major weakness, said Steve Dean, president of Fusion Power Associates, an industry association in Rockville, Maryland: "It doesn't talk about how much should be spent, or where the money will come from".

Indeed, although Bush can implement more than half of the energy strategy's 100 separate proposals without congressional approval, most of its more important elements must be put into effect by Congress, and the president will face a fight on many of them.

Perhaps the most difficult sections of the plan to get through Congress deal with the supply of and demand for petroleum. Bush foresees decreasing US oil demand by 3.4 million barrels a day by 2010 while increasing domestic supply by 3.8 million barrels a day. Much of the projected decrease in demand would be the result of improved energy efficiency in both transportation and residential, commercial and industrial energy use; the president's plan would produce this increased efficiency more from federal support for research and development than taxes and regulations aimed at conservation. In particular, Bush rejected increasing the average mileage standards that the federal government now demands from automobile manufacturers.

To increase US oil production, Bush would open the Arctic National Wildlife Refuge in Northern Alaska and areas of the outer continental shelf to oil drilling. This proposal was attacked by environmental and conservation groups, such as the Natural Resources Defense Council and the Sierra Club, which called the policy a sell-out to the energy industry.

Democrats in Congress warned that the Republican president will have to compromise, saying that he is unlikely, for instance, to get approval for both drilling in the wildlife refuge and keeping the mileage standards where they are.

Robert Pool

JAPANESE RESEARCH FUNDING

Cycle of feast or famine

Tokyo

To all appearances, biologists Satoshi Nishikawa and Kazunari Taira are doing well. Last month, the two researchers in the department of cellular and molecular biology of the Fermentation Research Institute received a government grant of ¥48 million ($360,000) to spend more or less as they please. And as most Japanese government researchers these days are struggling for adequate research funds and wrestling with red tape surrounding what money they do get, it would seem that Nishikawa and Taira have cause for celebration.

But there is a catch. Although the two scientists can spend the money on their choice of equipment, reagents, salaries for technicians and postdoctoral assistants and travel expenses for collaborators, their grant is good only to the end of the fiscal year. That gives them less than two months — not nearly enough time, they say, to spend it efficiently.

If this were an isolated case, it might be written off as one of the normal afflictions that develop in any bureaucratic system from time to time. But the experience of Nishikawa and Taira is symptomatic of chronic bureaucratic delays that hamper disbursement of funds under an otherwise imaginative grant scheme administered by the Science and Technology Agency (STA). The problem is particularly acute because the STA money fills an important niche in Japanese government funding of science.

Japan lacks a central organization such as the National Science Foundation in the United States or the research councils in Britain to which researchers of any affiliation can apply. Instead, government researchers have to rely primarily on their own ministry or agency for funds, and grants from these sources can be used only for rigidly defined purposes, usually not including such things as the employment of technicians or postdoctoral assistants.

To introduce more flexibility into this system, STA introduced in 1981 its "special coordination funds for promoting science and technology". The purpose was to create a substantial fund that would be open to government researchers of any affiliation and that could be used for multiple purposes. In large part, this aim has been achieved, and the special promotion fund has grown to more than ¥10,000 million ($75 million) a year, a significant part of the government's overall research grant budget.

But the timing of the disbursement of the funds has proved to be a problem. Whereas most government funds for research can be obtained fairly early in the fiscal year, which runs from April to March, the special promotion funds are seldom available before August or September and often come much later. And because the government sticks rigidly to a one-year fiscal cycle, all of the money must be spent by the end of the fiscal year and cannot be carried over to the next.

Even when a grant continues into the next fiscal year, funds are not available during the spring or summer because of bureaucratic delays in grant renewal. As a result, even scientists, such as oceanographers and climatologists, who need to take data throughout the year, cannot carry out surveys in the spring or summer with the STA special promotion funds.

The delays in disbursement are caused by hearings between STA and the Ministry of Finance, which determine the allotment of funds within each and every grant in minute detail. These negotiations begin only after the budget has been passed by the Diet, usually in March or April, and typically last up to several months for grant renewals and as much as four to six months for new grants. Grants for fiscal year 1990 were badly affected because passage of the budget was delayed by the opposition parties (see figure).

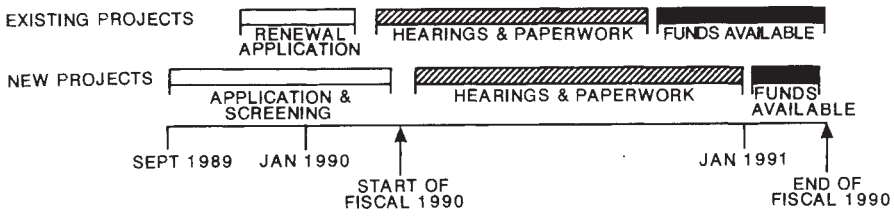

The results of these delays on scientists can be seen — in exaggerated form — in the case of Nishikawa and Taira. According to allotments laid down by STA and the Finance Ministry, their ¥48 million grant includes an allowance for 1,056 man-days of salaries for assistants, and travel funds for a collaborator at Hokkaido University in the north of Japan to come and work with them. But it is impossible for Nishikawa and Taira to spend 1,056 man-days of salaries in only two months, even if they could find anyone interested in signing on for such a short time. And their collaborator cannot come before the end of the fiscal year because the January–March period is particularly busy with examinations.

Fortunately for them, they are allowed some flexibility in how they spend the money. And so the two have gone on a spending spree, buying the most expensive equipment and reagents they can lay their hands on to try to use up all the money — because if they do not, the penny-pinching Ministry of Finance will cut their budget next year.

Taira says he is furious with the government bureaucrats responsible for this situation. "They don't care about scientists. They just think about paperwork."

He is not alone. Makoto Yuasa of the marine geology department of the Geological Survey of Japan says that the STA special promotion funds are always late. When the grant is small, the survey can borrow from other funds, but if the grant is large, Yuasa and his colleagues must sit and wait. And at the Ministry of International Trade and Industry's Agency of Industrial Science and Technology (AIST), Masayoshi Hamada, who administers the fund for AIST researchers, says he too has encountered many examples of problems caused by the delays in disbursement.

The situation is particularly bad for university researchers. Although in theory the special promotion fund is open to them, practice is somewhat different. The Ministry of Education, Science and Culture (MESC), which is in charge of funding at universities, has a running feud with STA about its area of responsibility, and the special promotion funds are seen as a direct intervention in traditional MESC territory. As a result, there is no mechanism for university researchers to receive money directly from the fund. Instead, the special promotion funds have to be fed indirectly through one of the national research laboratories belonging to another ministry or agency. And this leads to further bureaucratic delays.

One category of fund does get to researchers comparatively quickly. These are the 'emergency' special promotion funds designated for such things as natural disasters and epidemics. But even here bureaucracy intervenes.

Last November, Mount Unzen, a volcano on Japan's southern island of Kyushu which has been dormant for about 200 years, suddenly erupted. Researchers from Kyushu University, the Meteorological Agency and STA immediately applied for emergency funds. But the money was not granted until more than a month later, by which time the eruption had long since stopped. (Fortunately, the volcano re-erupted recently and the researchers now have something to spend their money on.)

Toshihiko Yamada, who administers the fund at STA, admits that there are problems. But he says that fiscal year 1990 was exceptionally bad because of delays in the passage of the budget in the Diet. And he says that he and his colleagues are trying their best this year to hold the annual negotiations with the Ministry of

Finance earlier.

The root of the problem is that although STA controls one of the largest science and technology budgets in the government, it has very little political power. The special promotion funds were introduced by the late Ichiro Nakagawa, a powerful member of the ruling Liberal Democratic Party (LDP), when he headed STA in the early 1980s. But Nakagawa was roundly defeated by Yasuhiro Nakasone in the run-up for prime minister in 1982. And Nakagawa subsequently committed suicide in a hotel in Hokkaido in 1983.

With Nakagawa's death, the special promotion fund lost its strongest political backer, and the Ministry of Finance, which was annoyed by the way in which Nakagawa and his supporters had bulldozed the new fund through the Diet, has been putting up bureaucratic barriers to the fund ever since. **David Swinbanks**

JAPANESE BUDGET

End of year splurge

Tokyo

THE rush to spend money at the end of the Japanese fiscal year is by no means confined to the special promotion funds of the Science and Technology Agency. Any motorist in Tokyo will testify to the horrendous traffic jams in the city in late March caused by local governments digging up the roads (whether they need to or not) in order to use up the fiscal year's

construction budget to make sure their budgets are not cut the following year.

And all booksellers know that February–March is the best time for their salesmen to visit universities and research institutes, because scientists are looking for ways to spend the rest of their book budget before the fiscal year ends. Booksellers set aside a *'dedu stoku'*, or 'dead stock', consisting of unsold books, which they sell off at a discount to researchers wanting to get rid of unused funds.

Many researchers say in private that they consider the annual splurge a disgraceful waste of taxpayers' money, but they cannot fight the system.

David Swinbanks

GULF OIL SPILL

Let nature take its course

London

THE Gulf states should resist the urge to clean oil from their smothered beaches, say a group of British ecologists at the Natural Environment Research Council (NERC) who were asked by the UK Department of the Environment to assess the environmental effects of the huge slick now drifting down the Saudi Arabian coast. The region's wildlife may take years to recover, but the additional disturbance caused by removing beached oil means this tactic would do more harm than good, says NERC's Brian Bayne.

Bayne's conclusion is based on studies of previous oil spills, notably the *Amoco Cadiz* wreck off the coast of Northern France in 1978, where saltmarshes that had been left alone recovered more quickly than those from which oil had been removed. Although his team rejects the idea of physical removal of the oil, Bayne believes it will be possible to accelerate the natural bacterial breakdown of oil by spraying fertilizing nutrients onto oiled beaches (see *Nature* **349**, 447; 7 February 1991). The 'latent' oil-feeding bacterial population is limited by a lack of nitrates in Gulf coastal waters, Bayne says.

The NERC report also recommends that the most ecologically vulnerable stretches of coastline should be protected using oil-diverting booms. Bayne is particularly concerned about the fate of the shallow water seagrass beds around the island state of Bahrain.

Most oil-damaged habitats are expected to recover in time, but Bayne says that smothered coral reefs may not be so lucky. The high salt content and relatively low temperature of the Gulf means that the corals are living near the limits of their physical tolerance. Damaged reefs may 'flip' to a completely different ecosystem, says Bayne, with corals unable to return.

The report urges that monitoring of the breakdown of spilled oil and the ecological damage and recovery should begin as soon as possible. This is difficult, given that much of the affected area is a war zone, but Bayne hopes surveys will begin within the next two months. The ecological impact of oil pollution in tropical waters has been studied extensively only once before, after an 8 million litre spill into the Caribbean in 1986, near the Panama Canal. That happened on the doorstep of the Smithsonian Tropical Research Institute's Galeta Marine Laboratory, so marine ecologists were able to make a thorough 'before and after' comparison. They found that reef corals and the seagrass fauna were badly hit. A similar study should be possible in the Gulf, using data collected before the war by Saudi and Kuwaiti scientists, although some Kuwaiti data may now have been destroyed.

Peter Aldhous

SOUTH AFRICAN DEVELOPMENT

Water project dropped

Johannesburg

THE Botswana government and Greenpeace International have issued a joint statement announcing that the southern Okavango Integrated Water Development Project has been abandoned. The plan to dredge the southern stretch of the Boro River, one of the main channels flowing through the Okavango Delta in northwest Botswana, met with opposition from Greenpeace, which had threatened an international boycott of beef and diamonds, the country's two main exports. But the government finally suspended work on the project when more than a thousand representatives of the delta's inhabitants converged on the town of Maun on 11 January to hold a 'kgotla' (crisis meeting) to protest against the scheme to Archie Mogwe, Minister of Mineral and Water Affairs.

The project was intended to provide water for both domestic and agricultural use in the Maun area, which lies at the foot of the delta, and for the De Beers diamond mine at Orapa, which accounts for a considerable portion of the country's foreign exchange earnings.

Some ecologists, were concerned that the project would inevitably lead to a dropping of the water level, which would have adversely affected the delta's ecosystems, which derive their rare characteristics from it being a broad but shallow body of water. The delta is fed by the Kavango River, which rises in the Angola high lands ad flows inland, creating a seasonal floodplain. Its inhabitants are largely dependent on the natural resources of the delta for their livelihood, for which they fish, and more recently, act as tourist guides.

De Beers appeared ambivalent about the implications of the scheme's abandonment for the future of Orapa, as the company set up its own water supply for the mine three years ago by drilling boreholes. Alternative arrangements will have to be made for improving Maun's domestic water supply, and plans for large-scale irrigation will have to be abandoned. But the interesting aspect of the Botswana government's about-face is that it appears to have been prompted by local opposition.

Michael Cherry

EPIDEMIOLOGY

Fluoride given the all clear

Washington

FLUORIDE, the water and toothpaste additive that has dramatically reduced tooth decay since the 1950s, does not cause cancer, US government officials said last week after the most comprehensive review* ever of health studies on the chemical. While the finding comes as little surprise — fluoride has been added to public water supplies for over three decades with apparently no ill effect — it may provide yet another example of the weakness of animal tests in determining human toxicity.

The only serious hint that fluoride might cause cancer in humans comes from a study with rats performed last year by the government's National Toxicology Program. A few male rats that were given nearly one hundred times a typical human flouride exposure did show some statistically significant carcinogenic activity — a finding that the researchers who performed the study characterized as "equivocal". Some animal studies have found that excess fluoride can cause skeletal and tooth damage, but the report notes that sensitivity to fluoride varies widely between species, making these results difficult to apply to humans.

Although the report recommends seven further studies on humans and bacteria to set optimum dietary levels, among other objectives, its only suggestion concerning further animal carcinogenicity tests is that the government should "evaluate the scientific merit" of such studies.

Christopher Anderson

**Review of Fluoride Benefits and Risks*, US Department of Health and Human Services, 1991.

RAMAN INSTITUTE

Storm at Bangalore institute

New Delhi

THE Raman Research Institute (RRI) in Bangalore, founded by the late Nobel laureate C. V. Raman, is passing through a crisis because of the treatment of 52-year-old Professor C. V. Vishveshwara, a theoretical physicist of international repute. His abrupt sacking, followed by the renewal of his service contract "under impossible working conditions", has sparked off a controversy.

The reasons given for terminating Vishveshwara's contract are that he failed to attract bright young people, to guide a single student towards a PhD or to build a school in general relativity and gravitation, the field of his specialization. He was also informed by V. Radhakrishnan, the director of RRI, who is C. V. Raman's son, that his scientific work was just "acceptable", implying that it was not outstanding. But Vishveshwara was not told why the institute waited for 14 years to discover his deficiencies.

The eight-member RRI council, which manages the institute, is within its legal rights to terminate contracts without giving reasons. But Vishveshwara's case has aroused sympathy within the scientific community because of his international stature. One of the pioneers in black-hole physics and one of India's best-known relativists, he is next only to the director in seniority and is the only Asian elected to the Berne-based international society on general relativity and gravitation.

A student of Charles W. Misner, Vishveshwara joined RRI as an associate professor in 1976 and was made full professor in 1980 for a five-year term. His contract had been routinely renewed twice, but when the next renewal came up in September 1990, he was asked to quit. His well-wishers believe that the director's decision, later endorsed by the RRI council, smacked of jealousy and vindictiveness. Radhakrishnan, who has not made any comments, says he will respond at an appropriate forum.

Vishveshwara's case was all set to be closed, but the council was forced to reconsider the issue in the wake of a memorandum signed by some 200 scientists as well as by appeals from several of his collaborators in the United States and Europe. At its last meeting in December 1990, the council agreed to renew the contract on condition that Vishveshwara would carry out only personal research in his field without interacting with other researchers at RRI.

The council also made it clear that the contract was being renewed "for extraneous reasons" and not on the merits of the case. Vishveshwara's room has also been moved from the physics block to the administrative block. Vishveshwara, who says that no self-respecting scientist would want to work under such humiliating conditions, has appealed against the "conditional" offer that his contract should be renewed.

At least one dissenting RRI council member has resigned, and several senior scientists, including nuclear physicist Raja Ramanna, have asked the president of the Indian Academy of Science, Professor C. N. R. Rao, to find a solution. A decision on Vishveshwara's appeal will be made at a special meeting of the Raman Trust, of which Rao is a member, on 2 March.

"Nothing that happened in the scientific community in recent years has disturbed it as much as the unfortunate developments in RRI", said S. R. Valluri, a former member of the council and fellow of the Indian Academy of Science. Pointing out that the harassment of Vishveshwara signalled the "erosion of ethics of Indian science", Valluri resigned from the academy, describing this step as a "penance" for the acts of fellow members of the academy who served on the RRI council.

The government's Department of Science and Technology, which supports RRI, has adopted an ostrich-like attitude, saying it cannot interfere in the problems of an autonomous institute. But Valluri in his resignation letter observed that academic freedom did not prevail in RRI which, some of its scientists say, has become a family fiefdom of the Indian Nobel laureate.

K. S. Jayaraman

Halley at large

COMET Halley has made an unexpected reappearance in the night sky, following an unprecedented outburst of activity at its nucleus. Observers at the European Southern Observatory first noticed the outburst on 12 February, and confirmed that Comet Halley, now well beyond the orbit of Saturn, was the source. The cause of the outburst is a complete puzzle. Until last year, solar heating maintained a vestigial cloud of gas and dust around the comet's nucleus. But now, the comet should consist solely of its dirty frozen nucleus. For it suddenly to take on the extended nebulous appearance observed by the European astronomers something must have made the nucleus erupt. A collision with another small body, interaction with solar wind and the sudden release of energy stored in the nucleus are possibilities entertained by astronomers. Roland Pease

European Southern Observatory.

Looking like just a faint smudge, Comet Halley has suddenly erupted into something at least 300,000 kilometres across. This image taken by O. Hainaut and A. Smetteon on 12 February, resembles those taken on subsequent nights, showing that Halley's reappearance is no flash in the pan.

RADIOASTRONOMY

Funding hiccup at Jodrell

Jodrell Bank, Cheshire

JUST as British radioastronomy is coming into its own, funding problems threaten to undermine its work. Britain's leading centre for radioastronomy, the University of Manchester's Nuffield Radio Astronomy Laboratory at Jodrell Bank, expects to find itself short of up to £800,000, nearly one-third of its annual running cost, when the Universities Funding Council (UFC) this week tells the universities how much money each will get in 1991–92.

Ironically, the problem has appeared just as British radioastronomy is poised to reap the scientific benefits of upgrading its most valued asset — the MERLIN radio telescope array (see this page).

Unlike many of the British laboratories now faced with a declining budget, the problem at Jodrell Bank is not simply the general one of underfunding in the British science base. Jodrell's particular difficulty is the new rigid formula that the UFC is using to calculate the money each university is given for research.

Although the formula does take into account the quality of research in university departments so that more is spent where the research output is strong, the formula will not justify the uniquely large sum of money Manchester must put aside to support radioastronomy at Jodrell. There has always been an element of "special funding" for Jodrell, says its director Rod Davies, but the UFC's predecessor, the University Grants Committee, never gave a detailed breakdown of each university's grant.

The problem is compounded by the government's decision to shift some of the UFC's research money to the research councils, beginning with £50 million in 1992–93. The idea is to make the research councils responsible for the indirect costs of research they support (see *Nature* **349**, 360; 31 January 1991), but Jodrell staff fear that the transfer will further undermine Manchester's capacity to fund the radioastronomy laboratory.

The obvious solution, Davies says, is for the £800,000 shortfall to come through the research council system, either from the Science and Engineering Research Council (SERC) or directly from the Advisory Board for the Research Councils (ABRC). SERC is already paying £2.3 million over three years to run the MERLIN telescope array as a national facility. But Davies says that Jodrell as a whole serves the entire British radioastronomy community, and so deserves increased research council support.

Nevertheless, Davies does not want Jodrell to become one of SERC's own laboratories. Jodrell can be run more efficiently within a university, he says.

Manchester officials saw the problem coming almost a year ago, but their discussions with SERC and the ABRC have so far failed to find a solution. With the research councils, and SERC in particular, tightening their belts to keep their spending within the disappointingly low 1991–92 science budget, Davies finds it difficult to see where the money will come from. The deadlock has also placed in an embarrassing position the SERC chairman, Sir Mark Richmond, as he has changed sides half-way through the negotiations. Until October last year, he was vice-chancellor at Manchester.

Despite the current impasse, Davies is optimistic: "It would be so daft", he says, if the reorganization of university funding could jeopardize a world-famous laboratory. If the money cannot be found, Manchester could be forced to stop funding the Lovell telescope, an instrument that has identified a number of rapidly spinning millisecond pulsars — among the most exciting discoveries by radioastronomers in recent years. **Peter Aldhous**

Making the most of MERLIN's potential

Jodrell Bank, Cheshire

MERLIN (the multi-element radio-linked interferometer network) takes advantage of the fact that a number of small radiotelescopes can be made to mimic a single large telescope by making simultaneous observations and combining their data electronically.

This solves a fundamental problem in radioastronomy: a radiotelescope's collection dish must be thousands of times larger than the mirror of an optical telescope to achieve the same resolution.

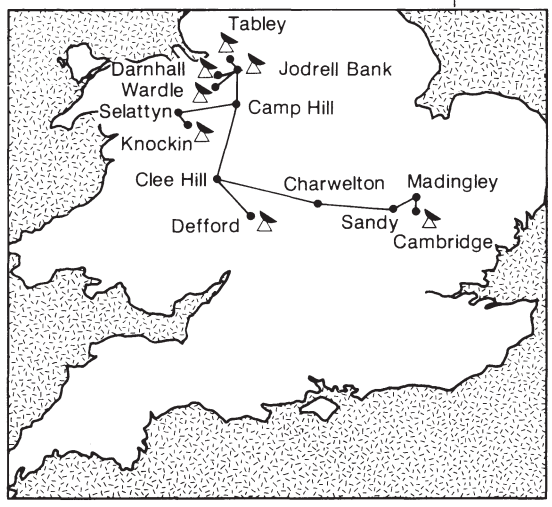

Map of the MERLIN array of radiotelescopes and repeater stations showing the microwave links to Jodrell bank.

Since 1980, six British telescopes have been run together, controlled from Jodrell. But MERLIN's sensitivity has now been increased by fitting the telescopes with helium-cooled radio receivers, improving the microwave links from each back to Jodrell, and upgrading the computers that are used to combine the data.

Even more valuable is a new 32-metre telescope at Cambridge (see *Nature* 348, 377; 29 November 1990) that has increased the maximum distance between pairs of MERLIN telescopes to 230 kilometres, improving MERLIN's angular resolution to better than that of the best ground-based optical telescopes. "It's the Hubble Space Telescope on the ground", says Rod Davies, Jodrell's director.

The full seven-telescope array should become fully operational in April. Among the first astronomers to benefit will be those interested in the radio observation of thermally active stars. Most stellar radioastronomy has so far concentrated on the few stars that "put on a show" in the radio spectrum, says Dennis Walsh, who collaborated with optical astronomers to discover the first gravitational lens at Jodrell in 1979. MERLIN is now sensitive enough to study "the silent majority" of stars, he says. MERLIN will also be used to investigate the astrophysics of star formation. The interiors of star-forming regions are opaque to optical and infrared telescopes, but can be probed using radioastronomy.

Walsh's own speciality — gravitational lenses — is high on the list of projects to be given telescope time. MERLIN will reobserve the first lens to be discovered, enabling astronomers to study the distribution of matter in a galaxy that is 'bending' radio emissions from a distant quasar to produce a double image. By linking MERLIN's observations with those from other European radiotelescopes, it may be possible to find a third quasar image that is predicted by theory but is likely to be quite faint.

There is also a plan to generate radio emission maps of the sky with MERLIN which will complement the optical maps now being drawn up using data from the European Space Agency's Hipparcos astrometry satellite. Simultaneous observations from very widely spaced radiotelescopes have been used previously to generate radio emission maps, but until now it has not been possible to include the radio emissions from most of the thermally active stars seen by Hipparcos.

Peter Aldhous

A long view of history

SIR—E. Guthy (*Nature* **348**, 670; 1990) is correct in pointing out that a long view of history absolves the Germans of greater aggressiveness than other European powers. What is striking in German history, however, at least before the Second World War, is the failure to form stable political systems capable of dealing with severe internal and external stress. Even Bismarck, masterful politician that he was, was not able to manage the system he had created without alternately targeting socialists, Catholics or (to a lesser extent) Jews for transient advantage. Moreover, the peculiar idea, springing from German romanticism but made explicit by Hegel, that the state itself possessed an organic life and natural rights apart from those of its citizens, was to have a long-lasting and terrible influence.

Guthy is somewhat disingenuous in his portrayal of Germany's beneficent influence on Central Europe in the years before the First World War. Certainly Austria would not have gone to war against Serbia in 1914 without encouragement from Germany. This, coming as it did from the Kaiser and general staff, bypassing the chancellor, illustrates the political failure. It is German historians who have taught us that war in 1914 was seen by many in Germany as necessary to resolve otherwise insoluble problems: "encirclement" by the Russians and the French; the implications of a socialist majority in the Reichstag; decline of the East Elbian aristocracy. And indeed German war aims, not just as advocated by more or less influential groups such as the Pan-German League, but articulated in the Brest-Litovsk Treaty, were not those of a power seeking only to preserve the *status quo* or redress recent losses.

German political evolution had been frozen at what was for Western Europe an intermediate stage on the road towards true representative government: the combination of an authoritarian executive with an elected parliament. As a result, there was no tradition of political accountability. During the war, Allied politicians knew the price of failure was loss of office; for the German government, it was revolution.

The instability of Imperial Germany, and its political failure, was of course exacerbated by the First World War. In the Weimar era, neither will nor resources were sufficient to suppress violent political deviance or to devise legitimate means of expression for the concerns that bred such violence. Although Hitler's regime was radically different from the Kaiser's, it was not totally discontinuous. In the former case an ideological, in the latter a military, dictatorship had been allowed to control the country. In fact one of the most interesting differences, and an indication that things do change, is the relative lack of influence of the military under the Nazis. Thus, the rejoinder to the fear of W. Frank Harris (*Nature* **347**, 510; 1990) that Germany in 2000 will act no differently than in 1900 or 1930 must be that different political structures are now in place. Moreover, the ultranationalist ideology popular among at least a significant minority of Germans in 1900 as well as 1930 seems much less prevalent now.

It is important to face problems openly. In the United States, the legacy of 300 years of slavery has not been erased entirely in the 100 since abolition. By now, certainly, Germany is experienced enough in democracy, and rich enough, to deal with the problems presented by unification, as long as everyone keeps the past, not in a closet, but in a quiet corner in the back of the mind.

WILLIAM H. THEODORE

6328 Lenox Road,
Bethesda, Maryland 20817, USA

Order, order!

SIR—John Maddox's News and Views article "Should camp-followers be policemen?" (*Nature* **348**, 107; 1990) raises again the issue of research article authorship. While it is widely acknowledged that the practice of a senior researcher adding his or her name to a paper in 'honorary co-authorship' is morally dubious, there is at least one pragmatic argument in favour of such a system — it can greatly facilitate literature searches. Searching against a (well known) senior author's name in reference listing (for example, *Index Medicus*, and especially the now widely available CD-ROM citation indexing) is likely to achieve a fruitful 'trawl' of relevant papers, highly desirable in these times of burgeoning publications.

R.D. EVANS

University of Oxford,
Nuffield Department of Anaesthetics,
Radcliffe Infirmary,
Oxford OX2 6HE, UK

SIR—Apportioning credit to each author of a multi-authored work continues to be a matter of guesswork. How is a reader to know, to mention examples with which I am familiar, that an author was listed only because he was department chair, or because he was a friend of the editor of a leading journal? What is one to make of a note added in proof advising readers to invert the published order of the authors in future references to the paper? Perhaps we need to devise a system to let employers, granting agencies, historians and (let's face it) gossips know what each author thought the others contributed.

Accordingly, I propose that we assign meaning to the punctuation marks used to separate authors' names. Thus, if authors believed that each contributed equally, a comma would continue to be used after each name. In more difficult cases, alternative punctuation would be used. For example, those authors who contributed equally to a multi-authored work might be listed together without commas, followed by a semicolon and the lesser authors. More imaginatively, the name of the department chair might be followed with a subscript star, the friend of the editor with a small double-headed arrow, and an author who contributed only money with a $, £ or ¥. Question and exclamation marks could be used in particularly interesting ways.

This system should appeal to scientists; it is arcane, expandable, infinitely arguable, wholly uninterpretable to readers not in the system and usable by bibiologographic services. The only major problem I can see is that a large percentage of authors would seem to gain nothing by such disclosure.

JEFFREY B. MILLER

Neuroscience Center,
Massachusetts General Hospital,
Boston, Massachusetts 02129, USA

Not so old

SIR—Perhaps a reasonably correct historical sense is not absolutely necessary in news items, but 'Britain's Astronomer Royal' (*Nature* **349**, 93; 1991) is a title that dates back only to 1972 when Sir Richard Woolley ceased to be 'Astronomer Royal of England'. It is the latter title that dates back to the seventeenth century and it was never 'an honorary position' but was coterminous with the directorship of the Royal Observatory at Greenwich until 1950 and then of the Royal Greenwich Observatory at Herstmonceux. At present there is no Astronomer Royal of Scotland so that the use of the term 'Britain' in Professor Wolfendale's appointment may be unwelcome to some Scottish readers. It may be further mentioned that, although the Andrews' Professor of Astronomy in the University of Dublin was conferred by George III (Letters Patent, 32 GeoIII, 1792) with the title "for ever" of Royal Astronomer of Ireland, it was tacitly understood that this provision lapsed in 1966 when the statutes of the university were revised.

PATRICK A. WAYMAN
Andrews' Professor of Astronomy
(Honorary)

Dunsink Observatory,
Dublin 15, Ireland

Letters submitted for Correspondence should be typed, double-spaced, on one side of the paper only.

New twist in the long saga of HIV

Nucleotide sequence data from Robert Gallo's laboratory now show that neither the French nor the US samples of virus isolated in 1983 correspond to the French LAV strain whose sequence appeared in 1985.

THE origin of the first AIDS virus has been a pervasive and somewhat destructive theme in AIDS research since French and US researchers got into a row about it eight years ago. Now, data from the laboratory of one of the principals — Robert C. Gallo of the US National Cancer Institute — add a curious twist to an old story (see Scientific Correspondence, page 745).

The new data cast doubt on the widely accepted view (some say canard) that the virus Gallo showed to be the cause of AIDS — called IIIB — is really a French virus in disguise. Spurred in part by a continuing NIH investigation of the integrity of his AIDS research, Gallo's colleagues, headed by Marvin Reitz, took advantage of modern polymerase chain reaction (PCR) techniques to go back to the freezer and sequence for the first time samples of viral isolates they received from Luc Montagnier and Jean-Claude Chermann of the Pasteur Institute in 1983.

The question was simply this: How does the sequence of IIIB, published in 1985, compare to that of the 1983 samples derived from a French male homosexual identified by the initials BRU. The expected answer would be that BRU and IIIB correspond. In fact, they do not. More surprising still, the data show that the BRU sequence, represen-ting the first putative AIDS virus, does not correspond to the sequence the French published in 1985 for their own virus, then known as LAV/BRU, where LAV stands for lymphadenopathy virus.

From the nucleotide sequences of several BRU samples that verifiably came from the Pasteur Institute in 1983, the new data add a new layer of mystery to the case, while providing strong circumstantial evidence that Gallo's IIIB did not come from the Pasteur Institute. As Gallo notes, the fact that LAV and IIIB were shown by 1985 sequence analysis to be nearly indistinguishable molecularly has led most AIDS researchers to conclude that they are, in fact, one and the same.

Assuming that the provenance of the viral isolates is correct (and there is no reason to doubt it), the new molecular analysis, and unpublished serological data, indicate that neither LAV nor IIIB (as published in 1985) is present in samples from the patient BRU. (The presence of Chermann among the signatories of today's correspondence bears on the authenticity of the 1983 French samples now analysed.)

Virologist Howard Temin of the McArdle Laboratory for Cancer Research at the University of Wisconsin, who is familiar with the new data, but who was not one of the referees of the correspondence, summarizes the situation this way. "We now do not know where LAV or IIIB came from. Therefore, we can't accuse anyone of anything. Do we care further? No, This is a non-issue as far as the AIDS epidemic is concerned. Now it is a non-issue as to the character of Dr Gallo. Let's get on with it." Temin also wonders why, in this case, people were so ready to assume chicanery, when science if full of examples of researchers doing parallel yet independent work."

A word on the nomenclature may help in making the outline of this story clearer. The virus that causes AIDS, now known as the human immunodeficiency virus (HIV) varies in molecular sequence from patient to patient. Even the few isolates described in Gallo's correspondence have separate designations. For simplicity in what follows, the viruses are referred to by only three terms: BRU refers to all the samples reported here to have come from the patient BRU; LAV refers to the Pasteur Institute isolate whose sequence was published in 1985; IIIB refers to the isolate from Gallo's laboratory whose sequence was also published in 1985, and which bears the uncanny likeness to LAV (or *vice versa*).

When Montagnier published the sequence of BRU in 1983, he suspected, but could not prove, that it might be the cause of AIDS. An inability to grow BRU in quantity limited possibilities for developing further data. Montagnier sent samples of BRU to Gallo, where cell biologist Mikulas Popovic was busy trying to get one of the laboratory's many isolates to grow in culture.

After repeated attempts with single isolates, Popovic, in November 1983, took isolates from ten different patients whose identity is known and, unconventionally pooled them to create a viral soup. His gamble paid off when IIIB emerged from that soup as an isolate that could be grown in quantity. By the spring of 1984, Gallo's laboratory had developed and patented an AIDS blood test based in part on IIIB.

Recently, NIH contracted with independent scientists to do molecular analyses of available samples of the isolates in Popovic's viral pool — at least seven of the ten have been retrieved — together with other isolates from Gallo's laboratory. The committee now also has the material from the 1983 samples described in the correspondence. One goal is to find the patient who was the source of IIIB. Now it would also be interesting to find the patient who was the source of LAV.

Gallo's laboratory received five samples of BRU in 1983. One, called MT2B, cannot be found. One sample, called RUB, was apparently used up. Is it possible that either of them was LAV? Perhaps, but Chermann, who was working with Montagnier at the time, avows that they, too, came from BRU.

Is it possible that BRU was doubly infected, by the isolate called BRU and by LAV? No such case of double infection by two widely different isolates of HIV has been reported, but an experiment can be done to test that possibility.

Yet another possibility is that Montagnier and Gallo each received viral isolates from the same patient. Gallo has records of the samples received from physicians in the United States and abroad. Presumably the Pasteur Institute does as well. Were the Institute to open its notebooks, it would be easy enough to see whether the French and US scientists received material from the same source.

Finally, it would be interesting to analysis by PCR any original 1983 viral samples that may still be frozen at the Pasteur Institute. A number of attempts to retrieve this tissue have been made, not only by Gallo and his colleagues, but also by NIH officials who are hoping to find the patients from whom these viruses are derived. But, so far as is known, no one has as yet received 1983 Pasteur Institute isolates either from the institute itself or from the official French national cell repository.

If Gallo's sequence data for BRU are indeed correctly attributed to the initial French isolate, it means that for the present, the origin of LAV is as much a mystery as the origin of IIIB. Although the value of the missing data is more historical and political than scientific, the issue has created an unhealthy diversion from the important business of stopping a deadly epidemic. All of Gallo's laboratory records, and now samples of viral material, have been opened to independent scrutiny by lawyers for the Pasteur Institute and committees of the NIH. Perhaps it is time for the French to come forward with its own records and early isolates.

Barbara J. Culliton

MATERIALS SCIENCE

Dropping below freezing point

Robert W. Cahn

BY letting droplets of pure molten rhenium fall through a 48-metre evacuated tube, workers at Grenoble have succeeded in cooling this high-melting-point metal almost a thousand kelvin below its melting point without it solidifying. The point of this study by Vinet *et al.* is to probe the limits to undercooling and to investigate the nucleation that precedes crystallization.

One can hardly become a materials scientist without encountering one of the central classics of this discipline, Turnbull's study of the limits of undercooling of molten metals[2,3]. When a molten metal is cooled, the amount by which it can overshoot the equilibrium melting temperature is normally determined by the presence of nucleation catalysts (an elegant name for minute specks of refractory dirt). Such specks ensure heterogeneous nucleation, caused by the existence of a low interfacial energy between a frozen nucleus and the speck. This always happens at a smaller undercooling than does true homogeneous nucleation, which is a purely statistical process in which a population of unstable solid embryos perpetually forms and remelts until the temperature falls far enough for a few to become stable and grow.

Turnbull's genial notion was to bypass heterogeneous nucleation by dividing the melt into tiny discrete droplets, typically tens of micrometres in diameter, surface-coating them to prevent coalescence and either supporting them on a substrate[2] or suspending them in an inert, immiscible fluid (the emulsion technique)[3]. The dirt specks are then restricted to a proportion of the droplets, and the remainder can freeze homogeneously.

The early (substrate) experiments were done with a range of metals melting at temperatures ranging up to 1,828 K (palladium), but the most precise experiments were done by the emulsion method with very low-melting-point metals such as mercury and bismuth. The undercooling was studied by dilatometry, which gave anomalous signals when a number of droplets froze and thus contracted. This kind of research has continued unabated since 1950, but rarely with the difficult materials now studied by Vinet *et al.*[1], who use the two metals with the highest melting points of all, tungsten (T_c = 3,690 K) and rhenium (T_c = 3,450 K).

Turnbull and Cech's early substrate experiments indicated that the maximum achievable undercooling observed by this technique was restricted to 0.18–$0.2T_c$. Turnbull[4] analysed this in terms of the classical theory of homogeneous nucleation, in which the predicted nucleation rate is proportional to $\exp(-K\sigma^3T_c^2/T[\Delta T]^2)$, where σ is the interfacial energy between liquid and solid, T_c is the equilibrium melting temperature, ΔT is the undercooling and K is Boltzmann's constant.

From the exponent, it was a reasonable assumption that the important independent variable was the normalized undercooling, $(\Delta T/T_c)$. Turnbull went further[4], showing that the interfacial energy between solid and liquid should be proportional to the heat of fusion, ΔH_f, of each metal (at least for close-packed crystal structures), so that the limiting normalized undercooling at which homogeneous freezing became unstoppable should indeed be about 0.18. It is easy to show that the theoretical nucleation rate for a given metal varies very rapidly indeed over a narrow temperature range: typically, a 10 per cent increase in undercooling will increase the homogeneous nucleation rate a million-fold — many experiments have confirmed this — and thus the critical undercooling can be quite narrowly defined.

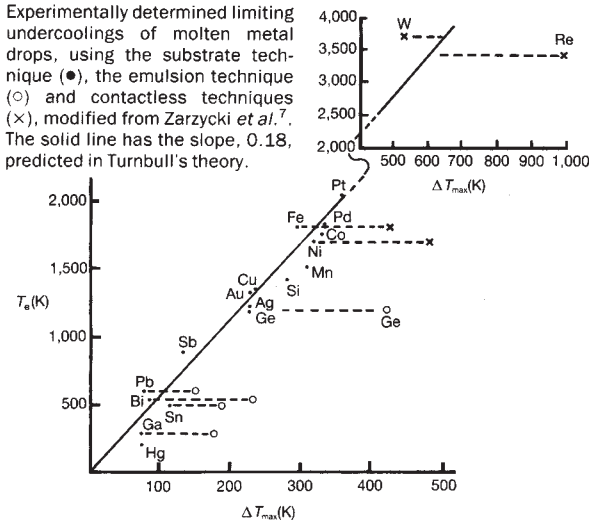

Experimentally determined limiting undercoolings of molten metal drops, using the substrate technique (●), the emulsion technique (○) and contactless techniques (×), modified from Zarzycki *et al.*[7]. The solid line has the slope, 0.18, predicted in Turnbull's theory.

In the early experiments, a modest standard cooling rate of around 0.3 K s^{-1} was used. Subsequent work showed that varying the cooling rate alters the achievable undercooling somewhat: a careful study by Chu *et al.*[5] on tin showed that the limiting undercooling increased from 95 to 103 K as the cooling rate is increased from 0.05 to 1.0 K s^{-1}.

Many experiments have been done with the substrate and droplet-dispersion approaches, and improved techniques (such as encapsulation in molten salts) permit increasingly high melting points to be examined. The emulsion technique in general yields greater undercoolings than does the substrate technique. The beginnings of microgravity research stimulated other methods, such as electromagnetic or acoustic levitation of droplets and the use of evacuated drop-tubes, and it became clear that such contactless methods often allowed undercoolings greatly to exceed those predicted by Turnbull's theory. Presumably, the absence of coatings and the cleanliness of the surface are responsible for this.

On the basis of this later work, some of it his own, Perepezko[6] proposed a modified limit to the possible undercooling, as much as 0.65 T_c. Clearly, Turnbull's theory predicting a linear relation between interfacial energy and the latent heat of fusion needs critical re-examination: it works well, but only for σ values deduced from substrate experiments. The graph reproduced here (from one by Zarzycki *et al.*, and including some recent results[8] on slowly cooled Si and Ge) gathers most data on undercooling of droplets and shows systematic variations according to the technique used.

A possible source of the experimental deviation from simple theory is a wider than expected variation in liquid/solid interfacial energy, σ. This energy is hard to measure directly. Glicksman and his colleagues[9,10] developed a method centred on measurement of the groove formed where a grain boundary impinges on the solid/liquid interface. For bismuth[11], the measured interfacial energy differed modestly, by 15 per cent, from that predicted by Turnbull's ΔH_f correlation. For lead[9], however, there was excellent agreement between the directly measured value of σ and that deduced from measurements of limiting undercooling by a variant of the substrate method; this constitutes one of the most convincing checks on the classical theory of homogeneous nucleation[12].

In their impressive new work on tungsten and rhenium, Vinet *et al.* used the drop-tube technique. Metal drops were allowed to fall freely under gravity down an evacuated tube and their freezing *en route* detected by the associated recalescence (a transient reheating due to the release of latent heat). Recalescence was detected by one of a number of radiation detectors arranged along the length of the tube, and the temperature at the moment recalescence began was calculated from the position of the drop, the theory of radiative cooling and the initial temperature of the molten drop. The Grenoble drop tube is 48 m long and kept at an ultrahigh vacuum of 4×10^{-10} mbar. The cooling rate is high, of the order of 1,000 K s^{-1}, but as we have seen, this should make only a modest difference, a few tens of degrees, to the achievable undercooling if the

nucleation is homogeneous.

Fifty drops of tungsten, made by electron-beam melting the end of a wire, with 150 K initial superheat, were allowed to fall down the tube: ten showed recalescence with a mean undercooling of 530 K, equivalent to $\Delta T/T_c$ of 0.14. The range of ΔT among the ten drops was small, 28 K, as expected from classical theory. The other forty drops presumably froze heterogeneously, not surprising when it is realized that the drops were over 4 mm in diameter. Ten rhenium drops, of about the same size, again at 150 K initial superheat, were tested, and all showed high undercooling: this time the mean ΔT was 975 K, with a very small spread (only 0.5 per cent). This corresponds to a remarkable value of $\Delta T/T_c$ of 0.28.

The authors point out that the extremely good vacuum ensured the cleanliness of the falling drops and diminished the likelihood of heterogeneous nucleation; this, together with the strikingly narrow range of ΔT observed for those drops which recalesced, makes it highly probable that true homogeneous nucleation had been observed. The undercooling found for rhenium is the highest absolute value observed for any metal hitherto, and the values of σ deduced for tungsten and rhenium are also the highest known for any metal. From the graph, however, it can be seen that the undercooling for tungsten (W), large as it is, is smaller than predicted by extrapolation from lower-melting-point metals; perhaps nucleation was heterogeneous after all.

Vinet *et al.* are planning to examine a range of other high-melting-point metals, such as platinum, tantalum, osmium and their alloys, by the same technique; when they have done this, it will be clearer how consistent the behaviour of these refractory metals is with that of low-melting-point metals. □

Robert W. Cahn is in the Department of Materials Science and Metallurgy, University of Cambridge, Pembroke Street, Cambridge CB2 3QZ, UK.

1. Vinet, B., Cortella, I., Favier, J.J. & Desré, P. *appl. Phys. Lett.* **58**, 97–99 (1991).
2. Turnbull, D. & Cech, R.E. *J. appl. Phys.* **21**, 804–810 (1950).
3. Turnbull, D. *J. chem. Phys.* **20**, 411–424 (1952).
4. Turnbull, D. *J. appl. Phys.* **21**, 1022–1028 (1950).
5. Chu, M.G., Shiohara, Y. & Flemings, M.C. in *Chemistry and Physics of Rapidly Solidified Materials* (eds Berkowitz, B.J. & Scattergood, R.O.) 3–10 (Met. Soc. AIME, New York, 1983).
6. Perepezko, J.H. & Paik, J.S. in *Rapidly Solidified Amorphous and Crystalline Alloys* (eds Kear, B.H., Giessen, B.G. & Cohen, M.) 49–63 (Elsevier, New York, 1982).
7. Zarzycki, J., Frischat, G.H. & Herlach, D.M. in *Fluid Sciences and Material Science in Space* (ed. Walter, H.U.) 599–636 (Springer, Berlin, 1988).
8. Evans, P.V., Devaud, G., Kelly, T.F. & Kim, Y.-W. *Acta Metall.* **38**, 719–726 (1990).
9. Nash, G.E. & Glicksman, M.E. *Phil. Mag.* **24**, 577–592 (1971).
10. Schaefer, R.J., Glicksman, M.E. & Ayers, J.D. *Phil. Mag.* **32**, 725–743 (1975).
11. Glicksman, M.E. & Vold, C.I. *Acta Metall.* **17**, 1–11 (1969).
12. Kelton, K. F. in *Solid state Physics* (eds Ehrenreich, H., Seitz, F. & Turnbull, D.) (Academic, New York, in the press).

LYMPHOCYTE HOMING

Skin-seeking memory T cells

Charles R. Mackay

THE constant migration of T cells and other leukocytes throughout the body allows the full repertoire of the immune system to protect tissues from challenge by pathogens. Leukocyte migration into tissues is particularly prominent during inflammatory responses, and results from cytokine-induced expression of adhesion molecules on the surface of vascular endothelial cells, which bind receptors on circulating leukocytes.

On pages 796 and 799 of this issue, Picker *et al.*[1] and Shimizu *et al.*[2] show that a molecule termed endothelial cell-adhesion molecule-1 (ELAM-1) is one of the receptors on inflamed endothelium for circulating T lymphocytes. More importantly, these papers demonstrate a striking bias in the class of T cells which bind ELAM-1 — only memory-type T cells, a functionally potent class of T cells, bind ELAM-1 and enter inflamed tissue; furthermore, the expression of ELAM-1 on inflamed endothelium is particularly prominent within skin, which has led to the suggestion that ELAM-1 acts as an adhesion molecule or 'vascular addressin' for a specific subset of skin-homing, memory T cells[1]. These findings support the concept that peripheral T cells segregate into distinct tissue-homing subsets as part of a rationalization of immunological resources.

Endothelial cell-adhesion molecule-1 is a member of the 'selectin' or 'LEC-CAM' family of adhesion molecules[3], which also includes MEL-14/LAM-1/Leu-8 and GMP-140. Selectins have a highly characteristic structure — an N-terminal lectin domain, an epidermal growth factor-like domain and a number of complement-binding protein-like domains. ELAM-1 was originally implicated in the binding of blood neutrophils and monocyte-like cells to inflamed endothelium[4]. Ligands for ELAM-1 expressed on neutrophils are sialylated, fucosylated polylactosamines, such as the sialyl Lewis x determinant, which bind to the lectin domain (as discussed recently by Springer and Lasky in News and Views[5]). The ligand for ELAM-1 on T cells has not yet been identified but it appears to be highly restricted in its expression to a specific subset of memory cells marked by a molecule termed cutaneous lymphocyte-associated antigen (CLA). Because T cells expressing this antigen bind selectively to COS cells transfected with ELAM-1, CLA may even serve as a ligand for ELAM-1.

Although ELAM-1 can be expressed on inflamed endothelium in almost any tissue, it does show a biased expression on inflamed endothelium of skin[1]. In contrast, the other major endothelial adhesion molecules for T cells, such as VCAM-1 and ICAM-1, show no tissue-specific restrictions. Hence ELAM-1 provides a certain degree of specificity, or at least bias, for a population of skin-homing T cells, whereas VCAM-1 and ICAM-1 probably act as general adhesion molecules.

The restricted expression of vascular adhesion molecules to specific tissues, and their ligands to specific subsets of lymphocytes, has long been thought to account for the non-random recirculation patterns of subsets of T cells. So the description in this issue of a skin-homing subset of memory T cells[1] gives more credence to claims for the other separate migration streams for T cells, such as those to the gut, the synovium of inflamed joints and lung-associated tissue[6-8]. A putative gut-homing subset of T cells also expresses a site-specific molecule recognized by the monoclonal antibodies HML-1 and Ber ACT8. In addition, a vascular addressin on mucosal endothelium and adhesion molecules on the gut-homing lymphocyte subset probably direct this migration pathway in a similar fashion to that described for the skin pathway. Interestingly, the homing of subsets of $\alpha\beta$ T cells to different tissues such as the skin and the gut resembles the way in which different families of $\gamma\delta$ T cells, distinguished by their use of different Vγ and Vδ T-cell receptor genes, home to different epithelial sites. The existence of several distinct migration streams for T cells makes sense, because the pathogens encountered in different sites — skin, gut and so on — will be characteristic of each tissue.

The findings of Picker *et al.*[1] and Shimizu *et al.*[2] that only memory-type T cells bind ELAM-1 are consistent with a number of reports on the accumulation of memory T cells in inflammatory lesions. Memory T cells are also the only T cells which recirculate through uninflamed tissues including skin[9], and so naive and memory-type T cells show clear differences in their distribution and migration patterns.

But what in fact are memory T cells, and what is the significance of their migration pathways? The traditional view has been that memory T cells represent a clonally expanded population of antigen-reactive cells that survive for years and that mediate an enhanced immune response upon re-encountering antigen. Alternatively, a somewhat heretical view is that most if not all memory T cells represent recently activated cells which are maintained by continuous antigenic stimula-

tion. Regardless of these interpretations, memory T cells are functionally much more potent than their naive precursors, and exhibit an altered surface phenotype which accounts for their behaviour and function. The expression of virtually all the leukocyte adhesion molecules is up-regulated on memory T cells, including those molecules that have been implicated in the binding of T cells to inflamed endothelium, such as VLA-4 and LFA-1.

Memory T-cell migration to inflamed or even normal skin seems to represent a rationalization of immune resources, because an inflammatory site is likely to contain antigens or pathogens which the host has encountered previously. Likewise, the surveillance of uninflamed tissue such as skin is best served by memory T cells. In contrast, new antigens drain to local lymph nodes, which are designed for the massive migration of lymphocytes of diverse specificities, especially naive T cells[9]. The differential migration patterns of naive and memory T cells may also have implications for peripheral T-cell tolerance, and the establishment of autoimmune disease, since the tissue antigens encountered by T cells in different migration streams will be different.

Until recently, determining how T cells mature in the thymus has overshadowed the study of T-cell behaviour in the periphery. The need for an understanding of the extra-thymic maturation of T cells, including the development of memory T cells with their specific migration pathways and their site-specific molecules, together with the need to clarify peripheral tolerance, represents an interesting shift in emphasis for immunologists. □

Charles R. Mackay is in The Basel Institute for Immunology, Grenzacherstrasse 487, CH-4057 Basel, Switzerland.

1. Picker, L. J., Kishimoto, T. K., Smith, C. W., Warnock, R. A., Butcher, E. C. *Nature* **349**, 796–799 (1991).
2. Shimizu, Y. *et al. Nature* **349**, 799–802 (1991).
3. Bevilacqua, M. P., Stengelin, S., Ma, J. R. G. & Seed, B. *Science* **243**, 1160–1165 (1989).
4. Bevilacqua, M. P. Pober, J. S., Mendrick, D. L., Cotran, R. S. & Gimbrone, M. A. *Proc. natn. Acad. Sci.* U.S.A. **84**, 9238–9242 (1987).
5. Springer, T. A. & Lasky, L. A. *Nature* **349**, 196 (1991).
6. Chin, W. & Hay, J. B. *Gastroenterology* **79**, 1231–1242 (1980).
7. Butcher, E. C. *Curr. Top. Microbiol. Immun.* **128**, 85–96 (1986).
8. Cahill, R. N. P. *et al. J. exp. Med.* **145**, 420–428 (1977).
9. Mackay, C. R., Marston, W. L. & Dudler, L. *J. exp. Med.* **171**, 801–817 (1990).

MOLECULAR ELECTRONICS

Totally organic transistors

David Bloor

THE first transistor to be made entirely of organic molecules has recently been devised and tested by Francis Garnier and co-workers[1] at the Laboratoire des Materiaux Moleculaires of the CNRS. One of the transistor's more unusual properties is its flexibility — it still functions when bent. This may mark the beginning of the end for the dominance of inorganic semiconductors in electronics.

Silicon microelectronic devices of increasing complexity continue to be developed and bring yet more compact and powerful systems into the home and office. The impact of other inorganic semiconductors is restricted to particular applications: for example, III–V compound semiconductors such as GaAs are used for microwave devices, light-emitting diodes, lasers and infrared sensors. Organic molecular materials, with a few exceptions, have been regarded as laboratory curiosities too unstable chemically and mechanically to be of practical significance. The exceptions are, however, not insignificant: polymeric photoresists are vital in the manufacture of silicon integrated circuits; the unique optoelectronic properties of molecular liquid crystals has lead to their widespread use for displays; organic semiconductors have largely displaced inorganic semiconductors as the active components in xerographic copiers. But despite these successes, molecular materials have not offered a serious challenge to established materials in the mainstream of electronic and optoelectronic devices. Recent progress in the preparation of pure, well-characterized organic materials and a better understanding of their physical and chemical properties may well change this.

The first step towards electronic devices with a polymer playing an active role was described in an earlier News and Views article[2]. This was made possible by the development of a precursor polymer route which enabled thin, pure semiconducting films of polyacetylene to be prepared by spin coating . These were incorporated in a metal–insulator–semiconductor arrangement similar to that of a silicon field-effect transistor (FET). However, the underlying device physics differs in two significant respects. First, when charge is induced in the polymer layer by applying a voltage to the gate, it does so as the result of the population or depopulation of states in the 'band' gap separating polyacetylene's valence and conductivity states. In silicon, charge is either added to the conduction band or removed from the valence band. The band-gap states in conducting polymers result from the structural relaxation of the polymer chain in the vicinity of an added charge to give 'solitonic' and 'polaronic' states (Fig. 1). The relaxation in the harder silicon lattice is much smaller and the effect on the electronic states is negligibile.

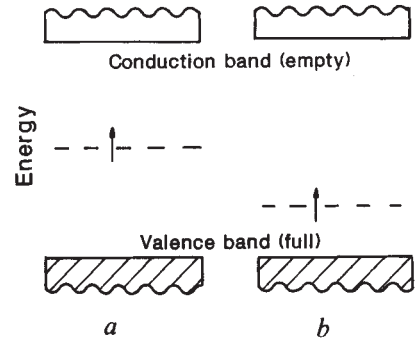

Fig. 1 *a*, Solitonic state in polymers, such as polyacetylene, with degenerate ground states. *b*, Polaronic levels in polymers, such as polyparaphenylenevinylene, with nondegenerate ground states. (↑, Single electrons.)

Second, structural defects in the polymer give rise to defect levels with a greater energy separation than the band gap. Thus, structural defects do not affect the semiconducting behaviour of the polymer. In silicon, structural defects produce localized energy states in the band gap which degrade the semiconducting properties. Thus amorphous silicon is a poorer semiconductor than single-crystal silicon, though it is still useful as a device material.

One severe problem which limits the performance of such polymeric transistors is the low mobility of the current carriers. The mobilities of electrons in semiconducting polymers, amorphous silicon and single crystal silicon are about 10^{-4}, 1 and 10 $cm^2 V^{-1} s^{-1}$, respectively. So while the current–voltage characteristics for polymeric FETs are reasonable, the operating speed is poor. However, it is not necessary to have long polymer chains to obtain suitable semiconducting properties. In fact, the disorder in the polymeric materials means that the defect-free regions of the polymer backbone are quite short. Thus, similar properties can be obtained with short molecules—oligomers.

It is an oligomeric analogue of the semiconducting polymer polythiophene containing six repeat units, sexithienylene, that Garnier and co-workers have now investigated[1]. The authors report the construction of an all-organic transistor based on sexithienylene. A polymeric insulating layer was used to separate the active sexithienylene layer from the gate electrode. The current carriers move in a thin layer close to the interface and Garnier and co-workers find that the nature of the interface has a large influence on carrier mobility in the oligomeric layer. Thus if a silicon oxide insulating layer is used, the electron mobility is 0.03 $cm^2 V^{-1} s^{-1}$. But with the polymeric insulator, the value is significantly larger, 0.5 $cm^2 V^{-1} s^{-1}$. This value is similar to that of amorphous silicon so that devices with comparable performance can be made. Large-area thin films are easily prepared on flexible sub-

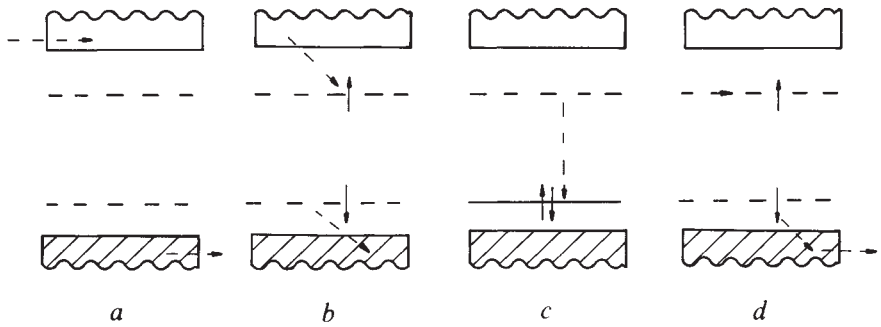

Fig. 2 Possible mechanisms for electroluminescence. *a*, Carrier tunnelling or thermionic emission into the conduction and valence bands. *b*, Formation of negative and positive polarons which combine to form a neutral polaron exciton. *c*, Emission by decay of excited polaron exciton. *d*, Direct injection of electrons to form negative polarons which combine with positive polarons followed by emission (as in *c*).

strates and the transistors produced are unaffected by bending. So, the way is open to large-area, conformable device arrays.

Although metal–insulator–semiconductor structures comprising an oxidized silicon substate and a semiconducting polymer layer do not compete with silicon FETs, they offer new devices not possible with conventional semiconductors. When charges are induced in the polymer by applying a voltage to the silicon, partially filled states are created in the band gap of the polymer. The polymer can then absorb light at wavelengths to which it is normally transparent, by promoting electrons from the valence band to the mid-gap states or from the mid-gap states to the conduction band[7]. Because the silicon substrate is also transparent at these wavelengths, the whole device functions as an electro-optic modulator. Other unusual characteristics have been reported. Metal–polyalkythiophene Schottky-barrier diodes behave with a pronounced temperature dependence[8] acting as diodes at room temperature but not at 100 °C. Polymers have also been manipulated to produce multilayer structures analogous to inorganic semiconductor 'quantum well' structures[9]. The potential of such structures to be used in devices remains to be explored.

Light-emitting diodes and lasers based on III–V semiconductors provide sources in the green, orange, red and infrared spectral regions. Blue sources, though available, are less efficient. Organic materials fluorescing at short wavelengths are well known, but only in 1987 was electroluminescence of high intensity produced[5]. This device combined an emitter layer, in which electrons were able to move, with a hole (electron-vacancy) transport layer. Recombination of electrons and holes at the interface produces the electroluminescence. This concept has been extended by Saito and co-workers[9] to provide efficent organic light-emitting diodes with output running across the visible spectrum into the blue. At present the devices lack long-term stability, but they are easy to prepare.

A parallel, more dramatic advance has been the observation of electroluminescence from semiconducting polymer diodes. This was first reported for polyparaphenylene[10], another polymer prepared by a precursor route. Polyparaphenylene was sandwiched between a positive electrode of oxidized aluminium, gold or indium oxide and a negative electrode of aluminium, magnesium silver alloy or silicon hydrogen alloy. The devices were made by spin coating the precursor polymer, which was thermally converted to the semiconducting form before the second electrode was applied. Similar results have been obtained with a soluble semiconducting polymer, poly-2-methoxy-5-(2-ethylhexoxy)-1,4-phenylene vinylene[11], although this was less efficient.

The exact mechanism of the electroluminescence in these materials is unclear. The charge carriers normally encountered in polyparaphenylene vinylene are bipolarons (paired charges) with low mobility. These are unlikely to contribute to the electroluminescence. Two possibilities are either that electrons tunnel to band states and relax to the final emissive exciton states (bound electron–hole states) via mobile polarons, or that they tunnel directly to the exciton levels (Fig. 2). These preliminary results are encouraging as control of polymer structure and micromorphology is likely to lead to improved device performance.

Progress since 1988 has been rapid and if the rate of progress is maintained practical polymer-based devices are likely to emerge. However, greater long-term

1. Garnier, F., Horowitz, G., Peng, X. & Fichou, D. *Adv. Mater.* **2**, 592–594 (1990).
2. Bloor, D. *Nature* **335**, 115–117 (1988).
3. Edwards, J. H., Feast, J. W. & Bott, D. C. *Polymer* **25**, 395–398 (1984).
4. Burroughs, J. H., Jones, C. A. & Friend, R. H. *Nature* **335**, 137–141 (1988).
5. Burroughes, J. H., Jones, C. A. Lawrence, R. A. & Friend, R. H. in *Conjugated Polymeric Materials. Opportunities in Electronics, Optoelectronics and Molecular Electronics* (eds Bredas, J. L. & Chance, R. R.) 221–245 (Kluwer, Dordrecht, 1990).
6. Ohmori, Y. *et al. Jap. J. appl. Phys.* **29**, L837 (1990).
7. Shimidzu, T. *Reactive Polym.* **11**, 177–189 (1989).
8. Tang, C. W. & Van Slyke, S. A. *Appl. Phys. Lett.* **51**, 913–915 (1987).
9. Adachi, C., Tsutsui, T. & Saito, S. *Phys. Lett.* **56**, 799–801; **57**, 531–533 (1990).
10. Burroughs, J. H. *et al. Nature* **347**, 539–541 (1990).
11. Braun, D. & Heeger, A. J. *Appl. Phys. Lett.* (in the press).

RÉSUMÉ

Splice after splice

A GENE in the *Euglena gracilis* chloroplast contains an intron within an intron. This is the surprising conclusion of D. W. Copertino and R. B. Hallick (*EMBO J.* **10**, 434–442; 1991) who show that the internal intron is excised while the external intron is still in place. Splicing out of the larger intron then produces the mature form of the RNA. Evolutionary considerations suggest that intron addition to chloroplast genes in *Euglena* is not uncommon, but it is unclear why the 'twintron' is processed in two separate splicing reactions. An intriguing possibility is that we may be seeing a primitive form of alternative splicing, a mechanism by which eukaryotes can use a single gene to produce related but distinct proteins, often with significantly different properties.

Radical prospects

AN international clinical trial holds out the promise that recombinant interferon-γ may be a safe and effective treatment for the rare inherited disorder chronic granulomatous disease (J. Gallin *et al. New Engl. J. Med.* **324**, 509–516; 1991). The disease, which exists in more than one form, affects the production of oxygen free radicals by phagocytes, diminishing the cells' ability to kill ingested bacteria. Only 14 out of 63 patients receiving interferon-γ experienced a serious infection, compared with 30 out of 65 who were given a placebo. The total number of serious infections was also reduced, yet phagocyte function was unchanged and so the mechanism of interferon action is unclear. However, if interferon can act in an oxygen-independent way, it may help not only those suffering from chronic granulomatous disease but also in the treatment of infectious ailments such as leprosy and leishmaniasis.

Strong stuff

NEUTRON stars may preserve their magnetic fields for 10^{18} years — an eternity on the timescale of the age of the Universe — according to calculations by E. Harrison (*Mon. Not. R. astr.Soc.* **248**, 419–423; 1991). The powerful fields are swept through space as the neutron star rotates, and are the source of the radio and optical pulses we recognize as pulsars. Curiously, pulsars seem to turn off after about 5 million years, when their rotation has slowed to around a cycle per second. One possibility proposed was that because the neutron stars have a superfluid and superconducting interior, the magnetic flux lines could effectively float out of the pulsar, which would consequently fade from view. Harrison now shows that the electromagnetic forces set up by the migration of the flux lines would completely negate any 'buoyancy' they may have. Another mechanism must silence the pulsars.

stability must be achieved for the devices before this possibility becomes a reality. The inorganic–polymer interface has been identified as the seat of failure in the electroluminescent devices. The work of Garnier *et al.* amply demonstrates the importance of control of the interface structure. It should also be noted that the earliest liquid crystal displays degraded rapidly, but now offer very long lifetimes. Thus, the use of purer materials and carefully designed device structures is essential if these research discoveries are to lead to mass-produced devices. □

David Bloor is in the School of Engineering and Applied Sciences, University of Durham, South Road, Durham DH1 3LE, UK.

CLUSTER PHYSICS

All surface and no bulk

Michael Grätzel

ATOMIC clusters can be made with high precision with any number of atoms from two or three to several thousands. Occupying a niche between molecules and bulk crystals, they offer a way to study the transition between these more conventional states of matter. In a study of the transition for the semiconductor material gallium arsenide, Smalley and colleagues[1] find that the gradual transition from molecular to bulk properties is punctuated by alternations between odd- and even-numbered clusters. They also find that, in contrast to metal clusters, it takes remarkably few atoms to make a bulk semiconductor.

The distinctive properties of the smallest semiconductor clusters, just a few nanometres in diameter, are determined by the quantum effects imposed by the confinement of valence electrons to small orbits, scarcely larger than atomic orbits. Quantum structures such as quantum wells, wires and dots (spatially restricted in one, two and three dimensions, respectively) are becoming widely studied because of these properties and because of the new technological possibilities they offer.

Recent experimental and theoretical studies have indicated that dramatic changes occur in the physical properties as one reduces the size of semiconductor clusters. For example, the gap between the electronic valence and conduction energy bands becomes greater, resulting in a shift to shorter wavelengths of the threshold 'edge' in absorption and fluorescence spectra. This is accompanied by a break up of the continuous character of the bands into discrete levels resembling molecular energy levels. And because the energy levels are roughly proportional to the inverse square of the particle's radius, the cluster's electron affinity (the energy associated with capturing an electron) should decrease in the same way.

As one approaches the nanometre size scale, however, a point is reached where it is no longer possible to ignore the influence of atoms on the cluster surface. In the case of semiconductor clusters this has been a distinct problem. These are generally prepared by arrested precipitation in solution, so that the surface atoms are in contact with foreign molecules which are expected to modify the properties of the whole cluster. The difference in the experiment of Smalley and colleagues[1] is that the clusters are prepared in the gas phase by laser vaporization of a GaAs wafer and subsequent cooling in supersonic gas expansion (Fig. 1). Cluster anions of a particular size are selected by mass spectrometry and have their electronic properties probed by ultraviolet photoelectron spectroscopy: the kinetic energy of the electron released by ultraviolet light of a particular wavelength indicates the ('vertical') electron affinity of the neutral cluster.

It turns out that clusters with 2–50 atoms and nearly equal numbers of gallium and arsenic atoms (nearly stoichiometric composition) have alternating electron affinities for odd and even numbers of atoms (Fig. 2). The strength of the alternation persists scarcely unaltered throughout the size range, the electron affinity of the even-numbered clusters being consistently 0.5–1 electronvolts (eV) lower than those of the odd-numbered ones. The only exception is for two- and three-atomed clusters, the electron affinity clusters, the electron affinity being larger for the monomolecular two-atom cluster. The odd–even alternation is also evident in the ionization potential of the neutral clusters, which was always lower for the odd-numbered clusters than for the even-numbered ones.

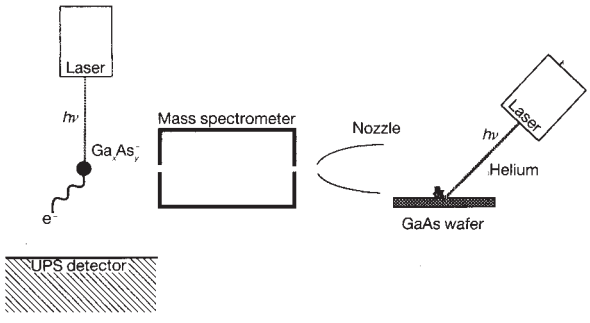

FIG. 1 Set up used by Smalley *et al.* to study Ga_xAs_y clusters. The clusters form as anions ($Ga_xAs_y^-$) in a plasma created by laser vaporization of a GaAs wafer. After selection in a mass spectrometer, a second laser detaches the excess electron which is analysed by the ultraviolet electron spectroscopy (UPS) detector to reveal the electronic states of the cluster.

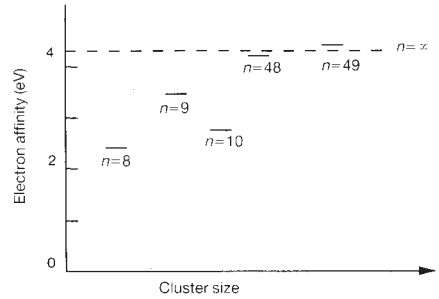

FIG. 2 Odd–even alternations in the electron affinity of gallium arsenide clusters (Ga_xAs_y) and the approach to the bulk value ($n = \infty$) as a function of the cluster size, $n = x + y$. (Data from Smalley and colleagues[1].)

The point is that the electron affinity and ionization potential give interesting clues about the nature of the electronic states of the clusters. In this case, they clearly establish that the even-numbered clusters have ground-states in which the electrons are spin-paired, corresponding to a closed-shell configuration. (Again, the exception is the diatomic GaAs molecule, whose ground state has two unpaired electrons: a spin triplet state.) The closed-shell configuration rules out the possibility of there being surface states formed by dangling bonds of the gallium and arsenic atoms occupied by unpaired electrons. Apparently, these are avoided by the transfer of an electron from gallium to arsenic, leaving the surface gallium atoms with vacant dangling-bond orbitals, and filled dangling bonds on the arsenic atoms.

Dangling bonds have already been extensively studied on bulk semiconductor surfaces. From a physical point of view, a singly filled dangling bond is a surface state whose energy is intermediate between the bulk valence and conduction bands. Because it can trap both electrons and holes (positively charged electron-vacancies) it can act as a site where these recombine. Chemically speaking, dangling bonds constitute reactive surface sites and are hence a source of thermodynamic instability: atoms with dangling bonds react with one another, changing the surface structure and bonding patterns. This chemical relaxation removes the dangling bonds from the band gap into the valence or conduction bands, so that they no longer act as recombination centres. The observations by Smalley and colleagues suggest that such reconstruction and relaxation occurs even on aggregates as small as a few atoms.

The addition of one more atom to the even clusters produces an odd-electron system which necessarily has an open-

shell configuration. The extra electron is in a largely non-bonding orbital whose energy is intermediate between the highest occupied and lowest unoccupied orbitals of the even-numbered cluster. This explains the alternation of the electron affinity and ionization potentials of the clusters[2].

The most astounding result from the investigation is the fast rate at which the electron affinity rises to its bulk value of 4.07 eV. Clusters with only 50 atoms have this electron affinity. The approach to the bulk property is even more rapid than is found with simple metal clusters such as potassium or copper. It also disagrees with the predictions of the usual semiclassical model[3] treating the clusters as uniformly charged spheres according to which even clusters containing as many as 1,000 atoms should have electron affinities several tenths of an electronvolt lower than the bulk value.

Interestingly, a recent investigation[4] of GaAs clusters in liquid quinoline shows also a smaller change in the energy gap between the occupied and unoccupied states than predicted by the model[4]. This is because, rather than being distributed uniformly throughout the cluster, the electrons are concentrated near a few surface atoms of the cluster which act as weak traps for the charge. And our recent study[5] shows that chelation of colloidal semiconductors enhances the rate of interfacial charge-transfer reactions, underlining the importance of the surface localization of the electrons.

All these observations underline the importance of charge localization for the behaviour of semiconductor particles. It seems that the answer to the question at which size a semiconductor starts to behave as a solid depends to a large degree on the state of the surface atoms. For GaAs, the corners between otherwise perfectly reconstructed surface facets act as shallow traps for conduction band electrons. The wavefunction for a trapped electron is localized and is not submitted to the same quantum confinement effects as the delocalized orbital of a conduction-band electron. Hence quantum confinement effects are expected to be less important in clusters where charge localization takes place. Intriguingly, such nanometre-sized clusters may turn out to be attractive models for studying the surface behaviour of bulk semiconductors. □

Michael Grätzel is in the Institut de Chimie Physique, Ecole Polytechnique Fédérale de Lausanne, CH-1015 Lausanne, Switzerland.

1. Jin, C., Taylor, K.J., Conceicao, J. & Smalley, R.E. *Chem. Phys. Lett.* **175**, 17–22 (1990).
2. O'Brien, S.C. *et al. J. chem. Phys.* **84**, 4074 (1986).
3. Brus, L.E. *J. chem. Phys.* **79**, 5566–5571 (1983).
4. Olshavsky, M.A., Goldstein, A.N. & Alivisatos, A.P. *J. Am. chem. Soc.* **112**, 9438–9439 (1990).
5. Frei, H., Fitzmaurice, D.J. & Grätzel, M. *Langmuir* **6**, 198–206 (1990).

ZOOLOGY

Marine quick-change acts

Jeremy J. D. Greenwood

A PIONEER in the study of the wonderful ability of cephalopods to change rapidly their body colours and patterns was William Holmes[1], who (amongst other things) showed that cuttlefish (*Sepia officinalis*) would adjust their normal countershading when they were turned on their backs. Fifty years later, Ferguson and Messenger, working like Holmes at the Naples Zoological Station, have extended these observations to two other species, have shown how rapid the colour adjustments are and have investigated the mechanism responsible for them[2].

Countershading, the phenomenon of the lower surface of an animal being paler than the upper surface, has the demonstrable effect of counteracting the difference of illuminance of the two surfaces, which is otherwise an important clue for the visual system in picking out three-dimensional objects from their backgrounds. It was first described by E. B. Poulton[3], who studied the pupa of the purple emperor butterfly *Apatura iris*. The pupa is up to 8.5-mm thick but, in Poulton's words, "By this beautiful and simple method [it] appears to be as flat as a leaf which is only a small fraction of 1 mm in thickness"[4]. That countershading is widespread was subsequently pointed out by A. H. Thayer[5]: not only are many cryptic insects countershaded but so are most fish and mammals, especially those that are strongly convex and that live in strongly lit environments.

In those animals that habitually live upside-down, such as the caterpillar of the eyed hawk-moth *Smerinthus ocellata*, countershading is inverted appropriately. This insect is typical of many others in being a leaf-mimic: the optical flattening produced by countershading is reinforced by pale stripes on the body that give the impression of veins on a leaf. In most fishes, in contrast, the value of countershading is probably that it produces simple crypsis: the dark upper surface of the fish blends in with the gloomy depths of the water when viewed from above, and the pale underparts are cryptic against the overhead light when viewed from below, any flattening effect of the countershading being relatively unimportant. Simply having pale underparts is a rather inadequate means of producing crypsis against illumination from above, as the animal is still silhouetted against the light. Fish therefore have silvery underparts which reflect the available light and reduce the contrast between their bodies and the surface illumination when they are viewed from below[6].

Ron Taylor/Ardea

Feat of imitation — an octopus turns blonde and black.

Cephalopods, except when engaged in displays, tend to be cryptic, matching their backgrounds closely in colour and pattern. Countershading is common. The animals' colours are the results of pigment held in small sacs, chromatophores, that can be expanded by attached muscles to expose the pigment over a wider area. Under nervous control, the muscles can operate quickly, giving startlingly rapid changes of colour which allow the animals to adjust their crypsis as they move over different backgrounds. Herein also lies the ability to adjust countershading. In all three species investigated by Ferguson and Messenger[2] (*Sepia officinalis*, the squid *Loligo vulgaris* and the octopus *Octopus vulgaris*) there is a rapid response when the animal is inverted: chromatophores on the entire ventral surface (now uppermost) are expanded, darkening that surface, whereas the dorsal surface becomes paler through the contraction of its chromatophores. If the animal is merely turned on its side, the response is appropriate: the side that is uppermost darkens and the lower side becomes pale. This adjustment, which can be seen in free-swimming cephalopods, makes their countershading superior to that of fish, which do not rapidly adjust their countershading and so do not maintain crypsis when temporarily rolled over.

Ferguson and Messenger show that, if a cephalopod is kept inverted for more than a few seconds, the ventral chromatophores do not remain expanded. This cannot be explained by supposing that chromatophores cannot be kept expanded for longer than that, because dorsal chroma-

tophores can be maintained tonically expanded for hours if necessary. Rather, the explanation is that under natural conditions an inverted cephalopod will rapidly turn over into its normal orientation, so it does not need to keep its altered countershading for long. This righting response is mediated mainly by the organs of balance (statocysts), though the eyes play some part. By surgical procedures, Ferguson and Messenger demonstrate that the countershading reflex in contrast is mediated entirely by the statocysts, which is surprising given that vision is the main sense determining other responses of the chromatophores.

These observations add to our picture of cephalopod behaviour but they leave many questions unanswered. Does countershading benefit cephalopods because it helps them to avoid predators or to ambush their own prey? Does it work by visually flattening the body or by reducing the contrast between the animal and its background? Does it help them to remain unseen or to be difficult to keep track of during a predatory chase? Cephalopod biologists are not alone in not having yet addressed these questions by experiment: although it is over a century since Poulton described countershading, there are no animals in which anyone has yet done so. □

Jeremy J. D. Greenwood is at the British Trust for Ornithology, Beech Grove, Tring, Hertfordshire HP23 5NR, UK.

1. Holmes, W. *Proc. zool. Soc. Lond.* **110**A, 17–35 (1940).
2. Ferguson, G.P. & Messenger, J.B. *Proc. R. Soc.* **B243**, 63–67 (1991).
3. Poulton, E.B. *Trans. Ent. Soc. Lond.*, E515–606 (1888).
4. Poulton, E.B. *The Colours of Animals* (Kegan Paul, Trench, Trubner & Co., London, 1890).
5. Thayer, A.H. *Pop. Sci. Mon.* **75**, 550–570 (1890).
6. Denton, E.J. & Nicol, J.A.C. *J. mar. biol. Ass. U.K.* **45**, 711–738 (1965).

HUMAN GENETICS

Methylation and the fragile X

Ian Craig

THE fragile-X syndrome is the most common form of mental retardation after Down's syndrome. In this disorder, mental handicap and the associated features of large ears and testes occur in males with a fragile site on the long arm of the X chromosome at the band position q27.3 (refs 1 and 2). The site appears as a non-staining gap in metaphase spreads[3] (Fig. 1). So far, the molecular events underlying the cytogenetic and clinical features have eluded researchers; but the recent reports by Vincent *et al.* in *Nature*[4] and by Bell *et al.* in *Cell*[5], provide a considerable advance towards that goal, as well as going some way to support the proposal[6] that DNA methylation is involved.

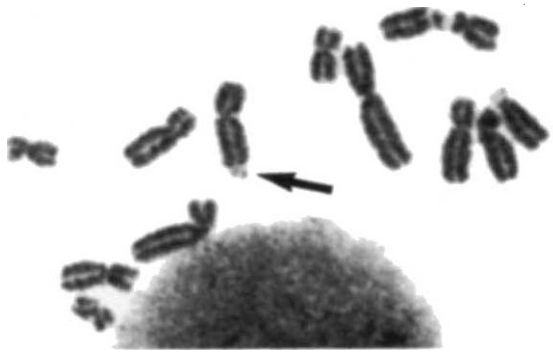

FIG. 1 Partial metaphase spread showing the fragile site at Xq27, appearing as a non-staining gap.

An unusual feature of the fragile-X syndrome, apart from its high mutation rate ($4-5 \times 10^{-4}$) (ref. 7), is its transmission by some males who show neither the fragile site nor clinical symptoms (Fig. 2). About 20 per cent of males known to carry the mutation fall into this category. Among females, a third of carriers express some of the features of affected males. Further complicating genetic counselling is that, although there is a high correlation between expression of the fragile site and mental retardation, lack of expression in females at risk (particularly in daughters of normal males who can transmit the defect) does not necessarily exclude them from being carriers. But recently DNA markers have been isolated that are closely linked to the fragile site, improving the confidence with which diagnosis can be made, but only where the mode of transmission (through the male or female) is clear[8-10].

To explain some of these unusual features of the fragile-X syndrome, various models with a two-step process in expression have been proposed. Laird[6] has suggested that the phenotype results from a mutation at Xq27 that prevents the reactivation of genes on the inactive X chromosome during oogenesis. Passage of the defect through the inactivation–reactivation process would therefore be a necessary precondition for full expression. Methylation is an obvious way by which an expression defect could be linked to reactivation. Both Vincent *et al.*[4] and Bell *et al.*[5] have now detected altered restriction-fragment patterns in DNA digests of fragile-X patients with probes that map close to the fragile site at Xq27.3. The differences could result from the blocking, by methylation, of recognition sequences in a cluster of rare restriction sites. With long-range mapping it has been shown that this cluster lies close to the fragile site and proximal to the regions detected by the probes used by the two groups. Vincent *et al.* showed with the distal probe DX5465, that three different enzymes that cut only rarely in the genome — *Bss*HII, *Eag*I and *Sac*II — failed to produce bands of normal size in affected males (ref. 11). Most characteristically, a band of about 620 kilobases (kb) observed in *Bss*HII digests of normal males was absent, or reduced in intensity, in affected males and replaced by more material at the limit of resolution. There was complete loss of normal bands in about three-quarters of the affected males. The appearance of a normal band at much reduced intensity in the remaining affected males indicates that gross sequence rearrangements are unlikely to be responsible. The results also indicate that, whereas phenotypically normal but transmitting males showed normal band patterns, their affected grandsons showed a high degree of methylation.

Probe M749

Bell *et al.*[5] did similar studies with the probe M749, which was isolated by microdissection and which maps immediately distal to the fragile site. The sizes of restriction fragments involved were similar to those observed by Vincent *et al.* and there is therefore good reason to suppose that the same cluster of rare restriction sites was being examined. Of 21 unrelated mentally retarded males carrying the fragile site, 19 had either little or none of the *Bss*HII band at about 600 kb; but two of the affected males showed apparently normal bands. Lack of direct correlation between methylation, clinical phenotype and fragile-X expression was further suggested by the finding of monozygotic twins who are discordant for the fragile-X syndrome, but who both show partial methylation (reduced intensity of the 600-kb band).

Although the exceptions are few, the lack of absolute correlation between methylation and the cytogenetical and/or clinical features is disappointing in terms of the possible diagnostic value of the observations. Difficulties also arise from possible tissue variations in methylation

1. Fryns, J.-P. in *The Fragile X Syndrome* (ed. Davies, K. E.) 1–30 (Oxford Univ. Press, 1989).
2. Sutherland, G. R. *Science* **197**, 265–266 (1977).
3. Lubs, H. A. *Am J. hum. Genet.* **21**, 231–244 (1969).
4. Vincent, A. *et al. Nature* **349**, 624–626 (1991).
5. Bell, M. V. *et al. Cell* **64**, 861–866 (1991).
6. Laird, C. D. *Genetics* **117**, 587–599 (1987).
7. Sherman, S. L., Morton, N. E., Jacobs, P. A. & Turner, G. *Ann. hum. Genet.* **48**, 21–37 (1984).
8. Dahl, N. *et al. Am. J. hum. Genet.* **45**, 231–244 (1969).
9. Oostra, B. A. *et al. Genomics* **6**, 129–132 (1990).
10. Suthers, G. K. *et al. Science* **246**, 265–266 (1989).
11. Rousseau, F. *et al. Am. J. hum. Genet.* (in the press).
12. Thibodeau, S. N. *et al. Hum. Genet.* **79**, 217–227 (1988).

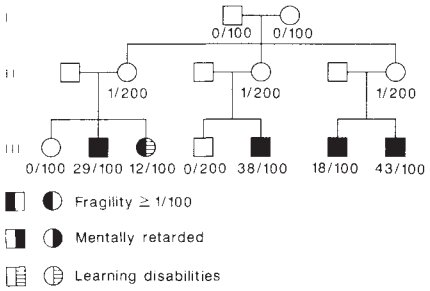

FIG. 2 Pedigree of family segregating for the fragile-X syndrome with a normal transmitting male I-1 (taken from ref. 12). Circles, females; squares, males.

and patterns of inactivation.

The relationship between methylation and the observation of fragility is not immediately obvious. Methylation of CpG-rich islands on the X chromosome is normally associated with the formation of heterochromatin, which seems to be at odds in this instance with the unravelling of chromosome structure that is seen (albeit only under conditions of thymidine stress). Perhaps the initial mutation interferes with the correct binding of DNA to the chromosome architecture. This may interfere with subsequent changes in organization associated with transitions between inactive and active states. The sequences responsible for the expression of the fragile site could be large and encompass much of the 2-megabase *Mlu*I DNA fragment that links the proximal and distal loci as reported by both of the groups. Clearly this region will yield many interesting sequences, including candidate disease loci and sequences important in inactivation and chromosome organization. The challenge will be how to recognize them. Indeed, yeast artificial chromosomes carrying the fragile-site region are already available: their dissection and introduction into animal cells will provide an important starting point. □

Ian Craig is in the Genetics Laboratory, Department of Biochemistry, University of Oxford, South Parks Road, Oxford OX1 3QU, UK.

CELL BIOLOGY

Membrane traffic COPs

Margaret S. Robinson

EUKARYOTIC cells contain at least two types of coated vesicles, both of which are involved in membrane traffic but which until now have seemed to differ in practically every other respect: structure, function and subcellular distribution. But reports last month in *Nature*[1,2] and now in *Cell*[3] reveal some unexpected similarities between the two.

Clathrin-coated vesicles, the first type to be discovered, bud from two membrane compartments of the cell: the plasma membrane and the trans-Golgi network (TGN)[4]. At first it was thought that all Golgi-associated coated vesicles were coated with clathrin, but on closer inspection a second population of vesicles was discovered which, for want of a better name, are usually referred to as non-clathrin-coated vesicles[5]. The non-clathrin-coated vesicles are associated with all five of the identifiable Golgi compartments — the intermediate or 'salvage' compartment, and the *cis*, medial and *trans* cisternae of the Golgi stack, as well as the TGN[5] — and their function is to carry newly synthesized proteins from one Golgi compartment to the next, enabling the proteins to acquire a series of post-translational modifications before they are sent from the TGN to their final destinations. Although clathrin-coated vesicles were purified and characterized biochemically over 15 years ago[6], the non-clathrin-coated vesicles have been much more difficult to isolate. However, two years ago a method for their purification was devised[7], and now Serafini *et al.*[1], Waters *et al.*[2] and Duden *et al.*[3] report the identification and characterization of some of the components of their coats. These papers demonstrate that the two types of vesicle are much more alike than was originally thought, thereby radically changing our view of them.

Earlier studies had mainly concentrated on the differences between the two. For instance under the electron microscope the coats on clathrin-coated vesicles appear as a lattice of hexagons and pentagons, and the ability of purified clathrin to form such cage-like structures in the absence of any membrane suggests that its self-assembly properties may provide the driving force required for membrane budding[7]. No such lattice has been evident on the non-clathrin-coated vesicles, although a hint of some sort of periodic structure can sometimes be seen in thin sections[8]. There are also differences in the sorting properties of the two types of coated vesicles. Clathrin-coated vesicles are highly selective, recruiting particular membrane proteins so that their concentration in the coated vesicle may be one hundred times their concentration in the original membrane[4]. In contrast, non-clathrin-coated vesicles do not seem to be particularly discriminating and are thought to be involved in bulk flow rather than in membrane sorting[5], although there may be a mechanism for excluding resident Golgi proteins from them.

These structural and functional differences are a reflection of the differences in the protein composition of the vesicle coats. Clathrin-coated vesicles are covered not only with clathrin, but also with protein complexes called adaptors[4] (see table). The adaptors are believed to connect the clathrin lattice to the cytoplasmic tails of selected transmembrane proteins, thus providing clathrin-coated vesicles with their characteristic specificity[4,8]. Different adaptors are associated with the plasma membrane and the TGN[9,10], and are thought to account for the different sorting properties of the clathrin-coated vesicles that bud from these two different compartments[2]. One of the adaptor subunits, β-adaptin, is very similar in the two complexes and contains a clathrin-binding site[9,11].

Comparisons

The purification of non-clathrin-coated vesicles by Serafini *et al.*[1], modified from the earlier method of Malhotra *et al.*[7], now makes it possible to compare the coat proteins on the two types of vesicles. Four major bands are seen on SDS polyacrylamide gels of non-clathrin-coated vesicles, which the authors name α-, β-, γ- and δ-COPs (for coat proteins). As shown in the table, the apparent molecular weights of the COPs are similar to those of clathrin heavy chain and some of the adaptor subunits. But the most compelling evidence that the two types of coated vesicles are alike is the cloning and sequencing by Duden *et al.*[3] of a complementary DNA that encodes a Golgi-associated protein of relative molecular mass 110,000 (M_r 110K), which is shown by Serafini *et al.* to be identical to β-COP. The deduced amino-acid sequence of β-COP is significantly homologous to that of β-adaptin[3].

This finding indicates that β-COP and β-adaptin must have evolved from a common ancestral gene, implying that there may at one time have been only a single type of coated vesicle in eukaryotes and that clathrin-coated and non-clathrin-coated vesicles probably form by a similar mechanism. There is also a family resemblance between β-adaptin and the other adaptin classes, α and γ (ref. 12). Using a computer program designed to search for distant relationships, Duden *et al.* found that they were able to align the N-terminal halves of β-COP and all three classes of adaptins[3]. Interestingly, it is the N-terminal domains of the adaptins that interact with the other subunits of the adaptor complex, and they also participate in clathrin binding, while the C-terminal domains of the adaptins, which are not homologous to β-COP, have been proposed to be involved in sorting[13].

The next step will be to characterize the other COPs and find out whether they can self-assemble into a structure which could provide a mechanism for vesicle budding.

Comparison of the coat proteins on the two types of coated vesicles

Clathrin-coated vesicles		COP-coated vesicles	
Clathrin heavy chain (180K)			
Clathrin light chains (30–40K)			
β-adaptin	(105K)	α-COP	(160K)
α or γ-adaptin	(92–108K)	β-COP	(110K)
~50K protein	(47–50K)	γ-COP	(98K)
~20K protein	(17–20K)	δ-COP	(61K)

In addition to the four COPs, smaller proteins are also associated with COP-coated vesicles, similar in size to clathrin light chains and the ~20K adaptor subunits. However, there are differences in the relative amounts of similarly sized proteins on the two types of coated vesicles: in particular, α-COP is considerably less abundant than clathrin heavy chain[2].

Serafini *et al.*[1] suggest that α-COP is the most likely candidate for a clathrin analogue on the non-clathrin-coated (or COP-coated) vesicles because of its similarity in size to clathrin heavy chain. Sequencing of the N terminus has already been carried out on the protein[2] so it should not be long before its cDNA has been cloned and its complete primary structure is known.

Characterization

The characterization of the COPs is facilitated by the large-scale purification method developed by Waters *et al.*[2] for isolating the proteins from cytosol (based on the fortuitous discovery that a precipitate which collected in their dialysis bags while they were attempting to purify another protein consisted almost entirely of COPs). The cytosolic COPs are thought to be in equilibrium with membrane-bound COPs, because, like clathrin-coated vesicles, COP-coated vesicles go through cycles of coating and uncoating. But whereas clathrin and adaptors exist in the cytoplasm as separate soluble pools, the cytoplasmic COPs purified by Waters *et al.* seem to be a complex containing all four proteins, including α-COP. The stoichiometry of the complex (or 'coatomer') still needs to be clarified, however, as the four COPs are not present in equimolar amounts and there are smaller proteins that copurify as well. One possibility that cannot be excluded is that, like adaptors, the coatomers may in fact be a heterogeneous mixture, with somewhat different complexes associating with the different Golgi compartments.

A powerful tool for examining this association and for investigating the role of COPs in vesicle budding and targeting will be the drug brefeldin A, which causes the Golgi stack to disappear and the resident Golgi proteins to back up into the endoplasmic reticulum[14]. By immunofluorescence microscopy, Donaldson *et al.*[15] have recently shown that brefeldin A causes β-COP (and presumably the entire COP complex) to dissociate from the Golgi membrane, possibly by interfering with the normal cycle of coating and uncoating. This event occurs within 30 seconds of addition of the drug, well before any changes in the appearance of the Golgi stack or in the distribution of resident Golgi proteins can be detected. So removal of the COPs may be responsible for the later changes that occur, a possibility that can now be tested using a system devised by Donaldson *et al.* in which the effects of brefeldin A can be reproduced in permeabilized cells[16].

How large is the β-COP/adaptin family likely to be? So far, three classes of adaptins have been identified, α, β and γ, which are somewhat more closely related to each other than to β-COP. A homologue of β-adaptin has been found in the yeast genome but so far the function of the protein product is unknown[17]. γ-COP (M_r 98K) may well turn out to be another member of the family. But what of all the many other transport vesicles in the cell, which have yet to be purified? Are they also coated with proteins belonging to the COP/adaptin family? Unfortunately, the similarity in amino-acid sequence between β-COP and the adaptins is not really strong enough to make it practical to use DNA probes to search for additional homologues. However, by using other methods for studying vesicular traffic that have proven successful in the past, particularly *in vitro* reconstitution and yeast genetics, it seems likely that in the next few years more members of the family will be discovered. □

Margaret S. Robinson is in the Department of Clinical Biochemistry, University of Cambridge, Addenbrooke's Hospital, Hills Road, Cambridge CB2 2QR, UK.

1. Serafini, T. *et al. Nature* **349**, 215–220 (1991).
2. Waters, M.G., Serafini, T. & Rothman, J.E. *Nature* **349**, 248–251 (1991).
3. Duden, R., Griffiths, G., Frank, R., Argos, P. & Kreis, T.E. *Cell* **64**, 649–665 (1991).
4. Pearse, B.M.F. & Robinson, M.S. *A. Rev. Cell Biol.* **6**, 151–171 (1990).
5. Orci, L., Glick, B.S. & Rothman, J.E. *et al. Cell* **46**, 171–184 (1986).
6. Pearse, B.M.F. *J. molec. Biol.* **97**, 93–98 (1975).
7. Malhotra, V., Serafini, T., Orci, L., Shepherd, J.C. & Rothman, J.E. *Cell* **58**, 329–336 (1989).
8. Glickman, J.N., Conibear, E. & Pearse, B.M. *EMBO J.* **8**, 1041–1047 (1989).
9. Ahle, S., Mann, A., Eichelsbacker, U. & Ungewickell, E. *EMBO J.* **7**, 919–929 (1988).
10. Robinson, M.S. *J. Cell Biol.* **104**, 887–895 (1987).
11. Ahle, S. & Ungewickell, E. *J. biol. Chem.* **264**, 20089–20093 (1989).
12. Robinson, M.S. *J. Cell Biol.* **111**, 2319–2326 (1990).
13. Kirchhausen, T. *et al. Proc. natn. Acad. Sci. U.S.A.* **86**, 2612–2616 (1989).
14. Lippincott-Schwarz, J., Yuan, L.C., Bonifacino, J.S. & Klausner, R.D. *Cell* **56**, 801–813 (1989).
15. Donaldson, J.G., Lippincott-Schwarz, J., Bloom, G.S., Kreis, T.E. & Klausner, R.D. *J. Cell Biol.* **111**, 2295–2306 (1990).
16. Donaldson, J.G., Lippincott-Schwarz, J. & Klausner, R.D. *J. Cell Biol.* (in the press).
17. Kirchhausen, T. *Molec. cell. Biol.* **10**, 6089–6090 (1990).

DAEDALUS

Sky sliding

MUCH of an aircraft's power is lost in atmospheric drag. On the molecular level, drag arises very simply. An air molecule hitting the skin of the aircraft does not merely bounce elastically off. Instead, it sticks for a short while, loading the craft with a new molecular passenger. It then disengages in some random direction, running away with the energy it acquired in its brief ride.

If the air molecules could somehow be persuaded to fly off the skin of the aircraft in the same rearward direction in which they met it, drag would be greatly reduced. In this connection Daedalus recalls that atoms in a solid do not move in an entirely random and isotropic manner. X-ray crystallographers, whose job it is to determine atomic positions, usually find that their thermal uncertainty is greater in some directions than in others. A short stub of atoms, like a hydroxyl or methyl group sticking out of an otherwise compact molecule, often wags almost linearly in one specific direction.

So, says Daedalus, the ideal aircraft skin should expose a perfect surface of such molecular stubs to the air. Their wagging-orientation at every point should be carefully lined up with the direction of the slipstream at that point. DREADCO's chemists are tracking down molecules with particularly good wagging groups. Among the most promising candidates so far are an iron-porphyrin complex, dimethyltartaric acid, and the anti-leprosy drug clofazimine. These substances are being formed into needle-crystals and compounded as densely as possible into an aviation paint. By brushing it on the aircraft everywhere parallel to the local slipstream, the crystals will be aligned to wag their surface groups along the direction of the airflow at that point.

An air molecule hitting the new paint will most likely attach itself to one of the surface wagging-groups. It will excite and share the molecular wagging motion back and forth along the line of the slipstream. When it disengages a little later, it will either be ejected forwards, in the teeth of the oncoming airstream, or backwards, back into that stream. The second choice, says Daedalus, is far more probable. The result: a slippery aircraft which loses no energy to the air-molecules hitting it.

Even better, the new paint will be slippery only in the slipstream direction. In other, non-wagging directions, it will be extra rough. It will arrest the molecules and fling them sideways, preferentially damping out the fluctuating flow-lines of surface turbulence and enhancing laminar flow. The improvements in stability and airworthiness, and the greatly reduced fuel costs, could well transform aviation. Air fares might even come down. David Jones

Sequence analysis of original HIV-1

SIR—In 1983, Barre-Sinoussi *et al.* reported[1] on the first isolate of the virus later shown[2-7] to be the cause of AIDS. In the summer and autumn of that year, the Laboratory of Tumor Cell Biology (LTCB) was sent samples of cell-free media and DNA from peripheral blood lymphocytes (PBLs) infected with that virus, called LAV-1/BRU. We have now analysed several of these samples by Southern blotting and by DNA sequence analysis of molecular clones generated by the polymerase chain reaction from the *env* and *nef* genes. We describe here the outcome of these studies.

In summary, we find that the sequence of the first published isolate[1] is distinct from that of others previously described, including both the sequences of HTLV-IIIB and LAV/BRU (LAV-1) published in 1985 by researchers from the LCTB[8] and the Pasteur Institute[9], respectively.

Reports of the first two isolates of what is now known as HIV-1 were soon followed by others[10,11] and molecular analysis showed extensive viral heterogeneity among them[12-15]. Because the complete sequences of the HTLV-IIIB and LAV-1/BRU are extremely similar, the relationship of the two viruses has been a subject of much speculation.

Over the past two years, prompted in part by allegations about the origin of HTLV-IIIB and also as part of a continuing study of the extent of the genetic change in HIV-1 among individuals over time, we have characterized the viral samples received at the LTCB in 1983, including most of the specimens from the Pasteur Institute.

In 1983, the LTCB received four samples of LAV-1/BRU from the Pasteur Institute. One, consisting of DNA extracted from PBLs, was sent by Jean-Claude Chermann (then at the Pasteur Institute and a signatory of this letter). Three samples were cell-free supernatants of LAV cultures, all of which were described as originally derived from the lymph node of patient BRU, cultured with PBLs or bone marrow from normal donors. A fifth sample consisted of a small amount of DNA labelled RUB, received from the Pasteur Institute in April 1983.

The first cell supernatant was given to one of us (R.C.G.) by Luc Montagnier in July 1983, whereupon M.P. attempted to grow it in cord-blood lymphocytes until 10 September, when the culture supernatant was frozen and saved (as LAV/C306 and LAV/C310). The two further supernatant samples sent by Montagnier were received on 23 September 1983, and were described as a further portion of the July sample (JBB/LAV) and as virus from patient BRU cultured with normal bone marrow (M2T/B) respectively. Both these samples were used in attempts at transmission by M.P. between late October and January 1984.

In July 1983, a sample of a DNA preparation labelled JBB/LAV was also received by former co-workers at the LTCB (Beatrice Hahn and Flossie Wong-Staal) from Chermann through the mail. Having been found free of both HTLV-1 and HTLV-2, this sample was not studied further, but stored as JBB/LAV DNA.

A search through records and freezers at the LTCB has located three of these four samples, and they have been further investigated as follows.

None of the RUB DNA could be located.

In May 1990, one of us (D.W.) used the frozen culture supernatant LAV/C306 and LAV/C310 derived from the July 1983 LAV sample in attempts at transmission to CEM cells and PBLs[16]. The work was done in a laboratory separate from the LTCB and in a module and incubator in which no HTLV-III had been grown. Virus could not be transmitted to the CEM cells, but the PBLs became productively infected, as judged by assays for reverse transcriptase and the appearance of cytopathic changes. DNA was prepared from the infected PBLs.

PERCENTAGE NUCLEOTIDE IDENTITY

	1985 Published sequences of		Molecular analysis in 1990 Samples received in 1983		
	HTLV-IIIB	LAV-1	1	2	3
HTLV-IIIB	—				
LAV-1	98.1	—			
Sample 1	91.3	91.5	—	—	
Sample 2	91.5	91.9	99.0	—	—
Sample 3	90.5	90.6	98.9	98.4	—

Sequence representing 900 bases of the *env* region of individual clones of each sample were compared (base pairs 7,000–7,900 using the numbering of Ratner *et al.*[8]). HTLV-IIIB and LAV-1 were taken from published sequences[8,9]. Sample designations and dates initially received are: Sample 1, JBB/LAV (September 1983); Sample 2, LAV/C306 (July 1983); Sample 3, JBB/LAV DNA (July 1983).

These results are consistent with our experience in 1983–84 that the JBB/LAV samples, in contrast to HTLV-III, showed a distinct preference for PBLs rather than immortalized T-cell lines. We were not able to grow virus from the LAV/C310 sample.

Similarly, in May 1989, M.P. used the 23 September 1983 sample called JBB/LAV (which he had retained) in attempts at transmission to H9 cells and PBLs. Transmission to H9 was not possible, but the PBLs became infected — they were positive for reverse transcriptase and antigen expression and showed cytopathic changes. The infected cells were sent, in July 1989, to LTCB for DNA purification.

We also learned that Hahn, now at the

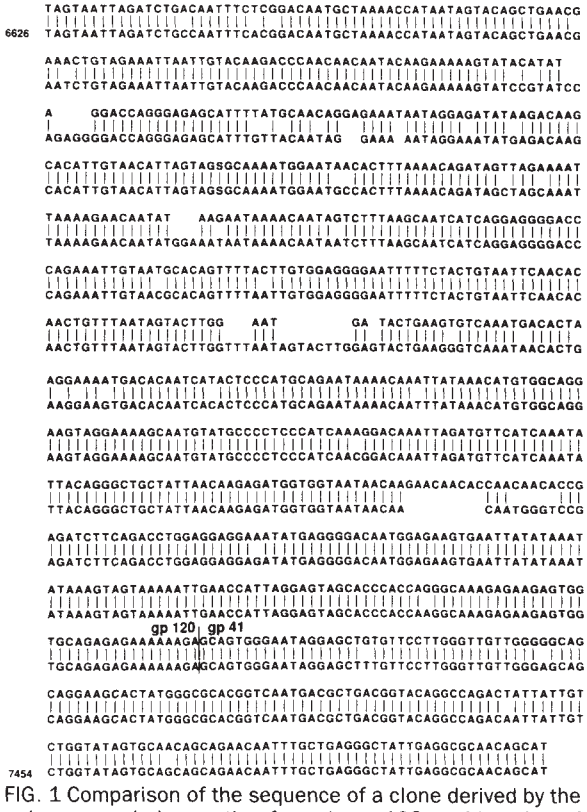

FIG. 1 Comparison of the sequence of a clone derived by the polymerase chain reaction from the gp120–gp41 region of JBB/LAV with that of LAV-1 (BRU)[9]. Numbers refer to nucleotide position in the complete LAV-1 provirus. Top, JBB/LAV; bottom, LAV-1 (BRU).

1. Barre-Sinoussi, F. *et al. Science* **220**, 868–871 (1983).
2. Sarngadharan, M.G., Popovic, M., Bruch, L., Schupbach, J. & Gallo, R.C. *Science* **224**, 506–508 (1984).
3. Gallo, R.C. *et al. Science* **224**, 500–503 (1984).
4. Popovic, M., Sarngadharan, M.G., Read, E. & Gallo, R.C. *Science* **224**, 497–500 (1984).
5. Brun-Vezinet, F. *et al. Science* **226**, 453–456 (1984).
6. Schupbach, *et al. Science* **224**, 503–505 (1984).
7. Safai, B. *et al. Lancet* **i**, 1438–1440 (1984).
8. Ratner, L. *Nature* **313**, 277–284 (1985).
9. Wain-Hobson, S., Sonigo, P., Danos, O., Cole, S. & Alizon, M. *Cell* **40**, 9–17 (1985).
10. Levy, J.A. *et al. Science* **225**, 840–842 (1984).
11. Shaw, G.M. *et al. Science* **226**, 1165–1171 (1984).
12. Starcich, B.R. *et al. Cell* **45**, 637–648 (1986).
13. Sanchez-Pescador, R. *et al. Science* **227**, 484–492 (1985).
14. Hahn, B.H. *et al. Science* **232**, 1548–1553 (1986).
15. Alizon, M., Wain-Hobson, S., Montagnier, L. & Sonigo, P. *Cell* **46**, 63–74 (1986).
16. Weiss, S.H. *et al. Science* **239**, 68–71 (1988).
17. Myers, G., Berzofsky, J.A., Rabson, A. B., Smith, T.F. & Wong-Staal, F. (eds) *Human Retroviruses and AIDS 1990*, (Los Alamos National Laboratory, 1990).

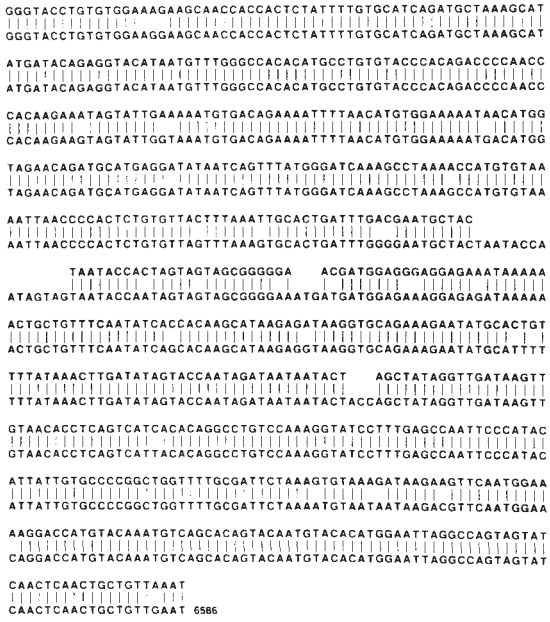

FIG. 2 Comparison of the sequence of a clone derived by the polymerase chain reaction from the *env* region of JBB/LAV with that of LAV-1 (BRU)[9]. Numbers refer to nucleotide position in the complete LAV-1 provirus. Top, JBB/LAV; bottom, LAV-1 (BRU).

University of Alabama at Birmingham, had retained the JBB/LAV DNA originally supplied by Chermann in July 1983; a portion of this sample was obtained from her in 1990.

It appears, however, that nothing remains of the M2T/B supernatant, and no derivatives of it have so far been located. Portions of the LAV-derived samples, uncultured since 1984, have been made available to the National Institutes of Health Office of Scientific Integrity.

DNA purified from the LAV/C306 and JBB/LAV materials described above have now been analysed by Southern blotting. The patterns obtained by restriction endonuclease digestion of these samples differ markedly from those from HIV-1 (HTLV-IIIB). Three of the five restriction endonucleases used (*Hin*dIII, *Pvu*II and *Sst*I) gave consistent patterns distinct from those obtained from HTLV-IIIB DNA (data not shown).

The two DNAs and Hahn's JBB/LAV DNA have also been used to generate, by the polymerase chain reaction, multiple 900-base pair (bp) clones from the envelope (*env*) gene. Multiple 600-bp clones of another portion of *env* were also obtained from JBB/LAV, as were multiple 1,000-bp clones from the *nef* gene of LAV/C306. Sequences were determined by standard Sanger protocols.

Comparisons of a 900-bp portion of *env* corresponding to bases 7,000 to 7,900 (numbering by ref. 8) show that clones from all three JBB/LAV samples are closely related to each other (98.4–99.0% sequence identity), whether or not the comparisons are between two clones from the same sample or between two clones from different samples (see table). This compares with the relatedness to the published HTLV-IIIB and LAV/BRU sequences, which is only 90.5–91.9% (see Fig. 1).

Similarly, clones from a second *env* region (600 bp from bases 6,300 to 6,900) from M.P.'s sample of JBB/LAV were found to be 99.4–100% identical to each other, but less closely related (94.1–94.6%) to both HTLV-IIIB and LAV-1/BRU (Fig. 2). Clones from the *nef* gene of LAV/C306 (bases 8,500 to 9,500) were similarly closely related to each other, but less closely to HTLV-IIIB and to LAV-1/BRU (Fig. 3). These sequences have been deposited at the Human Retrovirus and AIDS database[17].

These data clearly show that none of the LAV samples received in July and September 1983, which are still available for analysis (and which have never been in continuous cell-culture), was the source of HTLV-IIIB. Nor could the materials of which these are samples have been the origin of the published LAV-1 sequence[9].

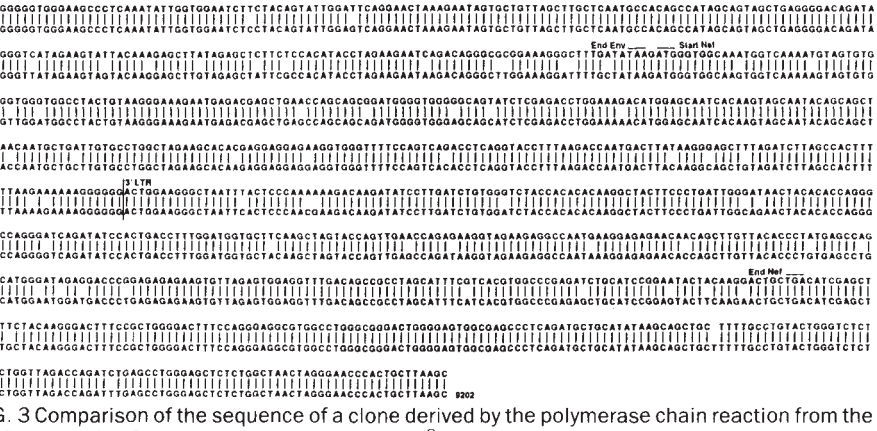

FIG. 3 Comparison of the sequence of a clone derived by the polymerase chain reaction from the *nef* region of JBB/LAV with that of LAV-1 (BRU)[9]. Numbers refer to nucleotide position in the complete LAV-1 provirus. Top, JBB/LAV; bottom, LAV-1 (BRU).

From the information available, it seems most likely that the single virus species (here called JBB/LAV) found in these samples is that derived from the patient BRU. The source of the HTLV-IIIB virus and sequence and, by inference, the LAV-1 sequence, may be difficult to determine and thus remain unknown.

We have pursued this question by testing early samples, but so far have not received samples stored at the Pasteur Institute for analysis. The issue of how two HIV-1 isolates that are so similar appeared in two different parts of the world has been distracting and divisive. We hope that our analyses will put the issue on a more factual basis.

HONG-GUANG GUO
Lofstrand Laboratories Limited, Gaithersburg, Maryland 20877, USA
JEAN-CLAUDE CHERMANN
INSERM, Marseilles, France
DAVID WATERS
Program Resources Inc., FCRDC, Frederick, Maryland 21701, USA
LEOTA HALL
AUDREY LOUIE
ROBERT C. GALLO
HOWARD STREICHER
MARVIN S. REITZ
Laboratory of Tumor Cell Biology, National Cancer Institute, National Institutes of Health, Bethesda, Maryland 20892, USA
MIKULAS POPOVIC
Bethesda, Maryland, USA
WILLIAM BLATTNER
Viral Epidemiology Section, National Cancer Institute, National Institutes of Health, Bethesda, Maryland 20892, USA

More mercury from crematoria

SIR—Mills (*Nature* **346**, 615; 1990) has drawn attention to the problem of mercury release from crematorium chimneys. On the basis of laboratory extraction of alloy on extracted teeth, he estimated that up to 3 g mercury could be released from cremation of a person with amalgam fillings. We have recently measured directly the amount of mercury and lead released from a crematorium chimney in a mid-size town in Switzerland.

The crematorium operates two electrically heated incinerators, each with a separate chimney. No filtering of gases is provided. The two incinerators differ in age (built in 1970 and 1981) and construction, the more modern one having a secondary thermal combustion chamber.

We took samples of combustion gas isokinetically from the chimney and analysed for dust-bound and vapour-phase mercury and lead during 16 cremations. We collected dust-bound

material on a quartz filter. Vapour-phase mercury was absorbed in a solution of 1% $KMnO_4$ in 10% sulphuric acid, and lead was absorbed in 5% HNO_3 in a solution of 3% peroxide. The quantity of metal in each sample was determined by cold-vapour and graphite-tube atomic absorption spectroscopy for mercury and lead, respectively. In addition, the temperature of each incineration and information about age, sex, weight, nationality, medication, where the person died and the type of coffin were provided.

We show the emissions of mercury and lead for each cremation in the figure. (Errors were estimated to be 25 and 30% for mercury and lead, respectively.) Clearly, emissions of both these elements vary considerably between cremations.

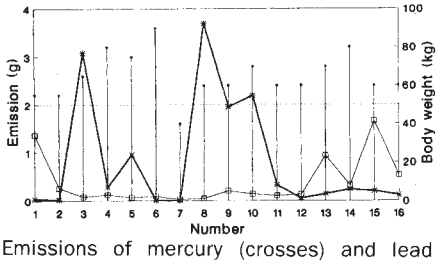

Emissions of mercury (crosses) and lead (open boxes) from a crematorium incinerator. Smaller, solid boxes, body weight.

The maximal emissions of mercury are in good agreement with the estimations of Mills, and the emissions of lead are somewhat smaller than those of mercury.

We found no correlation between emissions of these elements, between body weight and emissions, or between emissions and temperature of the cremation, incinerator-model, type of coffin, medical history, age or sex. We conclude that the mercury emissions are probably due to amalgam fillings, but we have no explanation for the origin of the lead emission peaks.

P. KÜNZLER
M. ANDRÉE

Dr Graf AG,
Stadtbachstrasse 42a,
CH-3013 Bern,
Switzerland

SIR—Two points may be added to Arnold P. Wendroff's letter (*Nature* **347**, 623; 1990). First, only about 10% of inhaled mercury enters the circulation through the lung alveoli, the remainder is absorbed by the bronchial secretions which are usually ingested. The result is that it tends to be mixed with food before digestion. Because it is toxic by virtue of its combination with protein, a diet rich in protein is likely to be protective. It is therefore difficult to predict the danger from heavy metal ingestion unless the amount of protein present in the diet is taken into account.

BRENNIG JAMES

Cherry Orchard,
Marlow Common, Bucks SL7 2QP, UK

No pulsar in SN1987A

SIR—Our previously reported observation (*Nature* **338**, 234–236; 1989) of what appeared to be an optical pulsar in the remnant from supervova 1987A turns out to be spurious. Despite repeated searches by us and others following the original observation in January 1989, the putative pulsar was not confirmed. In new data obtained in February 1990, however, we again detected the signal, in data from the supernova and, in comparison data taken on the Crab pulsar at the same time. From this, it is clear that the signal did not originate in the supernova, and we retract our reported discovery of the pulsar.

We believe that the observed signal is electrical noise from a closed-circuit television camera used for acquisition and guiding at the Cassegrain focus of the 4-metre telescope at Cerro Tololo Interamerican Observatory, where both sets of data were taken. The observed frequency of 1968.627 Hz is close to the 16th subharmonic of the nominal horizontal sync pulse of the camera (1968.75 Hz); the coincidence seems too close to be accidental.

We do not know how the signal coupled into our detector, and have not been able fully to reconstruct events during the observations. But we think there are plausible explanations for some of these things that made the original observation appear real. The most important are: (1) The signal disappeared when the telescope was pointed at a different object immediately after observing the supernova. It is likely that the offending guider camera was turned off between the two sets of observations to prevent damage from the increasing light of twilight.

(2) The signal was not observed with the same equipment on the same telescope, either before or after the detection run, until the run in February 1990. Several plausible explanations for this come to mind, any one or more of which might have occurred: there may have been subtle differences in the mounting of the detector system, changes in the adjustment of components, or a different guider camera (there are two such cameras at the telescope, which are used interchangeably). The system is extremely sensitive, and the detected signal was very small by normal standards: the interference current was equivalent to about 10^{-15} amps.

(3) Several highly suggestive properties of the observed frequency were totally fortuitous. The stability of the frequency over the 7-hour run was high (10^{-6}), a factor of 100 better than the stability specification for the camera. Furthermore, the observed small frequency change was quite smooth, and when the data were corrected for the Earth's motion, they were well fit by a sine wave, which suggested an external origin. (When a sine wave was subtracted from the data, the frequency residuals decreased by an order of magnitude. This was the basis for speculation that, for example, the pulsar might be in a binary orbit.) Similarly, the fact that the first two higher harmonics were in the same proportions as those seen in the Crab pulsar was a coincidence. All this was undoubtedly a combination of bad luck (or divine malice), misplaced pattern-finding skills, and the common human tendency to overinterpret a limited amount of data.

Searches for the pulsar continue, so far unsuccessfully.

J. KRISTIAN*

The Observatories,
Carnegie Institution of Washington,
813 Santa Barbara Street,
Pasadena,
California 91101, USA

*Co-authors of this letter are C. R. Pennypacker, J. Middleditch, M. A. Hamuy, S. Heathcote, J. N. Imamura, W. E. Kunkel, R. Lucino, D. E. Morris, R. A. Muller, S. Perlmutter, S. J. Rawlings, T. P. Sasseen, I. K. Shelton, T. Y. Steiman-Cameron and I. R. Tuohy.

Scientific Correspondence

Scientific Correspondence is intended to provide a forum in which readers may raise points of a scientific character. They need not arise out of anything published in *Nature*. In any case, priority will be given to letters of fewer than 500 words and five references. □

Signalling and superinduction

SIR—The process by which protein synthesis inhibitors accentuate and prolong the induction of specific genes that are normally only transiently induced in response to polypeptide growth factors, cytokines, hormones, interferons and phorbol esters is termed superinduction. This process is thought to be attributable to the loss of labile transcriptional repressors and messenger RNA-degrading enzymes, and is usually regarded as a direct consequence of the inhibition of protein synthesis[1–6]. Subramaniam *et al.*[6], for example, used this phenomenon to conclude that the serum response element is subject to negative regulation by labile repressors. Here we present evidence that supports an alternative explanation: some protein synthesis inhibitors may act positively to activate transcription through an intrinsic ability to interact with molecules involved in intracellular signalling.

When quiescent cells are stimulated with epidermal growth factor (EGF) or the tumour promoter tetradecanoyl phorbol acetate (TPA), the proto-oncogenes c-*fos* and c-*jun* are rapidly and transiently

induced[1-5,7]. Although EGF and TPA primarily activate distinct protein kinases, the EGF receptor and protein kinase C respectively, both agents can stimulate the rapid and transient phosphorylation of complexed and chromatin-associated forms of a phosphoprotein, pp33, of relative molecular mass 33K, and that of pp15, a chromatin-associated phosphoprotein of mass 15K (ref. 8). The speed and latency of these responses, their chromatin association and experiments with the protein kinase inhibitor 2-aminopurine indicate that they may be essential in the induction of c-*fos* and c-*jun*[5].

We recently observed that the protein synthesis inhibitors anisomycin and cycloheximide stimulate the rapid and sustained phosphorylation of pp33 and pp15. This raises the question of whether the signal activation is merely a further consequence of the inhibited protein synthesis. Our analysis of the effects of decreasing concentrations of anisomycin shows that the signalling responses are dissociable from the inhibition of protein synthesis. Thus, the ability of anisomycin to inhibit protein synthesis is lost at concentrations below 70 ng ml^{-1}, whereas the ability to stimulate intracellular signalling, induction and superinduction of c-*fos* and c-*jun* is observed at concentrations as low as 10 ng ml^{-1}. Analyses of protein synthesis inhibition, intracellular signalling, c-*fos* and c-*jun* mRNA levels and transcriptional activity using 25 and 50 ng ml^{-1} anisomycin are shown in the figure. At these concentrations, anisomycin alone does not produce any detectable inhibition of protein synthesis (*a*), but does produce complexed and chromatin-associated pp33 and pp15 phosphorylation (*b*), as well as the induction of c-*fos* and c-*jun*, measured both by nuclear run-on analysis (*c*) and northern blotting (*d*). In combination with EGF, no inhibition of protein synthesis is seen (*a*). However, the signalling responses (*b*), c-*fos* and c-*jun* transcription in the nucleus (*c*) and mRNA levels (*d*) are elevated. This shows that inhibition of protein synthesis is not a prerequisite for anisomycin-stimulated induction and superinduction, and implies that the compound must be able to interact more directly with the intracellular signalling pathways that regulate pp33/pp15 phosphorylation and c-*fos*/c-*jun* induction.

On balance, superinduction seems to be the result of several distinct processes. First, there is the enhancement of mRNA stability[4,5] variously attributed to the loss of labile mRNA-degrading enzymes, or of the necessity of ongoing translation for mRNA turnover[11]. Second, for genes such as c-*fos*, for which there is evidence of auto-repression[9,10], the inhibited translation of their protein product could lead to superinduction due to an inability to shut off transcription. It follows that both these effects can contribute to superinduction only after transcription has been activated. Third, loss of unspecified labile transcriptional repressors may lead to transcriptional activation[1-6], although there is no direct evidence for this. Finally, we have shown here that some protein synthesis inhibitors, even when applied at concentrations below those required for inhibition of protein synthesis, uniquely elicit the same chromatin-associated signals and proto-oncogene activation as EGF or TPA[5]. Thus, at sub-inhibitory concentrations, anisomycin seems capable of acting like a second-messenger agonist. Examination of how these bacterially secreted molecules interact with mammalian signalling biochemistry should provide insight into the nature and conservation of signal-transduction systems.

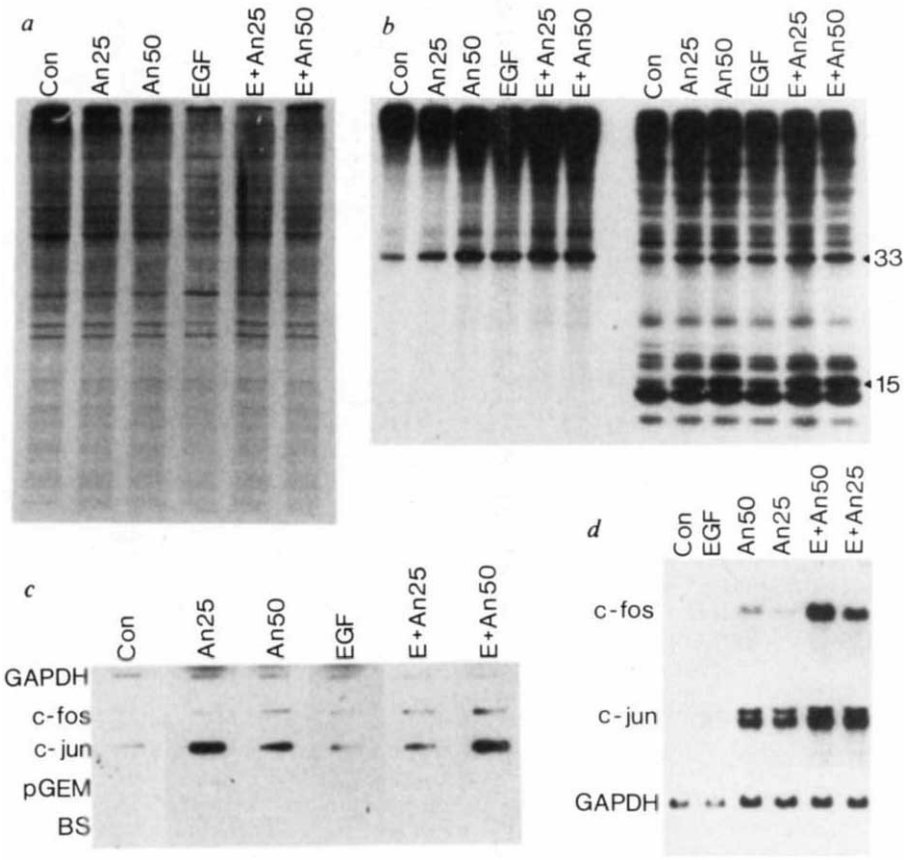

Anisomycin stimulates pp33/pp15 phosphorylation c-*fos*/c-*jun* induction and superinduction at sub-inhibitory concentrations. C3H 10T1/2 cells were quiesced in low-serum medium overnight and treated for 30 min with 25 or 50 ng ml^{-1} anisomycin, 50 ng ml^{-1} EGF or other combinations as indicated, after which cells were collected and processed as described below (see ref. 8 for details). *a*, ^{35}S-methionine (50 μCi ml^{-1}) was added to the medium 5 min after stimulation as indicated, cells lysed in Triton/DOC buffer 25 min later and aliquots of TCA-precipitated protein analysed by SDS-PAGE followed by autoradiography. *b*, Cells were ^{32}P-phosphate-labelled (0.5 mCi ml^{-1}) for 3 h before stimulation and collected 30 min later in Triton/DOC buffer. Fractions containing complexed and chromatin-associated proteins were prepared as described in ref. 8, and analysed by SDS-PAGE followed by autoradiography. *c*, Transcriptional run-on assays, as described in ref. 4, were performed using nuclei from cells stimulated as indicated for 30 min to analyse the transcriptional state of the c-*fos* and c-*jun* proto-oncogenes under these conditions. P-GEM and BS (Bluescript) are control plasmids. *d*, Cells were stimulated for 30 min with anisomycin, EGF or combinations of these. RNA prepared and analysed by northern blotting using probes against c-*fos*[8], c-*jun*[1] and glyceraldehyde phosphate dehydrogenase[8] (GAPDH). Lane assignations in each panel: con, unstimulated control cells; An25, 25 ng ml^{-1} anisomycin; An50, 50 ng ml^{-1} anisomycin; EGF, 50 ng ml^{-1} EGF; E+An25, 50 ng ml^{-1} EGF and 25 ng ml^{-1} anisomycin; E+An50, 50 ng ml^{-1} EGF and 50 ng ml^{-1} anisomycin.

LOUIS C. MAHADEVAN
Department of Biochemistry,
Oxford University,
South Parks Road,
Oxford OX1 3QU, UK

DYLAN R. EDWARDS
Heritage Medical Research Building,
University of Calgary,
3330 Hospital Drive NW,
Calgary, Alberta T2N 4N1, Canada

1. Ryseck, R. P., Hirai, S. J., Yaniv, M. & Bravo, R. *Nature* **334**, 535–538 (1988).
2. Quantin, B. & Breatnach, R. *Nature* **334**, 538–539 (1988).
3. Lamph, W. W., Walmsley, P., Sassone-Corsi, P. & Verma, I. *Nature* **334**, 629–631 (1988).
4. Greenberg, M. E., Hermanowski, A. L. & Ziff, E. B. *Molec. cell. Biol.* **6**, 1050–1057 (1986).
5. Almendral, J. M. *et al. Molec. cell. Biol.* **8**, 2140–2148 (1988).
6. Subramaniam, M., Schmidt, L. J., Crutchfield, C. E. & Getz, M. J. *Nature* **340**, 64–66 (1989).
7. Greenberg, M. E. & Ziff, E. B. *Nature* **311**, 433–438 (1984).
8. Mahadevan, L. C., Wills, A. J., Hirst, E. A., Rathjen, J. D. & Heath J. K. *Oncogene* **5**, 327–335, (1990).
9. Schontal, A., Herrlich, P., Rahmsdorf, H. J. & Ponta, H. *Cell* **54**, 325–334 (1988).
10. Sassone-Corsi, P., Sisson, J. C. & Verma, I. *Nature* **334**, 314–319 (1988).
11. Wilson, T. & Treisman, R. *Nature* **336**, 396–399 (1988).

Safety speculations

David L. Sills

Technological Risk. By H. W. Lewis. *Norton: 1990. Pp. 353. $22.95.*

WE live in an age that questions authority: of government, of religion, of art, of taste. Western civilization itself is in some quarters assailed as merely the product of 'dead white males'. The authority of science and technology is also widely questioned, and with some success, as exemplified by the impact of AIDS activists upon the availability of therapy and the conduct of research.

This *Zeitgeist* is the setting for H. W. Lewis's *Technological Risk*, but it is not the context that particularly interests him. Lewis, a distinguished American nuclear physicist with extensive experience on government and other risk-assessment panels, presents a somewhat different model of contemporary society. He believes that 'qualified scientists' are given less attention than journalists and other doomsayers, and he concludes his analysis with these characteristically breezy words:

> *The fact that, as a population, we are so uncomfortable with and ignorant of science and technology, and innumerate to boot, seems to make us irresistible targets. Beware of pseudo-experts with a mission and a grudge, especially if they are lawyers pretending to be scientists.*

This ignorance or this *Zeitgeist* — encouraged by such tragedies as Bhopal, Chernobyl and *Challenger* — has led to a rash of books on safety, risk and accidents, and *Technological Risk* takes its place in this literature. It is neither a blueprint for Doomsday nor an overly complacent description of the joys of science and technology. It is, rather, a balanced analysis: I would characterize its ideological position as somewhat right-of-centre. Lewis thinks that most technological risks are vastly over-stated, but he is far from complacent about others. Let me attempt a summary.

Lewis concludes not only that most risks are small but also that science and technology have vastly increased human happiness and welfare; he asserts that the quantitative assessment of risk is essential; and he admits that quantification is extremely difficult. (He places much emphasis upon probability and he uses throughout the book what he calls "the famous square-root-of-N rule, though no learned statistician would call it that." For example, in discussing the claim that the population living 'downwind' from the Three Mile Island nuclear power plant had excessive cancer mortality, he reports that the normal or expected mortality during the three years following the accident would have been 142, whereas the observed number was 144. The square root of 144 is 12, so "we would expect fluctuations of about 12 in this number, so the difference between 142 and 144 is of no significance whatever.")

One cannot quarrel (although some do) with the two risks he feels most strongly about: smoking leading to lung cancer and overpopulation leading to excessive CO_2 in the atmosphere and other threats as well. He quite properly attributes the Bhopal and *Challenger* accidents to "bad management", and he readily admits the dangers of lead poisoning, asbestos and of course the burning of fossil fuels — leading to acid rain, air pollution and the greenhouse effect.

Popperfoto

The crew of the ill-fated *Challenger* — victims of bad management?

Lewis understandably devotes more attention to demythologizing risks that he thinks are grossly overstated. He is very pro-nuclear power, but he thinks that more attention must be given to safety regulations. He thinks the concern over the proposed storage of high-level nuclear waste in special canisters in a Nevada mountain is misplaced: future people will probably welcome the discovery of these canisters, which will contain materials then in short supply. "High-level nuclear waste disposal is a non-risk", he asserts. And he is scornful of those who conclude that radon, X-rays, fluoridation, saccharin, formaldehyde, vinyl chloride and nonionizing radiation pose any risks.

Technological Risk is essentially nuts-and-bolts, but the theoretical chapter on the 'delusion of conservatism' is of considerable interest. The general principle expounded is: "The worst-case fixation leads to failure in the better-than-worst world." If aeroplane wings are made too strong, an aeroplane is unsafe to fly; heavily-armoured knights often did badly in mediaeval warfare; excessive testing of emergency diesel generators wears them out before the emergency; if aeroplanes did not fly in bad weather, more people would drive cars, which is even riskier, and so on. If this chapter had been expanded into a theory of safety (along the lines of Charles Perrow's theory of accidents (*Normal Accidents*, Basic Books, 1984), this would have been a more stimulating book.

I quarrel with only one of Lewis's major conclusions: his dismissal of the 55 mile-per-hour speed limit in the United States, which was adopted for energy conservation reasons during the 1973–74 Arab oil embargo and has been maintained as a safety measure. Lewis computes that this limit saves about 2,000 lives a year but costs about a billion hours in lost time for truckers, businessmen and others. Each life saved costs society approximately $5 million, he calculates, more than is spent in most regulatory activities. Well worth it, in my judgement. Let us find another way to subsidize the trucking industry.

Technological Risk is written in a breezy style that some will find refreshingly non-pompous; others may find it irritating if not insulting. Lewis describes his point of departure as "unabashedly American", but this should cause little difficulty for non-Americans except for the use of baseball to explain such concepts as probability and linear regression analysis. (I found these examples fascinating, but baseball, like some fine wines, does not travel well.) It is written for "intelligent readers, not specialists", and Lewis has concluded that the intelligent reader will not or cannot read technical reports. None are cited; the book has no footnotes, no references and no bibliography. A few reports of such organizations as the National Research Council are mentioned, without references. As he says in one technical discussion "if it sounds too complicated, trust the author."

I feel strongly that the United States and other industrial countries have benefited from participation by citizens in decisions concerning science and technology and they have grown beyond blind acceptance of the authority of one scientist. Documentation would not only have given the book greater authority, it would have made it more interesting. One of the publishing myths of our time is that readers do not like footnotes. On the contrary, many of us find them both essential and absorbing. □

David L. Sills is at 14 Crockett Street, Rowayton, Connecticut 06853, USA.

Unworldly genius

N. Kemmer

Dirac: A Scientific Biography. By H. S. Kragh. *Cambridge University Press: 1990. Pp.389. £35, $44.50.*

PAUL Dirac, one of the greatest brains of this century and also one of the strangest, unworldliest characters, deserves a lengthy biography, though the number of worthy tributes that appeared after his death in 1984 is already quite large. The 14 main chapters of *Dirac: A Scientific Biography* contain over 1,000 numerical superscripts related to 45 pages of annotations drawn from extensive and varied archival material. In addition there are a number of miscellaneous appendices.

The subtitle '*A Scientific Biography*' should not mislead readers to expect text devoted entirely to Dirac's scientific work. The text has accounts of his life and extraordinary character with outlines of his achievements skilfully interwoven.

It was a surprise to learn from the preface that the author had never met Dirac. (And also surprising that no information is given about the author.) No reader should skip chapter one; to understand Dirac's character one must appreciate his almost frightening background. His domineering single-minded father saw no other aim in educating his hugely talented son than a career in engineering. Dirac was denied all distracting contacts, but the academic hurdles he had to face proved to be so low that he had time for deep lone study of mathematical subjects. At a very early age he took up a studentship at St John's College, Cambridge and was taken further into postgraduate study when only 21. Cambridge received him still as a withdrawn, unworldly lad with a brain concentrated entirely on his mathematical thinking, which did not cease even on his long solitary walks every Sunday.

Dirac had intended to carry on with relativity, but instead his supervisor Ralph Fowler introduced him to the theory of atomic structure, which was still in a very incomplete state — but not for long. Heisenberg's pioneering paper that gave birth to quantum mechanics was sent in prepublication form to a privileged few, including Fowler. His student was able to study and, as always, to master it. Heisenberg received Dirac's version of his own theory in November 1925. The printed version had been published only four months earlier. In one quick transition the young student became a member of the select international community of research workers just beginning to absorb Heisenberg's ideas, which revolutionized our understanding of many branches of physics.

In the space left for this review I can only do justice to some of Paul Dirac's greatest contributions, barely touching on the accompanying story of his life, travels and honours — and eventual marriage. Even the whole chapter devoted to the humorous side of this strange man's life cannot receive more than brief mention. Dirac's major achievements can be summarized under two headings: electrodynamics and relativity. The latter continued his earlier interest, but the current difficulty was that the new quantum mechanics could not be reconciled with relativity. In 1927, Dirac hit on the strange-looking linear 'Dirac equation' for the electron; it settled the problem and eventually produced a Nobel prize for its discoverer.

Unfortunately it had one flaw: useless solutions with negative energy had to be avoided. Dirac found the way out. Pauli's exclusion principle forbids more than one electron to occupy any energy level. Dirac redefined the vacuum as having all negative energy levels filled. Positrons were still unknown, but predicted as holes in the vacuum; Dirac's theory was soon to be confirmed experimentally.

The story for electrodynamics is unhappier. Dirac himself was first to quantize it, creating the picture in which photons are created, annihilated and scattered. These events are well described in first approximation of the theory, but not further.

To Dirac the whole theory and related ones designed for new particles were wholly unacceptable and what is further remembered of his own work remained outside the mainstream of physics today. There is still much good reading in them.

However, I feel that Dirac was not quite fair to all the physicists who saw in the idea of renormalization the solution to the troubles of electrodynamics. The agreement between experiment and theory had become quite stunning and while the new procedure was not a thing of mathematical rigour, was it so different from his own departure from rigour when he introduced the infinity of occupied states in the vacuum?

Finally, I cannot help wishing that Paul Dirac was still with us for me to remind him that both S. Tomonaga and J. Schwinger chose a road to renormalization along which he himself had taken some first steps in his paper with V. Fock and B. Podolsky — and that the very different road trodden by R. Feynmann, the Lagrangian one, was familiar to you also, my dear Isolated Singularity! □

N. Kemmer is at 35 Salisbury Road, Edinburgh EH16 5AA, UK.

■ Also from Cambridge University Press comes *Unification of Fundamental Forces: The first of the 1988 Dirac Memorial Lectures* by Abdus Salam. Price is £8.95, $14.95.

Regulated change

Knut Schmidt-Nielsen

Rheostasis: The Physiology of Change. By Nicholas Mrosovsky. *Oxford University Press: 1990. Pp. 183. £40, $49.95.**

WHEN I first read the title of this book, *Rheostasis*, and the subtitle, *The Physiology of Change*, I thought that it somehow had to do with blood flow or possibly with a broader range of fluid flow topics. I was mistaken.

Before he introduces the novel term 'rheostasis' and defines it, Professor Mrosovsky discusses homeostasis, the concept of the constancy of the internal environment that was introduced by Claude Bernard and later popularized by Walter Cannon who coined the word 'homeostasis'. But then he asks "how does the sweeping concept of homeostasis stand up in the light of recent facts?" His answer to this question is what the book is all about.

Mrosovsky explains that changes in regulated levels have often been regarded as failures of homeostasis. But, he says, keeping the internal environment constant is not always imperative, nor does the body always seek constancy. Consider body temperature. Body temperature is not kept constant, it undergoes well regulated diurnal changes. And hibernation certainly entails a regulated drastic change in body temperature. There are many other regulated changes, and this book deals with such changes, for which Mrosovsky uses the term rheostasis.

'Rheostasis', then, is used "to describe a condition that is regulated at changing . . . levels or values". Or with more words: "*Rheostasis* refers to a condition or state in which, at any one instant, homeostatic defenses are still present but over a span of time there is a change in the regulated level. Therefore rheostasis includes a change in set-point, both when the term is used descriptively without specifying mechanism . . . and when it is used to indicate a mechanism comprising negative feedback with a reference signal."

The concept of constancy is so ingrained in all physiological thinking that it is useful to be reminded that changes may be both desirable and well regulated. Consider the fat content of the body, which normally is thought of as an energy reserve. If the fat content is maintained constant, it obviously cannot function as a reserve. And specifically, consider the pre-migratory accumulation of fat in a migrating bird, which may have nearly half its body weight as fat. This tremendous increase in

* To be published in the United Kingdom in April 1991.

fat content is a well regulated premigratory change.

Mrosovsky considers two categories of rheostasis, programmed rheostasis and reactive rheostasis. Programmed rheostasis (such as oestrus cycles or diurnal changes in temperature) are often cyclical, but need not be so. Reactive rheostasis occurs in response to stimuli. Fever is a classical example of reactive rheostasis; the higher body temperature level in fever is defended.

The two longest chapters in this short book deal with these two categories of rheostasis. They contain numerous examples of widely different physiological phenomena, some convincing and many less persuasive.

No doubt many of the examples qualify as rheostasis, but do they all? The criteria for considering a phenomenon as an illustration of rheostasis are not always clear, and in many cases a more plausible explanation may exist. In fact, the greatest weakness in the book is that rheostasis is presented "in terms of observed phenomena, rather than in terms of underlying mechanisms".

The lack of well defined criteria for rheostasis blurs the appropriateness of many of the examples and makes the overall presentation vague. With such uncertainty one may ask if the term 'rheostasis' is necessary or whether a new term is even desirable. The reasons for the choice of the word 'rheostasis' are discussed, but I find the term not well chosen. It grates on common sense that the meaning of a new term is not intuitively clear; in rheostasis there is an inherent conflict in combining the root 'rheo', meaning stream and flow, with a word, 'stasis', that emphatically implies standstill.

The value of Mrosovsky's ideas is that they provide a reasoned counter-measure to the ingrained, almost dogmatic assumption that constancy is the ultimate objective of physiological regulation. His book provides new perspectives that, I believe, will be a helpful basis for further discussions of the physiology of regulated change. □

Knut Schmidt-Nielsen is in the Department of Zoology, Duke University, Durham, North Carolina 27706, USA.

New in paperback

- *Principles of Animal Taxonomy* by George Gaylord Simpson, published by Columbia University Press at $21.50.
- *Creative Understanding: Philosophical Reflections on Physics* by Roberto Torretti, published by University of Chicago Press at $32.50, £25.95.
- *Ecological Economics: Energy, Environment and Society* by Juan Martinez-Alier, published by Basil Blackwell at £12.95; $18.95.
- *Environmentalism and the Future of Progressive Politics* by Robert C. Paehlke, published by Yale University Press at $16, £9.50. □

Bohr's institute

Jeremy Bernstein

Redirecting Science: Niels Bohr, Philanthropy and the Rise of Nuclear Physics. By Finn Aaserud. *Cambridge University Press: 1990. Pp. 356. £25. $47.50.*

WHEN one thinks of The Institute for Theoretical Physics, created by Niels Bohr in Copenhagen, one inevitably thinks of the photographs taken of conferences at the Institute, showing 30 or 40 of the world's best physicists. One is led to imagine that this is what it was like all the time at the Institute — a milling hive of intellectual activity. One of the values of this fine book, written by the Acting Director of the Niels Bohr Archive in Copenhagen, is to show how misleading this impression is. In the early 1930s, in a typical year, the Institute had ten visitors or less, and the group as a whole produced less than 30 scientific papers a year. To put this in perspective, the theory division at CERN has, at any given time, more than 120 visitors, to say nothing of a permanent staff that is larger than Bohr's entire Institute was at this time; each of these people produces at least one, and often several, papers a year.

Mary Evans

Niels Bohr — intellectually dominant.

During this period the work being done at the Institute was not in the mainstream of physics. Bohr, whose intellectual dominance determined the nature of the work being done there, was, on the one hand, thinking about philosophical problems in biology which, from the present point of view, seem of marginal interest and, on the other hand, doing physics that was actually wrong. He had come to the erroneous conclusion that nuclear beta decay violated the conservation of energy and was thus unable to accept the correct Fermi theory of beta decay which assumed the existence of the neutrino, invented by Pauli. The heart of *Redirecting Science* is the description of how, in the mid-1930s, Bohr changed his course, and that of the Institute, by going whole heartedly into experimental and theoretical nuclear physics.

Finn Aaserud's thesis is that this change of direction was much influenced by the nature of scientific funding. Bohr, it turns out, was an excellent fund raiser and was able to throw himself into this activity with the enormous energy he expended on anything that really interested him. The mind boggles when one tries to imagine Einstein writing a funding proposal to the Carlsberg Foundation — Carlsberg of the breweries — or the Rockefeller Foundation to ask for money for research. Both of these entities contributed heavily to Bohr's Institute. From reading *Redirecting Science*, my feeling is that the criteria used by these foundations were quite different. Bohr was a national hero in Denmark and I suspect that if he had asked the Carlsberg Foundation for money to support research in self-levitation he would have got it. On the other hand, as much as the Rockefeller people wanted the prestige of Bohr's name, they were fairly rigid about what their money could be used for. They were interested in biological applications. By coincidence, due to the racial policy of Adolf Hitler, several brilliant young scientists became available at this time, and George Hevesy came to the Institute from the University of Freiburg. Hevesy's programme to use radioactive isotopes as biological tracers fitted perfectly with the Rockefeller criteria, although it took some persuasion by Bohr to make the Foundation aware of this. In the event, the Rockefeller Foundation provided much of the funding for a cyclotron in Copenhagen. By the mid-1930s, Bohr's interest was focused almost entirely on nuclear physics where it remained for the rest of his active scientific life.

Although *Redirecting Science* may be of more direct interest to scholars of contemporary physics history, it is so agreeably written that it may find a wider audience. For me, it created the feeling of a truly elite institution of which my own personal aquaintance was a brief visit one summer in the 1960s. The elitism was one of intellect; the worst fate one could have was to have ideas that were uninteresting. Bohr would simply disengage, and that would be that. For the few who had the 'right stuff', being at Bohr's Institute was an unforgettable experience. This book teaches us that running such an institution required entrepreneurial skills as well as scientific genius. Bohr had an abundance of both. □

Jeremy Bernstein is at 2 Fifth Avenue, 18-L, New York, New York 10011, USA.

Gnomic genomes

Joseph F. Sambrook

Genes and Genomes. By Maxine Singer and Paul Berg. *Blackwell/University Science Books: 1990. Pp. 929. Hbk £49.50, $52; pbk £27.50.*

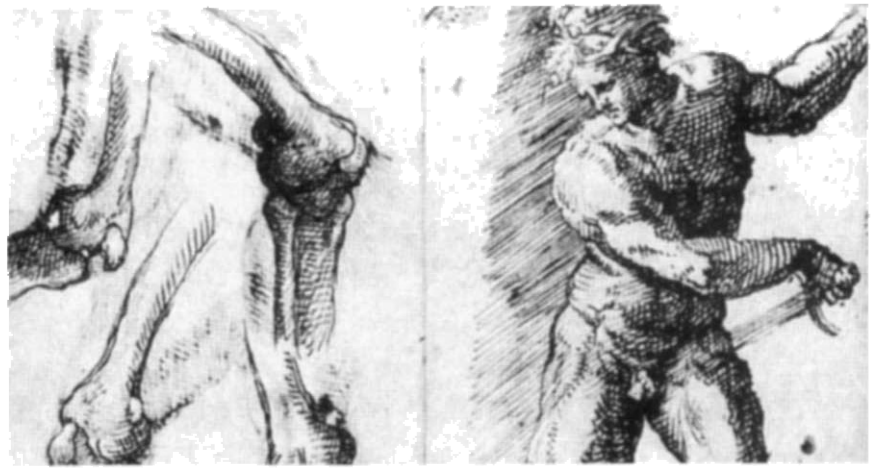

Inigo Jones's Italian sketch book taken from *Early Lithographed Books* by Michael Twyman and published by Farrand Press / The Book Press at £48.50, $87.50.

IN March 1960, Frances Partridge, the last survivor of the original Bloomsbury group of literary and artistic figures, went to dinner in Golder's Green at the house of the distinguished geneticist, Lionel Galton. Frances Partridge's diary : (*Hanging On: Diaries 1960–1963*, Collins, 1990) describes her reaction to viewing preparations of human chromosomes through an elegant light microscope that Galton kept at home.

> *Stained a pretty lavender-pink, there they were in double hanks tied round the waist, chromosomes from the blood or tissue of a child, before my very eyes. I could have listened to his exposition of normal and abnormal chromosomes for ever, and under his tutorship soon began to see which patterns were abnormal. He says that there is no cure for Mongolism despite what the newspapers say.*

After 60 years of hard training in left-wing aesthetics, it is not surprising that Frances Partridge should so clearly appreciate the delicate beauty of these objects while fretting about the starkness of the message that they carried.

Frances Partridge is now over 90 years old. Despite remaining disappointed that Down's syndrome cannot yet be cured and that its etiology is still not understood at the molecular level, she almost certainly would be delighted by the elegance and intellectual depth of the work on chromosomal organization and function that has been accomplished in the 30 years since she dined with Galton. Only a small fraction of this work has been assimilated into standard textbooks and *Genes and Genomes* is the first serious attempt to present an integrated and comprehensive view of chromosomes at the molecular level to graduate students and undergraduates.

Berg and Singer's book has a strong sense of the history of molecular genetics of eukaryotes. Scientific topics are often discussed in a chronological manner, usually taking the analogous situation in prokaryotes as a starting point. This approach serves the authors well while they are dealing with the early discoveries of eukaryotic molecular biology, but becomes rather strained when no obvious prokaryotic model is available. For example, the experiments on the structure of adenovirus messenger RNAs, which opened the way to the discovery of split eukaryotic genes and RNA splicing and had such profound consequences for the subsequent development of eukaryotic molecular biology, are described only in the most general terms – presumably because they then had no precedent in prokaryotic biology. The authors' views of the seminal events of the last 20 years are highly personal and inevitably reflect their own scientific interests and involvements. For example, more space is given to the design of eukaryotic viral vectors (12 pages) than to transgenic animals (two paragraphs); and the preface contains an extended account of the events of the mid 1970s that led to the establishment and subsequent lifting of the moratorium on recombinant DNA research in the United States. While this may stand as a sociological milestone, it was essentially a non-event in scientific terms and has little relevance to today's students.

The book is divided into four sections, which are successful to different extents. Part one is an elementary introduction to molecular biology that is intended for readers with only limited prior knowledge of biochemistry, cell biology and genetics. Part two describes some of the laboratory techniques used in molecular cloning. This section may be of help to people who have no previous exposure to recombinant DNA technology, but it gives no indication of the strengths and weaknesses of the various methods and in many places is quite seriously out-of-date. Part three is by far the most substantial section of the book; its 400 pages contain an excellent and lucid description of the general organization of chromosomes, of gene structure and the regulation of gene expression and of the nature and significance of moveable genetic elements and genomic rearrangements. These topics are treated in greater depth and with more insight than in any other undergraduate and graduate text currently available. *Genes and Genomes* is worth its purchase price for the excellence of part three alone. The final section of the book is less successful. The authors cram into 50 pages, descriptions of a large number of complex biological systems, including differential gene expression, restriction mapping of large genomes, generation and use of transgenic animals, embryological development, insertional mutagenesis, molecular virology and so on. The necessarily superficial treatment afforded to each of these topics stands in sharp contrast to the well-balanced excellence of part three. Graduate students who have read the book bewail the absence of problem sets, the omission of page numbers from cross-references and the lack of annotations in the long list of key references that are given at the end of each of the four major sections. It is not always obvious to students why many of these references are included nor why others are omitted. A one-sentence description of the scientific kernel of each paper would be extremely useful.

Throughout the book, the authors are at their best when dealing with genomes from the bottom up and, as a consequence, the reader is left with the impression that most, if not all, problems of genome structure and genetic behaviour can be solved by analysis of individual genes. Because this approach suffers from both theoretical and technical limitations, I hope that future editions of *Genes and Genomes* will include more detailed descriptions of 'top-down' methods of genomic analysis, and will describe how data obtained from analysis of linkage and segregation of genetic markers can be reconciled with physical maps of chromosomes. A book about genes and genomes that does not do justice to classical genetics misses the central issue that Frances Partridge grasped so clearly in 1960. □

Joseph F. Sambrook is in the Department of Biochemistry, The University of Texas, Southwestern Medical Center at Dallas, 5323 Harry Hines Boulevard, Dallas, Texas 75235-9038, USA.

Large-scale structure in the Universe

A. Kashlinsky & Bernard J. T. Jones

A variety of observations constrain models of the origin of large-scale cosmic structures. Enough observational data have accumulated to constrain (and perhaps determine) the power spectrum of primordial density fluctuations over a very large range of scales, independently of the particular cosmogonical theory assumed. Observations in the near future should be able to weed out many such theories.

THE Universe appears to be homogeneous, expanding and relatively simple on 'large scales' ($>10h^{-1}$ Mpc, with Hubble constant $H_0 = 100h^{-1}$ km s^{-1} Mpc^{-1}). On smaller scales the Universe is extremely inhomogeneous and complicated, containing a variety of distinct structures: galaxies, groups and clusters of galaxies, and superclusters. It is generally assumed that gravity was somehow responsible for the formation of the inhomogeneous part of the Universe through the 'galaxy formation' process. The clue to understanding the details and mechanism of galaxy formation may well be hidden in the various properties of the large-scale structure, and we aim here to discuss the connection between the two from both theoretical and observational perspectives. We will make the conventional assumption that gravity was predominantly responsible for formation of the large-scale structures, thus excluding theories such as explosions or cosmic strings; we also take the cosmological constant, Λ, to be zero.

The type of theory that one assumes for the origin of cosmic structure then depends to a large extent on the assumed density parameter Ω, the ratio of the cosmic density to the value required to make the Universe flat. Observationally, the value of Ω is not well known; most determinations lie in the range $0.1 < \Omega < 0.3$. Primordial nucleosynthesis implies $\Omega_B h^2 \approx 0.045$ (ref. 1), where Ω_B is the density in baryons alone, whereas the dynamics of galaxies and groups of galaxies indicate a mass-to-light ratio $M/L \approx (100\text{–}200)h$, which translates into $\Omega_B \approx 0.1\text{–}0.2$. The idea that $\Omega = 1$ is undoubtedly fuelled by the inflationary model of the early Universe, but there is no direct observational evidence for this supposition except from a very deep survey[2] in which ~1,000 approximate galaxy redshifts up to $z \approx 1$ were determined photometrically, resulting in an estimate $\Omega = 0.9 \pm 0.3$. But an estimate $\Omega \approx 0.2$, with considerable uncertainty, has been derived from the same data[3].

Primordial density fluctuations

To explain the existence of gravitationally bound structures in the Universe, one has to postulate the existence of small density fluctuations of relative amplitude $\delta(\mathbf{r})$ superimposed on the otherwise homogeneous and expanding background. Any density fluctuation can be expressed as a superposition of two independent components: adiabatic fluctuations, δ_{ad}, perturb matter and radiation together, keeping the entropy per baryon constant, whereas isocurvature fluctuations, δ_{iso}, perturb the entropy. The nature of the theory for the origin of cosmic structure is essentially determined by the assumed type of the primordial density fluctuations (PDF), along with an assumption about the nature of any dark material that may exist; the latter in turn determines Ω. To understand the formation of the hierarchy of objects from sub-galactic to supercluster scales, one has to understand whether large-scale structures formed first and later fragmented into smaller objects, or whether large scales formed by a continuous agglomeration of smaller objects into larger; this depends on the PDF spectrum, that is, the contribution of each scale to the total variance of $\delta(\mathbf{r})$. If the PDF spectrum is such that $\langle\delta^2\rangle^{1/2}$ increases smoothly towards small scales, structure formation would start on small scales and proceed to larger ones, but if the spectrum cuts off at some (large) scale, large structures would collapse first and fragment into smaller objects.

Power spectrum: origin and normalization. The total density variation at a single point receives contributions from density fluctuations on all scales. There are two ways to describe the spatial function $\langle\delta^2(\mathbf{r})\rangle$: in a volume that on average contains mass M, the mean square relative mass fluctuation $\langle(\delta M/M)^2\rangle$ is $\langle\delta_M^2\rangle$. Alternatively, the fluctuating field $\delta(r)$ can be described in terms of its Fourier components δ_k with distribution $P(k) = \langle|\delta_k|^2\rangle$. The two are linked by $\langle\delta_M^2\rangle = \sum_k P(k)W(kr)$, where $W(y) = [3(\sin y - y\cos y)/y^3]^2$. The underlying mass auto-correlation function is specified by the power spectrum as $\xi_N = \sum_{\mathbf{k}} P(k)\exp(-i\mathbf{k}\cdot\mathbf{r})$ and if, as is usually assumed, the PDF are gaussian (the phases of the Fourier components are random), the power spectrum defines all properties of the PDF field.

We do not understand the origin of the power spectrum and statistics of PDF, so it is usually assumed that PDF with an initial power spectrum $P(k) \propto k^n$ were either present as part of the initial conditions of the Universe or formed by some causal process which would presumably specify n and their amplitude. The case $n = 1$ is called the Harrison–Zel'dovich spectrum, which does the least violence to the geometry of space-time and which is generally (although not necessarily) expected in inflationary cosmologies. The amplitude of $P(k)$ should lead to the observed galaxy distribution today, and the standard practice is to normalize the original $P(k)$ on some scale relative to what it is on that scale now. The Universe can be seen only as far back as the last photon-scattering surface (when protons and electrons recombined to form neutral hydrogen and the Universe became transparent to the radiation background), and it makes sense to compute the r.m.s. value of the PDF, δ_{rec}, at that epoch (corresponding to redshift), $z_{rec} \approx 1{,}100$. This normalization can be done in several ways; what follows is our choice.

From observations of the galaxy distribution, the r.m.s. fluctuation in galaxy counts, $(\delta N/N)_{rms}$, is known to be unity in a sphere of radius $R_0 = 8h^{-1}$ Mpc (ref. 4). With the assumption that light traces mass (that is, that the visible Universe is a faithful representation of the mass distribution), the recombination PDF amplitude should have been such as to produce now $\langle\delta^2\rangle = 1$ on the mass scale $M_0 = 4\pi\rho_0 R_0^3/3 = 6\times10^{14}\,\Omega h^{-1} M_\odot$. The r.m.s. PDF amplitude at z_{rec} on a co-moving length-scale r can be written as

$$\delta_{rec} = A\left[\frac{\int P(k)W(kr)k^2\,dk}{\int P(k)W(kR_0)k^2\,dk}\right]^{1/2}$$

which for a power-law spectrum $P(k) \propto k^n$ leads to $\delta_{rec}(M) = A(M/M_0)^{-\alpha}$ with $\alpha = 1/2 + n/6$ and $-3 \leq n \leq 1$. The normalization A is computed by assuming that the fluctuation evolves from recombination as a mini-universe with density $\Omega_{eff} = (1+A)\Omega(z_{rec})$ into a mini-universe with $\Omega_{eff} = 2\Omega$, so that its density is now twice the cosmic mean. (For $\Omega < 0.5$ such fluctuations are underdense compared to the critical density, and will therefore never collapse.)

The amplitude δ_{ta} that fluctuations must have had at recombination in order to be on the point of collapse ('turning around')

today can likewise be calculated, as can δ_{col}, the amplitude required at z_{rec} for a fluctuation that has now completed its collapse. Table 1 shows A, δ_{ta} and δ_{col} for $z_{rec} = 1{,}100$.

If light does not trace mass, galaxy counts do not reflect the mass density, and δ_{rec} would be reduced by a bias parameter, $b = [(\delta N/N)_{r.m.s.}/(\delta\rho/\rho)_{r.m.s.}]$ for a sphere of radius R_0. It seems plausible that b could be different from unity, but there is no obvious way of predicting its value, which must for now be inferred from observations.

Large-to-small cosmogonies. If the PDF were purely baryonic and adiabatic, in which case they are damped at small scales by photon thermal conductivity, or if they were carried by massive neutrinos, in which case damping occurs by free streaming at epochs when neutrinos were relativistic, structure forms first on large scales (pancakes) which break up to create small-scale structure. The fluctuation spectrum thus produced has no high frequencies, and it is fairly straightforward to do simple numerical simulations of the evolution of small-amplitude PDF. Pictures of large-scale structure thus generated bore a striking resemblance to some sky surveys[5], but the purely baryonic model requires such large PDF amplitudes (because there is no dark matter and Ω is low) that it violates the limits on isotropy of the cosmic microwave background radiation. The amplitude problem might be solved by adding massive neutrinos as dark matter, which would make $\Omega = 1$ and also provide a large cutoff mass.

Small-to-large cosmogonies. If there are purely isocurvature fluctuations with no non-baryonic dark matter, then $\Omega = \Omega_B \approx 0.1$–$0.2$ is required by Big Bang nucleosynthesis. In this case, a power-law PDF spectrum will survive as a power-law on all scales, with no characteristic scale imprinted on it by physical processes at earlier epochs, and structure will form first on small scales, aggregating by hierarchical clustering to larger scales. The power laws usually considered have $-1 \leqslant n \leqslant 1$ ($n = 0$ being white noise), and Peebles[6] has proposed a 'minimal baryonic isocurvature' model, which fixes n on large scales, but requires an *ad hoc* reheating to generate a sufficiently smooth microwave background.

Alternatively, an adiabatic PDF spectrum would survive on all scales, realizing a small-to-large cosmogony, if $\Omega = 1$ were provided in the form of some weakly interacting massive particles—'cold dark matter' (CDM). Work on the CDM model has mostly been done numerically[7-10]. Apart from the initial amplitude of the spectrum, which determines the epoch of galaxy formation, the theory has no free parameters in its dynamics, but to relate mass and light distributions a bias parameter b is needed, as defined above. An attraction of the CDM model is that $\Omega = 1$, which makes the mass fluctuation in a sphere of radius $8h^{-1}$ Mpc equal to b^{-1}. Numerical simulations suggest $b = 2.5$, but this may have to be modified for consistency with observed galactic motions on large scales.

Theory versus observations

We will argue that the following observational data impose the strongest constraints on cosmogonic theories: redshifts, masses and co-moving densities of the most distant quasars and galaxies; galaxy and cluster correlation functions; peculiar velocities on scales $>10h^{-1}$ Mpc; and microwave background anisotropies. These observations cover mass scales from $\sim 10^9$ to $>10^{20} M_\odot$. (Mass and co-moving length scales are related by $M = 1.25 \times 10^{12} (r/1\ \mathrm{Mpc})^3 \Omega h^2 M_\odot$; so $r \propto h^{-1}$ implies $M \propto h^{-1}$.)

Birthdate of quasars and galaxies. The redshifts at which objects of different scale formed gives us a strong indication of the PDF spectrum. In general, in all large-to-small models, structure formation is very recent ($z_f \approx 2$–3), and has to be more recent for smaller Ω. Small objects (quasars and galaxies) must form after the first 'pancakes' formed and fragmented, so finding quasars and galaxies at high redshifts is a serious embarrassment. In small-to-large (hierarchical) models, on the other hand, there should be many quasars and galaxies at high z, but few large clusters. Quasars and galaxies have evidently completed their gravitational collapse, rather than merely turned around, by the redshift at which they are observed, and for this class of model the masses and abundances of high-redshift objects directly constrains the PDF. Table 2 shows, for various $P(k)$ and Ω in hierarchical models, the mass scales for which the r.m.s. PDF amplitude was equal to δ_{ta} or δ_{col} at z_{rec}. (We have taken the CDM power spectrum from ref. 11 for $\Omega = 1$ and $h = 0.5$.)

It has been established that quasars are fairly abundant at $z \gg 2$. Sixteen quasars are known at $z > 4$ (refs 12–14), and more are expected at still higher redshifts. Of the published quasars at $z \geqslant 4$, the brightest has absolute magnitude $M_V \approx -29$ and the most distant has $z = 4.73$. (Throughout this section we assume $h = 0.5$ where necessary.) The mass of such a quasar can be estimated by assuming its brightness to equal the Eddington value $L_{Edd} = (4\pi G m_p c/\sigma_T) M$, where m_p is the proton mass and σ_T the Thomson cross-section. L_{Edd} is the maximum luminosity that a spherically symmetric, gravitationally bound mass can generate, although data on quasar emission lines may be consistent with their having masss-to-light ratio a factor $\gamma = 10^{2\pm0.5}$ above the Eddington value, $(M/L)_{Edd} \approx 3.2 \times 10^{-5}$ (ref. 15). The Eddington argument implies a quasar mass $M_Q \approx 6 \times 10^{10} [\gamma (M/L)_{Edd} (L/L_*)] M_\odot$, where L_* is the Schechter luminosity corresponding to $M_V = -21.5$ (ref. 16). Efstathiou and Rees[17] estimate a similar mass. This mass refers only to that in the central engine of the quasar, and as it is generally believed that quasars are located in galactic nuclei, the total masses associated with them could be as high as a few times $10^{12} M_\odot$.

In hierarchical models with constant n, the typical mass of collapsed objects at any z is $M_{col}(z) \approx M_{col}(0) \psi(z)^{-1/\alpha}$, where $\psi(z) = \delta(0)/\delta(z)$ is the PDF growth factor between z and now. For $z > \Omega^{-1} - 1$, $\psi = (1+z)$, and is a slowly varying function of z at smaller redshifts. For hierarchical models with varying n, such as CDM, the value of n for the given mass scale should be used. In CDM models, the first galaxy-scale objects are thus expected to form at $z_f \approx 2$–3. Figure 1 shows $M_{col}(z)$ for various power spectra and Ω; quasars at $z > 4$ are marked with small circles. Their masses were estimated by the above prescription, and we note that this represents a lower bound.

It is clear from Fig. 1 that in the CDM model quasars must represent those rare fluctuations with $M \gg M_{col}$. According to the Press–Schechter formalism[18], the fraction $f_M\, \mathrm{d}M$ of such objects in the mass range $\mathrm{d}M$ is

$$f_M = (8\pi)^{1/2} (\delta_c/\sqrt{\langle\delta^2\rangle}) [\mathrm{d}\ln(\langle\delta^2\rangle)/\mathrm{d}M] \exp(-\delta_c^2/2\langle\delta^2\rangle)$$

where δ_c is the critical density that the fluctuation must have in order to turn around. The co-moving number density in objects with mass greater than M_Q is thus $N(>M_Q, z) = \rho(z) f_{QSO} \int_{M_Q}^{\infty} M^{-1} f_M\, \mathrm{d}M$. Here $f_Q(z)$ is the fraction of galaxies in the form of quasars; if all galaxies went through an early quasar phase, $f_Q \approx \min(1, Ht_Q)$, where $t_Q \approx \varepsilon M_Q c^2/L$ is quasar lifetime. The efficiency of quasar energy generation is $\varepsilon \approx 0.1$, and $t_Q = \gamma\varepsilon t_S$, where $t_S = Mc^2/L_{Edd} \approx 4 \times 10^8$ yr is the Salpeter timescale. The expected number of quasars in the range $2 \leqslant z \leqslant 4$ in the CDM model[17] agrees with observations if quasars are short-lived (so that they formed at redshifts not much greater than the ones at which they are observed) and radiate at the Eddington limit, so that $\gamma \approx 1$ rather than 100 (ref. 15). But then the abundance of high-luminosity quasars must decline exponentially for $z \geqslant 4$ (ref. 17), a requirement not supported by more recent observations[19].

Observations of galaxies at high redshift can be even more restrictive of cosmological models, because the total mass associated with the collapsed object can be estimated. But only a few galaxies have been found at $z > 1$: six at $z \approx 1.1$–1.2 and two steep-spectrum radio sources at $z = 3.4$ and 3.8 (refs 20, 21). To compare with theories for galaxy formation, models for evolution of the spectral distribution of galaxies of all luminosities are needed. For the two highest-redshift objects, modelling their

TABLE 1 Values of various density contrasts at recombination for various values of Ω

Ω	A	δ_{ta}	δ_{col}
1	8.6×10^{-4}	1.6×10^{-3}	2.6×10^{-3}
0.3	1.9×10^{-3}	4.3×10^{-3}	6.8×10^{-3}
0.1	4.4×10^{-3}	1.1×10^{-2}	1.8×10^{-2}
0.03	1.3×10^{-2}	3.4×10^{-2}	5.3×10^{-2}

colours with a rapid burst of star formation[22] leads to formation redshifts of 4.5 and 4.9, with luminous masses of 4 and $5.7\times10^{11}M_\odot$ for $\Omega=1$ and $h=1$. For low Ω (~0.1), $z=3.8$ and 4.2, with masses 1.6 and $2.5\times10^{12}M_\odot$, are needed. Much higher formation redshifts are needed if star formation proceeds gradually[21]. A deep survey of extremely faint galaxies[23] yielded $\sim1.5\times10^5$ galaxies per square degree to a limiting magnitude $B_J=26$.

The two high-redshift galaxies are also plotted on Fig. 1. These objects are clearly hard to explain by the CDM model, but they can be regarded as having formed from very rare fluctuations; more data on the abundance of high-redshift galaxies are needed for a quantitative comparison to be made.

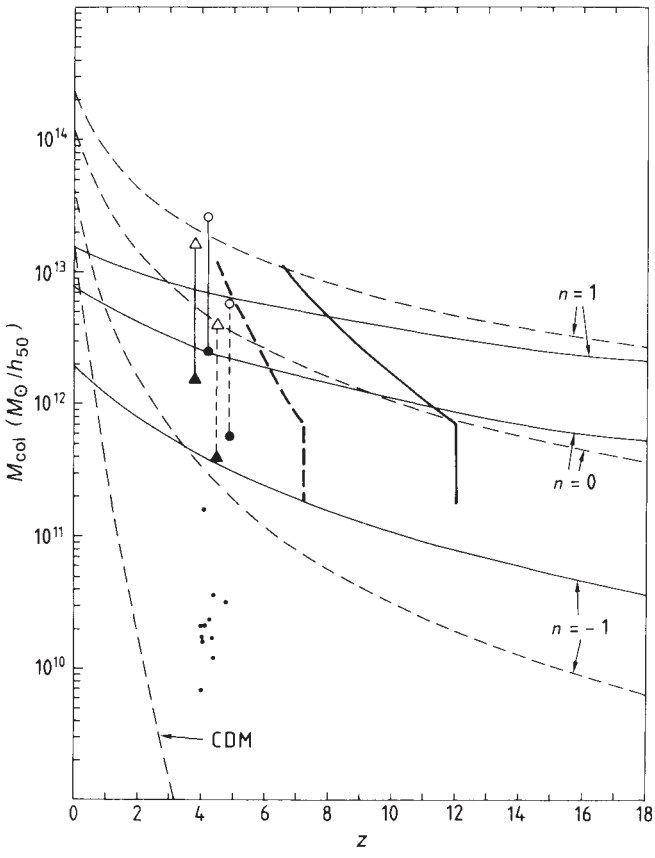

FIG. 1 The typical collapsed mass plotted against redshift, for various scenarios. The spectra are marked by their value of n, and the cold-dark-matter model with $\Omega=1$ is labelled 'CDM'. Solid lines correspond to $\Omega=0.1$, dashed ones to $\Omega=1$. Small dots mark the eleven quasars with $z>4$ that have been published. Large dots and triangles mark the high-redshift galaxies 4C41.7 and 0902+34, respectively, with redshifts of their formation and masses taken from ref. 22 (see text); filled symbols correspond to just the luminous mass and open ones to the total mass, adopted as ten times bigger. The symbols connected with continuous lines are for low Ω ($\Omega=0.1$); those with dashed lines, $\Omega=1$. 'Theoretical' lines marking the redshifts of formation of various mass haloes/galaxies (see text) are plotted with thick lines: solid thick line, $\Omega=0.1$; dashed thick line, $\Omega=1$. M_{col} is plotted in units of $M_\odot/h_{50}$, where $h_{50}=2h$.

The redshift of galaxy formation can be estimated theoretically by assuming that galactic haloes form with isothermal density profile and without dissipation, the latter being the (perhaps naive) assumption in hierarchical models. Galaxies are then born when they have achieved a certain overdensity with respect to the critical density of the Universe at that time. One can refine this argument using the well established Faber-Jackson relation[24] $L=L_*(\sigma/\sigma_*)^4$ for elliptical galaxies with absolute magnitudes $19.5\leq-M_V\leq22.5$, and $L\propto\sigma^3$ for $18.0\leq-M_{-V}<19.5$; $h=0.5$ is assumed. The $L\propto\sigma^3$ law implies that the low-luminosity ellipticals have roughly constant mass density, and must therefore have formed at about the same epoch.

Numerical experiments[25] show that the isothermal density profiles of galactic haloes imply a central velocity dispersion $\sigma=1.67H_0R_t$, R_t being the total radius of the halo, which is assumed to have a negligible core radius. The outer edge of the virialized halo then has density contrast $\delta_c=4(1.67)^2/3=3.72$ with respect to the critical density of the Universe at the time of halo formation. In conjunction with the Faber-Jackson relation, we obtain $(1+z_f)^2(1+\Omega z_f)=(4/\delta_c)(\sigma_*^6/L_*^2)(M/L)^2\times(M/M_*)^{1/2}(H_0G)^{-2}$ for the redshift of formation of a galaxy of total (halo) mass M with luminosity $M_V\leq-19.5$. The right-hand side of this expression scales as h^3 and is approximately equal to (halo crossing time/Hubble time)^2. We adopt $\sigma_*=225\,\mathrm{km\,s^{-1}}$, $L_*=1.5\times10^{10}h^{-2}$ and $M/L=150h$. The last assumption means that dark matter amounting to $\Omega=0.1$, as indicated by the dynamics of galactic systems, was attached to the haloes when they formed and could have been lost later as hierarchical clustering proceeded. We then find $(1+z_f)^2(1+\Omega z_f)=315(2h)^3(M/10^{12}M_\odot)^{1/2}$. These lines are drawn on Fig. 1 for $\Omega=1$ (dashed-thick) and $\Omega=0.1$ (continuous-thick). Evidently galaxy formation (more precisely the collapse of their haloes) should have finished by $z\approx4.5$ if $\Omega=1$ and ~6.5 if $\Omega=0.1$. In an open Universe, galaxy formation would have begun earlier and lasted longer than in the $\Omega=1$ case. The reader is invited to judge how well these lines correspond to the 'typical collapsed mass' lines for various power spectra and Ω. This argument will be modified if M/L depends on galactic luminosity, but the qualitative results are unlikely to change.

These lines are not in conflict with the data on high-redshift galaxies, because the gas that is collapsing in the potential well of the new halo to produce the luminous part of the galaxy[26] will need time to cool[27] and fragment[28], and because the redshifts of the high-z galaxies are only a lower bound on their formation redshift.

Correlation functions. Two-point correlation functions, ξ, measure the lowest-order deviations of the galactic distribution from Poisson (random) form. The function ξ carries different information about the power spectrum depending on the physical scale on which it is calculated. On small scales (<8–$10h^{-1}$ Mpc), structure is nonlinear, and a consequence of gravity[29] rather than the initial PDF even for hierarchical models, which start with significant power on these scales. But on larger scales, fluctuations are still in a linear stage of evolution ($\delta<1$), and ξ carries direct information about the initial PDF. We denote the mass auto-correlation function on linear scales as ξ_N.

The two-point galaxy correlation function on nonlinear scales is well approximated by $\xi_{gg}=(r/r_0)^{-1.77}$, with $r_0\approx5h^{-1}$ Mpc[29,30]. Hierarchical models reproduce this reasonably well in N-body simulations[7-10], with only 'logarithmic' dependence on the fluctuation power-law exponent n, but pancake models with massive neutrinos indicate a larger amplitude than is observed[31,32], and for the baryonic adiabatic model the situation is unclear[33]. On linear scales one expects $\xi_{gg}\approx b^2\xi_N$ for biased galaxy formation[34], or $\xi_{gg}\approx\xi_N$ if light traces mass and large-scale structures formed hierarchically[35]. For $P(k)\propto k^n$,

TABLE 2 Values of turned-around and collapsed masses for various $P(k)$ and Ω

	M_{ta}				M_{col}			
Ω	$n=-1$	$n=0$	$n=+1$	CDM	$n=-1$	$n=0$	$n=+1$	CDM
1	1.7×10^{14}	3.2×10^{14}	4.5×10^{14}	1.2×10^{14}	4.25×10^{13}	1.3×10^{14}	2.25×10^{14}	1.7×10^{13}
0.1	7.3×10^{12}	1.9×10^{13}	3×10^{13}	—	1.8×10^{12}	7.4×10^{12}	1.5×10^{13}	—

Values given are for the present epoch ($z=0$), in units of $M_\odot$. We assume a Hubble scaling parameter $h=0.5$.

$\xi \approx -\sin(\pi n/2) r^{-(3+n)}$, so the sign and slope of ξ_{gg} on linear scales should provide direct information about the power spectrum there. The Durham deep-redshift sample[16], which is confined to narrow solid angles in the sky, indicates a correlation function with scale length $\sim 7h^{-1}$ Mpc, beyond which there is a break in the slope. There is persistent evidence that the correlation function is not a power law, but has a 'shoulder' on scales $2\text{-}5h^{-1}$ Mpc, although this could arise because the data are in redshift space rather than true position[36]. There is also persistent evidence that the correlation function becomes negative at $\sim 20h^{-1}$ Mpc, never turning positive again, but this may be because the survey appears to avoid notable galaxy clusters; a newly compiled catalogue of more than 2 million galaxies[30] brighter than $B_J = 20.5$, covering a large fraction of the sky, reveals a strictly positive ξ_{gg} up to $\sim(50\text{-}100)h^{-1}$ Mpc, with slope and sign consistent with $n \approx -1$ on these scales. On larger scales ξ_{gg} falls off rapidly, indicating a change or cutoff in $P(k)$.

For the rich Abell clusters, the cluster-cluster correlation function[37,46] ξ_{cc} has greater amplitude than would be expected for the galaxy distribution on the same large scales. In addition, ξ_{cc} is positive and proportional to r^{-2} on scales up to $\sim(50\text{-}100)h^{-1}$ Mpc (the upper limit is controversial[38,39]) and is larger for richer clusters (see also ref. 40). These trends are confirmed for catalogues of poorer clusters[41,42]. Projection effects[38] may reduce the amplitude of ξ_{cc} to ~ 1 at $\sim 14h^{-1}$ Mpc, rather than $25h^{-1}$ Mpc as was first thought[37], and make it consistent with zero on scales $\geqslant 50h^{-1}$ Mpc, but the general trends of ξ_{cc} mentioned above are confirmed[43,44] for the Southern Abell catalogue[45].

The larger amplitude of ξ_{cc} can be explained if[34] galaxies formed only where the density field was a factor $b \approx 2.5$ larger than the average, as would be the case in biased galaxy formation models. A generalization[35,47] of the Press-Schechter prescription to correlated PDF can explain the larger ξ_{cc} if the clusters formed by gravitational clustering from a PDF with $n=-1$ on scales at least up to $50\text{-}100h^{-1}$ Mpc, because for $\xi_N > 0$ and $n < 0$, the correlation amplitude is greater for bigger objects. This would also mean that poor groups should have $\xi < \xi_N$ on linear ($>10h^{-1}$ Mpc) scales, but the dependence of the correlation amplitude on mass is complex[47]. Observational tests of this are difficult[48-50], mainly because of uncertainty in defining a 'group', and because of the poor quality of current samples for determining ξ on scales $>10h^{-1}$ Mpc.

If ξ_{cc} is indeed positive even up to $\sim 50h^{-1}$ Mpc (ref. 38), its slope (and not just sign) is inconsistent with the CDM model if $\Omega = 1$ (ref. 47); $n \approx -1$ is needed on these scales. Furthermore, the increase in the correlation amplitude for different mass scales within the clustering hierarchy depends on cluster or group richness in a complicated but unique way for a given $P(k)$. The 'typical' turned-around mass today had an r.m.s. amplitude of δ_{ta} at recombination (see Table 2). It is is easy to see that the Abell clusters should indeed be the (rare) massive members of the hierarchy. Thus the dependence of the amplitude of ξ_{cc} on richness or mass reveals the power index n on mass scales of $(10^{13}\text{-}10^{15})M_\odot$, or co-moving length scales of $\sim(1\text{-}10)h^{-1}$ Mpc, while its dependence on r gives information on $P(k)$ on scales of $\sim(10\text{-}100)h^{-1}$ Mpc. The magnification (or decrease for small groups) of the correlation function by gravitational clustering can provide independent information on $P(k)$ for a large range of scales.

There have been several attempts to improve on the original Press-Schechter prescription for identifying structures that form[52,123] from a random density field. Appel and Jones[51] address the problem of defining the window function scale at a given overdensity b. They determine a window radius from the density field in the vicinity of a maximum: it is the radius at which the smoothed density field at a local maximum has a density excursion that is the threshold (bias) value. This defines a unique set of objects that are essentially isolated and which have a mass function similar, for the CDM model, to the Press-Schechter function.

Peculiar velocities are produced by local ('peculiar') gravity and therefore map the mass distribution whether light traces mass or not. Present data on peculiar velocity flows is limited to a nearby volume of $<100h^{-1}$ Mpc in radius (10,000 km s^{-1} in recession velocity). The best established peculiar velocity is certainly that causing the dipole anisotropy of the microwave background radiation (MBR), which is $\Delta T/T = (1.2 \pm 0.03) \times 10^{-3}$ in the direction right ascension $= 11.2 \pm 0.04$ h, declination $= (-7 \pm 0.05)°$ (ref. 53). Ascribing this to motion of our Galaxy, along with the Local Group, with respect to the MBR rest frame gives a peculiar velocity of 650 ± 30 km s^{-1} on a scale of at least $\sim 5h^{-1}$ Mpc. In linear theory, the direction of the peculiar velocity should coincide with the direction of peculiar gravity, which is given by the dipole in the mass distribution and whose magnitude decreases like M/r^2. Because the flux of radiation goes like L/r^2, then if M/L is constant the direction of the dipole velocity (after subtracting the Virgocentric infall) should coincide with that of the light dipole in galaxy catalogues. This has been tested for a variety of optical[54,55] and IRAS (Infrared Astronomy Satellite)[56-58] catalogues; the light dipoles are in reasonable alignment with the MBR dipole, the mass distribution responsible for this motion lies outside the Local Group, and much of it comes from a sphere of radius $\sim 40h^{-1}$ Mpc.

On larger scales, large redshift surveys and good distance indicators are needed. For disk galaxies, two promising distance indicators are based respectively on the Tully-Fisher relation between total luminosity and the asymptotic rotational velocity width of the 21-cm hydrogen line, which has been applied at wavelengths from the blue to the infrared[59], and the infrared colour/absolute magnitude correlation[60,61]. Application of the Tully-Fisher distance indicator to a sample of 132 spiral galaxies[62] revealed large deviations, of up to 10,000 km s^{-1}, from the Hubble flow. This so-called Rubin-Ford effect was strongly criticized by Hart and Davies[63], who found only small peculiar velocities (<300 km s^{-1}) on a scale of $35h^{-1}$ Mpc, but re-analysis of a subsample of 64 galaxies from the original 132 using the infrared Tully-Fisher relationship seems to confirm the original effect[64,65]. Aaronson *et al.*[66] applied the infrared Tully-Fisher distance indicator to a sample of spiral galaxies in ten clusters, and found a mean Hubble constant $h = 0.9$, with deviations characterized by $\langle v_p^2 \rangle \leqslant 200$ km s^{-1} on scales $\leqslant 100h^{-1}$ Mpc.

To get redshift-independent distances to elliptical galaxies there is a Faber-Jackson relation $D_n \propto \sigma_0^{4/3}$ (refs 67, 68), where D_n is the isophotal diameter of the galaxy, where the surface brightness falls to 20.75 B mag per arcsec^2, and σ_0 is the central velocity dispersion. Lynden-Bell *et al.*[69] (hereafter referred as 7S) applied this distance indicator to a sample of ~ 400 elliptical galaxies over $\sim 6{,}000$ km s^{-1} in depth and found a large peculiar velocity of 600 ± 100 km s^{-1} on a scale of $\sim 50h^{-1}$ Mpc. This

peculiar velocity points towards the Hydra-Centaurus system and roughly coincides with the MBR dipole direction, the dipole determined from spiral galaxy samples and the optical light dipole direction[54]. It also coincides roughly with the long axis of the quadrupole component of the local velocity field[72].

A word of caution is in order here. The new distance indicator was established purely from galaxies in the Coma cluster, but some correlation between galaxy properties and their environments (tidal interactions, mergers, gas removal) is both known and expected: the D_n-σ_0 relation may not apply equally to all elliptical galaxies. Of the ~400 ellipticals in the 7S sample, some are in rich clusters, some in poor ones and a fraction are in the field, but the sample is not large enough to estimate any effects from environment or evolution[70].

The 7S group identified[69,71] a large-scale enhancement (the 'Great Attractor', GA) in the distribution of galaxies as a possible cause of the velocity deviations they discovered. The existence of the GA was presaged in the identification[72] from the Aaronson *et al.* survey[73] of a quadrupole component in the Virgocentric flow. The long axis of the quadrupole (confirmed by others[74]) was found to point in the direction of the Hydra-Centaurus complex. The importance of the quadrupole component is that it is unambiguously gravitational in origin. The remarkable flows in the direction of the GA receive some support from a survey of spirals for which distances have been determined using the infrared Tully-Fisher distance indicator[75]. (Another word of caution: the two surveys do not agree in detail in their velocity maps of the nearby Universe, at distances $<100h^{-1}$ Mpc.) The GA can be modelled by a density distribution proportional to r^{-2}, centred ~3,500 km s^{-1} away from us towards the Hydra-Centaurus region, with total mass $\sim 10^{16} M_{\odot}$.

There are local contributions to the Local Group motion[55] as well as those from the directions of Perseus and Hydra-Centaurus. Conversely, the search for the GA led other groups[76,77] to suggest a 'super attractor' far beyond the Hydra-Centaurus system. Recently Raychaudhury[78] re-analysed the Scaramella *et al.* sample of Abell clusters[76] and concluded that there are two unusual concentrations of Abell clusters—one in the region of the GA and one in the region originally suggested in refs 76 and 77.

The existence of large-scale peculiar velocities sets further constraints on cosmogonical models. A simple but very accurate estimate for v_p follows by arguing that a particle that has experienced peculiar acceleration g_p for a time t would have acquired $v_p \approx g_p t$. Writing $g_p = G\delta M/r^2 = 4\pi G\delta\rho r/3 = 0.5\Omega H_0 v_H \delta$ leads to $v_p/v_H \approx f(\Omega)\delta/3$ where v_H is the Hubble velocity and $f(\Omega) = 3H_0\Omega t \approx \Omega^{0.6}$. The ratio v_p/v_H is what gives directly the PDF amplitude on a given scale. (Essentially the same result can be derived in a more sophisticated way by using the linearized continuity equation, which leads to $\nabla \cdot v_p = -H_0 f(\Omega)\delta$.) Because the peculiar velocity is generated by gravity, a conservative force, it should be irrotational, so that the Fourier component of v_p is $ikH_0 f(\Omega)\delta_k/k^2$. The r.m.s. amplitude of v_p is thus related to $P(k)$ via $\langle v_p^2 \rangle = 4\pi H_0^2 f^2(\Omega) \int P(k) W_v(kr)\, dk$, where W_v is the velocity window function, usually[79] chosen to be the Fourier transform of a Gaussian window in r-space.

This equation, however, contains information only about the r.m.s. magnitude of v_p on a given scale, and more information about peculiar motions in different models can be obtained from the various types of velocity correlation function. The easiest such function to work with analytically is the dot velocity correlation[80], $\nu(\mathbf{r}) = \langle \mathbf{v}_p(\mathbf{x}) \cdot \mathbf{v}_p(\mathbf{x}+\mathbf{r}) \rangle$, which measures the coherence length of the velocity field and is related to the difference between the peculiar velocities of two points separated by distance r. On linear scales, ν is related to the primordial mass autocorrelation function by[81] $\nabla^2 \nu = -H_0^2 f^2(\Omega)\xi_N$. For $P(k) \propto k^n$, $\xi_N(r) \propto r^{-(n+3)}$, so $\nu(r) = a_1 r^{-1} - a_2 n r^{-(n+1)}$ for $n > -1$ (for $n = -1$ the peculiar gravitational potential diverges and a large-scale cutoff must be introduced). The constant a_1 comes from normalizing the velocity field to nonlinear scales and depends on Ω; a_2 is defined here to be positive and depends on H_0 and Ω. As n increases, the peculiar velocities on a given scale (proportional to $\sqrt{\nu(r)}$) decrease. Noting that $\xi_N(r)$ measures the excess probability of finding another turned-around object at a distance r from the given one, one sees that if $n = 0$ then $\xi_N = 0$, and the average peculiar mass in the vicinity of a given turned-around structure is zero. The peculiar gravity is then dominated by the central mass, leading to keplerian fall-off in $\langle v_p^2 \rangle$ at large r. If $n < 0$, $\xi_N(r) > 0$, and the peculiar gravity on a given scale is greater than in the white noise ($n = 0$) case, leading to a slower decrease of $\langle v_p^2 \rangle$ with r, and vice versa for $n > 0$. But because $\xi_N(r) \propto r^{-(n+3)}$ and decreases very steeply with r for positive n, the decrease in $\langle v_p^2 \rangle$ with r for positive n is not significantly more dramatic than in the white-noise case.

To summarize, the smaller n is, the more power PDF have on large scales, and the greater would be both the amplitude and the coherence length of the peculiar velocity field. If light does not trace mass, as in biased galaxy-formation scenarios, the peculiar velocity on a given scale would be smaller by a factor of b than that given by the above expressions if δ is normalized through the observed galaxy (light) distribution.

The velocity resulting from the MBR dipole does not impose any strong constraints on the models, as it can be interpreted as a local ($5h^{-1}$ Mpc) motion on a nonlinear scale at which δ is given by the normalization at R_0. It therefore depends only marginally on the particular model or PDF spectrum. But when the dipole velocity is combined with the 7S data, the latter imply a very large coherence length for the peculiar velocity field, which is inconsistent with most predictions, notably those of the CDM and biased models[82]. (Kaiser[83] argues that this interpretation may not be so straightforward because of uncertainties in the exact value of the velocity window size in the 7S data.) Bertschinger and Juszkiewicz[84] show that the GA is a 7σ fluctuation in CDM models, while Peebles[80] argues that the large coherence length of the velocity field is consistent with the minimal baryonic isocurvature (MBI) model, assuming complete reionization, which would also presumably solve the problem of MBR anisotropies.

Groth *et al.*[85] argue that the observed velocity field in the 7S sample is correlated more strongly than would be expected on the basis of the CDM model, particularly at large separations, but Gorski *et al.*[86] have refined their calculations. They split the velocity correlation tensor into 'parallel' and 'transverse' components and show, by comparing their analysis with N-body simulations, that the scalar velocity correlation used by Groth *et al.*[85] may be misleading. The Aaronson *et al.*[66] and IRAS samples show velocity correlations on scales of $150h^{-1}$ Mpc; the 7S elliptical galaxy sample shows the same correlation length scale, but with a considerably greater amplitude. (The 7S correlations are very sensitive to the velocities of a small number of galaxies in the sample.) The correlations in the first two samples are not unusual for CDM models with a bias parameter of $b \leq 2$, but the CDM model cannot reproduce the amplitude of the 7S sample. The MBI model automatically generates long-range correlations, but even then cannot come to terms with the 7S sample. Juszkiewicz *et al.*[87] analysed a baryon-dominated isocurvature model with $n = -1$, no reionization and $\Omega = 0.4$; their model is normalized without biasing ($b = 1$) and the power spectrum has a prominent feature at the matter-radiation Jeans length. They find that the expected streaming motions in the model are consistent with both IRAS and 7S data.

The difficulty presented by the 7S data can be understood through the Press-Schechter formalism for gravitational clustering, which should be an adequate model for PDF on these linear scales, where $\langle \delta^2 \rangle \propto M^{-\alpha}$ for both hierarchical and pancake models. Taking $l_{GA} \approx 50h^{-1}$ Mpc to be the scale of typical GA motions, we expect for a given PDF spectrum to find the density fluctuation variance $\delta_e \approx (l_{GA}/R_0)^{-3\alpha} \ll 1$ on that scale. But on any scale $v_p/v_H \approx f(\Omega)\delta/3$, and on the GA scale, where

$v_p/v_H \approx 0.1$, $\delta_{GA} \approx 0.3\Omega^{0.6}$. For example, if $\Omega \approx 0.3$, $\delta_{GA} \approx 0.67$, whereas for $\Omega = 1$, $\delta_{GA} \approx 0.3$. The probability for such a region to have formed by now is, for gaussian PDF, $P_{GA} = (\sqrt{2}\pi\delta_e)^{-1} \int_{\delta_{GA}}^{\infty} \exp(-\delta^2/2\delta_e^2)\, d\delta$; for $\delta_{GA} \gg \delta_e$ it becomes $P_{GA} \approx (\sqrt{2}\pi\delta_{GA}/\delta_e)^{-1} \exp(-\delta_{GA}^2/2\delta_e^2)$. For $\Omega \approx 0.3$, $P_{GA} \approx 3\times10^{-5}$, 3.6×10^{-23} and 0 for $n = -1$, 0 and +1 respectively. For $\Omega = 1$, $P_{GA} = 4\times10^{-2}$, 5.4×10^{-6} and 1.7×10^{-27}. As expected, such regions are very implausible for positive n, but for spectra with $n < 0$, which carry significant power on large scales, they are rare but not at all unlikely.

There is another reason[81] why the GA should be identified with these rare regions in a Universe with $n < 0$: the GA region is by definition rich in elliptical galaxies, and from the morphology-density relation[88] such a region is likely to contain rich clusters. So the GA represents a massive member of the clustering hierarchy and, as was discussed above, if $n < 0$ and if light traces mass, the more massive clusters should have a boosted correlation function. Consequently, rare regions of high peculiar mass would typically be composed of objects more massive than the general hierarchy members, and there should be a bias in the velocity field such that the dynamics of massive clusters should on the average exhibit larger peculiar velocities. This 'velocity bias' origin for the large peculiar velocities of the GA region is supported by the recent findings of unusually high concentration of rich clusters there[78].

There is also the important problem of relating the alignment of the peculiar gravitational acceleration of the Local Group, as determined from galaxy catalogues, with the dipole velocity that originates on large scales. The alignment angles have different probabilities for different power spectra. The peculiar velocity field of the Local Group has been constructed for both CDM and BDM (baryonic dark matter) models; Juszkiewicz *et al.*[87] find the two models indistinguishable at the 2σ level, both being consistent with the observations out to 10,000 km s^{-1}, but Lahav *et al.*[89] apply a somewhat different statistical analysis and conclude that the biased CDM model with $b \approx 1.7$ is consistent with the small misalignment of the dipoles, whereas in baryon isocurvature models with $n < 0$ only a small fraction of observers will see the observed alignment of the MBR dipole with the mass distribution.

MBR anisotropies. The microwave background retains an imprint of the cosmic conditions, notably the PDF spectrum[90], from the last scattering surface, which in the absence of reheating would be at z_{rec}. Current upper limits on MBR anisotropies on scales from several arcseconds to degrees strongly constrain galaxy-formation models. The angular scale θ at z_{rec} contains information about the mass scale $M(\theta) = 1.4\times10^{12}(\theta/1\ \text{arcmin})^3(\Omega^2 h)^{-1} M_\odot$, so that 1 arcmin subtends a co-moving scale of $\sim 1h^{-1}$ Mpc at recombination.

There are three important angular scales in observations of MBR anisotropies: for θ less than several arcminutes, primordial MBR fluctuations are suppressed by Silk damping and, if detected, would reveal information about the pre-recombination Universe[91,92] or would be of local origin; observational limits on fluctuations in the range several arcminutes $\leq \theta \leq 3°$, corresponding to $10^{13} \leq M(\theta)/M_\odot \leq 10^{17}$, are of greatest relevance to galaxy formation; for $\theta \geq 3°$ (which is approximately the horizon scale at Z'_{rec}), fluctuations are dominated by the Sachs-Wolfe effect (the gravitational redshift resulting from mass fluctuations).

Most of the results we discuss here will soon be superseded by new data from the COBE (Cosmic Background Explorer) satellite. There are three past measurements of particular significance[93-95]. The RELICT experiment[93,96] sets constraints of $(\sum_{i=2}^{25} a_i^2)^{1/2} < 7\times10^{-5}$ and $\Delta T/T < 1.6\times10^{-5}$ on the large scale; it also provides the strongest limit on the quadrupole anisotropy, $\sqrt{C_2} < 5\times10^{-5}$, and a limit $\sqrt{C_4} < 7\times10^{-5}$ on the octupole anisotropy. Second, Davies *et al.*[94] report a marginal positive detection of a temperature fluctuation on an angular scale of ~8°. The amplitude of this 'hot spot' is not incompatible with the RELICT limits, and can theoretically be produced in a number of ways[97,98]; the position of the hot spot on the sky roughly coincides with the recently reported 'Great Wall' in the galaxy distribution[99]. Third, Readhead *et al.*[95], at the Owens Valley Radio Observatory (OVRO), measure $\Delta T/T < 1.5\times10^{-5}$ at $\theta = 7.15$ arcmin, which provides the tightest constraint on pancake theories.

In addition, the IRAM experiment[100] gives $\Delta T/T \leq 2.6\times10^{-4}$ at $\theta \approx 11$ arcsec, and from the VLA (Very Large Array)[101-103] comes a limit $\Delta T/T \leq 2\times10^{-4}$ for θ from 18 to 60 arcsec. On these small angular scales, any MBR fluctuations come mostly from faint radio sources. The limits say little about the Universe at recombination, but can constrain the extent of reheating of the cosmic plasma since then. The IRAM measurements also strongly limit the presence of any clumped dust distribution[104].

Fluctuations on scales >1° are important because they are relatively easy to measure and because they are unaffected by any reheating of the intergalactic medium (the Sachs-Wolfe effect is independent of the position of the surface of last scattering). The expected MBR anisotropies have been computed in a variety of cosmogonic models[105-108], but different authors do not agree on what calculational technique should be used, and get different results for the same model. Nevertheless, several models can clearly be ruled out, while others await better data from COBE.

The OVRO results, on the 7.15-arcmin scale, are most useful in constraining theories: the standard CDM picture, for example, with $\Omega_B = 0.1$ and $h = 0.5$ gives $\Delta T/T = 0.4\times10^{-5}$ on this scale, which is quite safe. But as discussed above, that model may not have sufficient large-scale structure to account for the large-scale velocity correlations, and the temperature fluctuations and the velocity correlations are intimately related[109]. The BDM model ($n = -1$) is in conflict with the quadrupole anisotropy limit[110], but can be saved by modifying the ionization history; reionization must then have occurred at a redshift <100 but larger than the redshift of the new last scattering surface (~5-10). COBE data will probably make or break this model.

In summary, the current limits on $\Delta T/T$, if taken at face value, conflict with theoretical predictions from pancake models, and from those invoking baryon isocurvature PDF with $n \leq 0$. But in the latter type, the first compact objects would form immediately after recombination, and $\Delta T/T$ could then be changed by reheating or gravitational lensing effects. Reheating and reionization would provide a large enough optical depth to erase fluctuations on scales up to several degrees[111,112], and new fluctuations would be generated in the hot plasma[113], but the current limits do not rule out models with reheating[112,114]. Gravitational lensing by compact objects can also affect MBR fluctuations[115,116]. It has been argued that lensing would erase anisotropies[116], increase them[117], or erase them on large scales and increase them on small scales[118]. Detailed computations should resolve this uncertainty[119].

An important new question is whether the large peculiar velocities discussed in the previous section arose from PDF that are consistent with the observed limits on MBR anisotropies. Juszkiewicz *et al.*[109] and Martinez-Gonzalez and Sanz[120] calculate the 'minimal' MBR anisotropy associated with a given streaming motion, meaning that the PDF spectrum is chosen to produce the required velocity field but to minimize the observed temperature fluctuations. Although it is a near thing, no MBR anisotropy experiments are yet in conflict with the observed peculiar motions.

The MBR spectrum is also an important diagnostic of the pre-recombination Universe. COBE has set the best constraints on the deviation of the spectrum from black-body[121], giving a comptonization parameter $y \leq 10^{-4}$ for wavelengths between 0.05 and 1 cm. This eliminates any significant amount of hot intergalactic gas[122], meaning that the optical depth due to hot intergalactic gas is small for z up to at least ~5-10, and that

most of the soft cosmic X-ray background must come from compact sources.

Conclusions

There is no one theory that can account for all the data. The occurrence of high-redshift quasars and galaxies constrains $P(k)$ on scales $<10^{12}M_{\odot}$, and requires more power than CDM and pancake models can provide. Correlation functions on linear scales now constrain the power spectrum on co-moving scales of $1<r/(h^{-1}\,\mathrm{Mpc})<100$, and indicate $n\approx-1$, which is inconsistent with CDM models. The data on the GA motions constrain the power spectrum on similar scales, and also suggest baryonic isocurvature models with $n<0$. MBR anisotropies (or upper limits on them) constrain the power spectrum over a large range of scales: arcminute-scale measurements correspond to $r\approx$ several h^{-1} Mpc, while degree-scale anisotropies contain information on scales $>100h^{-1}$ Mpc. Present limits rule out everything but the $\Omega=1$ CDM model, except that in the baryonic isocurvature models the first generation of compact objects, formed soon after recombination, could erase fluctuations on arcminute scales. Pancake models are inconsistent with the OVRO limits at 7 arcmin. Finally, although we did not discuss the issue here, the observations of large structures in galaxy catalogues (voids, filaments and the like) pertain to the power spectrum on scales of $\sim(20\text{–}50)h^{-1}$ Mpc, and lean towards pancake or $n<0$ hierarchical models.

But we should end on an optimistic note. The coming decade will bring significant advances in space-based astronomy, which will markedly advance our understanding of the structure of the Universe. The COBE satellite, already in orbit, will map out the microwave sky, and the Hubble Space Telescope, when it overcomes its current problems, will bring new and better data in visible light. The Advanced X-Ray Astronomy Facility (AXAF), due to be launched later this decade, should be able to see structure in the X-ray sky (<10 keV), and the soon to be launched γ-ray observatory (GRO) should be able to set further constraints on, or perhaps even detect, dark matter if it is made of CDM particles whose annihilations in the halo of our Galaxy could then produce a γ-ray flux. And there will be new and deeper surveys from the ground. At the end of all this, we hope, there will be but one theory for the origin of the large-scale structure in the Universe. □

A. Kashlinsky is at NORDITA, Blegdamsvej 17, DK-2100 Copenhagen, Denmark. Bernard J. T. Jones is in the Department of Astronomy, University of Sussex, Falmer, Brighton BN1 9QH, UK.

1. Kolb, E. W. & Turner, M. S. *The Early Universe* Ch. 4 (Addison-Wesley, 1990).
2. Loh, E. D. & Spillar, E. J. *Astrophys. J. Lett.* **307,** 1–4 (1986).
3. Caditz, D. & Petrosian, V. *Astrophys. J. Lett.* **337,** 65–68 (1989).
4. Davis, M. & Peebles, P. J. E. *Astrophys. J.* **267,** 465–482 (1983).
5. de Lapparent, V., Geler, M. J. & Huchra, J. P. *Astrophys. J. Lett.* **302,** 1–5 (1986).
6. Peebles, P. J. E. *Astrophys. J. Lett.* **315,** 73–76 (1987).
7. Frenk, C. S., White, S. D. M. & Davis, M. *Astrophys. J.* **271,** 417–430 (1983).
8. Davies, M., Efstathiou, G., Frenk, C. S. & White, S. D. M. *Astrophys. J.* **292,** 371–394 (1985).
9. White, S. D. M., Frenk, C. S., Davis, M. & Efstathiou, G. *Astrophys. J.* **313,** 505–516 (1987).
10. Frenk, C. S., White S. D. M., Davis, M. & Efstathiou, G. *Astrophys. J.* **327,** 507–525 (1988).
11. Bond, J. R. & Efstathiou, G. *Astrophys. J. Lett.* **285,** 45–48 (1984).
12. Schneider, D. P., Schmidt, M. & Gunn, J. E. *Astr. J.* **98,** 1507–1522 (1989).
13. Schneider, D. P., Schmidt, M. & Gunn, J. E. *Astr. J.* **98,** 1951–1958 (1989).
14. Hazard, C. *et al.* preprint (1990).
15. Wandel, A. & Mushotzky, R. *Astrophys. J. Lett.* **306,** 61–65 (1986).
16. Shanks, T., Hale-Sutton, D., Fong, R. & Metcalfe, N. *Mon. Not. R. astr. Soc.* **237,** 589–610 (1989).
17. Efstathiou, G. & Rees, M. J. *Mon. Not. R. astr. Soc.* **230,** 5P–11P (1988).
18. Press, W. & Schechter, P. *Astrophys. J.* **187,** 425–435 (1974).
19. McMahon, R. *et al.* preprint (1990).
20. Chambers, K. C., Miley, G. K. & van Breugel, W. *Astrophys. J.* (in the press).
21. Lilly, S. J. *Astrophys. J.* **333,** 161–167 (1988).
22. Chambers, K. C. & Charlot, S. *Astrophys. J. Lett.* **348,** 1–4 (1990).
23. Tyson, J. A. *Astr. J.* **96,** 1–23 (1988).
24. Davies, R., Efstathiou, G., Fall, S. M., Illingworth, G. & Schecter, P. L. *Astrophys. J.* **266,** 41–57 (1983).
25. Goodman, J. & Narayan, R. *Mon. Not. R. astr. Soc.* **231,** 97–114 (1988).
26. White, S. D. M. & Rees, M. J. *Mon. Not. R. astr. Soc.* **183,** 341–358 (1978).
27. Rees, M. J. & Ostriker, J. P. *Mon. Not. R. astr. Soc.* **179,** 541–559 (1977).
28. Kashlinsky, A. *Mon. Not. R. astr. Soc.* **200,** 585–603 (1982).
29. Peebles, P. J. E. *Astrophys. J. Lett.* **189,** 51–53 (1974).
30. Maddox, S. J., Efstathiou, G., Sutherland, W. J. & Loveday, J. *Mon. Not. R. astr. Soc.* **242,** 43P–47P (1990).
31. White, S. D. M., Frenk, C. S. & Davis, M. *Astrophys. J. Lett.* **274,** 1–5 (1983).
32. Peebles, P. J. E. *Astrophys. J.* **258,** 415–424 (1982).
33. Peebles, P. J. E. *Astrophys. J.* **248,** 885–897 (1981).
34. Kaiser, N. *Astrophys. J. Lett.* **284,** 9–12 (1984).
35. Kashlinsky, A. *Astrophys. J.* **317,** 19–25 (1987).
36. Kaiser, N. *Mon. Not. R. astr. Soc.* **227,** 1–21 (1987).
37. Bahcall, N. & Soneira, R. *Astrophys. J.* **270,** 20–38 (1987).
38. Sutherland, W. & Efstathiou, G. *Mon. Not. R. astr. Soc.* **248,** 159–167 (1991).
39. Olivier, S., Blumenthal, G. R., Dekel, A., Primack, J. R. & Stanhill, D. *Astrophys. J.* **356,** 1–13 (1990).
40. Borner, G., Mo, H. & Chu, Y. *Astr. Astrophys.* **219,** 29–33 (1989).
41. Shectman, S. A. *Astrophys. J. Suppl. Ser.* **57,** 77–90 (1985).
42. Postman, M., Geller, M. J. & Huchra, J. P. *Astr. J.* **91,** 1267–1273 (1986).
43. McGill, C. & Couchman, H. *Mon. Not. R. astr. Soc.* **236,** 51P–56P (1989).
44. Batuski, D. J., Bahcall, N. A., Olowin, R. P. & Burns, J. O. *Astrophys. J.* **341,** 599–610 (1989).
45. Abell, G., Corwin, H. G. & Olowin, R. P. *Astrophys. J. Suppl. Ser.* **70,** 1–138 (1989).
46. Klypin, A. A. & Kopylov, A. I. *Soviet Astr. Lett.* **9,** 41–44 (1983).
47. Kashlinsky, A. preprint (1991).
48. Jing, Y. & Zhang, J. *Astr. Astrophys.* **190,** L21–L23 (1988).
49. Maia, J. & da Costa, L. N. *Astrophys. J.* **349,** 477–479 (1990).
50. Ramella, M., Geller, M. J. & Huchra, J. P. *Astrophys. J.* **353,** 51–58 (1990).
51. Appel, L. & Jones, B. J. T. *Mon. Not. R. astr. Soc.* **245,** 522–530 (1990).
52. Bardeen, J., Bond, J. R., Kaiser, N. & Szalay, A. S. *Astrophys. J.* **304,** 15–61 (1986).
53. Smoot, G. F. *et al. Astrophys. J. Lett.* **291,** 23–27 (1985).
54. Lahav, O. *Mon. Not. R. astr. Soc.* **225,** 213–220 (1987).
55. Lynden-Bell, D., Lahar, O. & Burstein, D. *Mon. Not. R. astr. Soc.* **241,** 325–345 (1989).
56. Yahil, A., Walter, D. & Rowan-Robinson, M. *Astrophys. J. Lett.* **301,** 1–5 (1986).
57. Lahav, O., Rowan-Robinson, M. & Lynden-Bell, D. *Mon. Not. R. astr. Soc.* **234,** 677–701 (1988).
58. Rowan-Robinson, M. *et al. Mon. Not. R. astr. Soc.* **247,** 1–18 (1990).
59. Aaronson, M. & Huchra, J. *Astrophys. J.* **265,** 1–17 (1983).
60. Tully, B., Mould, I. R. & Aaronson, M. *Astrophys. J.* **257,** 527–537 (1982).
61. Wyse, R. F. G. *Mon. Not. R. astr. Soc.* **199,** 1P–8P (1982).
62. Rubin, V. C., Thonnard, N., Ford, W. K. & Roberts, M. S. *Astrophys. J.* **81,** 719–732 (1976).
63. Hart, L. & Davies, R. D. *Nature* **297,** 191–196 (1982).
64. Collins, A., Joseph, R. D. & Robertson, N. A. *Nature* **320,** 506–508 (1986).
65. James, P. A., Joseph, R. D. & Collins, C. A. *Mon. Not. R. astr. Soc.* **229,** 53–59 (1987).
66. Aaronson, M. *et al. Astrophys. J.* **302,** 536–563 (1986).
67. Dressler, A. *et al. Astrophys. J.* **313,** 42–58 (1987).
68. Djorgovski, S. & Davis, M. *Astrophys. J.* **313,** 59–68 (1987).
69. Lynden-Bell, D. *et al. Astrophys. J.* **326,** 19–49 (1988).
70. Silk, J. *Astrophys. J. Lett.* **345,** 1–4 (1989).
71. Dressler, A. *et al. Astrophys. J. Lett.* **313,** 37–42 (1987).
72. Lilje, P., Yahil, A. & Jones, B. J. T. *Astrophys. J.* **307,** 91–96 (1986).
73. Aaronson, M. *et al. Astrophys. J. Suppl. Ser.* **50,** 241–262 (1982).
74. Stavely-Smith, L. & Davies, R. D. *Mon. Not. R. astr. Soc.* **241,** 787–801 (1989).
75. Aaronson, M. *et al. Astrophys. J.* **338,** 654–676 (1989).
76. Scaramella, R., Baiesi-Pillastrini, G., Chincarini, G., Vettolani, G. & Zamorani, G. *Nature* **338,** 562–564 (1989).
77. Lahav, O., Edge, A. C., Fabian, A. C. & Putney, A. *Mon. Not. R. astr. Soc.* **238,** 881–895 (1989).
78. Raychaudhury, S. *Nature,* **342,** 251–255 (1989).
79. Kaiser, N. *Astrophys. J. Lett.* **273,** 17–20 (1983).
80. Peebles, P. J. E. *Nature* **327,** 210–211 (1987).
81. Kashlinsky, A. *Astrophys. J. Lett.* **343,** 5–7 (1989).
82. Vittorio, N., Juszkiewicz, R. & Davis, M. *Nature* **323,** 132–133 (1986).
83. Kaiser, N. *Mon. Not. R. astr. Soc.* **231,** 149–167 (1988).
84. Bertschinger, E. & Juszkieweicz, R. *Astrophys. J. Lett.* **334,** 59–62 (1988).
85. Groth, E., Juszkiewicz, R. & Ostriker, J. P. *Astrophys. J.* **346,** 558–565 (1989).
86. Gorski, K., Davis, M., Strauss, M. A., White, S. D. M. & Yahil, A. *Astrophys. J.* **344,** 1–19 (1989).
87. Juszkiewicz, R., Vittorio, N. & Wyse, R. *Astrophys. J.* **349,** 408–414 (1990).
88. Dressler, A. *Astrophys. J.* **236,** 351–365 (1980).
89. Lahav, O., Kaiser, N. & Hoffman, Y. *Astrophys. J.* **352,** 448–456 (1990).
90. Kaiser, N. & Silk, J. *Nature* **324,** 529–537 (1986).
91. Hogan, C. *Astrophys. J. Lett.* **284,** 1–4 (1984).
92. Efstathiou, G. in *Physics of the Early Universe* NATO ASI series (eds Peacock, J. A., Heavens, A. F. & Davies, A. T.) 361–463 (Reidel, Dordrecht, 1990).
93. Strukov, I. A. *et al.* in *IAU Symp.* 130 (eds Audouze, J., Pelletan, M.-C. & Szalay, A.) (Reidel, Dordrecht, 1987).
94. Davies, R. D. *et al. Nature* **326,** 462–466 (1987).
95. Readhead, A. C. S. *et al. Astrophys. J.* **346,** 566–587 (1989).
96. Klypin, A. A. *et al. Sov. Astr. Lett.* **298,** L1 (1987).
97. Vittorio, N. in *Large-Scale Motions in the Universe* (eds Rabin, V. C. & Coyne, G. V.) 397–417 (Princeton University Press, 1989).
98. Scaramella, R. *Astrophys. J.* **346,** 607–612 (1989).
99. Geller, M. J. & Huchra, J. *Science* **246,** 897–903 (1989).
100. Kreysa, E. & Chini, A. in *Proc. 3rd ESO/CERN Symp. Astronomy, Cosmology and Fundamental Particles* (eds Caffo, M. *et al.*) (Reidel, Dordrecht, 1989).
101. Martin, B. & Partridge, B. *Astrophys. J.* **324,** 794–800 (1988).
102. Fomalont, E. *et al. Astr. J.* **96,** 1187–1191 (1988).
103. Hogan, C. & Partridge, B. *Astrophys. J. Lett.* **341,** 29–31 (1989).
104. Bond, J. R., Carr, B. J. & Hogan, C. J. *Astrophys. J.* (in the press).
105. Efstathiou, G. & Bond, J. R. *Mon. Not. R. astr. Soc.* **227,** 33P–38P (1987).
106. Gouda, N., Sasaki, M. & Suto, Y. *Astrophys. J.* **341,** 557–574 (1989).
107. Sugiyama, N., Sasaki, M. & Tomita, K. *Astrophys. J. Lett.* **338,** 45–48 (1989).
108. Holtzman, J. A. *Astrophys. J. Suppl. Ser.* **71,** 1 (1989).
109. Juszkiewicz, R., Gorski, K. & Silk, J. *Astrophys. J. Lett.* **323,** 1–6 (1987).
110. Gorski, K. & Silk, J. *Astrophys. J. Lett.* **346,** 1–4 (1989).
111. Peebles, P. J. E. *Astrophys. J. Lett.* **243,** 119–122 (1981).
112. Peebles, P. J. E. *Astrophys. J. Lett.* **315,** 73–76 (1987).
113. Vishniac, E. T. *Astrophys. J.* **322,** 597–604 (1987).
114. Efstathiou, G. & Bond, J. R. *Mon. Not. R. astr. Soc.* **218,** 103–121 (1986).
115. Blanchard, A. & Schneider, J. *Astr. Astrophys.* **184,** 1–6 (1987).

116. Kashlinsky, A. *Astrophys. J. Lett.* **331,** 1-4 (1988).
117. Cole, S. & Efstathiou, G. *Mon. Not. R. astr. Soc.* **239,** 195-200 (1989).
118. Sasaki, M. *Mon. Not. R. astr. Soc.* **240,** 415-420 (1989).
119. Kashlinsky, A. preprint (1990).
120. Martinez-Gonzalez, E. & Sanz, J. L. *Astrophys. J.* **347,** 11-15 (1989).
121. Mather, J. *et al. Astrophys. J. Lett.* (in the press).
122. Lacey, C. & Field, G. *Astrophys. J. Lett.* **330,** 1-4 (1988).
123. Peacock, J. A. & Heavens, A. F. *Mon. Not. R. astr. Soc.* **243,** 133-138 (1990).

ARTICLES

Sequence and expression of a metabotropic glutamate receptor

Masayuki Masu, Yasuto Tanabe, Kunihiro Tsuchida, Ryuichi Shigemoto* & Shigetada Nakanishi†

Institute for Immunology and * Department of Morphological Brain Science, Kyoto University Faculty of Medicine, Kyoto 606, Japan

The complementary DNA of a metabotropic glutamate receptor coupled to inositol phosphate/Ca^{2+} signal transduction has been cloned and characterized. This receptor shows no sequence similarity to conventional G protein-coupled receptors and has a unique structure with large hydrophilic sequences at both sides of seven putative membrane-spanning domains. Abundant expression of this messenger RNA is observed in neuronal cells in hippocampal dentate gyrus and CA2-3 and in cerebellar Purkinje cells, suggesting the importance of this receptor in specific hippocampal and cerebellar functions.

EXCITATORY amino-acid receptors, the main transmitter receptors mediating synaptic excitation in the mammalian central nervous system (CNS), play a crucial part in modification of the efficacy of synaptic transmission and in neuronal cell degeneration[1-4]. Hence this receptor family has become the focus of many investigations to elucidate the mechanisms of neuronal plasticity, cognitive processes, memory acquisition, learning, and some neurological disorders such as epilepsy, stroke and neurodegenerative diseases[1-4]. These receptors have been classified into four main subtypes on the basis of pharmacological and electrophysiological studies[1,2]: receptors for *N*-methyl-D-aspartate (NMDA), α-amino-3-hydroxy-5-methyl-4-isoxazole propionate (AMPA), kainate and 2-amino-4-phosphonobutyrate (AP4). They are thought to contain integral cation-specific ion channels and hence are called ionotropic receptors[1]. Complementary DNAs for AMPA/kainate receptors have recently been cloned and the receptors have been shown to be subtypes of the same family with ionotropic receptor structures[5,6].

Recently, an additional and novel glutamate receptor representing a fifth class has been identified by studies of brain slices and cultured cells and those of *Xenopus* oocytes injected with brain poly(A)$^+$ RNA (refs 4, 7, 8). This receptor is coupled to G protein(s) and stimulates the inositol phosphate/Ca^{2+} intracellular signalling pathway[4]. It also differs in agonist selectivity from the known ionotropic glutamate receptors and shares no antagonists with any other glutamate receptors[9]. Thus this receptor, termed the metabotropic glutamate receptor (mGluR), is different from the family of the ionotropic glutamate receptors both functionally and pharmacologically. The molecular characteristics of mGluR, however, have remained elusive. We report here the isolation of an mGluR cDNA clone, pmGR1, from a rat cerebellum cDNA library by applying a cloning approach involving the use of a *Xenopus* oocyte expression system combined with electrophysiology[10]. Our characterization of the cloned receptor indicated that it represents a metabotropic type of glutamate receptor coupled to the stimulation of inositol phosphate/Ca^{2+} second messenger. But the deduced amino-acid sequence of the cloned mGluR differs from the structural characteristics common to the family of known G protein-coupled receptors. This investigation provides evidence indicating the existence of a novel G protein-coupled receptor. The abundant expression of mGluR messenger RNA in neuronal cells in dentate gyrus and CA2-3 as well as in Purkinje cells is also revealed by *in situ* hybridization analysis, suggesting that this receptor is important in hippocampal and cerebellar functions.

Cloning and characterization of mGluR

For the isolation of a functional mGluR cDNA clone, a rat cerebellum cDNA library was constructed in an RNA expression vector from an mRNA fraction giving a high level of mGluR expression in *Xenopus* oocytes. A mixture of cDNA clones containing a functional mGluR cDNA clone was identified by testing for mGluR expression in oocytes after injection of the mRNAs synthesized *in vitro* from the cDNA mixtures. A single mGluR cDNA clone (λGEM-mGR1) was purified by serially subdividing the response-evoking cDNA mixture. The cDNA insert was excised from the λGEM-mGR1 and inserted into plasmid pBluescript (clone pmGR1).

Application of L-glutamate to an oocyte injected with mRNA derived from clone pmGR1 evoked a long-lasting current (Fig. 1*a*), which is characteristic of the response of receptors involved in intracellular metabolic processes[11]. Neither normal oocytes nor water-injected oocytes showed any response to application of glutamate. The properties of the cloned receptor and its involvement in intracellular signal transduction were investigated by a series of experiments in *Xenopus* oocytes injected with mGluR transcript synthesized *in vitro*.

Effects of glutamate on inositol phosphate formation were examined by measuring inositol 1,4,5-trisphosphate ($InsP_3$). This increased in the oocytes injected with mRNA after exposure to glutamate for 15 min, whereas no increase in $InsP_3$ formation was detected in noninjected oocytes (Fig. 1*b*). Consistent with the previous report of the agonist selectivity of mGluR (ref. 9), quisqualate and trans-1-aminocyclopentane-1,3-dicarboxylate (ACPD) elicited comparable stimulation of $InsP_3$ formation but NMDA or kainate failed to increase $InsP_3$ formation. Furthermore, the stimulation of $InsP_3$ formation was greatly reduced by pretreatment of the oocytes with pertussis toxin (PTX), indicating that glutamate responses are mediated by a PTX-

† To whom correspondence should be addressed.

sensitive G protein.

Effect of glutamate on intracellular Ca^{2+} mobilization was investigated by injection of a Ca^{2+} chelater, EGTA, in oocytes coinjected with mGluR mRNA and I_{SK} mRNA. I_{SK} is a membrane protein that induces a Ca^{2+}-independent potassium channel activity by membrane depolarization[12] and was used as a control to examine the possible nonspecific effect of EGTA on oocyte function. Intracellular injection of EGTA completely abolished glutamate response of mGluR but not a voltage-dependent potassium channel activity of I_{SK} (Fig. 1*c*), indicating that intracellular Ca^{2+} mobilization underlies the induction of electrophysiological response of mGluR.

Reversal potential of glutamate-inducing currents was approximately −22 mV in an ND96 bathing solution (Fig. 1*d*), which is in good agreement with an equilibrium potential of Cl^- in oocytes[11]. This reversal potential was shifted in accordance with the Nernst equation by alteration of external chloride concentration. Thus, activation of the cloned receptor results in increase in Cl^- conductance in *Xenopus* oocytes. These findings are consistent with the previous reports of mGluR characterized in oocytes injected with rat brain poly(A)$^+$ RNA (refs 8, 9) and demonstrate that the cloned mGluR activates a PTX-sensitive G protein, leading to stimulation of $InsP_3$ formation and intracellular Ca^{2+} mobilization. The subsequent effector in the *Xenopus* oocyte is a Ca^{2+}-dependent chloride channel[11] but it is possible that mGluR is coupled to different effectors in neuronal cells through the activation of $InsP_3/Ca^{2+}$ signal transduction.

The functional mGluR cDNA clone allows the precise characterization of an agonist profile of mGluR without any ambiguity due to cross-reactivity of multiple subtypes of the glutamate receptors. We therefore electrophysiologically determined the agonist selectivity of mGluR in *Xenopus* oocytes. Glutamate, quisqualate, ibotenate and ACPD were effective in inducing electrophysiological responses, and quisqualate was the most potent among the agonists analysed. The values of effective dose for half-maximal response (ED_{50}) of quisqualate, ibotenate, glutamate and ACPD were determined to be 2×10^{-7}, 6×10^{-6}, 9×10^{-6} and 5×10^{-5} M, respectively (Fig. 2). These values were in general agreement with the results found in oocytes injected with brain poly(A)$^+$ RNA (ref. 9). Also, L-aspartate, kainate, AMPA and AP4 displayed weak agonist properties (each applied at 1 mM), although these compounds were reported to be ineffective in poly(A)$^+$ RNA-injected oocytes[9]. Because the amplitudes of responses observed by these compounds were about two orders lower than that of glutamate (1 mM), the discrepancy between our result and the previous one[9] is probably due to the difference in sensitivity of the two systems using the cloned receptor transcript and brain poly(A)$^+$ RNA. No response was observed for NMDA (1 mM) in a Mg^{2+}-free solution supplemented with glycine (3 μM). The characterization of the agonist profile strongly indicates that the cloned receptor represents a metabotropic type of glutamate receptor indistinguishable from the one observed in oocytes injected with brain poly(A)$^+$ RNA (ref. 9).

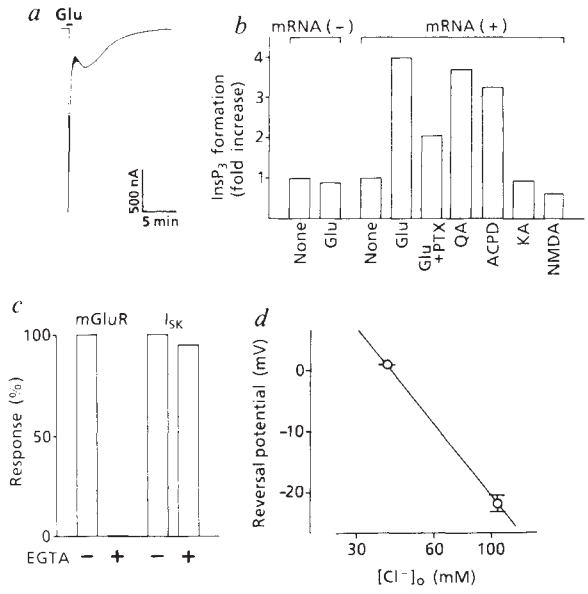

FIG. 1 Electrophysiological and biochemical characterization of the cloned mGluR in *Xenopus* oocytes. *a*, Current response to application of L-glutamate (1 mM) was recorded from an oocyte injected with the *in vitro* synthesized mGluR mRNA (5 ng) under voltage clamp at −60 mV. Downward deflection indicates inward current. *b*, Stimulation of $InsP_3$ formation is expressed as folds increase of $InsP_3$ levels in glutamate-untreated oocytes. The ligands applied (1 mM each) are as follows: glutamate (Glu), quisqualate (QA), ACPD, kainate (KA) and NMDA; Glu + PTX means glutamate exposure in PTX-treated oocytes. *c*, The mGluR and I_{SK} activities of oocytes injected with 10 mM EGTA (5–10 nl per oocyte) are compared to these activities of EGTA-uninjected oocytes. *d*, Reversal potentials of glutamate response are plotted against different chloride concentrations. The straight line has a slope of 54 mV per 10-fold change in $[Cl^-]_o$. Vertical lines represent s.e.m.

METHODS. The mGluR cDNA clone (pmGR1) was isolated as follows. Rat cerebellum poly(A)$^+$ RNA was subjected to centrifugation on sucrose density gradient[33] (5–25%). A fraction giving potent mGluR expression in *Xenopus* oocytes was electrophysiologically identified and was used for the subsequent construction of a cDNA library with λGEM-2 vector[10,33]. This library was divided into fractions, each containing approximately 2.8×10^4 cDNA clones. Each fraction was subjected to *in vitro* transcription by SP6 RNA polymerase in the presence of the capping nucleotide[33], followed by electrophysiological measurement of response to glutamate (1 mM) in oocytes injected with the *in vitro* synthesized mRNAs. A single mGluR cDNA clone (λGEM-mGR1) was obtained by repeating the *in vitro* mRNA syntheses and electrophysiological measurements after stepwise fractionation of the response-evoking cDNA mixture[33]. The *NheI-NotI* fragment containing the whole cDNA and its preceding SP6 promoter sequences was excised from the phage clone λGEM-mGR1 and inserted into pBluescript-II KS+ (pmGR1). Electrophysiological measurements for both mGluR and I_{SK} were carried out in a standard ND96 solution (96 mM NaCl, 2 mM KCl, 1.8 mM $CaCl_2$, 1 mM $MgCl_2$ and 5 mM HEPES pH 7.6). In *b*, oocytes were enzymatically defolliculated by collagenase treatment (2 mg ml^{-1}) for 1 h and then injected with the mRNA. A part of the mRNA-injected oocytes was pretreated with 2 μg ml^{-1} PTX for 24 h. Noninjected oocytes were also prepared as controls. $InsP_3$ levels were measured in duplicate, using an $InsP_3$-binding assay kit (Amersham) as described[34]. Each value was obtained from a group of 15 oocytes. In *c*, the mGluR and I_{SK} activities represent the mean of at least five sets of data. In *d*, reversal potentials were obtained from intersections of current-voltage curves at standard and low-chloride solutions; for the low-chloride solution, 64 mM Cl^- in the ND96 solution was replaced with the same concentration of *N*-methylglucamine.

Structure

The cDNA insert of clone pmGR1 was sequenced in both strands[13]. A large open reading frame of 3,597 base pairs was

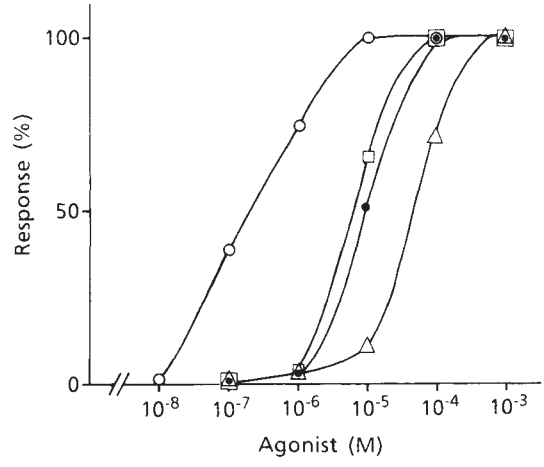

FIG. 2 Dose-response curves of the cloned mGluR for agonists. Current responses to serial application of different concentrations of agonists were recorded electrophysiologically in oocytes injected with the mGluR mRNA (5 ng). ○, quisqualate; □, ibotenate; ●, L-glutamate; △, ACPD. Each point represents the mean of at least three sets of data.

```
  CTCTGACCTGAGACCAATAGCTGTGTCTACCCGGACTCAGCGTCCAGCTCACCGCCACTAACGCGCCGCGCATTGGACACCTGATCCACACACCTTCGGGCACCAGTGAAAAACCGCG  -241
ACTTGATTTTCTGGAAGAACGCCCCCAGGGTGTGGGAGCGGTCGTGGAGGACCAGCAGGAGGAAGCGGAGGGGAGAGGGGCAGTAGTGGAGGCAGAGAAAGCGTTGAACCAGCTGTGTTG  -121
GCCGAAGGCACGAAACGGCAAAAGGCAGCGGTGAGCATCTGTGTGGTTCCCGCTGGGAACCTGCAGGCAGGACCGGCGTGGGAACGTGGCTGGCCCGCGGTGGACCGCGTCTTCGCCACA    -1
 1                SP                                                                                                          40
MetValArgLeuLeuLeuIlePhePheProMetIlePheLeuGluMetSerIleLeuProArgMetProAspArgLysValLeuLeuAlaGlyAlaSerSerGlnArgSerValAlaArg
ATGGTCCGGCTCCTCTTGATTTTCTTCCCAATGATCTTTTTGGAGATGTCCATTTTGCCCAGGATGCCTGACAGAAAAGTATTGCTGGCAGGTGCCTCGTCCCAGCGCTCCGTGGCGAGA  120
                                                                                                                            80
MetAspGlyAspValIleIleGlyAlaLeuPheSerValHisHisGlnProProAlaGluLysValProGluArgLysCysGlyGluIleArgGluGlnTyrGlyIleGlnArgValGlu
ATGGACGGAGATGTCATCATCGGAGCCCTCTTCTCAGTCCATCACCAGCCTCCAGCCGAGAAGGTACCCGAAAGGAAGTGTGGGGAGATCAGGGAACAGTATGGTATCCAGAGGGTGGAG  240
                                                                                                                           120
AlaMetPheHisThrLeuAspLysIleAsnAlaAspProValLeuLeuProAsnIleThrLeuGlySerGluIleArgAspSerCysTrpHisSerSerValAlaLeuGluGlnSerIle
GCCATGTTCCACACGTTGGATAAGATTAACGCGGACCCGGTGCTCCTGCCCAACATCACTCTGGGCAGTGAGATCCGGGACTCCTGCTGGCACTCTTCAGTGGCTCTCGAACAGAGCATC  360
                                                                                                                           160
GluPheIleArgAspSerLeuIleSerIleArgAspGluLysAspGlyLeuAsnArgCysLeuProAspGlyGlnThrLeuProProGlyArgThrLysLysProIleAlaGlyValIle
GAATTCATCAGAGACTCCCTGATTTCCATCCGAGATGAGAAGGATGGGCTGAACCGATGCCTGCCTGATGGCCAGACCCTGCCCCCTGGCAGGACTAAGAAGCCTATTGCTGGAGTGATC  480
                A                                                                                                          200
GlyProGlySerSerSerValAlaIleGlnValGlnAsnLeuLeuGlnLeuPheAspIleProGlnIleAlaTyrSerAlaThrSerIleAspLeuSerAspLysThrLeuTyrLysTyr
GGCCCTGGCTCCAGCTCTGTGGCCATTCAAGTCCAGAATCTTCTCCAGCTGTTCGACATCCCACAGATCGCCTATTCTGCCACAAGCATAGACCTGAGTGACAAAACTTTGTACAAATAC  600
                                                                                                                           240
PheLeuArgValValProSerAspThrLeuGlnAlaArgAlaMetLeuAspIleValLysArgTyrAsnTrpThrTyrValSerAlaValHisThrGluGlyAsnTyrGlyGluSerGly
TTCCTGAGGGTGGTCCCTTCTGACACTTTGCAGGCAAGGGCGATGCTCGACATAGTCAAGCGTTACAACTGGACCTATGTCTCAGCAGTCCACACAGAAGGGAATTACGGCGAGAGTGGA  720
                                                                                                                           280
MetAspAlaPheLysGluLeuAlaAlaGlnGluGlyLeuCysIleAlaHisSerAspLysIleTyrSerAsnAlaGlyGluLysSerPheAspArgLeuLeuArgLysLeuArgGluArg
ATGGATGCTTTCAAAGAACTGGCTGCCCAGGAAGGCCTCTGCATCGCACACTCGGACAAAATCTACAGCAATGCTGGCGAGAAGAGCTTTGACCGGCTCCTGCGTAAACTCCGGGAGCGG  840
                                                                                                                           320
LeuProLysAlaArgValValValCysPheCysGluGlyMetThrValArgGlyLeuLeuSerAlaMetArgArgLeuGlyValValGlyGluPheSerLeuIleGlySerAspGlyTrp
CTTCCCAAGGCCAGGGTTGTGGTCTGCTTCTGCGAGGGCATGACAGTGCGGGGCTTACTGAGTGCCATGCGCCGCCTGGGCGTCGTGGGCGAGTTCTCACTCATTGGAAGTGATGGATGG  960
                                                                                                                           360
AlaAspArgAspGluValIleGluGlyTyrGluValGluAlaAsnGlyGlyIleThrIleLysLeuGlnSerProGluValArgSerPheAspAspTyrPheLeuLysLeuArgLeuAsp
GCAGACAGAGATGAAGTCATCGAAGGCTATGAGGTGGAAGCCAACGGAGGGATCACAATAAAGCTTCAGTCTCCAGAGGTCAGGTCATTTGATGACTACTTCCTGAAGCTGAGGCTGGAC  1080
                                                                                                                           400
ThrAsnThrArgAsnProTrpPheProGluPheTrpGlnHisArgPheGlnCysArgLeuProGlyHisLeuLeuGluAsnProAsnPheLysLysValCysThrGlyAsnGluSerLeu
ACCAACACAAGGAATCCTTGGTTCCCTGAGTTCTGGCAACATCGCTTCCAGTGTCGCCTACCTGGACACCTCTTGGAAAACCCCAACTTTAAGAAAGTGTGCACAGGAAATGAAAGCTTG  1200
                                                                                                                           440
GluGluAsnTyrValGlnAspSerLysMetGlyPheValIleAsnAlaIleTyrAlaMetAlaHisGlyLeuGlnAsnMetHisHisAlaLeuCysProGlyHisValGlyLeuCysAsp
GAAGAAAACTATGTCCAGGACAGCAAAATGGGATTTGTCATCAATGCCATCTATGCCATGGCACATGGGCTGCAGAACATGCACCATGCTCTGTGTCCCGGCCATGTGGGCCTGTGTGAT  1320
                                                                                                                           480
AlaMetLysProIleAspGlyArgLysLeuLeuAspPheLeuIleLysSerSerPheValGlyValSerGlyGluGluValTrpPheAspGluLysGlyAspAlaProGlyArgTyrAsp
GCTATGAAACCCATTGATGGCAGGAAGCTCCTGGATTTCCTCATCAAATCCTCTTTTGTCGGAGTGTCTGGAGAGGAGGTGTGGTTCGATGAGAAGGGGGATGCTCCCGGAAGGTATGAC  1440
                                                                                                                           520
IleMetAsnLeuGlnTyrThrGluAlaAsnArgTyrAspTyrValHisValGlyThrTrpHisGluGlyValLeuAsnIleAspAspTyrLysIleGlnMetAsnLysSerGlyMetVal
ATTATGAATCTGCAGTACACAGAAGCTAATCGCTATGACTATGTCCACGTGGGGACCTGGCATGAAGGAGTGCTGAATATTGATGATTACAAAATCCAAATGAACAAAAGCGGAATGGTA  1560
                                                                                                                           560
ArgSerValCysSerGluProCysLeuLysGlyGlnIleLysValIleArgLysGlyGluValSerCysCysTrpIleCysThrAlaCysLysGluAsnGluPheValGlnAspGluPhe
CGATCTGTGTGCAGTGAGCCTTGCTTAAAGGGTCAGATTAAGGTCATACGGAAAGGAGAAGTGAGCTGCTGCTGGATCTGCACGGCCTGCAAAGAGAATGAGTTTGTGCAGGACGAGTTC  1680
                                                                                                                           600
ThrCysArgAlaCysAspLeuGlyTrpTrpProAsnAlaGluLeuThrGlyCysGluProIleProValArgTyrLeuGluTrpSerAspIleGluSerIleIleAlaIleAlaPheSer
ACCTGCAGAGCCTGTGACCTGGGGTGGTGGCCCAACGCAGAGCTCACAGGCTGTGAGCCCATTCCTGTCCGTTATCTTGAGTGGAGTGACATAGAATCTATCATAGCCATCGCCTTTTCT  1800
                I                                                                                                      II  640
CysLeuGlyIleLeuValThrLeuPheValThrLeuIlePheValLeuTyrArgAspThrProValValLysSerSerArgGluLeuCysTyrIleIleLeuAlaGlyIlePheLeu
TGCCTGGGCATCCTCGTGACGCTGTTTGTCACCCTCATCTTCGTTCTGTACCGGGACACACCCGTGGTCAAATCCTCCAGTAGGGAGCTCTGCTATATCATTCTGGCTGGTATTTTCCTC  1920
                                                                                                                           680
GlyTyrValCysProPheThrLeuIleAlaLysProThrThrThrSerCysTyrLeuGlnArgLeuLeuValGlyLeuSerSerAlaMetCysTyrSerAlaLeuValThrLysThrAsn
GGCTATGTGTGCCCTTTCACCCTCATCGCCAAACCTACTACCACATCCTGCTACCTCCAGCGCCTCCTAGTTGGCCTCTCTTCTGCCATGTGCTACTCTGCTTTAGTGACCAAAACCAAT  2040
                                                                                                                           720
ArgIleAlaArgIleLeuAlaGlySerLysLysLysIleCysThrArgLysProArgPheMetSerAlaTrpAlaGlnValIleIleAlaSerIleLeuIleSerValGlnLeuThrLeu
CGTATTGCACGCATCCTGGCTGGCAGCAAGAAGAAGATCTGCACCCGGAAGCCCAGATTCATGAGCGCTTGGGCCCAAGTGATCATAGCCTCCATTCTGATTAGTGTACAGCTAACACTA  2160
                                                                                                                           760
ValValThrLeuIleIleMetGluProProMetProIleLeuSerTyrProSerIleLysGluValTyrLeuIleCysAsnThrSerAsnLeuGlyValValAlaProValGlyTyrAsn
GTGGTGACCTTGATCATCATGGAGCCTCCCATGCCCATTTTGTCCTACCCGAGTATCAAGGAAGTCTACCTTATCTGCAATACCAGCAACCTGGGTGTAGTGGCCCCTGTGGGTTACAAT  2280
    V                                                                                                                      800
GlyLeuLeuIleMetSerCysThrTyrTyrAlaPheLysThrArgAsnValProAlaAsnPheAsnGluAlaLysTyrIleAlaPheThrMetTyrThrThrCysIleIleTrpLeuAla
GGACTCCTCATCATGAGCTGTACCTACTATGCCTTCAAGACCCGCAACGTGCCGGCCAACTTCAATGAGGCTAAATACATCGCCTTCACCATGTACACTACCTGCATCATCTGGCTGGCT  2400
                                                                                                                           840
PheValProIleTyrPheGlySerAsnTyrLysIleIleThrThrCysPheAlaValSerLeuSerValThrValAlaLeuGlyCysMetPheThrProLysMetTyrIleIleIleAla
TTCGTTCCCATTTACTTTGGGAGCAACTACAAGATCATCACTACCTGCTTCGCGGTGAGCCTCAGTGTGACGGTGGCCCTGGGGTGCATGTTTACTCCGAAGATGTACATCATCATTGCC  2520
                                                                                                                           880
LysProGluArgAsnValArgSerAlaPheThrThrSerAspValValArgMetHisValGlyAspGlyLysLeuProCysArgSerAsnThrPheLeuAsnIlePheArgArgLysLys
AAACCTGAGAGGAACGTCCGCAGTGCCTTCACGACCTCTGATGTTGTCCGCATGCACGTCGGTGATGGCAAACTGCCGTGCCGCTCCAACACCTTCCTCAACATTTTCCGGAGAAAGAAG  2640
                                                                                                                           920
ProGlyAlaGlyAsnAlaAsnSerAsnGlyLysSerValSerTrpSerGluProGlyGlyArgGlnAlaProLysGlyGlnHisValTrpGlnArgLeuSerValHisValLysThrAsn
CCCGGGGCAGGGAATGCCAATTCTAACGGCAAGTCTGTGTCATGGTCTGAACCAGGTGGAAGACAGGCGCCCAAGGGACAGCACGTGTGGCAGCGCCCTCTCTGTGCACGTGAAGACCAAC  2760
                                                                                                                           960
GluThrAlaCysAsnGlnThrAlaValIleLysProLeuThrLysSerTyrGlnGlySerGlyLysSerLeuThrPheSerAspAlaSerThrLysThrLeuTyrAsnValGluGluGlu
GAGACGGCCTGTAACCAAACAGCCGTAATCAAACCCCTCACTAAAAGTTACCAAGGCTCTGGCAAGAGCCTGACCTTTTCAGATGCCAGCACCAAGACCCTTTACAATGTGGAAGAAGAG  2880
                                                                                                                          1000
AspAsnThrProSerAlaHisPheSerProProSerSerProSerMetValValHisArgArgGlyProProValAlaThrThrProProLeuProProHisLeuThrAlaGluGluThr
GACAATACCCCTTCTGCTCACTTCAGCCCTCCCAGCAGCCCTTCTATGGTGGTGCACCGACGCGGGCCACCCGTGGCCACCACACCACCTCTGCCACCCCATCTGACCGCAGAAGAGACC  3000
                                                                                                                          1040
ProLeuPheLeuAlaAspSerValIleProLysGlyLeuProProProLeuProGlnGlnGlnProGlnGlnGlnProProProGlnGlnGlnProGlnGlnGlnProLysSerLeuMetAspGln
CCCCTGTTCCTGGCTGATTCCGTCATCCCCAAGGGCTTGCCTCCTCCTCTCCCGCAGCAGCAGCCACAGCAGCCGCCCCCTCAGCAGCCCCCGCAGCAGCCCAAGTCCCTGATGGACCAG  3120
                                                                                                                          1080
LeuGlnGlyValValThrAsnPheGlySerGlyIleProAspPheHisAlaValLeuAlaGlyProGlyThrProGlyAsnSerLeuArgSerLeuTyrProProProProProProGln
CTGCAAGGCGTAGTCACCAACTTCGGTTCGGGGATTCCAGATTTCCATGCGGTGCTGGCAGGCCCGGGGACACCAGGAAACAGCCTGCGCTCTCTGTACCCGCCCCCGCCTCCGCCGCAA  3240
                                                                                                                          1120
HisLeuGlnMetLeuProLeuHisLeuSerThrPheGlnGluGluSerIleSerProProGlyGluAspIleAspAspAspSerGlyArgPheLysLeuLeuGlnGluPheValTyrGlu
CACCTGCAGATGCTGCCCCTGCACCTGAGCACCTTCCAGGAGGAGTCCATCTCCCCTCCTGGGGAGGACATCGATGATGACAGTGAGAGATTCAAGCTCCTGCAGGAGTTCGTGTACGAG  3360
                                                                                                                          1160
ArgGluGlyAsnThrGluGluAspGluLeuGluGluGluGluAspLeuProThrAlaSerLysLeuThrProGluAspSerProAlaLeuThrProProSerProPheArgAspSerVal
CGCGAAGGGAACACCGAAGAAGATGAATTGGAAGAGGAGGAGGACCTGCCCACAGCCAGCAAGCTGACCCCTGAGGATTCTCCTGCCCTGACGCCTCCTTCTCCTTTCCGAGATTCCGTG  3480
                                                                                                                 1199
AlaSerGlySerSerValProSerSerProValSerGluSerValLeuCysThrProProAsnValThrTyrAlaSerValIleLeuArgAspTyrLysGlnSerSerSerThrLeu
GCCTCTGGCAGCTCAGTGCCCAGTTCCCCCGTATCTGAGTCGGTCCTCTGCACCCCTCCAAATGTGACCTACGCCTCTGTCATTCTGAGGGACTACAAGCAAAGCTCTTCCACCCTGTAG  3600
TGTGTGTGTGTGTGTGGGGGGGGGGGGGAGTGCGCATGGAGAAGCCAGAGATGCCAAGGAGTGTCAACCCTTCCAGAAATGTGTAGAAAGCAGGGTGAGGGATGGGGATGGAGGACCACG  3720
GTCTGCAGGGAAGAAAAAAAAAATGCTGCGGCTGCCTTAAAGAAGGAGAGGGACGATGCCAACTGAACAGTGGTCCTGGCCAGGATTGTGACTCTTGAATTATTCAAAAACCTTCTCTAG  3840
AAAGAAAGGGAATTATGACAAAGCACAATTCCATATGGTATGTAACTTTTATCGAAAAAAATAATAAAACGTAAAAATAAAATC                                      3924
```

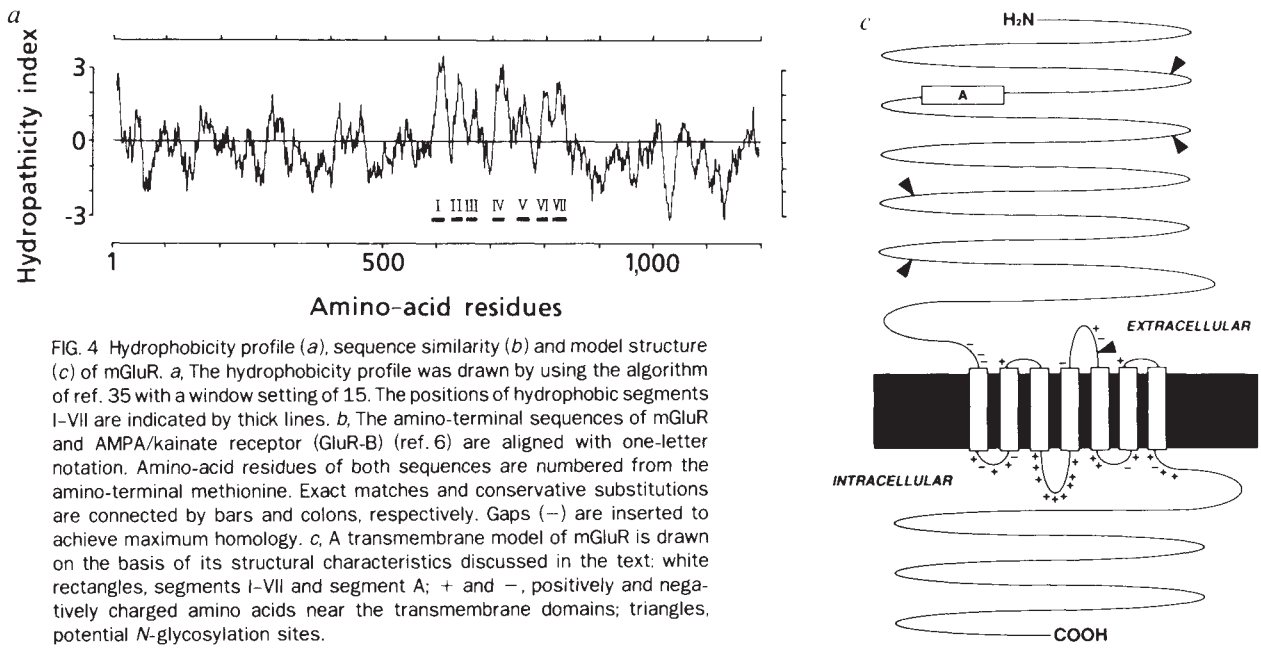

FIG. 4 Hydrophobicity profile (*a*), sequence similarity (*b*) and model structure (*c*) of mGluR. *a*, The hydrophobicity profile was drawn by using the algorithm of ref. 35 with a window setting of 15. The positions of hydrophobic segments I–VII are indicated by thick lines. *b*, The amino-terminal sequences of mGluR and AMPA/kainate receptor (GluR-B) (ref. 6) are aligned with one-letter notation. Amino-acid residues of both sequences are numbered from the amino-terminal methionine. Exact matches and conservative substitutions are connected by bars and colons, respectively. Gaps (–) are inserted to achieve maximum homology. *c*, A transmembrane model of mGluR is drawn on the basis of its structural characteristics discussed in the text: white rectangles, segments I–VII and segment A; + and –, positively and negatively charged amino acids near the transmembrane domains; triangles, potential *N*-glycosylation sites.

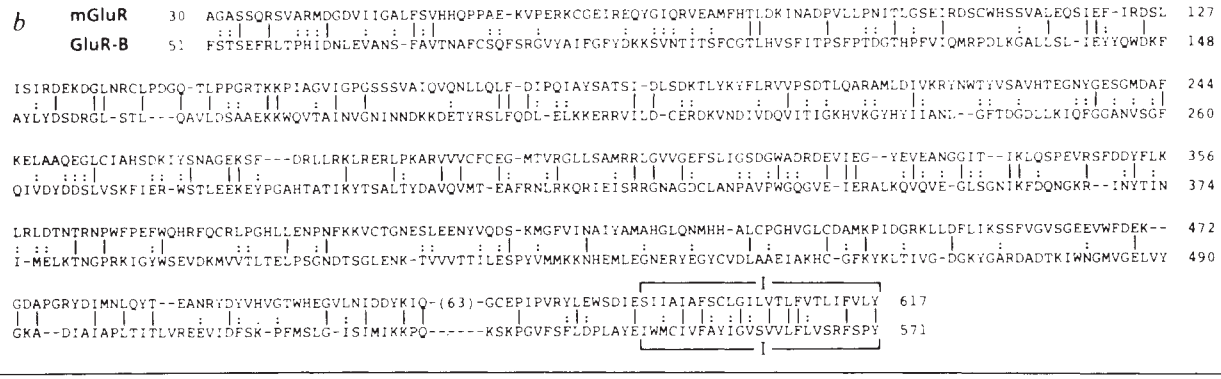

found within the total length of 4,282 base pairs (Fig. 3), and this frame was the only one without multiple termination codons. The nucleotide sequence surrounding the initiation codon agrees well with the consensus sequence[14]. The predicted polypeptide consists of 1,199 amino acids, with a calculated relative molecular mass of 133,229. This protein is thus considerably larger than the other members of G protein-coupled receptors[15,16]. Computer-aided sequence analysis revealed no overall homology to other protein sequences or to any members of the G protein-coupled receptors. A family of the G protein-coupled receptors possesses many conserved amino acids at mutually corresponding positions[15,16]. But almost none of these amino acids was found in the sequence of the mGluR. A hydrophobicity analysis showed that there are at least eight hydrophobic segments consisting of 20–25 uncharged amino-acid residues and two large hydrophilic sequences, one composed of roughly 570 amino-acid residues at the amino terminus and the other consisting of roughly 360 residues at the carboxy terminus (Figs 3 and 4*a*). All reported members of G protein-coupled receptors for large glycoprotein hormones have been shown to possess a large amino-terminal extracellular domain attached to seven membrane-spanning domains[17,18]. mGluR, like these glycoprotein receptors[18], shows clusters of cysteine residues in the amino-terminal sequence preceding the hydrophobic domains. But no example indicating the presence of a large amino-terminal sequence has been thus far reported for G protein-coupled receptors for small molecule neurotransmitters[15,16]. Thus, both the amino-acid sequence and the structural architecture of mGluR differ from those of the conventional G protein-coupled receptors.

The topology of the predicted mGluR protein is not easily deduced from its primary structure, which has no apparent sequence similarity to the other known proteins. Several structural characteristics of this protein can , however, be deduced from its sequence. (1) The amino terminus (residues 1–20) shows a characteristic feature of the signal peptide, including hydrophobicity and the presence of consecutive leucine residues[19]. This sequence may serve as a signal peptide, similar to the amino termini preceding the extracellular domains of glycoprotein hormone receptors[17,18]. The large hydrophilic amino-terminal sequence of mGluR is therefore likely to be extracellular. (2) There is a cluster of seven hydrophobic segments at about

◄ FIG. 3 The cDNA sequence for rat mGluR and its deduced amino-acid sequence. Seven hydrophobic segments (I to VII) and the sequence consisting of 24 consecutive uncharged amino-acid residues (segment A) are indicated by enclosures with solid lines and dashes, respectively; positions of segments I–VII were assigned on the basis of hydrophobicity analysis, and their termini were tentatively defined. Other lines and marks are as follows: solid line shown with SP, the predicted signal peptide; wavy lines, stretches of proline/glutamine and glutamic acid/aspartic acid residues; triangles, potential *N*-glycosylation sites[22]; stars, possible phosphorylation sites[23,24]; line below the nucleotide sequence, a possible polyadenylation signal.

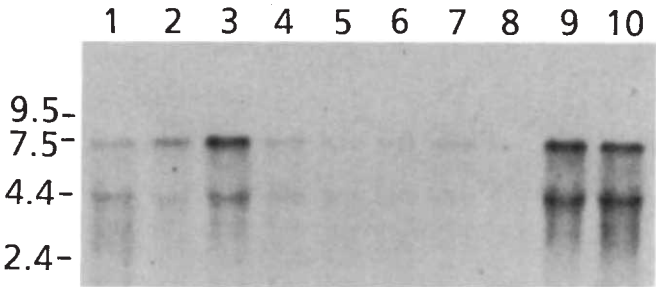

FIG. 5 RNA blot analysis of mGluR mRNA. Total RNAs (10 μg each) analysed[12] were as follows: 1, whole brain; 2, cortex; 3, hypothalamus; 4, midbrain; 5, striatum; 6, hippocampus; 7, medulla/pons; 8, spinal cord; 9, olfactory bulb; 10, cerebellum. The cDNA probe and size marker (kb) used were the 1,236 base pair *Pma*CI fragment of pmGR1 and the RNA ladder (BRL), respectively. Identical hybridization bands were also observed by two different cDNA probes (the 960-bp *Pvu*II-*Pma*CI and 1,088-bp *Pma*CI-*Xba*I fragments of pmGR1). The level of mGluR mRNA in the hypothalamus was high in this experiment, probably because of inclusion of a part of the thalamus in the hypothalamic preparation used.

two-thirds downstream from the amino terminus of this protein, and these hydrophobic segments probably represent seven membrane-spanning domains. (3) Around the seven putative membrane- spanning domains, positively charged residues predominate in the sequences between hydrophobic segments III and IV and between segments V and VI as well as in the sequence immediately following segment VII (for numbering of hydrophobic segments, see Fig. 3). There is deviation of charge distribution of amino acids in many integral membrane proteins, and positively charged amino acids generally prevail in the cytoplasmic region near the transmembrane domain[20]. The amino terminus and carboxy terminus of the seven putative transmembrane regions can thus be postulated to be located on the extracellular and cytoplasmic sides, respectively. (4) A more careful search of sequence similarity with related receptors revealed that there is some sequence similarity between the amino termini of mGluR and AMPA/kainate receptors (Fig. 4*b*). The observed sequence similarity is not convincingly high (exact matches, 16.7%; exact matches plus conserved substitutions, 36.0%) but it extends over the whole amino-terminal hydrophilic domain up to hydrophobic segment I. Also, two large regions between the two sequences (residues 235–372 and residues 473–617 of mGluR) were evaluated to be significantly homologous beyond the probability that the number of matches could have arisen by chance; this accident probability was calculated to be 1.2×10^{-5} by statistical analysis[21]. (5) There are several peculiar sequences comprising a stretch of proline/glutamine or glutamic acid/aspartic acid in the carboxy terminus of this protein (Fig. 3). Similar proline/glutamine-rich and glutamate/aspartate-rich sequences are observed in the cytoplasmic regions of adrenergic and muscarinic receptors[15]. On the basis of these structural characteristics, a tentative transmembrane model of mGluR has been constructed as illustrated in Fig. 4*c*. In this model, several potential sites of post-translational modification can be pointed out in this receptor: five consensus sites for *N*-glycosylation[22] in the extracellular

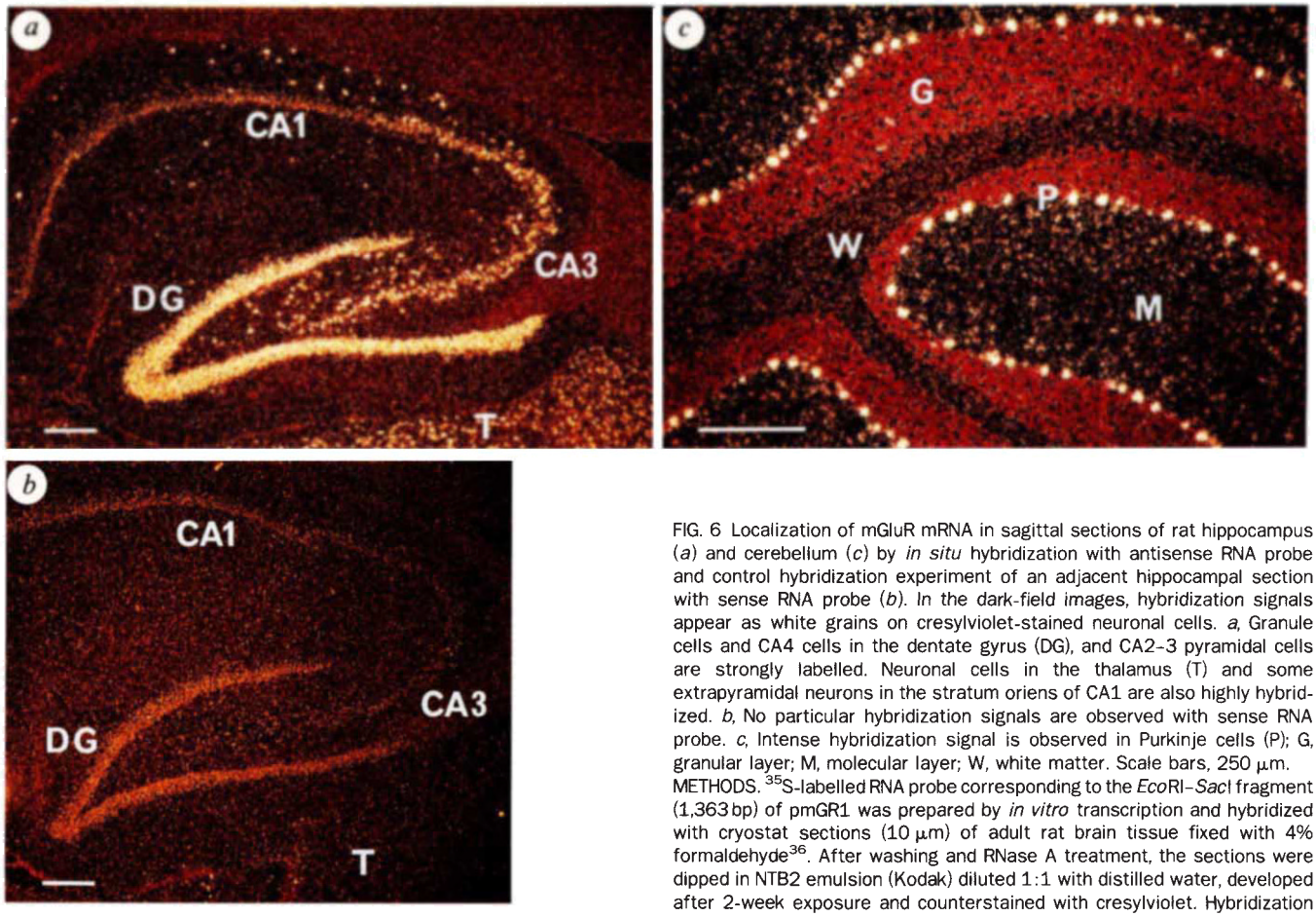

FIG. 6 Localization of mGluR mRNA in sagittal sections of rat hippocampus (*a*) and cerebellum (*c*) by *in situ* hybridization with antisense RNA probe and control hybridization experiment of an adjacent hippocampal section with sense RNA probe (*b*). In the dark-field images, hybridization signals appear as white grains on cresylviolet-stained neuronal cells. *a*, Granule cells and CA4 cells in the dentate gyrus (DG), and CA2-3 pyramidal cells are strongly labelled. Neuronal cells in the thalamus (T) and some extrapyramidal neurons in the stratum oriens of CA1 are also highly hybridized. *b*, No particular hybridization signals are observed with sense RNA probe. *c*, Intense hybridization signal is observed in Purkinje cells (P); G, granular layer; M, molecular layer; W, white matter. Scale bars, 250 μm.
METHODS. ^{35}S-labelled RNA probe corresponding to the *Eco*RI-*Sac*I fragment (1,363 bp) of pmGR1 was prepared by *in vitro* transcription and hybridized with cryostat sections (10 μm) of adult rat brain tissue fixed with 4% formaldehyde[36]. After washing and RNase A treatment, the sections were dipped in NTB2 emulsion (Kodak) diluted 1:1 with distilled water, developed after 2-week exposure and counterstained with cresylviolet. Hybridization patterns similar to those shown in (*a*) and (*c*) were observed with a different non-overlapping antisense RNA probe corresponding to the *Bgl*II-*Cla*I fragment (1,236 bp) of pmGR1.

domains (Asn 98, Asn 223, Asn 397, Asn 515 and Asn 747); and many serine and threonine residues for regulatory phosphorylation[23,24] in the cytopoasmic domains (Fig. 3). Three Asn-X-Thr sequences (Asn 920, Asn 925 and Asn 1,181), however, are present in the carboxy terminus of this protein, and there is a stretch of 24 consecutive uncharged amino acids (segment A in Fig. 3) in the hydrophilic amino-terminal region, although this sequence is not very hydrophobic. Thus, additional structural and biochemical evidence is necessary for the determination of the precise topology of this receptor, and the number and/or orientation of membrane crossings may change.

Expression of mGluR mRNA

RNA blot analysis and *in situ* hybridization were performed to examine the expression of mGluR mRNA in different brain regions. RNA blot analysis gave rise to two hybridization bands with estimated mRNA sizes of about 4.4 and 7.4 kb (Fig. 5). The two mRNAs are probably derived from the same mGluR gene because these bands remained by hybridization with different parts of the cDNA sequence under high-stringency conditions. The RNA blot analysis showed that mGluR is distributed throughout different brain regions and is the highest in the cerebellum and olfactory bulb. *In situ* hybridization revealed expression of mGluR mRNA in many neuronal cell groups in the CNS. Prominent expression of mGluR mRNA is observed in granule cells and CA4 cells in the hippocampal dentate gyrus, CA2-3 pyramidal cells (Fig. 6*a*), and cerebellar Purkinje cells (Fig. 6*c*). No particular hybridization signals are observed using sense RNA probes as a control (Fig. 6*b*). Interestingly, expression of mGluR mRNA in CA1 pyramidal cells is less than that in CA2-3 pyramidal cells; the number of grains per cell in CA1 pyramidal cells, when calculated under brightfield illumination, was about one-tenth of that in CA2-3 pyramidal cells (data not shown). The mRNA is also abundantly expressed in mitral and tufted cells in the olfactory bulb (data not shown) and most neuronal cells in the thalamic nuclei. The observed distribution of mGluR mRNA thus suggests that this receptor subtype may not only mediate many of the central actions of glutamate but also have an important role in hippocampal and cerebellar functions.

Discussion

This paper reports the cloning and characterization of a cDNA for a new glutamate receptor classified as a metabotropic receptor. The cloned mGluR is coupled to a G protein sensitive to PTX and results in stimulation of $InsP_3$ formation and intracellular Ca^{2+} mobilization. The signal transduction of mGluR thus seems to be similar to that of other G protein-coupled receptors linked to the inositol phosphate/Ca^{2+}-signalling pathway[15,16]. But mGluR has a unique structural architecture with large hydrophilic sequences in both amino- and carboxy-terminal sides of the seven putative transmembrane domains and shares no sequence similarity with other G protein-coupled receptors. This investigation thus demonstrates the existence of a novel class of G protein-coupled receptors. The large hydrophilic amino-terminal region, which has some sequence similarity to the AMPA/kainate receptors, may share a common evolutionary origin with the AMPA/kainate receptors and may be involved in glutamate binding. This region is, however, extremely large and could have additional regulatory functions other than glutamate binding. The hydrophilic carboxy-terminal domain also shows a unique sequence comprising stretches of some peculiar amino acids, and may be involved in additional or different signal transduction underlying a distinct function of mGluR in the CNS.

Numerous lines of evidence have indicated that glutamate receptors play a key part in many neuronal functions including neuronal plasticity and neurotoxicity in the CNS. Although the physiological importance of the ionotropic glutamate receptors has been emphasized[1-3], the role of metabotropic glutamate receptor in the CNS function has been reported only recently. Our *in situ*-hybridization analysis revealed prominent expression of mGluR mRNA in hippocampal and cerebellar neuronal cells known to be involved in evoking long-term potentiation (LTP)[25] and long-term depression (LTD)[26]. It has recently been reported that LTP in the mossy fibre-CA3 synapses as well as in the stratum radiatum-CA1 synapses are suppressed by PTX pretreatment of the hippocampus[27,28]. Interestingly, in the stratum radiatum-CA1 synapses, PTX has been suggested to act on presynaptic terminals which are mainly derived from pyramidal cells of CA3 (ref. 28). Furthermore, these hippocampal pyramidal cells are known to contain extremely high levels of phosphoinositide cycle elements such as $InsP_3$ receptor[29,30]. Similarly, the phosphoinositide cycle elements are considerably enriched in cerebellar Purkinje cells and are thought to be linked mainly to the metabotropic glutamate receptor in these cells[30,31]. Furthermore, LTD in the parallel fibre-Purkinje cell synapses is evoked by quisqualate, but not by NMDA (ref. 32), although it is not yet definite whether quisqualate-evoking LTD is mediated through the metabotropic or the ionotropic receptor. Thus this study, in conjunction with others, raises an intriguing question as to whether and, if so, how mGluR, in addition to ionotropic receptors, is involved in the central actions of glutamate such as LTP and LTD. The cloned mGluR cDNA should lead to a better understanding of the mechanisms and regulation of excitatory amino-acid receptors underlying the neuronal functions of the CNS. □

Received 12 November 1990; accepted 10 January 1991.

1. Monaghan, D. T., Bridges, R. J. & Cotman, C. W. *A. Rev. Pharmac. Tox.* **29,** 365-402 (1989).
2. Watkins, J. C., Krogsgaard-Larsen, P. & Honoré, T. *Trends pharmac. Sci.* **11,** 25-33 (1990).
3. Meldrum, B. & Garthwaite, J. *Trends pharmac. Sci.* **11,** 379-387 (1990).
4. Sladeczek, F., Récasens, M. & Bockaert, J. *Trends Neurosci.* **11,** 545-549 (1988).
5. Hollmann, M., O'Shea-Greenfield, A., Rogers, S. W. & Heinemann, S. *Nature* **342,** 643-648 (1989).
6. Keinänen, K. *et al. Science* **249,** 556-560 (1990).
7. Nicoletti, F., Iadarola, M. J., Wroblewski, J. T. & Costa, E. *Proc. natn. Acad. Sci. U.S.A.* **83,** 1931-1935 (1986).
8. Sugiyama, H., Ito, I. & Hirono, C. *Nature* **325,** 531-533 (1987).
9. Sugiyama, H., Ito, I. & Watanabe, M. *Neuron* **3,** 129-132 (1989).
10. Masu, Y. *et al. Nature* **329,** 836-838 (1987).
11. Dascal, N. *CRC crit. Rev. Biochem.* **22,** 317-387 (1987).
12. Takumi, T., Ohkubo, H. & Nakanishi, S. *Science* **242,** 1042-1045 (1988).
13. Sanger, F., Nicklen, S. & Coulson, A. R. *Proc. natn. Acad. Sci. U.S.A.* **74,** 5463-5467 (1977).
14. Kozak, M. *Nucleic Acids Res.* **15,** 8125-8148 (1987).
15. O'Dowd, B. F., Lefkowitz, R. J. & Caron, M. G. *A. Rev. Neurosci.* **12,** 67-83 (1989).
16. Nakanishi, S. *et al. Recent Prog. Hormone Res.* **46,** 59-84 (1990).
17. McFarland, K. C. *et al. Science* **245,** 494-499 (1989).
18. Sprengel, R. *et al. Molec. Endocr.* **4,** 525-530 (1990).
19. von Heijne, G. *Eur. J. Biochem.* **133,** 17-21 (1983).
20. Boyd, D. & Beckwith, J. *Cell* **62,** 1031-1033 (1990).
21. Kitamura, N. *et al. J. biol. Chem.* **260,** 8610-8617 (1985).
22. Hubbard, S. C. & Ivatt, R. J. *A. Rev. Biochem.* **50,** 555-583 (1981).
23. Kemp, B. E. & Pearson, R. B. *Trends biol. Sci.* **15,** 342-346 (1990).
24. Kishimoto, A. *et al. J. biol. Chem.* **260,** 12492-12499 (1985).
25. Nicoll, R. A., Kauer, J. A. & Malenka, R. C. *Neuron* **1,** 97-103 (1988).
26. Ito, M. *A. Rev. Neurosci.* **12,** 85-102 (1989).
27. Ito, I., Okada, D. & Sugiyama, H. *Neurosci. Lett.* **90,** 181-185 (1988).
28. Goh, J. W. & Pennefather, P. S. *Science* **244,** 980-983 (1989).
29. Hwang, P. M., Bredt, D. S. & Snyder, S. H. *Science* **249,** 802-804 (1990).
30. Ross, C. A., Bredt, D. & Snyder, S. H. *Trends Neurosci.* **13,** 216-222 (1990).
31. Furuichi, T. *et al. Nature* **342,** 32-38 (1989).
32. Kano, M. & Kato, M. *Nature* **325,** 276-279 (1987).
33. Yokota, Y. *et al. J. biol. Chem.* **264,** 17649-17652 (1989).
34. Varnold, R. L. & Smith, L. D. *Development* **109,** 597-604 (1990).
35. Kyte, J. & Doolittle, R. F. *J. molec. Biol.* **157,** 105-132 (1982).
36. Angerer, L. M., Cox, K. H. & Angerer, R. C. *Meth. Enzym.* **152,** 649-661 (1987).

ACKNOWLEDGEMENTS. We thank T. Miyata for statistical analysis of sequence homology. This work was supported by the Ministry of Education, Science and Culture of Japan. Sequence data has been deposited with the GeneBank/EMBL Data Bank.

Gravitational micro-lensing of the relativistic jets of quasars

Gopal-Krishna & Kandaswamy Subramanian

Tata Institute of Fundamental Research, PO Bag No. 3, Poona University Campus, Pune 411007, India

GRAVITATIONAL microlensing of quasars has been invoked to account for their observed optical variability[1–3]—the timescale being as short as a few years for microlenses the size of Jupiter moving at ~300 km s^{-1} (ref. 4). But some blazars (conspicuously active quasars) show ultra-rapid variability on timescales as short as 1 hour in the optical[5–7] and 1 day at centimetre wavelengths[8–11]. Blazars are known to contain relativistic jets directed within ~10° of the line of sight[12], and bright knots in these jets could appear to move superluminally with respect not only to the blazar nucleus but also to any galaxy near the line of sight. We argue here that any such superluminal motion[13], if microlensed by a star in an intervening galaxy, can produce the requisite ultra-rapid variations, even in the absence of intrinsic flux variations in the jet. Moreover, the same mechanism can naturally account for the commonly observed ~1-day variability of compact radio sources at centimetre wavelengths[14].

Consider a quasar at redshift $z = z_S$ ejecting a radiating 'blob' that moves from S to S′ with a velocity $\mathbf{v}$ in time t (Fig. 1). An intervening lensing galaxy centred at L ($z = z_L$) bends the light such that S and S′ are seen by the observer O along the lines OI and OI′. The vectors describing the positions of the source, $\mathbf{r}$, and the images, $\mathbf{x}$, are related by:

$$\mathbf{r} = \mathbf{x} + D\boldsymbol{\alpha}(\mathbf{x}) \tag{1}$$

where all the positions (distances) are projected onto the lens plane, unless stated otherwise. $\boldsymbol{\alpha}$ is the vectorial bending angle and $D = D_L D_{LS}/D_S$, with D_L, D_{LS} and D_S being, respectively, the lens, source-lens and source angular-diameter distances in the Robertson-Walker Universe. The projected separation between S and S′ $= \delta r_i = v_i t \sin\theta (D_L/D_S)$, and corresponds to an image displacement from I to I′ given by $\delta x_i = T_{ij}\delta r_j$, where T_{ij} is the inverse of the jacobian matrix $A_{ij} = \partial r_i/\partial x_j$. It can readily be shown that, according to the observer, the image moves with an apparent velocity $\mathbf{V}$ in the lens plane, given by

$$V_i = \frac{\delta x_i}{\delta t_{obs}} = \frac{T_{ij} v_j (D_L/D_S)\sin\theta}{(1+z_S)(1-(|\mathbf{v}|/c)\cos\theta)} \tag{2}$$

Here δt_{obs} is the difference between the arrival time of the signals emitted from S and S′ (at times 0 and t), as seen by the observer, and we have assumed that t is much greater than the extra differential time delay introduced by the lens. Equation (2) implies that as $|\mathbf{v}| \to c$, the image can move superluminally, both owing to the lensing action[15] ($T_{ij}v_j$) and the standard beaming effect[13,16,17].

The timescale, τ, for flux variability owing to the 'superluminal microlensing' is the time taken for the image to cross the region of high amplification associated with the microlens. Because the lens magnifies equally both the velocity $\mathbf{v}$ and the source along $\mathbf{v}$, the magnifying effect of the lens cancels out and we are left with:

$$\tau \approx \bar{d}_S \frac{(1-(|\mathbf{v}|/c)\cos\theta)(1+z_S)}{(D_L/D_S)\cdot|\mathbf{v}|\sin\theta} \tag{3}$$

Here $\bar{d}_S/2$ is the radius of the source (projected onto the lens plane). For significant amplification to occur, this radius should be smaller than the radius of influence, r_L, of the microlens:

$$r_L \approx (4GmD/c^2)^{1/2} \approx 10^{-2}(D/500\ \mathrm{Mpc})^{1/2}(m/M_\odot)^{1/2}\ \mathrm{pc} \tag{4}$$

where m is the mass of the microlens. Now τ is minimized when $\sin\theta = \gamma^{-1}$ where γ is the Lorentz factor $[1-(v/c^2)]^{-1/2}$. Thus,

$$\tau_{min} \sim \frac{d_S(1+z_S)}{\gamma c} = 0.8\left(\frac{d_S}{10^{15}\ \mathrm{cm}}\right)\left(\frac{\gamma}{10}\right)^{-1}(1+z_S)\ \mathrm{hours} \tag{5}$$

where d_S is the source diameter, $\bar{d}_S(D_S/D_L)$.

Note that this timescale is akin to the flux rise time, τ_R, computed by Schneider and Weiss[3] for arbitrary optical depths to microlensing, except for the additional factors that account for the apparent superluminal motion of the source (in fact, $\tau = 2\tau_R$). Further, the predicted time interval between the outbursts is of the same order as τ for optical depths >0.5 and source radii a few times smaller than r_L (ref. 3). Because such optical depths may be needed[18] for large amplifications, the light curve may exhibit a quasi-periodic variability on the timescale τ, as the source crosses the web of caustics formed by the effect of the high optical depth[3,19].

Finally, the observed flux density of a flat-spectrum source (such as most blazars) can be related to that measured in the emitter's frame, as:

$$S_{obs} \approx S_{em}\cdot A[(1+z_S)\gamma\{1-(v/c)\cos\theta\}]^{-3} \tag{6}$$

where $A = \sum_n |\det(T_{ij})|$, summed over all the microlensed images. In general, A includes amplification due to both the lensing galaxy and the microlenses.

It is clear, therefore, that the superluminal microlensing scheme allows the amplification of flux and velocity over and above that owing to beaming or lensing alone. Moreover, even an intrinsically non-varying source can seem, because of microlensing, to vary significantly on a short timescale, which is determined by the superluminal velocity of the image relative to the lens (but is independent of the amplification factor A). Thus, even with a modest $\gamma(\sim 5)$, a value of $\tau \sim 1$ hour can be obtained for optical emission, which is typically thought to originate from a region with an intrinsic size[20] of 10^{-3}–10^{-4} pc, probably coincident with the base of the blazar's relativistic jet[17,21]. This is consistent with the shortest microvariability timescales reported for BL Lac objects[5]. From equation (4), the microlenses should have $m \gtrsim 10^{-4} M_\odot$ and could therefore be planets or stars. Also, in this model, microlensing of radio-quiet quasars would not be expected to cause micro-variability

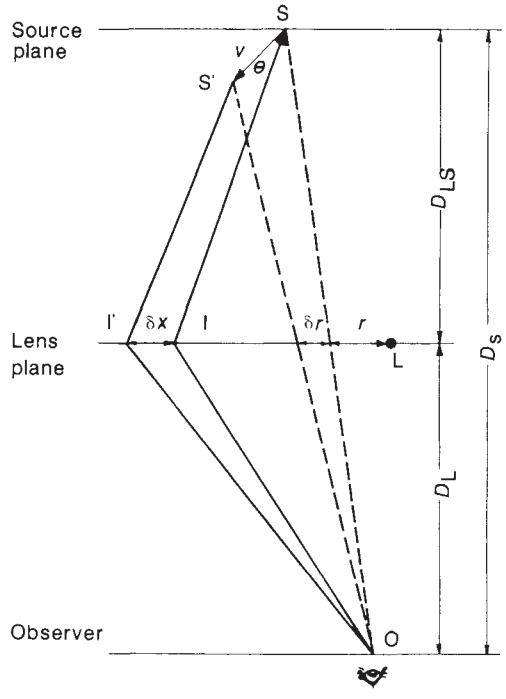

FIG. 1 A schematic diagram of a relativistically moving 'blob' emitted from a quasar being gravitationally lensed by an intervening massive body (see text.)

($\tau \lesssim 1$ h), if their emission mechanism does not involve bulk relativistic motion.

In the radio band, the brightness temperatures, T_b, inferred from the rapid variability ($\tau \sim 1$ day) of blazars at centimetre wavelengths ($\lambda < 6$ cm) are often known to greatly exceed the brightness temperature limit, $T_{max} \approx 10^{12}$ K set by the inverse Compton catastrophe[22,10]. This is explained in the standard beaming model[17] by postulating very large values of $\gamma(\sim 100)$[9,10] and a correspondingly small value of $\theta \sim \gamma^{-1} \ll 1°$, which allows a larger intrinsic source size than that inferred from causality. In our lensing-beaming model, we obtain a value for the source diameter

$$d_S \approx \frac{\gamma c \tau}{(1+z_S)} \approx \frac{10^{-2}}{(1+z_S)} \left(\frac{\gamma}{10}\right)\left(\frac{\tau}{1\ \text{day}}\right) \text{pc} \qquad (7)$$

which is identical to that obtained from the standard model. But because the lens is additionally amplifying the source flux, the excess of T_b over T_{max} can be partly credited to the lensing, lessening the demand on γ and θ, as we shall now see. For a flux variation, ΔS (typically ~ 0.1 Jy) of a flat-spectrum source, we obtain for the variable component:

$$T_b\,(\text{intrinsic}) = 3 \times 10^{17} \left[\left(\frac{\tau}{1\ \text{day}}\right)^{-2} \left(\frac{D_S}{1{,}170\ \text{Mpc}}\right)^{2} \left(\frac{\Delta S}{0.1\ \text{Jy}}\right) \times \left(\frac{\lambda}{6\ \text{cm}}\right)^{2} \left(\frac{1+z_S}{\gamma}\right)^{3} \frac{1}{A} \right] \lesssim 10^{12}\ \text{K} \qquad (8)$$

Taking $z_S = 1$, Hubble's constant $H_0 = 75$ km s^{-1} Mpc^{-1}, deceleration parameter $q_0 = 0.5$, then equation (8) implies a minimum value of $\gamma \approx 135$ in the absence of lensing ($A = 1$). In our model, however, the lens alone could produce an amplification of a factor of ~ 10 (see, for example, ref. 18), which gets further boosted by the microlensing, say by a factor of ~ 2. Thus, for $A \approx 20$, equation (8) gives $\gamma \approx 50$, as compared to $\gamma \approx 135$ for the standard beaming model.

An interesting constraint on the timescale, τ, of variability (induced by microlensing) arises from the above-mentioned considerations; namely that the source diameter $\bar{d}_S (\propto c\gamma\tau)$ should not exceed $2r_L$ (equation (4)), and that the intrinsic T_b inferred from τ and γ should be below $T_{max} (\sim 10^{12}$ K). Using equations (4), (7) and (8), the above two conditions translate to $m > K_1 \gamma^2 \tau^2$ and $\tau^2 \gamma^3 > K_2$, where K_1 and K_2 are constants derived from certain given values of z_S, A, λ, ΔS and T_{max}. Thus, $\tau <$ constant $\times\, m^{3/2}$. Evidently, the timescale for the microvariability would be maximized, in practice, for a critical mass m_* above which stars are exceedingly rare. Taking a clue from our Galaxy where $m_* \sim 2M_\odot$ (refs 23, 24), we get $\tau_{max} \sim 4$ days, corresponding to $\gamma \approx 28$ and a source size $d_S = 0.05$ pc, using typical values, $z_S = 1.0$, $z_L = 0.05$ (ref. 18), $\Delta S = 0.1$ Jy, as given above, and $\lambda = 10$ cm. Of course, timescales shorter than τ_{max} could arise via microlensing by lighter stars ($m < M_\odot$), of which there are plenty. But this would entail higher values of γ and correspondingly smaller values of $\theta (\sim \gamma^{-1})$ (see equation (8)), for which the probability shrinks rapidly. These countervailing trends indicate that timescales $\tau \sim \tau_{max}$ (a few days) are most likely to be detected at $\lambda \sim 10$ cm. Interestingly, evidence for such preferred daylike timescales has in fact been reported[14]. Another phenomenon that naturally follows from our model is the preferred association of rapid radio variability with the same sources every time they are looked at[9], as the variability is closely linked to the existence of a foreground lensing galaxy. Further, as mentioned earlier, a web of caustics[3,19] is likely to form for high optical depth, leading to quasi-periodic flux variations, as recorded for some radio sources[10].

In a popular model[21], the flux outbursts are primarily associated with transverse shocks propagating down the relativistic jet, which compress the turbulent magnetic field. Although this picture is supported by polarimetry results, from the very-long-baseline interferometry (VLBI)[25] of several blazars where the radio knots (identified with the shocks) show polarization vectors aligned with the parsec-scale jet, such an alignment has not been observed in quasar jets. Moreover, on the scales identified with the optically radiating base[17,21] of the same jet, the preferred alignment of the optical polarization vector with the radio jet is found to occur during the periods of inactivity, rather than during the outbursts (see ref. 26). Note that it is these inner scales that are more relevant to our microlensing model. Furthermore, it is not obvious how the observed preferred timescales for radio variability would naturally arise in such intrinsic models.

We now consider our beaming-lensing model from a statistical viewpoint. First, we emphasize that by considering core-dominated radio sources, we are pre-selecting the ones with jets pointing nearly towards us ($\theta \lesssim 10°$), whose detection has been strongly favoured because of the large amplification bias caused by Doppler boosting[12]. One should ask what fraction of these would be microlensed, taking into account the effect of amplification bias resulting from the microlensing. Following Tyson[27], but using his latest deep galaxy counts[28] (150 galaxies/(arcmin)^2 above $m_R = 26$), the probability of finding a galaxy within 1-2 arcsec of a compact radio source (with typical $z > 1$) is ~ 0.3. Some fraction, f, of these closely aligned galaxies could lie at appropriate redshifts and therefore act as lenses with high optical depth ($\gtrsim 0.5$) for microlensing. For such optical depths, taking a slope of -2.5 for the logarithmic differential counts of strong flat-spectrum radio sources[29], the number density of sources in the vicinity of the lens is expected to be enhanced by a factor of ~ 4 due to the amplification bias[3]. It follows that a fraction $\sim 1.2f$ of all the sources could be microlensed. This may well be significant for reasonable values of $f(\sim 0.1)$ as inferred from the models for explaining the faint galaxy counts[24] and direct spectroscopy[30], which indicates that even for faint galaxies (B magnitude of 24), the median redshift is only 0.4. On the observational side, several lens candidates in the directions of blazars have already been reported[31]. In fact, it has been proposed[18] that some BL Lac objects may result from microlensing of distant optically violent variable quasars.

Considering some other potential ramifications of our model, we note that as the variable compact component may well be polarized differently from the underlying, relatively steady emission, the net polarization can be expected to vary rapidly due to the superluminal microlensing, as reported in some optical[7] and radio[10] studies. Second, although microlensing is inherently achromatic, frequency-dependent variability could arise because source structure may itelf vary with wavelength, for example as a result of opacity effects, like that seen in the VLBI images of 3C273 on sub-milliarcsecond scales[32]. But in the best studied source showing short-timescale radio variability, namely 0917+624 (refs 9,10), the intensity extrema are broadly coincident[33] over the wavelength range 2-20 cm, consistent with the microlensing picture. Finally, the superluminal effects can similarly be invoked to interpret the observed timescales of metre-wavelength variability (a few years)[34] of compact radio sources in terms of refractive scintillations caused by intervening plasma irregularities located at intergalactic distances, possibly associated with cooling flows in clusters of galaxies[35]. □

Received 6 September; accepted 19 December 1990.

1. Chang, K. & Refsdal, S. *Nature* **282**, 561-564 (1979).
2. Narasimha, D., Subramanian, K. & Chitre, S. M. *Mon. Not. R. astr. Soc.* **210**, 79-88 (1984).
3. Schneider, P. & Weiss, A. *Astr. Astrophys.* **171**, 49-65 (1987).
4. Gott, J. R. *Astrophys. J.* **243**, 140-146 (1981).
5. Miller, H. R., Carini, M. T. & Goodrich, B. D. *Nature* **337**, 627-629 (1989).
6. Kidger, M. R. & de Diego, J. A. *Astr. Astrophys.* **227**, L25-L28 (1990).
7. Kulshreshtha, A. K., Joshi, U. C. & Deshpande, M. R. *Nature* **311**, 733-734 (1984).
8. Epstein, E. E., Landau, R. & Rather, J. D. G. *Astr. J.* **85**, 1427-1433 (1980).
9. Quirrenbach, A. *et al. Nature* **337**, 442-444 (1989).
10. Quirrenbach, A. *et al. Astr. Astrophys.* **226**, L1-L4 (1989).
11. Signal, A. K. & Gopal-Krishna *Mon. Not. R. astr. Soc.* **215**, 383-393 (1985).

12. Blandford, R. D. & Rees, M. J. in *Pittsburgh Conf. BL Lac Objects* (ed. Wolfe, A. M.) 328 (Univ. of Pittsburg, 1978).
13. Rees, M. J. *Mon. Not. astr. Soc.* **135,** 345–360 (1967).
14. Heeschen, D. S., Krichbaum, Th., Shalinski, C. J. & Witzel, A. *Astr. J.* **94,** 1493–1507 (1987).
15. Chitre, S. M. & Narlikar, J. V. *Mon. Not. R. astr. Soc.* **187,** 655–659 (1979).
16. Scheuer, P. A. G. & Readhead, A. C. S. *Nature* **277,** 182–185 (1979).
17. Blandford, R. D. & Konigl, A. *Astrophys J.* **232,** 34–48 (1979).
18. Ostriker, J. P. & Vietri, M. *Nature* **344,** 45–47 (1990).
19. Wambsganss, J., Paczynski, B. & Katz, N. *Astrophys. J.* **352,** 407–412 (1990).
20. Impey, C. *Mon. Not. R. astr. Soc.* **209,** 245–269 (1984).
21. Marscher, A. P. & Gear, W. K. *Astrophys. J.* **298,** 114–127 (1985).
22. Kellermann, K. I. & Pauling-Toth, I. I. K. *A. Rev. Astr. Astrophys.* **19,** 373–410 (1981).
23. Scalo, J. M. *Fund. Cosmic Phys.* **11,** 1–278 (1986).
24. Guiderdoni, B. & Rocca-Volmerange, B. *Astr. Astrophys.* **227,** 362–378 (1990).
25. Gabudza, D. L., Cawthorne, T. V., Roberts, D. H. & Wardle, J. F. C. *Astrophys. J.* **347,** 701–712 (1989).
26. Sikora, M., Zbyszewska, M. & Begelman, M. C. in *BL Lac Objects* (eds Maraschi, L., Maccacaro, T. & Ulrich, M. H.) 381–387 (Springer, Berlin, 1989).
27. Tyson, J. A. *Astrophys. J.* **272,** L41–L44 (1983).
28. Tyson, J. A. & Seitzer, P. *Astrophys. J.* **335,** 552–583 (1988).
29. Pauliny-Toth, I. I. K. *et al. Astr. J.* **83,** 451–474 (1978).
30. Cowie, L. L. & Gardner, J. *Astrophys. J. Suppl. Ser.* (in the press).
31. Falomo, R., Melnick, J. & Tanzi, E. G. *Nature* **345,** 692–694 (1990).
32. Zensus, J. A., Unwin, S. C., Cohen, M. H. & Biretta, J. A. *Astr. J.* **100,** 1777–1784 (1990).
33. Quian, S. J. *et al.* Preprint no. 405, Max-Planck Institut für Radioastronomie (1990).
34. Spangler, S., Fanti, R., Gregorini, L. & Padrielle, L. *Astr. Astrophys.* **209,** 315–326 (1989).
35. Gopal-Krishna *Current Sci.* (in the press).

ACKNOWLEDGEMENTS. We thank R. Nityananda, S. M. Chitre, G. Swarup and P. J. Wiita for their comments.

New measurement of solar gravitational deflection of radio signals using VLBI

D. S. Robertson, W. E. Carter & W. H. Dillinger

Laboratory for Geosciences, Office of Ocean and Earth Sciences, National Oceanic and Atmospheric Administration, Rockville, Maryland 20852, USA

RADIO observations using very-long-baseline interferometry (VLBI) can measure the deflection of electromagnetic radiation by the Sun's gravitational field with an accuracy of better than 1 milliarcsecond, and can thus be used to test General Relativity. For an object at an angle α from the centre of the Sun, the expected deflection is[1] $(1+\gamma)\,(M_s/r_e)((1+\cos\alpha)/(1-\cos\alpha))^{1/2}$, where M_s is the mass of the Sun in geometrized units[2] (1.477×10^5 cm), r_e is the distance from the Earth to the Sun in cm, and γ is a parameter whose value is 1 if General Relativity is correct but which takes on different values in other theories of gravity. For $\gamma=1$, the deflection is 1,750 mas at the Sun's limb, 4 mas at $\alpha=90°$ and 0 at $\alpha=180°$. Our analysis of ten years of VLBI data, including observations of objects in the range $2.5°<\alpha<178°$, yields an estimate $\gamma=1.0002$ with a formal standard error of 0.00096 and an estimated standard error of 0.002. This determination is comparable in accuracy and in good agreement with the determination from Mars–Viking time-delay measurements[3].

In the late 1960s Shapiro[4,5] recognized that VLBI measurements of the relativistic deflection of signals from extragalactic radio sources by the gravity field of the Sun could potentially yield an accurate estimate of γ. The National Oceanic and Atmospheric Administration's POLARIS and IRIS projects[6] and the National Aeronautic and Space Administration's Crustal Dynamics Project (CDP)[7] produce large sets of VLBI observations having the requisite angular resolution and broad distribution of Sun angles required to estimate γ. Figure 1 shows the expected changes in gravitational deflection during the solar year (calculated for $\gamma=1$) for the radio sources that are presently in the IRIS observing schedules.

We have analysed a set of 342,810 group-delay observations from the POLARIS, IRIS and CDP projects. The data include observations of 74 radio sources collected by 29 VLBI observatories between 1980 and 1990. All of the observations were made with the Mark-III VLBI system[8]. Two observing frequencies (X- and S-band) were used to eliminate the refractive effects of charged particles (both in the solar corona and in the Earth's ionosphere) along the line of sight to the radio sources. The distribution of observations as a function of Sun angle is shown in Fig. 2, along with a smooth curve showing the theoretical deflection. A total of 214 observations were obtained within three degrees of the Sun, where the deflection is larger than 155 mas, and an additional 592 observations were within six degrees, where the deflection is larger than 77 mas.

Scintillations in the solar corona degrade the signal for sources close to the sun, reducing the signal-to-noise ratio (SNR) of the VLBI delay determinations. For example, when OJ287 changes from a Sun angle of 37.5° to 2.6°, its SNR at S-band on the Ft Davis–Wettzell baseline drops from ~35 to ~12, whereas at X-band the drop is from ~100 to ~75. Fortunately, the S-band noise contributes only at the 10% level to the combined S–X observable, and the total noise is commonly dominated by effects such as unmodelled atmosphere refraction. The primary effect of the decreased SNR is to place a practical limit on how close to the Sun we can make observations.

In 1984 we reported a determination of γ (based on a subset of the data reported here) that was about an order of magnitude poorer[9]. Improvements in the current solution include a larger set of more accurate observations of a better optimized set of sources. The accuracy of the determination of γ scales roughly with the length of the baseline, and our earlier determination was dominated by observations that used the 3,000-km baseline from Westford, Massachusetts to Fort Davis, Texas. By contrast, much of the new data involves baselines in the range of 7,000–10,000 km. Thirty-one of the present observations that are within 3° of the Sun were made with baselines >7,500 km. Also, observations of the radio sources 3C273B and 3C279 were deleted from our current solution because of their large and variable brightness structure. Significant improvements have also been made in the data-processing software, including improved modelling of atmospheric refraction, adjustment of tectonic plate-motion velocities, and adjustments to the Earth tide Love numbers.

In addition, T. A. Herring and I. I. Shapiro (personal communication) pointed out that in ref. 9 we had underestimated the effect of errors in the nutation series used at the time, and of errors in the relativistic model used to calculate the theoretical delays. These problems corrupted the estimates of γ at the level

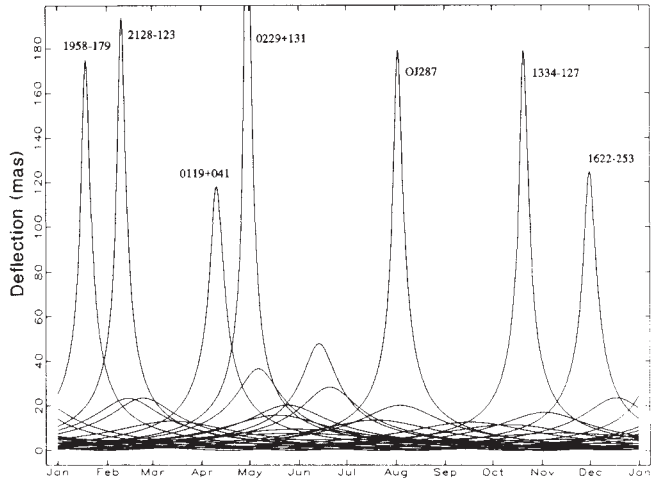

FIG. 1 Relativistic deflection in mas for the 26 sources that are currently observed in the IRIS programme. Seven sources give peaks larger than 100 mas. The sources in the Southern Hemisphere have relatively few observations because regular VLBI observations have only recently begun there. 0229+131, whose peak (>300 mas) is off scale, has not been successfully observed for deflections larger than 137 mas.

TABLE 1 Error budget

1	Formal error	0.96
2	Atmospheric refraction	0.64
3	Nutation	0.78
4	Earth orientation	0.28
5	Source structure	0.64
6	Love number *h*	0.02
7	Love number *l*	0.19
8	Tectonic displacement	0.11
9	Ocean loading	0.27
10	Barometric loading	0.54
11	Antenna deformation	0.21
12	Theoretical model error	0.01
	Root-sum-square total	1.70

Units are 0.001 times γ.

of about twice the quoted formal error. To correct these problems, the present solution uses theoretical calculations of interferometric group delays computed using an algorithm developed by Shapiro[10,11] (see also Herring[12] and Ryan[13]), which includes the effect of the gravity field of the Earth as well as that of the Sun. This algorithm yields estimates of theoretical delays to within 2 picoseconds (<1 mm equivalent path length) of the algorithm developed by Hellings[14], when gravitational effects on the radio-wave propagation in the vicinity of the Earth are added to the latter. The nutation errors are dealt with by solving for daily offsets to the nutation series.

The parameters estimated in the least-squares solution for γ include the positions and velocities of the VLBI observatories, the coordinates of the radio sources, pole position, UT1 and nutation offsets for each 24-h observing session, clock polynomial coefficients, Earth tide Love numbers (h and l), and the coefficients of a continuous, piecewise linear model for the atmosphere refractivity at zenith, with rate breaks every half-hour. The atmosphere rate breaks were constrained with a 1σ *a priori* constraint of 50 ps h^{-1}.

Estimates for the error contributions from a variety of sources calculated from a series of numerical experiments are given in Table 1. To estimate the atmospheric refraction error, a dozen different estimates of γ were produced with different piecewise linear atmosphere models. The interval between the atmosphere rate breaks was varied from 0.5–2 h, and the rate constraints were varied from 25 ps h^{-1} to 75 ps h^{-1}. The atmosphere uncertainty shown in line two of Table 1 represents the r.m.s. variation of those solutions.

The nutation error was estimated from a solution using the IAU 1984 model, which is known to have an error in the annual term of ~2 mas. The estimate for γ changed by 0.0039. The formal errors for the adjusted nutation parameters are in the range of 0.2 mas, so we have scaled the estimate for the remaining nutation error by about twice this amount or ~20% of the adjustment found in this test.

The Earth rotation error was estimated by fixing the pole positions at values obtained from satellite laser ranging, whose errors have been shown to be no worse than 2 mas[15]. The estimate for γ changed by 0.00056. As the formal errors of the determinations of VLBI pole position are in the range of 0.5 mas, we have scaled the estimate for the pole position error by twice the formal error, or 50% of the adjustment found in this test.

The estimate of the source-structure error was derived by comparing solutions with and without observations of 3C273B as it is known to have time-variable structure at the level of ~3–4 mas[16–20]. The estimated value for γ changed by 0.0021. In contrast, most of the other sources in our observing schedule, including the sources that pass close to the Sun, such as OJ287, have much smaller structures, of the order of 1 mas or less. We therefore estimate the structure effects from these sources to be ~30% of the effect for 3C273B.

The error estimates for the Love numbers, h and l, were calculated by estimating numerically the derivative of the estimate of γ, with respect to these parameters by varying each Love number in successive least-squares solutions. The resulting derivatives were multiplied by twice the 1σ formal errors of the estimates of h and l in our standard solution.

The errors due to tectonic displacement of the stations were estimated by deleting the station velocity parameters from the standard solution (that is, by fixing the station velocities at the values from the International Earth Rotation Service (IERS) standard AM0-2 plate motion model[21]). The estimate for γ changed by only 0.00011. Removing the AM0-2 velocities, that is, fixing the station velocities at zero, changed the estimate for γ by only 0.00008.

The theoretical calculations in the solution for γ included the IERS standard ocean-loading model[21]. The uncertainties in this model are not well known. With this model removed from the solution, the estimated value for γ changed by 0.00054. Assuming that the errors in the ocean-loading model are possibly as large as 50%, we have scaled this difference by 0.5 when estimating the possible error in γ.

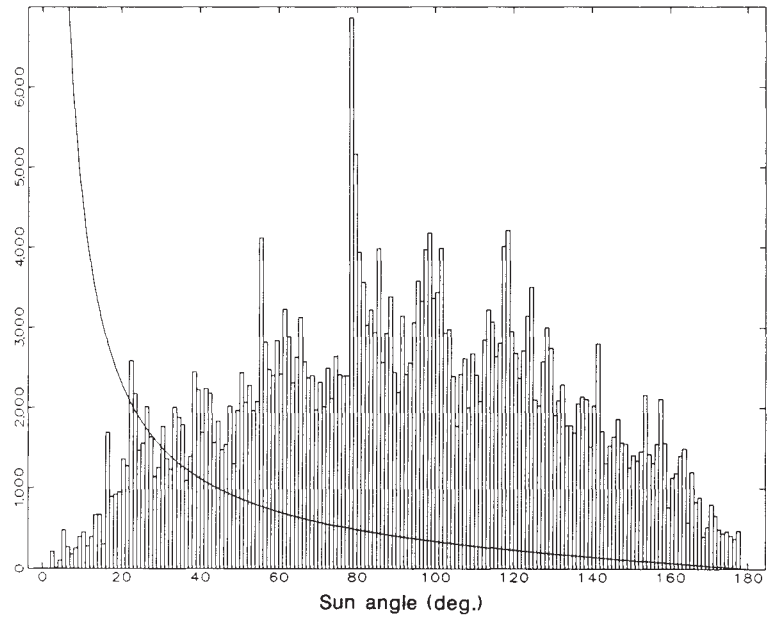

FIG. 2 Histogram showing the Sun-angle distribution of the VLBI observations, in degrees. The smooth curve shows the expected deflection of the source position in units of 0.01 mas, calculated for $\gamma=1$. The closest observation to the Sun was made at a distance of 2.534 degrees with the radio source 2128−123, observed with the 7832-km baseline from Wettzell (Germany) to Hartebeesthoek (South Africa) on 9 February 1987. The deflection for this observation was about 184 mas. Other sources that were successfully observed close to the Sun include OJ287 at 2.601 degrees, 1958−179 at 2.789 degrees and 0229+131 at 3.411 degrees.

The remaining three entries in Table 1 are much rougher estimates than the preceding quantities, because, at present, we lack the software to model these effects. We have estimated these errors by scaling from the magnitude of the ocean-loading effects calculated above. For example, the effects of barometric loading of the atmosphere on the station positions are believed to be ~2.5 cm in the vertical, which is comparable to the magnitude of the ocean loading effects[22,23]. We therefore estimate the error from neglecting this effect to be comparable to neglecting the ocean-loading altogether. Antenna deformation is believed to be in the range of 1 cm or less, and its effects here have been calculated by scaling the ocean-loading effects down to 1 cm. The calculation of the theoretical model error is based on the 2 ps differences between Shapiro's and Hellings's derivations.

Summing (in a r.m.s. sense) the various error components in Table 1 yields an uncertainty in γ of 0.0017; making further allowance for errors that have not been accounted for, we feel that a reasonable error estimate for this estimate of γ should be in the range of 0.002.

The measurements made use of here were collected for e research programmes unrelated to the study of relativity, programmes which are expected to continue at least another decade. For this reason alone we can expect the determination of γ to improve with time. In addition, future observations are expected to be more accurate as a result of both technological and operational improvements in the VLBI measurement programs. Anticipated improvements in instrumentation include double-spanned bandwidth, an eightfold increase in the recorded bandwidth and improved delay- and phase-calibration equipment (A. R. Whitney, A. E. E. Rogers and T. A. Clark, personal communication). Improvements in atmosphere modelling using increased coverage of low-elevation observations should improve the overall accuracy of the determinations[24,25]. Two Southern Hemisphere radio sources that are not currently included in our routine observing programmes (2128 − 123 and 1958 − 179), which are strong enough to produce good data at small Sun angles, are currently being added to the IRIS observing programme[6]. New observing stations, especially in the Southern Hemisphere[26], will increase the number of measurements and improve their distribution in the sky. The next sunspot minimum should be accompanied by reduced solar corona activity, allowing observations closer to the solar limb.

We therefore conclude that in another decade, improvements in the determination of γ by a factor of 2 to 5 seem inevitable, and a full order of magnitude is not impossible. Of course, at some point, subtle systematic errors such as atmospheric refraction errors or unmodelled barometric pressure loading will begin to dominate the statistical errors. At that point, further improvements in the determination of γ will depend critically on improvements in our ability to model these systematic effects. □

Received 5 September; accepted 20 December 1990.

1. Misner, C. W. *et al. Gravitation* 1103 (Freeman, San Francisco, 1973).
2. Misner, C. W. *et al. Gravitation* 36 (Freeman, San Francisco, 1973).
3. Reasenberg, R. D. *et al. Astrophys J.* **234,** L219–L221, (1979).
4. Shapiro, I. I. *Science* **157,** 806–808 (1967).
5. Shapiro, I. I. & Knight, C. A. in *Earthquake Displacement Fields and the Rotation of the Earth* (eds Mansinha, L., Smylie, D. E. & Beck, A. E.) 285–301 (Reidel, Dordrecht, 1970).
6. Carter, W. E. *et al. J. geophys. Res.* **90,** 4577–4587 (1985).
7. Coates, R. J. *et al. IEEE Trans. Geosci. Remote Sens.* **GE23,** No. 4, 360–368 (1985).
8. Rogers, A. E. E. *et al. Science* **219,** 51–54 (1983).
9. Robertson, D. S. & Carter, W. E. *Nature* **310,** 572–574 (1984).
10. Shapiro, I. I. *Relativistic Corrections to the Delay Observable* Int. Memo. 1–24 (Harvard/Smithsonian Center for Astrophysics, Cambridge, 1983).
11. Shapiro, I. I. *Relativistic Delay of Signal from Source Due to Gravitational Potential of the Earth* Int. Memo. 3–1 (Harvard/Smithsonian Center for Astrophysics, Cambridge, 1983).
12. Herring, T. A. *General Relativity Delay Expression* Int. Memo. 1–30 (Harvard/Smithsonian Center for Astrophysics, Cambridge, 1989).
13. Ryan, J. *CALC-7.0 Release Document* Internal Memo 12–16 (NASA Goddard Space Flight Center, Greenbelt, 1989).
14. Hellings, R. W. *Astr. J.* **91,** 650–659 (1986); *Erratum Astr. J.* **92,** 1446 (1986).
15. Robertson, D. S. *et al. Science* **229,** 1259–1261 (1985).
16. Biretta, J. A. *et al. Astrophys. J.* **292,** L5–L8 (1985).
17. Unwin, S. C. *et al. Astrophys. J.* **289,** 109–119 (1985).
18. Cohen, M. H. *et al. Astrophys. J.* **315,** L89–L92 (1987).
19. Charlot, P. *et al.* in *Proc. IAU Symp. No.* 129 (eds Reid, M. J. & Moran, J. M.) 33–34 (Kluwer, Dordrecht, 1988).
20. Kawaguchi, N. & Takahashi, Y. in *Proc. IAU Symp. No.* 129 (eds Reid, M. J. & Moran, J. M.) 45–46 (Kluwer, Dordrecht, 1988).
21. McCarthy, D. D. (ed.) *IERS Standards* IERS tech. Note 3, International Earth Orientation Service (Observatoire de Paris, Paris, 1989).
22. Rabbel, W. & Zschau, J. *J. Geophys.* **56,** 81–89 (1985).
23. Van Dam, T. M. & Wahr, J. M. *J. geophys. Res.* **92,** 1281–1286 (1987).
24. Davis, J. L. *et al. Radio Sci.* **20,** 1593–1607 (1985).
25. Davis, J. L. *et al.* in *Proc. IAU Symp.* No. 129 (eds Reid, M. J. & Moran, J. M.) 367–368 (Reidel, Dordrecht, 1988).
26. Carter, W. E. *et al. J. geophys. Res.* **93,** 14947–14953 (1988).

ACKNOWLEDGEMENTS. We would like to thank I. I. Shapiro and C. M. Will for their perceptive and helpful comments in reviewing this paper.

Texturing of magnetic materials at high temperature by solidification in a magnetic field

P. de Rango*, M. Lees*, P. Lejay*, A. Sulpice*, R. Tournier*, M. Ingold†, P. Germi† & M. Pernet†

* Centre National de la Recherche Scientifique, Centre de Recherches sur les Très Basses Temperatures, associé à l'Université Joseph Fourier, BP 166X, 38042 Grenoble Cedex, France
† Centre National de la Recherche Scientifique, Laboratoire de Cristallographie, BP 166X, 38042 Grenoble Cedex, France

THE ability to impose a preferred orientation, or 'texture', on a crystalline material is important in many fields of materials science. In general, crystalline materials are more or less anisotropic in their properties, depending on their lattice structure, and texturing allows the most favourable direction (for example, for current flow or magnetic susceptibility) to be used in applications. Ferromagnetic materials can be textured by 'magnetic annealing'—the orientation of powdered material in a magnetic field, usually followed by a sintering step—but this must be done at temperatures below the material's Curie temperature. Here we present a new method of texturing materials that have a residual anisotropy in their magnetic susceptibility at high temperature, by solidification in a magnetic field. This one-step process, which may be called 'paramagnetic annealing', is demonstrated by application to the high-temperature superconductor $YBa_2Cu_3O_7$.

Farrel *et al.*[1] have demonstrated that at room temperature the anisotropy energy associated with the paramagnetic state of $YBa_2Cu_3O_7$ is strong enough to induce alignment of particles in a magnetic field (the *c* axis aligns parallel with the applied field). As yttrium is non-magnetic, this anisotropy energy is attributed to the paramagnetic susceptibility associated with the Cu—O planes[2]. This energy has been used to produce aligned sintered ceramics from particles suspended in a liquid and oriented at room temperature[3,4]. Until now, this approach has not been extended to solidification from a melt, because it was doubted that sufficient anisotropy would remain at temperatures high enough to induce partial melting of $YBa_2Cu_3O_7$ ($T >$ 1,000 °C). But we have confirmed that this condition is satisfied by orienting collections of single crystals of $RBa_2Cu_3O_7$ (R = rare earth element) in liquid silver at 1,020 °C (ref. 5). A second requirement for magnetic alignment is that one must be able simultaneously to obtain both liquid and crystallites that are of a size sufficient that the anisotropy energy associated with the crystals ($\Delta E = \mu_0 \Delta\chi V H_A^2/2$, where V is the volume of each particle, H_A is the annealing field and $\Delta\chi = \chi_{\parallel} - \chi_{\perp}$ is the anisotropy of the paramagnetic susceptibility) is larger than the energy associated with thermal disordering effects ($\sim kT$). Using the room-temperature value[6] of $\Delta\chi$ for $YBa_2Cu_3O_6$ (this quantity decreases slowly as temperature increases because of strong magnetic correlations in the Cu—O layers), ΔE is 5,000 times larger than kT for $V = 1\ \mu m^3$, $T = 1{,}500$ K and $H_A = 5$ T.

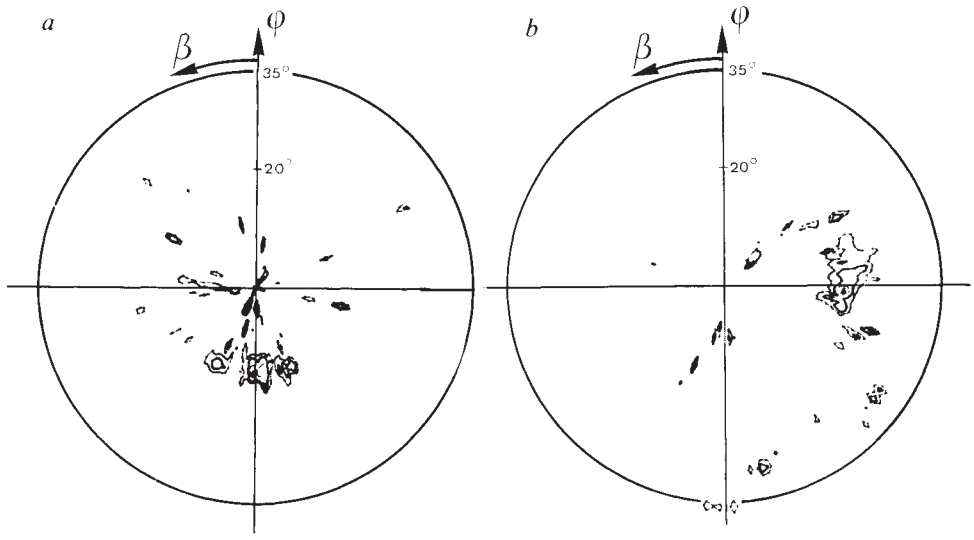

FIG. 1 *a*, (007) pole figure ($\theta_B = 27.50°$) measured by diffraction on a 7-mm-diameter surface cut perpendicular to the annealing field H_A for $YBa_2Cu_3O_7$ textured at 1,050 °C in a 5-T field. No pole appears for $\phi > 35°$. *b*, (200) pole figure ($\theta_B = 23.76°$) measured by diffraction on a 2-mm-diameter surface cut parallel to the annealing field H_A for the same sample. No pole appears for $\phi > 38°$. In both cases, the outermost contour corresponds to an intensity of 15% and subsequent contours increase from 30% to 60% to 90%.

We have attempted to produce a bulk textured sample of $YBa_2Cu_3O_7$ by application of a magnetic field whilst the sample is in the liquid state. A pellet was prepared by mixing stoichiometric quantities of Y_2BaCuO_5, $BaCuO_2$ and CuO. We have found that this starting composition leads to the formation of a liquid phase at lower temperature (≈1,050 °C) than that required for $YBa_2Cu_3O_7$ itself. The chemical precursor was heated at a rate of 100 °C h^{-1}. The sample was then annealed at 1,050 °C for 2 h in a 5-T magnetic field, and cooled at a rate of 20 °C h^{-1} to allow $YBa_2Cu_3O_7$ to form via a peritectic reaction. Note that the high-temperature cooling rate is relatively rapid compared with that used in the melt-growth process[7-9] (~1 °C h^{-1}).

We obtained X-ray diffraction pole figures of the sample using the Schulz reflection technique[10]. The intensity is measured by fixing the Bragg angle θ_B and rotating the sample simultaneously around the surface normal (angle β) and the tilt axis (angle ϕ). These figures show the diffraction intensities, corrected for geometric defocusing, on a polar stereographic projection. Isointensity lines indicate the relative intensity of the pole; 100% corresponds to the maximum diffracted intensity. Figure 1*a* and *b* shows pole figures for two orthogonal directions with β ranging from 0 to 360° and ϕ ranging from 0 to 35° with a step of 1.8°. The (007) pole figure defines the *c*-axis alignment; the localization of these poles within a very small area indicates that the crystallites are aligned strongly with their *c* axes parallel to H_A. In an orthogonal direction, the (007) poles are extremely weak whereas the (200) poles are localized within a small area. Taken together, these results allow us to conclude that the sample exhibits at least a fibrous texture in which the fibre axis coincides with the direction of the applied magnetic field and lies about 15° from the normal of the projection plane of Fig. 1*a*. (This displacement of the fibre axis is attributed to a misalignment of the crucible containing the sample relative to the annealing field and misalignment introduced during the cutting and mounting of the sample before obtaining the pole figures.) The large size of the crystallites (as seen in micrographs) explains the discontinuous contour around the fibre axis. As the pictures of the two surfaces studied remain coherent, we can conclude that the observed texture is a bulk, and not a surface, property.

We have examined the faces parallel and perpendicular to H_A using the scanning electron microscope. For the face parallel to H_A we observe a highly textured microstructure throughout the entire sample, with plate-like grains stacked with their *c* axes aligned parallel to the direction of the applied field. Some misorientation was observed on the circumference of the pellet which may explain the weak distribution observed in the pole figures.

The magnetic hysteresis was measured at 4 K on a 2×2×2 mm cube, with the measuring field *H* parallel and perpendicular to H_A (Fig. 2). These measurements confirm the existence of an anisotropy of about a factor of two, with the orientation of the *c* axis parallel to H_A. This value compares well with those observed for $YBa_2Cu_3O_7$ crystallites aligned in epoxy resin.

To verify that the observed orientation has not been induced by the presence of a thermal gradient or other external causes, another sample was prepared using exactly the same procedure but without the application of a magnetic field during the annealing. The magnetization hysteresis measured for this sample exhibits a very small anisotropy relative to that obtained for the sample prepared in the presence of a field (Fig. 2). Note that the diamagnetism of the sample prepared in zero field is four times smaller than that of the sample annealed under a field of 5 T. This indicates that annealing in a field not only introduces crystallographic orientation but also improves the quality of the intergranular contacts. Several samples have also been prepared at different annealing temperatures in the solid state, with a magnetic field applied whilst the sintering and crystal growth

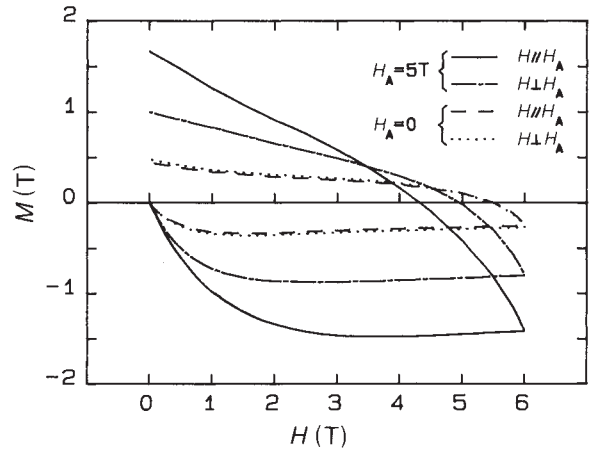

FIG. 2 Magnetization hysteresis at 4 K measured on 2×2×2 mm cubes cut from two samples, with the measuring field *H* parallel and perpendicular to the vertical axis of the furnace used for the thermal treatment. For a sample textured in an annealing field $H_A = 5$ T, there is an anisotropy of about a factor of two. (The critical-current densities j_c deduced from these curves using the Bean model are $j_c^{ab} = 4.2 \times 10^5$ A cm^{-2} and $j_c^c = 2.5 \times 10^5$ A cm^{-2}.) For a sample prepared using the same thermal treatment but without the application of a magnetic field, no significant anisotropy is observed and the diamagnetism is four times smaller.

take place. In all cases no significant anisotropy is observed, indicating that melting is necessary to obtain alignment.

Our method has several advantages over existing techniques. The temperatures and magnetic fields required during sample preparation are relatively modest. The direction of the crystal orientation can be controlled carefully and easily. In addition, because of the relatively rapid cooling rates used during the thermal treatment cycle, the sample production times are significantly shorter than those commonly experienced in melt-texture-growth techniques[7-9]. If the alignment is due to the presence of anisotropic magnetic particles into a liquid, the efficiency of the process will depend on the size and the number of nuclei that are aligned by the field, and consequently on the heating rate, the time and the temperature of the annealing and the cooling rate, all of which govern the grain growth. The process could be adapted for industrial production of textured samples and may prove to be generally applicable to all magnetic substances that have a residual magnetic anisotropy at high temperature. □

Received 17 October 1990; accepted 8 January 1991.

1. Farrel, D. E. *et al. Phys. Rev.* B **36,** 4025-4027 (1987).
2. Livingston, J. D., Hart, H. R. Jr & Wolf, W. P. *J. appl. Phys.* **64,** 5806-5808 (1988).
3. Nakagawa, Y., Yamasaki, H., Obara, H. & Kimura, Y. *Jap. J. appl. Phys.* **28,** L547-L550 (1989).
4. Lees, M. *et al.* in Proc. Int. Conf. '*From Modern Superconductivity Towards Applications*' (ed. Tournier, R. & Suryanarayanan, R.) 49-54 (IITT International Gournay-sur-Marne, 1990).
5. De Rango, P., Lees, M., Lejay, P., Sulpice, A. & Tournier, R. in Proc. Int. Conf. '*From Modern Superconductivity Towards Applications*' (ed. Tournier, R. & Suryanarayanan, R.) 21-26 (IITT International, Gournay-sur-Marne, 1990).
6. Miljak, M., Collin, G. & Hamzic, A. *J. Mag. Mater.* **76 & 77,** 609-611 (1988).
7. Jin, S. *et al. Appl. Phys. Lett.* **52,** 2074-2076 (1988).
8. Salama, K., Selvamanickam, V., Gao, L. & Sun, K. *Appl. Phys. Lett.* **54,** 2352-2354 (1989).
9. Meng, R. L. *et al. Nature* **345,** 326-328 (1990).
10. Schulz, L. G. *J. appl. Phys.* **20,** 1030 (1949).

Estimates of the effect of Southern Ocean iron fertilization on atmospheric CO_2 concentrations

F. Joos*, J. L. Sarmiento† & U. Siegenthaler*

* Physics Institute, University of Bern, CH-3012 Bern, Switzerland
† Atmospheric and Oceanic Sciences Program, Princeton University, Princeton, New Jersey 08544, USA

IT has been suggested[1-3] that fertilizing the ocean with iron might offset the continuing increase in atmospheric CO_2 by enhancing the biological uptake of carbon, thereby decreasing the surface-ocean partial pressure of CO_2 and drawing down CO_2 from the atmosphere. Using a box model, we present estimates of the maximum possible effect of iron fertilization, assuming that iron is continuously added to the phosphate-rich waters of the Southern Ocean, which corresponds to 16% of the world ocean surface. We find that after 100 years of fertilization, the atmospheric CO_2 concentration would be 59 p.p.m. below what it would have been with no fertilization, assuming no anthropogenic CO_2 emissions, and 90–107 p.p.m. less when anthropogenic emissions are included in the calculation. Such a large uptake of CO_2 is unlikely to be achieved in practice, owing to a variety of constraints that require further study; the effect of iron fertilization on the ecology of the Southern Ocean also remains to be evaluated. Thus, the most effective and reliable strategy for reducing future increases in atmospheric CO_2 continues to be control of anthropogenic emissions.

A flux of dead biogenic organic matter from the ocean surface continuously transports carbon (and nutrients) to depth and thus influences the surface concentration of total dissolved inorganic carbon (ΣCO_2). Model studies have shown that variations in the efficiency of biological uptake and export of organic carbon in the Southern Ocean, where concentrations of the nutrients P and N are high, can lead to alterations of atmospheric CO_2 in excess of 100 p.p.m.[4-7]. Recently, it has been suggested that biological production in these regions may be limited by a restricted supply of iron[8-11]. Although the hypothesis that iron is the ultimate limiting factor there is controversial[12-14], we adopt it here to obtain upper-limit estimates of the possible reduction in atmospheric CO_2. Because the ratio of iron to carbon incorporated in plants is rather low, between 1:10,000 and 1:100,000[15,16], the amount of iron required to carry out this fertilization is relatively modest: $\sim 10^6$ tons of iron per year assuming that all the iron goes into organic matter. Our model study differs from that of Peng and Broecker[17] in the area fertilized (16% of the world ocean rather than 10%), and in that we include scenarios with anthropogenic CO_2 emissions for which we find that fertilization has a greater effect than when we assume no man-made emissions.

We consider there to be three factors that exert the most important control on the response of atmospheric CO_2 to an

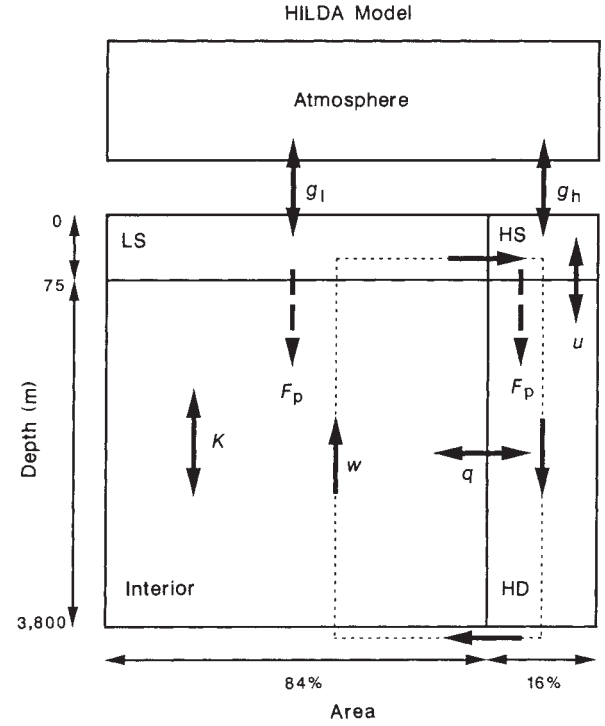

FIG. 1 Structure of the model used for our study, which is based on a model developed by G. Shaffer (personal communication) and one of us (J.L.S.). The ocean interior is resolved by a vertical stack of boxes connected by advection (w) and diffusion (K). The high-latitude regions are simulated by two well-mixed boxes which are connected to each other by mixing (u). The parameter q is a rudimentary representation of the ventilation of the interior oceans by high-latitude waters. The model parameters obtained by fitting bomb and natural ^{14}C are: $K = 465 + 7{,}096 \times \exp(-(z - 75\,m)/253\,m)\,m^2\,yr^{-1}$; $w = 0.44\,m\,yr^{-1}$ (equivalent to $4.24 \times 10^6\,m^3\,s^{-1}$); $u = 38\,m\,yr^{-1}$ ($69.8 \times 10^6\,m^3\,s^{-1}$); $q = 0.00186\,yr^{-1}$ ($79.5 \times 10^6\,m^3\,s^{-1}$); gas-exchange rate ($g_l$, g_h) at 280 p.p.m. = 15.1 mol $m^{-2}\,yr^{-1}$; ocean surface area = $3.62 \times 10^{14}\,m^2$; depth of mixed layer = 75 m; average depth of ocean = 3,800 m. We solve conservation equations for the perturbation of phosphate and CO_2 ($c_{pert.} = c_{actual} - c_{unpert.}$) with an initial condition for $c_{pert.}$ of 0 everywhere. The relation between changes of ΣCO_2 and P_{CO_2} is calculated using the equations of Peng *et al.*[24]. The phosphate and carbon removed from the surface high-latitude box are regenerated to the dissolved form in the deep box below (dashed arrows, F_p = perturbation flux of particulate carbon and phosphorus). A small amount of this excess phosphate makes its way through the deep sea to low-latitude surface waters, where it is removed and regenerated below with an exponential scale depth of 1,160 m obtained from a fit to oceanic nutrient data by G. Shaffer and J.L.S. Multiplying the resulting phosphate fluxes by the C:P Redfield ratio (130) gives the corresponding carbon fluxes. LS, low-latitude surface; HS, high-latitude surface; and HD, high-latitude deep boxes.

TABLE 1 Projected changes in atmospheric CO_2 partial pressures resulting from various scenarios beginning in 1990

Scenario*	After 50 years A Unfertilized	B Fertilized	Effect of fertilization (B − A)	After 100 years C Unfertilized	D Fertilized	Effect of fertilization (D − C)
		High-latitude area fraction = 9.7%†				
Initialized at pre-industrial levels						
Our model	0	−26	−26	0	−39	−39
Peng and Broecker‡	—	—	—	0	−34	−34
Constant-emission	80	46	−34	156	98	−58
Business-as-usual	150	114	−36	430	362	−68
		High-latitude area fraction = 16.0%				
Initialized at pre-industrial levels	0	−41	−41	0	−59	−59
Constant-emission	79	24	−55	151	61	−90
Business-as-usual	146	88	−58	417	310	−107

* The scenario which is initialized at pre-industrial levels of atmospheric CO_2 has no anthropogenic source of CO_2 to the atmosphere, thus the CO_2 drawdown by the ocean results in a reduction below the initial pre-industrial value of 278.3 p.p.m. In the 'constant-emission' scenario, atmospheric CO_2 content is prescribed using observations until 1990[23], after which the CO_2 emission to the atmosphere is fixed at the model-determined value of 6.15 Gt C yr^{-1} in 1990. In the 'business-as-usual' scenario, the atmospheric CO_2 content is prescribed until 1989, after which the annual emission increases according to the IPCC business-as-usual scenario[22], in which the man-made emissions increase linearly with time from 6.0 Gt C yr^{-1} in 1990 to 22.4 Gt C yr^{-1} in 2100. The 1990 atmospheric CO_2 partial pressure is 355 p.p.m.

† The area fraction of 9.7% in our model corresponds to the same area in m^2 as chosen by Peng and Broecker[17].

‡ The Peng and Broecker[17] model is initialized at 280 p.p.m. and has a phosphate reduction of 1.6 mmol m^{-3}. The result given here is for their scenario with 17.5×10^6 m^{-3} s^{-2} of water upwelling in the high latitudes and being placed directly into the deep ocean.

enhanced carbon uptake resulting from iron fertilization. First is the reduction in average Σ CO_2 per unit area that occurs when fertilization is started. We take the supply of phosphate from depth as a reasonable guide to the maximum potential biological uptake of carbon, although we recognize that light supply, our ability to spread iron efficiently over the large ocean areas involved, the behaviour of the ocean ecosystem, and other processes may interfere long before the phosphate is depleted. (Carbon cycling is linked to that of phosphate through the Redfield ratio of C : P = 130 in organic matter.[18]) Second is the area over which the fertilization occurs. We use a recent analysis of National Oceanic Data Center phosphate data (S. Levitus and R. G. Najjar, personal communication) to estimate that the Southern Ocean's (>30° S) water volume in the depth range 0–75 m with phosphate ≥1.0 mmol m^{-3} amounts to 15.8% of the world ocean volume in the same depth range. The average phosphate content of this volume is 1.63 mmol m^{-3}. We therefore take the high-latitude box of our 'standard' model to consist of 16% of the world ocean area (with 9.7% as an alternative case corresponding to the area used by Peng and Broecker[17]), and we determine the enhancement to the biological production by forcing a reduction of phosphate by 1.5 mmol m^{-3} in the surface box of this area. Third is the reduction in CO_2 partial pressure resulting from a given carbon removal. We have found that this is considerably larger at high rather than at low CO_2 levels because of the nonlinear relation between P_{CO_2} and Σ CO_2. We use three different anthropogenic CO_2 emission scenarios to examine the contribution of this nonlinearity, one in which the ocean and atmosphere are initialized at the pre-industrial value of 278 p.p.m. with no anthropogenic sources, a 'constant-emission' scenario, and a 'business-as-usual' scenario (see Table 1 legend for descriptions of the scenarios).

The rate at which atmospheric CO_2 is taken up by the oceans also depends on the rate at which the ocean circulation and mixing transport to the abyss the excess CO_2 that invades the fertilized region from the atmosphere. As discussed below, we find that this factor is less critical than those mentioned above. Figure 1 shows the model we use to simulate the ocean circulation and mixing. Parameter values are obtained by fitting the model to pre-bomb ^{14}C observations as well as the GEOSECS bomb inventory estimates of Broecker *et al.*[19] (U.S. and F.J., to be published elsewhere). However, the bomb inventory estimates in the Southern Ocean were not considered adequate for use in the fitting exercise because the bomb signal is not easy to discern from the natural ^{14}C background; the data in the Southern Ocean are scanty, especially from pre-bomb time; and the bomb inventories south of 46° S show considerable variation. Instead, we checked our model with high-latitude CFC-11 observations, obtaining a standing crop of 1,976 nmol m^{-2} for 1984, comparable to an estimate of 1,950 ± 550 nmol m^{-2} obtained for the same period from measurements south of 46° S by Weiss *et al.*[20] in the South Atlantic, by the Pacific Marine Environmental Laboratory of the National Oceanic and Atmospheric Administration in the South Pacific (R. H. Gammon and D. Weisgarver, personal communication), and by R. Weiss (personal communication), also in the South Pacific.

Figure 2 summarizes results from the iron fertilization assuming the business-as-usual and constant-emission CO_2 scenarios. Without fertilization, the increase in atmospheric CO_2 from its 1990 value of 355 p.p.m. is 146 p.p.m. after 50 years, and 417 p.p.m. after 100 years in the business-as-usual scenario (Fig. 2*a*). When iron fertilization is initiated, an additional flux of organic carbon out of the high-latitude surface box is stimulated. Its size is approximately constant at 5.5 Gt C yr^{-1} after an initial peak in the first year. This increased carbon flux leads to a massive decrease in the high-latitude surface P_{CO_2} (see Fig. 2*b*), and a resulting enhancement of atmospheric CO_2 uptake so that the atmospheric CO_2 now increases by only 88 p.p.m. after 50 years (60% of the increase in the unfertilized scenario) and by 310 p.p.m. after 100 years (74% of the increase in the unfertilized scenario). The decrease in atmospheric P_{CO_2} resulting from iron fertilization reduces the low-latitude air–sea difference so that the response of the low latitude regions is opposite in sign to that of the high latitudes (Fig. 2*b*). After 100 years, the additional CO_2 flux from the atmosphere to the high-latitude box in the iron fertilization scenario is 2.65 Gt C yr^{-1}. This is partly balanced by a reduction of 0.51 Gt C yr^{-1} in the low-latitude uptake of anthropogenic CO_2, for a net annual oceanic uptake of 2.13 Gt C yr^{-1} due to iron fertilization.

The effect of the nonlinearity of the carbon chemistry equations can be discerned by comparing the three scenarios shown in Table 1. The constant-emission scenario with fertilization of 16% of the world ocean shows a reduction of 90 p.p.m. in the increase of atmospheric CO_2 resulting from 100 years of iron fertilization, compared with 59 p.p.m. for the scenario initialized at 278 p.p.m. The further increase in atmospheric CO_2 in the business-as-usual scenario has a still larger effect: 107 p.p.m. The dependence on the prevailing atmospheric CO_2

concentrations can be understood when considering that P_{CO_2} depends in a nonlinear way on ΣCO_2. The higher the atmospheric concentration of CO_2, the larger the change in oceanic P_{CO_2} for a given reduction of ΣCO_2 due to iron fertilization (see Fig. 2*c*). We find that the percentage reduction in atmospheric CO_2 concentration which would occur after 100 years of iron fertilization decreases with higher CO_2 levels (21% for pre-industrial initialization, 14% for the business-as-usual scenario). This is in contrast to the assertion of Peng and Broecker[17] that the relative reduction is constant.

Peng and Broecker[17] emphasize that the key to evaluating the impact of iron fertilization is the rate of vertical exchange in the Southern Ocean. We find that the uncertainty in the calibration of the high-latitude transport parameters u and w gives error limits of $^{+14\%}_{-24\%}$ for the absolute value of the iron-induced reduction in atmospheric CO_2 for the pre-industrial scenario. Therefore, the precise magnitude of the vertical exchange seems not to be as critical as uncertainties in other processes. This is also supported by the fact that Peng and Broecker's result agrees well with ours for the same pre-industrial scenario (Table 1), although their high-latitude vertical exchange, which is calibrated with bomb-produced radiocarbon, is considerably weaker than our vertical exchange calibrated by oceanic distribution of CFC-11.

The effect of ocean area is readily apparent from the results summarized in Table 1. An increase in the fertilized area from 9.7% to 16% leads to an almost linear increase in the effect of iron fertilization of ~60%. Broecker[21] argues that their choice of the smaller area was intended to compensate for the fact that much of the Antarctic is in darkness during part of the year. We attempted to compensate for this effect by fertilizing the ocean for only six months of the year. The CO_2 uptake in the business-as-usual case went down from 107 p.p.m. to 88 p.p.m. far less than the drop to 68 p.p.m. which occurs when using the smaller area.

To be effective, iron fertilization has to be applied continuously so that the atmosphere–ocean system does not revert to its unfertilized state. This is shown in Fig. 3, which shows what happens if iron fertilization is terminated after 50 years. At 50 years the ocean in the business-as-usual iron fertilization simulation has taken up 57.9 p.p.m. more CO_2 than the non-fertilized ocean. If fertilization is stopped at this point, the difference between the fertilized and non-fertilized scenarios reduces to 35.5 p.p.m. after 100 years.

Changes in the Earth's equilibrium temperature are logarithmically related to the atmospheric CO_2 content, with a doubling of CO_2 leading to an equilibrium warming of between 1.5 °C and 4.5 °C, with a preferred value of 2.5 °C (ref. 22). A useful index of the significance of a given CO_2 increase is the factor $\ln(P_{CO_2}/278)/\ln(2)$ which, multiplied by 2.5 °C, will give the equilibrium warming resulting from a given CO_2 increase. Thus, the atmospheric CO_2 concentration of 771 p.p.m. reached by 2090 in the business-as-usual scenario will give an equilibrium warming of 3.7 °C. The 107-p.p.m. additional oceanic uptake

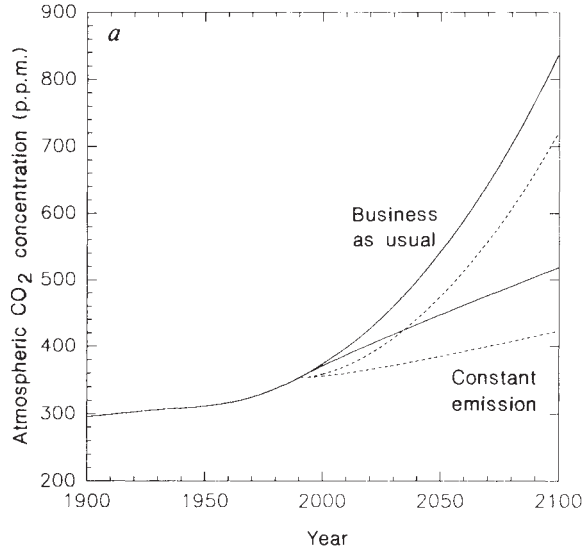

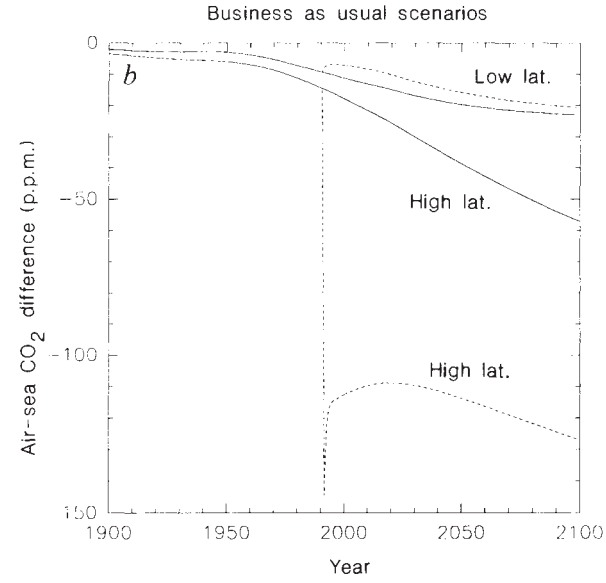

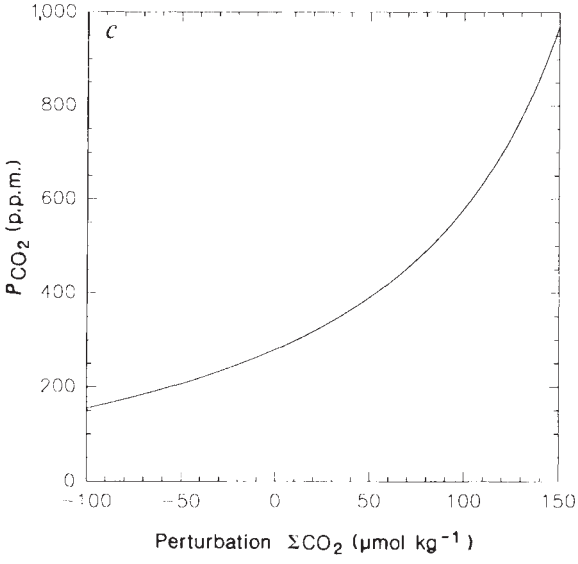

FIG. 2 *a*, Future atmospheric CO_2 concentration in the business-as-usual and constant-emission scenarios. The solid line is our prediction without iron fertilization, the dashed line shows what might occur with iron fertilization. *b*, The air–sea CO_2 difference of the iron-fertilized business-as-usual scenario (dashed lines) and the non-fertilized business-as-usual scenario (solid lines). *c*, Dependence of the partial pressure of CO_2 on ΣCO_2 in high-latitude surface water ($T = -0.22$ °C). With increasing CO_2 concentrations, the slope of the curve increases, and so does the change in P_{CO_2} for a given change in ΣCO_2.

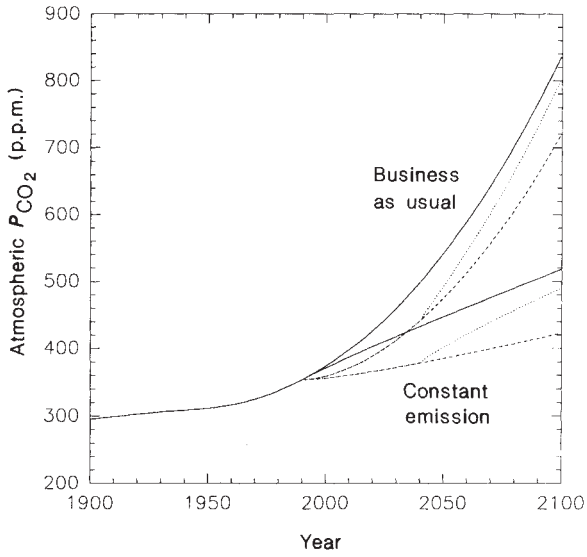

FIG. 3 The effect of stopping iron fertilization after 50 years (dotted line) is depicted for the business-as-usual and constant-emission scenarios. The solid line is the unfertilized scenario, the dashed line is the scenario for continuous fertilization.

resulting from iron fertilization gives an equilibrium warming of 3.1 °C instead. On the other hand, the unfertilized constant-emission scenario, which reaches 505 p.p.m. in 2090, gives a significantly smaller equilibrium warming of 2.2 °C, which is reduced to 1.4 °C with the 90 p.p.m. additional oceanic uptake resulting from iron fertilization. These numbers can be compared with the 0.9 °C equilibrium warming that can be expected from the present atmospheric CO_2 content of 355 p.p.m. It should be kept in mind that the transient warming is smaller than, and not necessarily proportional to the equilibrium warming, due primarily to the uptake of heat by the ocean.

The most important conclusion we draw from our calculations is that, although the effect of iron fertilization is large enough to justify further study, the effect of a significant change in the emissions of CO_2 is even larger. We emphasize the preliminary nature of our calculations and the fact that all the assumptions we have made have been biased so as to yield an upper limit. □

Received 5 November 1990; accepted 5 February 1991.

1. Booth, W. *Washington Post*. A1 20 May (1990).
2. Baum, R. *Chem. Engng News* **68**, 21–24 (1990).
3. Martin, J. H., Fitzwater, S. E. & Gordon, R. M. *Global biogeochem. Cycles* **4**, 5–12 (1990).
4. Knox, F. & McElroy, M. B. *J. geophys. Res.* **84**, 2503–2518 (1984).
5. Siegenthaler, U. & Wenk, T. *Nature* **308**, 624–626 (1984).
6. Sarmiento, J. L. & Toggweiler, J. R. *Nature* **308**, 621–624 (1984).
7. Sarmiento, J. L., Toggweiler, J. R. & Najjar, R. *Phil. Trans. R. Soc.* **A325**, 3–21 (1988).
8. Martin, J. H. & Fitzwater, S. E. *Nature* **331**, 341–343 (1988).
9. Martin, J. H. & Gordon, R. M. *Deep-Sea Res.* **35**, 177–196 (1988).
10. Martin J. H., Gordon, R. M., Fitzwater, S. & Broenkow, W. W. *Deep-Sea Res.* **36**, 649–680 (1989).
11. Martin, J. H. *Paleoceanography* **5**, 1–13 (1990).
12. de Baar, H. J. W. *et al. Mar. Ecol. Prog. Ser.* **65**, 105–122 (1990).
13. Banse, K. *Limnol. Oceanogr.* **35**, 772–775 (1990).
14. Dugdale, R. C., & Wilkerson, F. P. *Global biogeochem. Cycles* **4**, 13–20 (1990).
15. Anderson, G. C. & Morel, F. M. M. *Limnol. Oceanogr.* **27**, 789–813 (1982).
16. Morel, F. M., & Hudson, R. J. in *Chemical Processes in Lakes* (ed. Stumm, W.) 251–270 (Wiley, New York, 1985).
17. Peng, T.-H. & Broecker, W. S. *Nature* **349**, 227–229 (1991).
18. Toggweiler, J. R. & Sarmiento, J. L. in *The Carbon Cycle and Atmospheric CO_2: Natural variations Archean to Present* Vol. 32, Geophysical Monograph Series (eds. Sundquist, E. T. & Broecker, W. S.) 163–184 (American Geophysical Union, Washington, DC. 1985).
19. Broecker, W. S. Peng, T.-H., Östlund, G. & Stuiver, M. *J. geophys Res.* **90**, 6953–6970 (1985).
20. Weiss, R. F., Bullister, J. L., Warner, M. J., Van Woy, F. A. & Salameh, P. K. *Ajax Expedition Chlorofluorcarbon Measurements* (Scripps Institution of Oceanography Reference 90-6, La Jolla, 1990).
21. Broecker, W. S. *Global biogeochem. Cycles* **4**, 1–2 (1990).
22. Houghton, J. T., Jenkins, G. J. & Ephraums, J. J. (eds) *Climate Change*, The IPCC Scientific Assessment (Cambridg, University Press, 1990).
23. Siegenthaler, U. & Oeschger, H. *Tellus* **39B**, 140–154 (1987).
24. Peng, T. H., Takashi T. & Broecker, W. S. *Tellus* **39B**, 439–458 (1987).

ACKNOWLEDGEMENTS. We appreciate the great help given to F.J. by M. Warner in setting up our CFC runs, and his generosity and that of R. Gammon in helping us to obtain the CFC data needed to estimate the CFC inventories. R. Fink developed our carbonate system algorithm and R. Slater helped with the phosphate data analysis. J. R. Toggweiler and J. Orr provided helpful comments on the manuscript. F.J. and U.S. acknowledge the hospitality of the Atmospheric and Oceanic Sciences Program during their extended visit to Princeton. This work was funded by subcontracts with Martin Marietta Systems, Inc., under contract with the Carbon Dioxide Research Division, US Department of Energy; by a follow-up contract directly from the Carbon Dioxide Research Division of the Department of Energy; and by the National Science Foundation.

Biases from natural sulphurization in palaeoenvironmental reconstruction based on hydrocarbon biomarker distributions

Math E. L. Kohnen, Jaap S. Sinninghe Damsté & Jan W. De Leeuw

Organic Geochemistry Unit, Faculty of Chemical Technology and Materials Science, Delft University of Technology, De Vries van Heystplantsoen 2, 2628 RZ Delft, The Netherlands

BIOMARKERS (chemical fossils) are sedimentary organic compounds whose basic skeletons suggest an unambiguous link with known contemporary natural products, and were synthesized by biota present at the time of the deposition of the sediment. These compounds are commonly used to assess palaeoenvironmental conditions of deposition of Recent and ancient sediments[1–3]. Saturated hydrocarbons are relatively easy to analyse and contain a lot of geochemical information, and are therefore the most widely used class of biomarkers in palaeoenvironmental reconstruction[2–5]. Hydrocarbon biomarkers are biosynthesized as such or are derived from functionalized biosynthetic lipids, such as alkenes, alcohols and acids, by diagenetically induced defunctionalization. Functionalized lipids may, however, also undergo an abiogenic reaction with hydrogen sulphide or polysulphides ('natural sulphurization') during the early stages of diagenesis, and this may lead to selective removal of specific hydrocarbon biomarker precursors. Here we investigate the influence of natural sulphurization on hydrocarbon biomarker signatures in immature sediments from Italy and off Peru. We show that, if not taken properly into account, this process may lead to a severe bias in the interpretation of the geological record.

Sedimentary functionalized lipids react with reduced sulphur species (H_2S and HS_x^-) to form organic sulphur compounds (OSCs) and sulphur-bound lipid moieties in macromolecules (see ref. 6 for a review). The onset of sulphurization of organic matter is controlled by the reactive iron (for example, ferrihydrite and haematite) content of the sediment, because organic matter reacts with reduced sulphur more slowly than do sedimented iron minerals and thus does so only after reactive iron oxides have first been converted to iron sulphides. In the region of upwelling in the Peru margin, sulphur incorporation into sedimentary organic matter starts in the top metre of the sediment column[7], indicating that this process occurs in the early stages of diagenesis. Moreover, the identification of OSCs in a Recent Black Sea sediment (age $3\text{–}6 \times 10^3$ yr) also points to an early diagenetic sulphurization of organic matter[8]. Ten Haven *et al.*[9] examined the extracts of almost 100 thermally immature deep-sea sediments and found that approximately 70% of the samples contain OSCs. The widespread occurrence of OSCs, and the fact that reduced inorganic sulphur species are present in any anoxic organic-matter-containing Recent marine sediment[10], suggest that natural sulphurization of specific functionalized lipids is a ubiquitous process. It seems inevitable that this selective removal of the precursors of hydrocarbon biomarkers will alter the hydrocarbon biomarker distribution in immature sediments, and thus the interpretation of the geological record as revealed by their apparent distribution. Hydrocarbon biomarkers are used in many (palaeo)environmental reconstruction studies of immature sediments[11–16] and of par-

ticulate organic matter in the water column recovered from sediment traps[17]. Although the major biota contributing to the sedimentary organic matter are deduced from the presence of specific biomarkers (such as hydrocarbons, alcohols and acids), the absence of specific biomarkers does not necessarily imply that the biosynthetic precursors and the corresponding biota were not present in the palaeoenvironment. Similarly, the absence of carbonate micro-fossils in sediments deposited below the carbonate compensation depth does not imply the absence of such species in the environment.

To investigate the bias introduced into hydrocarbon biomarker signatures in immature sediments by natural sulphurization, we have analysed immature sediment samples from the Messinian Vena del Gesso basin (Northern Apennines, Italy) and the Peru upwelling area. The Vena del Gesso basin is an evaporitic basin filled with thick beds of gypsum associated with thinner carbonate and shaly intercalations[18]. The sample investigated (VDG-4A) is taken from a fresh outcrop of a non-evaporitic bituminous shale intercalation. The immature character of these consolidated sediments is reflected by the low vitrinite reflectance (~0.25%) of the trace indigenous vitrinite particles encountered. The Peru sediment is taken from ODP Leg 112, site 679 (11°03.81′ S, 76°16.33′ W), at a depth of ~1 m. Although both samples can be classified as thermally immature, the older and once more-deeply-buried Vena del Gesso sediment has a longer geological history and hence has undergone more diagenetic changes. Figure 1*a* shows the distribution of the hydrocarbon biomarkers of the Vena del Gesso sample. To release the naturally sulphurized hydrocarbon biomarkers, the maltene fractions (the fraction of sediment extract that is soluble in *n*-heptane) were desulphurized using Raney nickel, which cleaves C—S bonds selectively and quantitatively[19]. Both the 'free' and the 'free+S-bound' hydrocarbon biomarker fractions were hydrogenated before being compared. The distributions of the 'free' hydrocarbon biomarkers is significantly different to that of the 'free+S-bound' compounds (Fig. 1 and Table 1), clearly demonstrating the bias introduced by natural sulphurization, and the consequent possibility of incomplete or even erroneous reconstructions of depositional environments.

In the Vena del Gesso sediment, the distribution of the long-chain *n*-alkanes (C_{25}–C_{33}) is dramatically changed after desulphurization (Fig. 1). This is also expressed by the change in the 'carbon preference index' (the ratio of odd- to even-carbon-numbered *n*-alkanes[20]; Table 1), which is a frequently used measure of the contribution of terrigenous organic matter in sediments[18]. Based on the investigation of only the 'free' long-chain *n*-alkanes, one might come to the conclusion that the organic matter in this sediment contains an appreciable terrigenous contribution, whereas, after taking into account the naturally sulphurized long-chain *n*-alkanes, it can be concluded that there is only a small contribution of terrestrial organic matter. Pristane (**II**, see Fig. 2) and phytane (**III**) are acyclic isoprenoid biomarkers that are ubiquitous in sediments; the pristane/phytane ratio is thought to reflect the oxicity of the depositional environment[22], although more recently this ratio has also been interpreted in terms of palaeosalinity[23,24]. Although this parameter is not often applied to Recent sediments (such as the Peru sediment), it is frequently used in consolidated immature sediments (such as the Vena del Gesso sediment). In

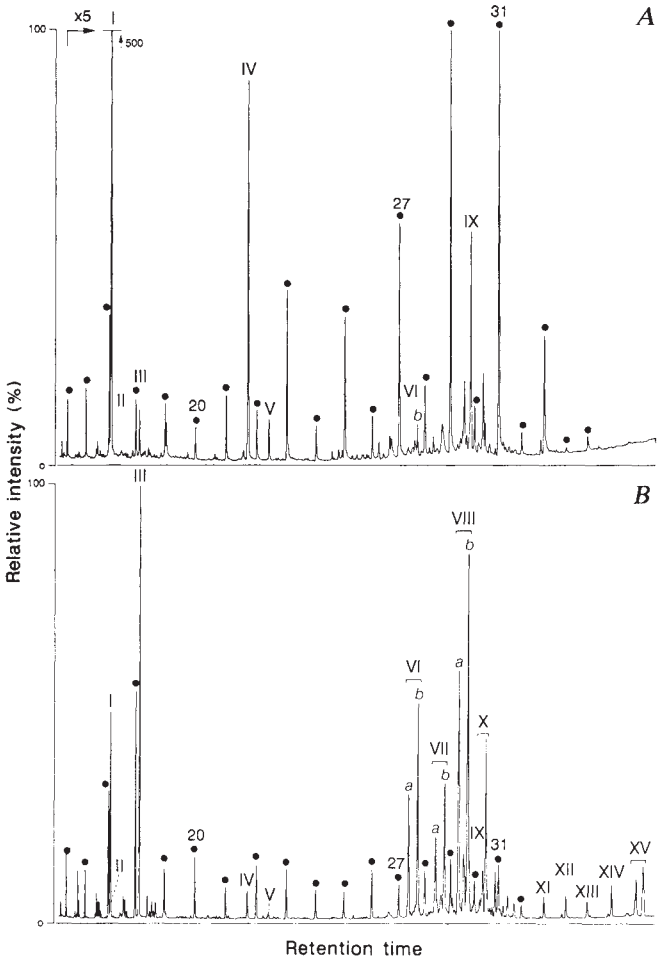

FIG. 1 Gas chromatograms (conditions: 25 m × 0.32 mm fused-silica capillary column coated with CP Sil-5 (0.12 μm); temperature program: 70–130 °C at 10 °C min^{-1}, 130–320 °C at 4 °C min^{-1}, held for 20 min, on column injection) of *A*, hydrogenated 'free' hydrocarbon biomarkers, and *B*, hydrogenated 'free+S-bound' hydrocarbon biomarkers isolated from the untreated and the desulphurized maltene fraction, respectively, of the extract from the Vena del Gesso sediment. The maltene fraction was separated from the extract (obtained by sonication using mixtures of CH_3OH and CH_2Cl_2) by precipitating the asphaltenes in *n*-heptane. Subsequently 6,6-d_2-3-methyleicosane (**IV**) was added as an internal standard. An aliquot of the maltene fraction was desulphurized using Raney nickel[19]. Both the reaction mixture obtained after desulphurization and an untreated aliquot of the maltene fraction were fractionated on a column into an apolar and a polar fraction as described previously[29]. A hydrocarbon fraction (R_f = 1.0–0.8) was isolated from the apolar fraction using thin-layer chromatography (SiO_2, 0.25 mm thickness) with *n*-hexane as developer. The hydrocarbon fractions were hydrogenated[8] and subsequently analysed with gas chromatography and GC–MS (GC–MS conditions were similar to those reported previously[32]). Key: *a*, 5β(H), 14α(H), 17α(H) steranes; *b*, 5α(H), 14α(H), 17α(H) steranes. Arabic numbers refer to number of carbon atoms of *n*-alkanes (indicated by black dots). Roman numbers refer to structures indicated in Fig. 2.

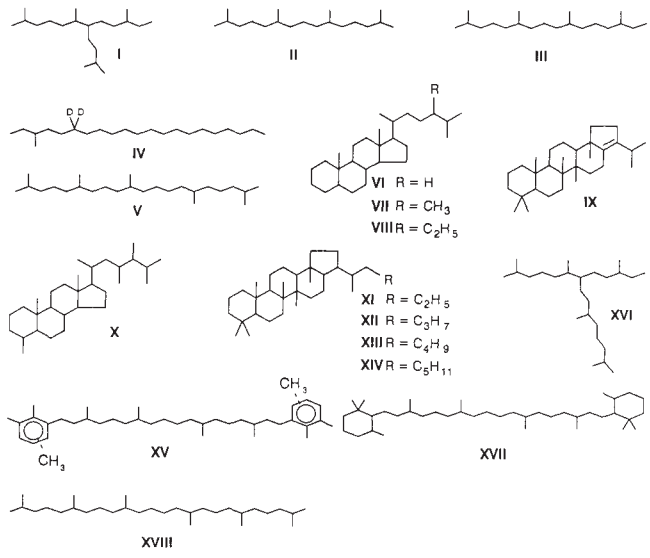

FIG. 2 Structures of compounds.

TABLE 1 Concentrations of selected biomarkers and biomarker ratios in the 'free' hydrocarbon and the 'free + S-bound' hydrocarbon fractions

	Vena del Gesso-4a			Peru upwelling area		
	'Free'	'Free + S-bound'	Naturally sulphurized fraction*	'Free'	'Free + S-bound'	Naturally sulphurized fraction*
Octadecane	9.0×10	5.5×10^3	98	2.0×10^3	2.0×10^3	0
Octacosane	1.7×10^2	1.7×10^3	90	2.0×10	3.2×10	38
Nonacosane	9.6×10^2	1.9×10^3	49	3.4×10	5.8×10	41
Pristane (**II**)	2.2×10^2	3.3×10^2	33	3.6×10	3.5×10	0
Phytane (**III**)	9.0×10	1.1×10^4	99	7.1×10	1.4×10^3	95
C_{20} HBI†(**I**)	4.0×10^3	4.6×10^3	13	<1	<1	n.a.
C_{25} HBI† (**XVI**)	<1	<1	n.a.	<1	1.,2×10^2	100
PME‡ (**V**)	1.0×10^2	2.5×10^2	60	5.0×10	7.0×10	29
Squalane (**XVIII**)	<1	<1	n.a.	1.5×10^2	1.7×10^2	12
Cholestanes§ (**VI**)	1.6×10^2	1.2×10^4	99	3.0×10	2.0×10^2	85
Dinosterane (**X**)	<1	8.5×10^3	100	<1	<1	n.a.
Pentakishomo-Hopane‖ (**XIV**)	<1	1.1×10^3	100	<1	<1	n.a.
Diaromatic Carotenoid (**XV**)	<1	4.3×10^3	100	<1	<1	n.a.
β-Carotane (**XVII**)	<1	<1	n.a.	2.0×10	1.2×10^4	100
CPI#	8.0	1.1	n.a.	1.3	1.2	n.a.
Pristtane/phytane¶	2.5	2.9×10^{-2}	n.a.	5.5×10^{-1}	2.5×10^{-2}	n.a.

n.a. = not applicable. Concentrations of biomarkers (mg per kg extract) are obtained by integrating their peak areas and that of the internal standard (IV) in the FID trace.

* [('S-bound')/('free + S-bound')] ×100 (in %).

† HBI = highly branched isoprenoid.

‡ PME = 2,6,10,15,19-pentamethyleicosane.

§ 5α(H), 14α(H), 17α(H)-cholestane and 5β(H), 14α(H), 17α(H)-cholestane.

‖ 17β(H), 21β(H), 22R-pentakishomohopane.

¶ Peak area of pristane is determined in an FID trace obtained using a DB17 column.

\# CPI = Carbon preference index (ref. 20) of the *n*-alkanes (C_{24}–C_{34}):

$$\mathrm{CPI}=\frac{1}{2}\left[\frac{C_{25}+C_{27}+C_{31}+C_{33}}{C_{24}+C_{26}+C_{28}+C_{30}+C_{32}}+\frac{C_{25}+C_{27}+C_{29}+C_{31}+C_{33}}{C_{26}+C_{28}+C_{30}+C_{32}+C_{34}}\right]$$

both samples, the pristane/phytane ratio is changed drastically after desulphurization (Table 1), demonstrating that it may be heavily biased in immature sediments. This bias stems from the fact that the precursors of phytane react selectively with inorganic sulphur species during early diagenesis[24]. The contribution of marine organic matter is also underestimated when using the regular steranes (**VI–VIII**), which are those derived from sterenes after hydrogenation, as biomarkers for algal material, because these compounds are present only at very low levels in the 'free' hydrocarbon fraction whereas they are highly prevalent in the 'free + S-bound' hydrocarbon fraction (Fig. 1 and Table 1).

In both samples, several diagnostic biomarkers are virtually absent in the 'free' hydrocarbon biomarker fraction but are present in significant amounts after desulphurization (Fig. 1 and Table 1), demonstrating again that studies using solely the 'free' hydrocarbon biomarkers may miss valuable information about the depositional environment. Dinosterane (**X**), a biomarker for dinoflagellate algae[25], shows up only after desulphurization: its presence is in agreement with microscopic examinations, which reveal dinoflagellate cysts in the sediment. The presence of sulphur-linked diaromatic carotenoids (**XV**) attests to the activity of photosynthetic bacteria in the depositional environment of the Vena del Gesso sediment[26,27]. Another clue to bacterial activity is furnished by the appearance of pentakishomohopane (**XIV**) after desulphurization (Fig. 1). The presence of a C_{25} highly branched isoprenoid alkane (**XVI**) in the desulphurized sample of the Peru sediment (Table 1) is reminiscent of the presence of C_{25} highly branched isoprenoid alkenes in other samples[28], which have possibly been biosynthesized by diatoms in the palaeoenvironment. The most striking bias in the biomarker distribution is illustrated by the β-carotane carbon skeleton (**XVII**) in the Peru sediment: this compound is absent in the hydrocarbon fraction, but it is present as a major 'S-bound' moiety and thus dominates the 'free + S-bound' hydrocarbon biomarker distribution (Table 1).

On the other hand, the abundances of a number of biomarkers (for example, a C_{20} highly branched isoprenoid alkane (**I**), pristane (**II**), 2,6,10,15,19-pentamethyleicosane (**V**), squalane (**XVIII**)) in the naturally sulphurized fraction are relatively low (Table 1), indicating that 'free' hydrocarbon biomarkers in immature organic-sulphur-rich sediments are lipids that did not react with sulphur during early diagenesis, probably because they were biosynthesized without a reactive functionality.

It follows from these results that, in sediments with a high organic-sulphur content, the sulphur-bound biomarkers should be taken into account for a complete and thus more correct characterization of the (palaeo)environment. This can be achieved easily by simple desulphurization, which releases the naturally sulphurized biomarkers. Preliminary results[29] indicate that the same bias can be expected for the distributions of oxygenated biomarkers (such as alcohols, acids and ketones), compounds that are also used frequently to reconstruct palaeoenvironments from analysis of immature sediments[30,31]. □

Received 29 October 1990; accepted 4 January 1991.

1. Johns, R. B. (ed.) *Biological Markers in the Sedimentary Record* (Elsevier, Amsterdam, 1986).
2. Brassell, S. C. & Eglinton, G. in *Organic Marine Geochemistry* (ed. Sohn, M. L.) 10–32 (American Chemical Society, Washington, 1986).
3. Volkman, J. K. in *Lacustrine Petroleum Source Rocks* (eds Fleet, A. J., Kelts, K. & Talbot, M. R.) 103–122 (Blackwell, Oxford, 1988).
4. Mackenzie, A. S. in *Advances in Petroleum Geochemistry* Vol. 1 (eds Brooks, J. & Welte, D. H.) 115–214 (Academic, London, 1984).
5. Philip R. P. *Fossil Fuel Biomarkers. Methods in Geochemistry and Geophysics* Vol. 23 (Elsevier, Amsterdam, 1985).
6. Sinninghe Damsté, J. S. & de Leeuw, J. W. in *Advances in Organic Geochemistry 1989* (eds. Durand, B. and F. Behar) 1077–1101 (1990).
7. Mossmann, J., Aplin, A. C., Curtis, C. D. & Coleman, M. L. in *Proc. ODP Sci. Results* **112** (eds Suess, E. *et al.*) 455–464 (Ocean Drilling Program, College Station, Texas, 1990).
8. Kohnen, M. E. L. *et al. Geochim. cosmochim. Acta* **54,** 3053–3063 (1990).
9. Ten Haven, H. L., Rullkötter, J., Sinninghe Damsté, J. S. & de Leeuw, J. W. in *Geochemistry of Sulfur in Fossil Fuels* (eds Orr, W. L. & White, C. M.) 613–632 (American Chemical Society, Washington, DC, 1990).
10. Berner, B. A. *Phil. Trans. R. Soc. Lond.* **315,** 25–38 (1985).

11. Simoneit, B. R. T. & Mazurek, M. A. *Init. Rep. DSDP* **63,** 837–853 (1982).
12. Rulkötter, J., von der Dick, H. & Welte, D. H. *Init. Rep. DSDP* **64,** 837–853 (1982).
13. Von der Dick, H., Rulkötter, J. & Welte, D. H. *Init. Rep. DSDP* **71,** 1015–1032 (1983).
14. Rulkötter, J., Mukhopadyay, P. K. & Welte, D. H. *Init. Rep. DSDP* **75,** 1069–1087 (1984).
15. Volkman, J. k., Allen, D. I., Stevenson, P. L. & Burton, H. R. in *Advances in Organic Geochemistry 1985* (eds Leythaeuser, D. & Rullkötter, J.) 671–681 (1986).
16. Grimalt, J. & Albaigés, J. *Geochim. cosmochim. Acta* **51,** 1379–1384 (1987).
17. Wakeham, S. G. *Geochim. cosmochim. Acta* **54,** 1325–1336 (1990).
18. Vai, G. B. & Ricci Lucci, F. R. *Sedimentology* **24,** 211–244 (1977).
19. Sinninghe Damsté, J. S., Rijpstra, W. I. C., de Leeuw, J. W. & Schenck, P. A. in *Advances in Organic Geochemistry 1987* (eds Novelli, L. & Matavelli, L.) 593–606 (1988).
20. Bray, E. E. & Evans, E. D. *Geochim. cosmochim. Acta* **22,** 2–15 (1961).
21. Eglinton, G. & Hamilton, R. J. in *Chemical Plant Taxonomy* (ed. Swain, T.) 187–217 (Academic, New York, 1963).
22. Didyk, B. M., Simoneit, B. R. T., Brassell, S. C. & Eglinton, G. *Nature* **272,** 216–222 (1978).
23. Ten Haven, H. L., de Leeuw, J. W., Rullkötter, J. & Sinninghe Damsté, J. S. *Nature* **330,** 641–643 (1987).
24. De Leeuw, J. W. & Sinninghe Damsté J. S. in *Geochemistry of Sulfur in Fossil Fuels* (eds Orr, W. L. & White, C. M.) 417–443 (American Chemical Society, Washington, DC, 1990).
25. Summons, R. E., Volkman, J. K. & Boreham, C. J. *Geochim. cosmochim. Acta* **51,** 3075–3082 (1987).
26. Liaaen-Jensen S. in *Marine Natural Products* (eds Faulkner, D. J. & Fenical, W. H.) 1–73 (Academic New York, 1978).
27. Liaaen-Jensen S. in *Photosynthetic Bacteria* (eds Clayton, R. K. & Sistrom, W. R.) 233–248 (Plenum, New York, 1978).
28. Nichols P. D., Volkman, J. K., Palmisano, A. C., Smith, G. A. & White, D. C. *J. Phycol.* **24,** 90–96 (1988).
29. Meunier-Christmann, C. thesis, University of Strasbourg (1988).
30. Ten Haven, H. L., Baas, M., de Leeuw, J. W. & Schenck, P. A. *Mar. Geol.* **75,** 137–156 (1986).
31. Ten Haven, H. L., Rullkotter, J., Stein, R. & Welte, D. H. in *Proc. ODP Sci. Results* **112,** (eds Suess, E. *et al.*) 591–606 (Ocean Drilling Program, College Station, Texas, 1990).
32. Kohnen, M. E. L., Sinninghe Damsté, J. S., Rijpstra, W. I. C. & de Leeuw, J. W. in *Geochemistry of Sulfur in Fossil Fuels* (eds Orr, W. L. & White, C. M.) 444–485 (American Chemical Society, Washington, DC, 1990).

ACKNOWLEDGEMENTS. We thank G. Eglinton and J. R. Maxwell for providing the sediment sample from the Peru upwelling area, H. Brinkhuis for microscopic analysis of the Vena del Gesso sample, M. Baas for analytical assistance, and J. K. Volkman for his constructive review. This work was partly supported by the Netherlands Foundation for Earth Science Research (AWON) with financial aid from the Netherlands Organisation for Scientific Research (NWO).

Hydrothermal activity and metallogenesis in the Lau back-arc basin

Y. Fouquet*, U. Von Stackelberg†, J. L. Charlou*, J. P. Donval*, J. Erzinger‡, J. P. Foucher*, P. Herzig§, R. Mühe‖, S. Soakai¶, M. Wiedicke§ & H. Whitechurch#

* IFREMER Centre de Brest, BP 70, 29280 Plouzane, France
† Bundesanstalt für Gewissenschaften und Rohstoffe (BGR), 3000 Hannover 51, Germany
‡ Institut für Geowissenschaften, Justus-Liebig-Universität, 6300 Giessen, Germany
§ Institut für Mineralogie und Lagerstättenlehre, RWTH Aachen, 5100 Aachen, Germany
‖ Geologisches Institut, Universität Kiel, 2300 Kiel 1, Germany
¶ Ministry of Lands Survey and Natural Resources, Nuku'alofa, Tonga
# Ecole et Observatoire de Physique du Globe de Strasbourg, 5 rue Descartes, 67084 Strasbourg Cedex, France

IN 1989, the submersible Nautile discovered one of the most active hydrothermal fields on the modern ocean floor, in the Lau back-arc basin (Fig. 1). The field contains high-temperature white and black smokers, and as we report here, its characteristics contrast strongly with those of the hydrothermal fields found at normal mid-ocean ridges. The main differences are the acidity (pH as low as 2), chemistry and temperature (up to 400 °C) of the hydrothermal fluids, the composition of the ore deposits, and the volcanic and tectonic environments. The fluids also have very high concentrations of trace metals, and primary gold is present in the accompanying mineral deposits. Our data show that these back-arc deposits in the Lau Basin are intermediate between typical mid-ocean-ridge mineralization and massive sulphide deposits of the Kuroko type.

The Lau Basin is a typical example of an active back-arc basin between a remnant (Lau ridge) and an active volcanic arc (Tofua volcanic arc) (Fig. 1*a*). The northern spreading axis at the centre of the basin consists of tholeiitic basalt. The southern segment, located 75 km closer to the Tofua volcanic arc, is made up of a differentiated series of Fe–Ti basalts, andesites, dacites and rhyolite[1–4]. This area shows a clear influence of the subducted slab on the composition of the lava[4,5].

Here we report observations from the Valu Fa ridge, the southernmost part of the southern segment between 21° and 23° S, only 40 km west of the Tofua volcanic arc[2,6–10] (fig. 1*b*). The water depth ranges from 1,700 to 2,000 m. The sulphide deposits are underlain by basaltic andesites and andesites at the Vai Lili field and by andesites and dacites at the Hine Hina field. The physical properties of the crust and construction processes are such that they do not produce the same fissures, faults and offsets that occur in typical mid-ocean ridge (MOR) systems. In particular, the high gas content of the magmas produces highly vesicular and brecciated lavas which facilitate extensive circulation of sea water and hydrothermal fluids in the crust and create pathways for ascending hydrothermal solutions[8,11,12]. These conditions provide an effective mechanism for abundant and widespread sea-floor and sub-surface mineralization.

Very-high-temperature black (320–400 °C) and white smokers (250–320 °C) were discovered at the central Valu Fa Ridge[6] (Fig. 1*b*, area 2). About 10 groups of smokers were observed in area 2. The active zone, not entirely mapped, is at least 400 m long and 100 m wide and controlled by a normal fault. In the Vai Lili area the hydrothermal plume rises up to 200 m (ref. 6) above the bottom. The temperature anomalies on the bottom are up to 30 °C a few metres from the vents, compared with only some tenths of degrees at hydrothermal sites in MOR systems. This is due to the importance of intense diffuse discharge from the side of the chimney and from the highly porous and brecciated andesite at the base. Away from the sulphidic chimneys there are important zones of widespread low-temperature discharge (100 × 100 m) where the ambient sea-

TABLE 1 Composition of Lau Basin, mid-ocean ridge and Kuroko sulphide deposits

	White Church (zone 3)	Vai Lili (zone 2)	Hine Hina (zone 1)	Mid-ocean ridge	Kuroko
*N**	13	11	5	33	39
SiO_2(wt%)	25.12	10.48	1.76	5.15	
Al_2O_3 (wt%)	1.79	1.39	1.12	0.08	
S (wt%)	18.21	28.51	43.64	35.12	16.20
Ca (wt%)	0.14	1.48	0.07	4.49	
Fe (wt%)	7.17	10.46	34.57	25.96	13.72
Cu (wt%)	3.32	7.05	3.32	7.83	1.88
Zn (wt%)	11.17	26.27	10.87	8.17	6.25
Pb (wt%)	0.23	0.17	0.59	0.05	1.78
Ba (wt%)	20.84	11.76	2.09	0.08	
Mn (p.p.m.)	799	783	44	100	
Co ((p.p.m.)	2	2	5	960	
Ni (p.p.m.)	2	11	4		
As (p.p.m.)	473	1,581	4,586	154	
Se (p.p.m.)	2	0	22	163	
Sr (p.p.m.)	3,166	1,621	1,037	498	
Mo (p.p.m.)	46	30	20	50	
Ag (p.p.m.)	107	143	517	49	215
Cd (p.p.m.)	338	784	323	233	
In (p.p.m.)	<10	92	<10		
Sn (p.p.m.)	<10	5	2		
Sb (p.p.m.)	86	41	25		
Au (p.p.m.)	2	0.6	1.7	0.26	1.58

Calculated average of representative sulphide samples from the three main hydrothermal fields from the Valu Fa Ridge (zones 1, 2, 3). Metal content of dried substances were determined by X-ray fluorescence (P. Cambon and J. Etoubleau, IFREMER/Brest). Gold was analysed by neutron activation method. Values for mid-ocean ridge (East Pacific Rise, 13° N) are from ref. 26 and values for Kuroko from ref. 27.

* *N*, number of determinations.

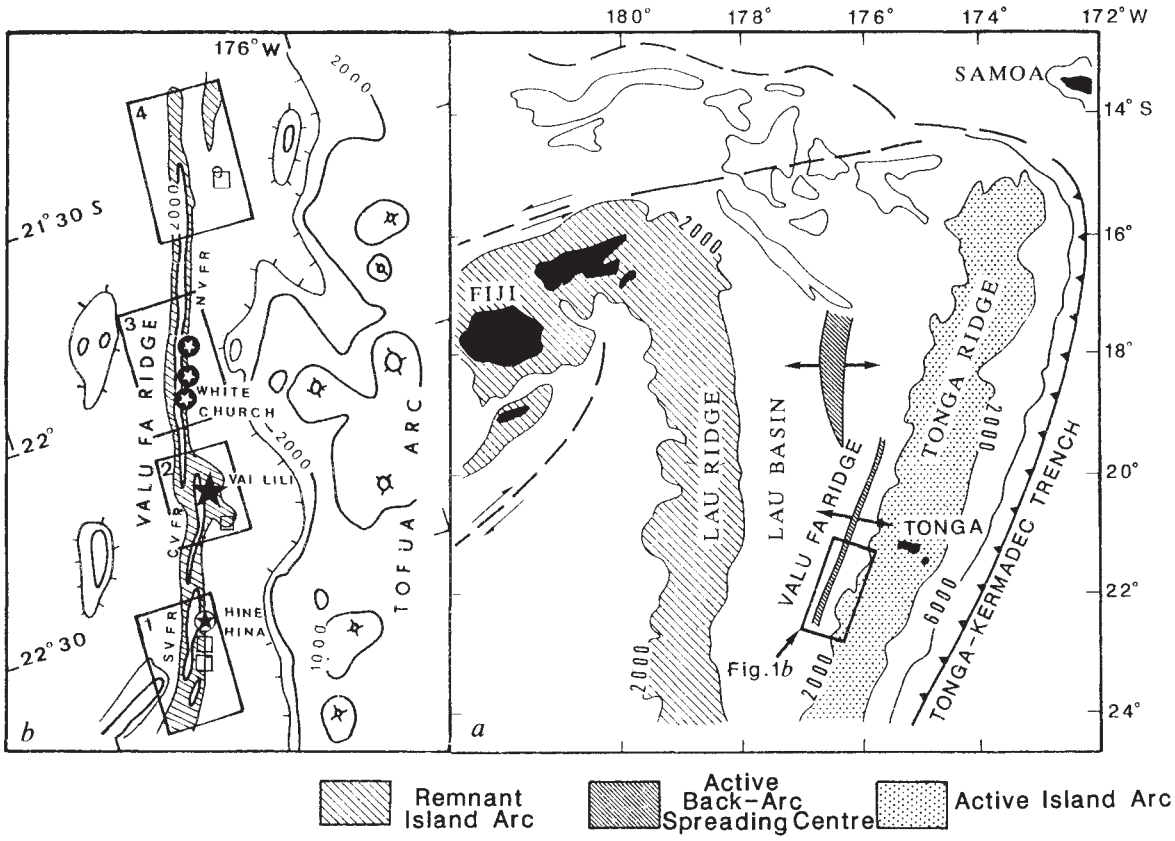

FIG. 1 *a*, General map of the Lau back-arc basin and *b*, location of hydrothermal fields along the Valu Fa Ridge near the active Tofua island arc. The four diving areas (1, 2, 3, 4) are shown together with the names of the three main hydrothermal fields (White Church, Vai Lili and Hine Hina). Nine hydrothermal deposits have been found. Four of them are formed of Mn/Fe oxides related to low-temperature diffuse discharge on broad areas or on top of seamounts (□). One deposit is formed of massive sulphides occurring underneath the extensive low-temperature Mn crust ((✪)). Three deposits are barite dominant chimneys associated with sulphides (✪). The last deposit is the most active area where black smokers, white smokers, barite chimneys and massive sulphides were observed (★).

water temperature anomalies are up to 3 °C. The Vai Lili field is among the most active hydrothermal fields known. At the Hine Hina field surrounding sea water shows enrichments of silica (up to 0.422 mmol kg^{-1}) and methane (up to 4,400 nl l^{-1}) associated with depletion of dissolved oxygen.

Hydrothermal fluids with temperatures ranging from 240 °C to 342 °C (as measured by the submersible probe[6]) were collected at Vai Lili using standard titanium syringes. After extraction of the gas phase, pH, sulphate, methane and silica were determined on board. With one exception, the samples contained >90% hydrothermal fluid. The fluid composition was calculated for a Mg-free end member. All samples have a calculated endmember pH of 2, the lowest measured in deep oceanic hydrothermal fluids (Table 2). Even when the measured temperature is close to the boiling point there is no direct evidence of boiling, but boiling may be responsible for the salinity being higher than that of sea water. The endmember concentration of SiO_2 is about 14 mmol and chloride concentrations lie between 700 and 800 mmol. Iron and copper concentrations are strongly dependent on the fluid temperature. Compared with fluids from MOR hydrothermal vents, the concentrations of boron and Ba in fluids from the Vai Lili field are high (Table 2), but the boron concentrations are close to values found in similar hydrothermal systems such as the Mariana back-arc basin[13]. The manganese content of the endmember is very high (6–7 mmol), with Fe/Mn ratios of about 0.2. The concentrations of dissolved metals (Zn, Pb, As and Cd) are significantly higher than in MOR fluids[14–20] (Table 2). These data, as well as alkali metal ratios, Sr isotopes $^{87}Sr/^{86}Sr = 0.7044$) and B isotopes ($\delta^{11}B = 24.5‰$), are explained by the interaction of the andesitic basement rocks with sea water at greenschist-facies conditions and demonstrate the difference between Valu Fa ridge and MOR hydrothermal systems.

Sulphide deposits from chimneys, sulphide mounds and stockwork were sampled precisely, using the submersible arms. The mean values of sulphide composition for the three main hydrothermal fields is reported in Table 1. The most striking contrasts with MOR deposits are the importance of barium and the very low iron and high arsenic and lead concentrations in the outer part of the deposits. In addition we found primary visible grains (5 μm) of native gold in the outer part of barite/sulphides chimneys from the Vai Lili area where the gold concentration is up to 20 p.p.m. (ref. 21). Previous observation of secondary native gold in the Atlantic was related to weathering of sulphides[22]. In this area (Fig. 1*b*, area 2) a complete cross-section through a massive sulphide deposit was made along a 20-m-high fault scarp. From the top to the base we successively sampled: active smokers up to 17 m high and talus of broken copper/zinc chimneys (barite, anhydrite, chalcopyrite, sphalerite); immature porous zinc sulphides (barite, sphalerite, galena, tennantite, native gold); massive zinc-rich sulphides (sphalerite, pyrite, chalcopyrite); massive copper-rich sulphides (chalcopyrite, pyrite); and stockwork mineralizations in altered andesite showing centimetre-thick veins of chalcopyrite followed by veins of silica, barite and sphalerite.

Crusts of manganese oxide (some up to 10 cm thick) have been produced by extensive (several kilometres long) low-temperature discharge related to the high permeability of the andesite[2,6,12]. At various locations, near-surface rocks show strong alteration, they are highly silicified and impregnated by pyrite, and occurrences of alunite and cristobalite have been described[2]. These Mn deposits are located at the top (Hine Hina field) or next to (Vai Lili and White Church Fields) the sulphide ore bodies. Medium-to-high-temperature barite/sulphide mineralization, observed in many places, constitutes the upper

TABLE 2 Composition of endmember fluids for different ocean hydrothermal waters

Element	Standard sea water	EPR (21° and 13° N)	Guaymas	Marianas	Lau Basin
Temperature (°C)	2	273–354	315	287	334
pH	7.8	3.1–3.8	5.9	4.4	2
SiO_2(mmol kg^{-1})	0.16	15.6–22	9.3–13.8	14	14
Cl (mmol kg^{-1})	541	489–760	580–637		650–800
SO_4 (mmol kg^{-1})	28	0	0		0
B (μmol kg^{-1})	419				770–870
Na (mmol kg^{-1})	465	432–596	472–513		520–615
Li (μmol kg^{-1})	26	591–1,448	630–1,076		580–745
K (mmol kg^{-1})	9.8	23.2–29.8	32.5–49	31	55–80
Rb (μmol) kg^{-1})	1.3	14.1–33	57–86	30	60–75
Mg (mmol kg^{-1})	53	0	0		0
Ca (mmol kg^{-1})	10.2	11.6–55	26.6–41.5		28–41
Sr (μmol kg^{-1})	87	62–182	158–253	90	105–135
Ba (μmol kg^{-1})	0.14	>43	15–54		20–60
Cs (nmol kg^{-1})	2.2	115–246		800	280–370
Fe (μmol kg^{-1})	<0.001	600–10,170	8–180		1,200–2,900
Mn (μmol kg^{-1})	<0.001	361–2,932	128–236		5,800–7,100
Cu (μmol kg^{-1})	0.007	2–44	<0.02–1.1		15–35
Zn (μmol kg^{-1})	<0.01	2–106	0.1–40		1,200–3,100
Cd (nmol kg^{-1})	1	17–180	0–46		700–1,500
Pb (nmol kg^{-1})	0.01	14–359	0–652		3,800–7,000
As (nmol kg^{-1})	27		283–1,074		6,000–11,000
Fe/Mn	1–5		0.1–0.8		0.2–0.4
Cs/Rb $\times 10^{-3}$	1.5	8.2–11.3			4.7–5
$^{87}Sr/^{86}Sr$	0.7091		0.7054		0.7044
$\delta^{11}B$‰*	39.5	32.2		20	24.5

Data for East Pacific Rise (EPR), 13° N, are from ref. 14; data for EPR, 21° N, are from ref. 15; data for Guaymas Basin are from ref. 16; data for Marianas Basin are from ref. 13; the Cs/Rb ratios for the EPR are from ref. 20.
* Relative to NBS SRM 951.

part of the sulphide deposits. The tectonic control of hydrothermal discharge is better established at high-temperature discharge areas than at low-temperature discharge areas.

Although the basic ore-forming processes in back-arc environments are similar to those described at MOR spreading centres, specific properties of the fluids and deposits are largely controlled by the physicochemical properties of the crust which in turn reflects the tectonic setting. Both mineralogical and geochemical compositions of sulphides and fluids indicate the differences between back-arc and ocean-ridge environments. The vertical zonation of the Vai Lili sulphide ore body is close to the normal sequence of typical Kuroko deposits[23] where the outer deposit is black ore (barite, sphalerite, pyrite, galena) and the core is yellow ore (pyrite, chalcopyrite). The Kuroko-type occurrences of Japan are Miocene volcanogenic ore deposits[23]. As is the case for the Lau Basin deposits, these deposits are rich in Ba, Zn, Cu, Pb and Au, and are associated with felsic calc-alkaline rocks of a back-arc spreading centre. In addition, characteristics of the Valu Fa deposits such as the association with brecciated andesites and dacites within a back-arc environment are consistent with the Kuroko model (Table 3). This model is not applicable for back-arc basins in general, however, because the type of ore deposit largely depends on the basement rocks which can be related to the maturity of the back-arc system. In a nascent back arc such as the Okinawa Basin[24], the back-arc system is being created within continental crust, and the hydrothermal model should include interaction between continental crust and sea water. In mature back-arc basins, such as the North Fiji Basin[25], the basaltic oceanic crust that has been created prevents interaction of the sea water with the continental rock and sediments, and the hydrothermal system and associated deposits are therefore similar to those of mid-ocean ridges. Owing to the presence of a differentiated series with island-arc affinities the Lau Basin environment is intermediate between oceanic and continental back-arc environments. This intermediate position is also found for the sulphide compositions[26,27] (Table 1). This indicates that back-arc tectonic environment has a high metallogenic potential, evolving from the continental-controlled Kuroko type in young basins, to the basaltic-controlled MOR type in mature basins. Because of their volcanic environment, tectonic setting and chemical composition, the Lau Basin deposits can be considered to be a transitional type between Kuroko and mid-ocean types. □

TABLE 3 Characteristics of Kuroko, Lan Basin and mid-ocean-ridge sulphide deposits

	Kuroko	**Lau Basin**	**Mid-ocean ridges**
Geodynamic environment	Back-arc spreading	Back-arc spreading	Oceanic spreading
Basement	Continental crust	Island-arc crust	Oceanic crust
Tectonic environment	Caldera	Faulting along ridge	Axial graben
Volcanic environment	Basalt Andesite Dacite Rhyolite	Basalt Andesitic basalt Andesite Dacite Rhyolite	Basalt
Chemistry of deposits	Ba, Ca, Zn Cu, Pb, Au	Ba, Zn, Cu Pb, As, Au	Fe, Zn, Cu
Igneous rocks associated with mineralization	Brecciated dacite and rhyolite	Brecciated andesitic basalt Andesite Dacite	Basalt (pillow and lava flows)

Received 20 September 1990; accepted 8 January 1991.

1. Jenner, G. A. *et al. J. Volcan. geotherm. Res.* **32,** 209–222 (1987).
2. von Stackelberg, U. *et al. Mar. Min.* **7,** 431–442 (1988).
3. Frenzel, J. M., Mühe, R. & Stoffers, P. *Geol. Jb.* D**92,** 395–471 (1990).
4. Sunkel, G. *Mar. Min.* **9,** 205–234 (1990).
5. Boespflug, X. Thesis, Univ. Brest (1990).
6. Fouquet, Y. *et al. Eos* **71,** 678–679 (1990).

7. Morton, J. L. & Sleep, N. H. in *Geology and Offshore Resources of Pacific Island Arcs-Tonga Region* (eds School, D. W. and Vallier, T. L.) 441–443 (1985).
8. von Stackelberg, U. *et al. BGR* Circ. **2,** 3–14 (1985).
9. Foucher, J. P. *et al. C.r. hebd. Seanc. Acad. Sci., Paris* **307,** 509–616 (1988).
10. Parson, L. *et al. Geology* **18,** 470–473 (1990).
11. Herzig, P., von Stackelberg, U. & Petersen S. *Mar. Min.* **9,** 271–301 (1990).
12. von Stackelberg, U. & von Rad, U. *Geol. Jb.* (in the press).
13. Campbell, A. C., Edmond, J. M., Colodner, D., Palmer, M. R. & Falkner K. K. *Eos* **68,** 1531 (1987).
14. Michard, A. *et al. Earth planet. Sci. Lett.* **67,** 297–307 (1984).
15. Von Damm, K. L. *et al. Geochem. cosmochim. Acta* **49,** 2221–2237 (1985).
16. Von Damm, K. L. *et al. Geochem. cosmochim. Acta* **49,** 2197–2220 (1985).
17. Von Damm, K. L. & Bischoff, J. L. *J. Geophys. Res.* **92,** 334–346 (1987).
18. Campbell, I. H. *et al. Nature* **335,** 514–519 (1988).
19. Donval, J. P. *et al. Terra Cognita* **1,** 325 (1988).
20. Palmer, M. R. & Edmond, J. M. *Proc. 28th Int. Geol. Congress* **2,** 567 (Washington, 1989).
21. Herzig, P., Fouquet, Y., Hannington, M. & Stackelberg, U. *Eos* **71,** 1680 (1990).
22. Hannington, M. D., Thompson, G., Rona, P. A. & Scott, S. D. *Nature* **333,** 64–66 (1988).
23. Ohmoto, H. & Skinner, B. J. *Econ. Geol. Monogr.* **5,** 1–8 (1983).
24. Halbach, P. *et al. Nature* **338,** 496–499 (1989).
25. Auzende, *et al. C.r. hebd. Seanc. Acad. Sci., Paris* **309,** 1787–1795 (1989).
26. Fouquet, Y., Auclair G., Cambon, P. & Etoubleau, J. *Mar. Geol.* **84,** 145–178 (1988).
27. Tanimura, S., Date, J., Takahashi, T., Ohmoto, H. *Econ. Geol. Monogr.* **5,** 9–54 (1983).

ACKNOWLEDGEMENTS. The NAUTILAU cruise was an IFREMER/BGR joint project to study hydrothermal activity in the Lau Basin. The campaign was supported by France and Germany. We thank the crew members and the Nautile team, Mr Tongilava (Ministry of Land Survey and Natural Resources) for his help and the permission to work within the Tongan Exclusive Economic Zone, J. Cann for discussions and K. Von Damm for a review.

Seismic excitation by the space shuttle Columbia

Hiroo Kanamori*, Jim Mori†, Don L. Anderson* & Thomas H. Heaton†

* Seismological Laboratory, California Institute of Technology, Pasadena, California 91125, USA
† United States Geological Survey, 525 South Wilson Avenue, Pasadena, California 91106, USA

SEISMIC stations in southern California recorded the atmospheric shock waves generated by the space shuttle Columbia on its return to the Edwards Air Force base on 13 August 1989 (Fig. 1). In addition to the shock wave, the broad-band IRIS–TERRAscope station at Pasadena recorded a distinct pulse with a period of ~2–3 seconds, which arrived 12.5 seconds before the shock wave (Fig. 2). This pulse was also recorded at the University of Southern California, near downtown Los Angeles, where it arrived 3 seconds after the shock wave. The origin of this pulse could not be readily identified. We show here that it was a seismic P wave excited by the motion of high-rise buildings in downtown Los Angeles, which were hit by the shock wave. The proximity of the natural period of the high-rise buildings to that of the Los Angeles basin enabled efficient energy transfer from shock wave to seismic wave.

The shock-wave arrival times can be best explained with Mach cones (the conical shock-wave fronts produced by the passage of supersonic aircraft) propagating N40E across the Los Angeles (LA) basin. The velocity varies from 1,300 m s^{-1} (Mach 4.4) on the coast to 700 m s^{-1} in the Mojave desert. The shock wave excited by a supersonic aircraft is called an N wave because of its distinctive N-shaped pulse[1] (Fig. 3). Cook and Goforth[2] describe two kinds of seismic effects of sonic booms: a moving strain in the immediate vicinity of the surface loads, caused by the N-wave overpressure, and coupled seismic waves, which follow the passage of the N wave. The N waves shown in Fig. 3 are of the first kind. The positive pressure causes downward ground motion near the seismograph site, which is consistent with the observed polarity. We estimated the pressure from these records by approximating the shock front with a plane wave incident on a half-space. Following equation (9.187) of ref. 3, we calculated the response of the half-space to an N wave, convolved it with the instrument response, compared it with the observed seismogram, and thus estimated the pressure changes to be from 0.7 to 2.2 mbar, which are similar to those measured directly by pressure gauges for the earlier space shuttles[4].

The most unusual observation was the very distinct long-period (about 2 to 3 s) pulse with an amplitude of about 1 μm observed at Pasadena (PAS) 12.5 s before the arrival of the shock wave. The initial horizontal particle motion is in the northeast direction, and is in phase with the vertical motion, indicating that this pulse is a seismic P wave arriving at the station from the southwest. The time difference of 12.5 s between the shock wave and the P pulse suggests that the origin of the P pulse is located near downtown Los Angeles, 14.5 km southwest of Pasadena (see Fig. 1 inset). A broadband instrument at station SCS (at the University of Southern California) also recorded this pulse as well as the shock wave (Fig. 2). Unlike the Pasadena record, this record shows the P pulse arriving about 3 s after the shock wave. The amplitude is 10 μm, ten times larger than that at Pasadena. These observations support the interpretation that the P pulse originated from downtown Los Angeles.

To excite the P wave in this area, the shock-wave energy must have been transferred to the ground there through some coupling mechanism. The most prominent feature in downtown Los Angeles is a group of high-rise buildings with a natural period of 1–6 s. This led us to believe that the P pulse was excited by the high-rise buildings which were hit simultaneously by the

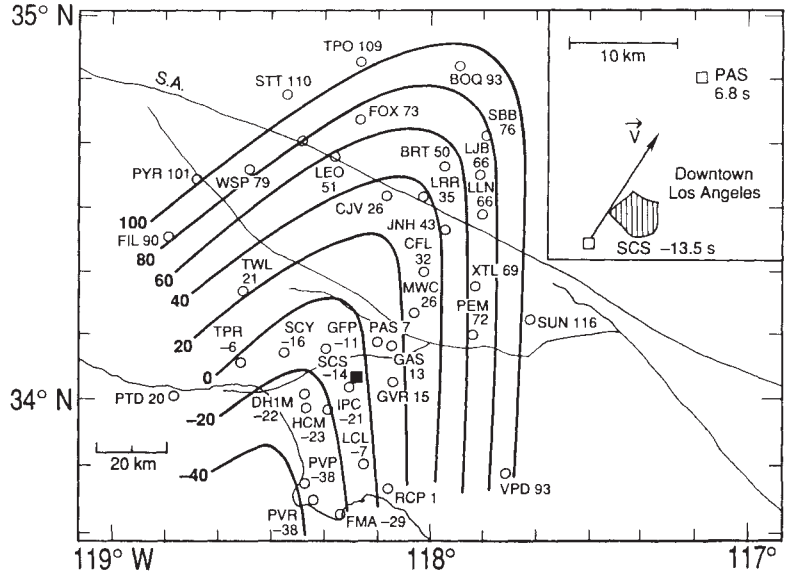

FIG. 1 Arrival times of the shock waves excited by the space shuttle Columbia, recorded by seismic stations of the Southern California Seismic Network and The University of Southern California Los Angeles Basin Seismic Network. The numbers below the station codes are the arrival times (in seconds from an arbitrary reference time). Hyperbolas at 20 s intervals are fitted to the arrival-time data. The inset shows the stations PAS and SCS (at the University of Southern California) with respect to downtown Los Angeles. The vector V indicates the shuttle path. The arrival-time difference between PAS and SCS is 20.3 s.

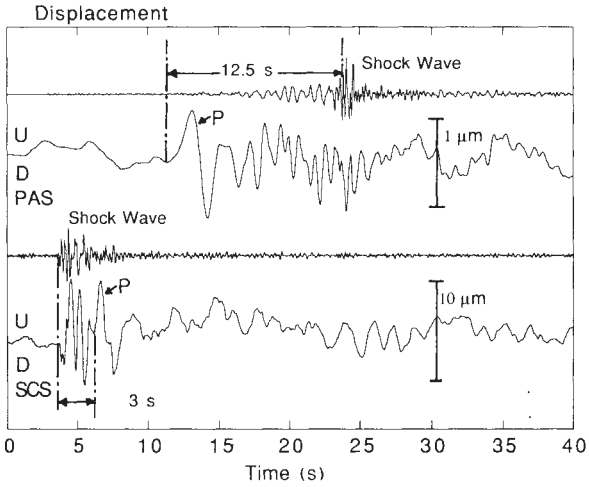

FIG. 2 Comparison of the displacement records at PAS and SCS (for station locations, see Fig. 1) displayed on a common timescale. A high-pass-filtered record is shown above the displacement record for each station to indicate the arrival time of the shock wave. Note that at PAS the long-period P pulse arrives 12.5 s before the shock wave, whereas at SCS it is 3 s after the shock wave.

shock waves. According to the Los Angeles City Fire Department (F. Border, personal communication), there are about 100 buildings taller than 20 stories in downtown Los Angeles and the Wilshire district.

Because of the weak damping of the building, the oscillation of the individual building hit by a shock wave lasts for a long time. The resulting ground motion will be a long, damped oscillation instead of an impulse. If, however, many buildings with different periods are excited simultaneously, the first cycle will contribute constructively to excitation of ground motion, but the later cycles will interfere destructively with no significant net contribution; the resulting ground motion will be impulsive, as observed. This situation may be viewed as an inverse Fourier transform of a delta function.

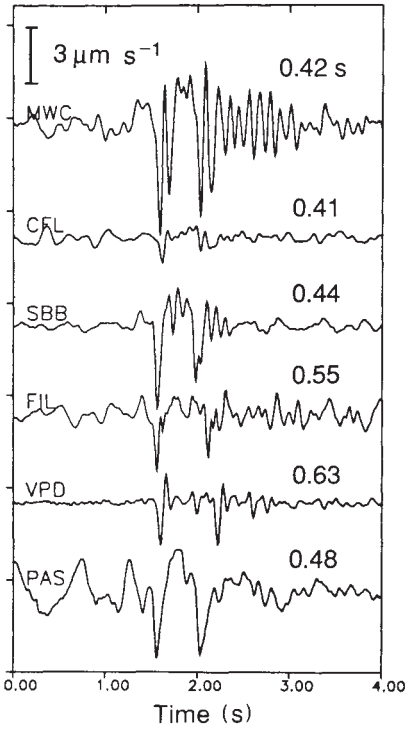

FIG. 3 Examples of N waves. The records represent ground-motion velocity in a frequency range of 1–10 Hz. The numbers to the right are the separations (in s) between the two pulses of an N wave.

The excitation of seismic waves by shaking of a building has been demonstrated by Jennings[5]. Shaking of the Millikan Library building (nine stories) on Caltech Campus excited seismic waves which were observed with a seismograph at Mount Wilson, 11 km away. The observed acceleration on the roof of the Millikan Library was 0.02 *g*, and the observed amplitude at Mount Wilson was 0.02 μm.

The efficient excitation of the seismic pulse with a period of 2–3 s by the buildings suggests, by reciprocity, that seismic-wave energy coming into the Los Angeles basin will be transferred efficiently to the buildings with this range of natural period. This points to the importance of investigating the long-period site response of the Los Angeles basin[6,7]. The importance of site effects has been demonstrated repeatedly for recent major earthquakes, such as the 1985 Mexico earthquake and the 1989 Loma Prieta earthquake.

As many recent studies have suggested, large earthquakes with a long fault length, such as those expected on the San Andreas fault, excite a highly significant amount of energy at periods longer than 1 s. In view of the high probability of large ($M > 7.5$) earthquakes on the San Andreas fault in the next 30 years[8], and possible large earthquakes on the blind faults beneath the Los Angeles basin[9], it is important to assess the long-period response of the Los Angeles basin quantitatively so that more comprehensive hazard mitigation measures can be taken. □

Received 22 October 1990; accepted 8 January 1991.

1. Carlson, H. W. & Maglieri, D. J. *J. acoust. Soc. Am.* **51,** 675–685 (1972).
2. Cook, J. C., Goforth, T. & Cook, R. K. *J. acoust. Soc. Am.* **51,** 729–741 (1972).
3. Ben Menachem, A. & Singh, S. J. *Seismic Waves and Sources* 1-1-1108 (Springer, New York, 1981).
4. Garcia, F. J., Jones, J. H. & Henderson, H. R. *NASA tech. Pap. 2475,* 1–42 (National Aeronautics and Space Administration, Washington, DC, 1985).
5. Jennings, P. C. *Bull. seismol. Soc. Am.* **60,** 2037–2043 (1970).
6. Liu, H.-L. & Heaton, T. *Bull. seismol. Soc. Am.* **74,** 1951–1968 (1984).
7. Helmberger, D. V. & Vidale, J. E. *Bull. seismol. Soc. Am.* **78,** 109–121 (1988).
8. Working Group on California Earthquake Probabilities, *US Geological Survey Open-File Report 88-398* (US Geological Survey, US Department of the Interior, Washington, DC, 1988).
9. Hauksson, E. *J. Geophys. Res.* **95,** 15365–15394 (1990).

ACKNOWLEDGEMENTS. We thank B. Sturtevant, P. Jennings, J. Beck and D. Harkrider for discussions, D. Goldstein, for information on the space shuttle parameters, D. Maglieri for the references to seismic measurements of sonic booms, and F. Borden, Los Angeles City Fire Department, for providing the building statistics in the city of Los Angeles.

Gene flow between African- and European-derived honey bee populations in Argentina

Walter S. Sheppard*, Thomas E. Rinderer†, Julio A. Mazzoli‡, J. Anthony Stelzer† & Hachiro Shimanuki*

* Bee Research Laboratory, USDA-ARS, Building 476, BARC-E, Beltsville, Maryland, 20705, USA
† Honey Bee Breeding, Genetics and Physiology Research Laboratory, USDA-ARS, 1157 Ben Hur Road, Baton Rouge, Louisiana, 70820, USA
‡ Catedra de Genética, Facultad de Agronomia, Universidad de Buenos Aires, 1417 Buenos Aires, Argentina

IN the Neotropics, introduced European honey bees (*Apis mellifera* L.)[1,2] have been largely supplanted by bees descended from an African race, *A. m. scutellata* Lepetier, which were introduced into Brazil in the 1950s. Recent restriction enzyme analyses indicate that mitochondrial DNA in some neotropical populations is almost entirely of African origin[3,4], and these data have been cited as evidence for asymmetrical gene flow between African- and European-derived populations[3,4]. Evaluation of the nature of hybridization in the Neotropics is, however, confounded by possible

population size advantages for the African-derived group[5–7]. As an alternative approach, genetic interactions can be studied in transition areas between zones ecologically and climatically adaptive for both racial groups. We describe here results of a survey transecting regions populated by African- and European-derived honey bees in Argentina. Mitochondrial DNA, morphological and isoenzyme analyses show that substantial hybridization occurs between the two racial groups.

For several decades the northward expansion of African-derived (Africanized) honey bee populations has been tracked with behavioural, morphological and biochemical studies[8–13]. In general, behavioural studies have shown that certain characters of the African race, especially those with adaptive value in the tropics (including swarming and absconding propensities, defensive behaviour, and opportunistic use of resources), are predominant within the Africanized population. Alloenzyme evidence for varying degrees of hybridization between African- and European-derived honey bee populations in the Neotropics has recently been reported[14,15]. Although the frequency of malate dehydrogenase allele Mdh^{100} is >0.95 in African *A. m. scutellata* and >0.90 in some neotropical Africanized populations[3,12,13], the mean frequency of Mdh^{100} in 118 Africanized colonies within the Brazilian state of Sao Paulo was ~0.78, indicating sources other than *A. m. scutellata* for some genes[14,15].

We investigated the genetic interaction between European- and African-derived honey bee populations in an area of geographical overlap in the New World. We hypothesized that hybridization should be most evident between areas most suitable ecologically and climatically for the two racial groups. In the Russian steppes, for example, an area of natural introgression occurs between the endemic ranges of two honey bee races (*A. m. mellifera* and *A. m. carnica* Pollman)[16]. In the temperate New World, portions of Argentina provide the best current areas of interface between African- and European-derived populations[17,18]. The northern portion of the country, as far south as the sugar cane-growing region of Tucuman, is an area saturated by Africanized honey bees (AHB)[17] to the complete exclusion of commercial beekeeping with European-derived populations. From Buenos Aires province southward, the country is considered to be free of Africanized honey bees and, after the arrival of these bees in Argentina in 1968, has become the main area for the production of European-type queens for commercial use[17]. The region between these two areas is regarded as a transition zone between the two racial types[17] (Fig. 1).

Mitochondrial DNA (mtDNA) genotypes of 106 feral colonies from the northern 'AHB-saturated' region and the southern 'AHB-free' region were consistent with expectations (Table 1). That is, 59 of 67 colonies in the north and 33 of 39 colonies in the south exhibited mtDNA restriction patterns indicative of African and European races, respectively (Fig. 2). Morphological analyses of the same colonies yielded similar results: 63 of 67 colonies in the AHB-saturated region have Africanized morphology and 30 of 39 colonies in the AHB-free zone display European morphology (Table 1). In the area of transition both mtDNA types were detected in relatively high frequency. The predominance of Africanized morphology in samples from this region suggests that the main interface may be south of previous estimates[17]. Additional samples are, however, required to determine the current position, shape and width of the transition zone and to allow estimation of the relative contributions of selection and dispersal to its maintenance[19].

In 28 colonies, including 16 of 65 sampled from the transition zone, mtDNA and morphological analyses gave contradictory indications. That is, colonies exhibited Africanized morphology and European mtDNA, or vice versa. In addition, isoenzyme analysis of these colonies showed that, outside the area of transition, high frequencies of the nuclear allele Mdh^{100} remain significantly associated with Africanized morphology (Table 1). Within colonies from the transition area, where hybridization and backcrossing between the two racial types is more likely, high Mdh^{100} frequencies were not significantly associated with Africanized morphology.

In 11 of 12 colonies exhibiting contradictory mtDNA genotypes and morphology outside the transition area, morphology reflected climatic/ecological expectations (that is, Africanized morphology in the north and European morphology in the south). Thus, although nuclear genes responsible for morphology (and probably behaviour) seem to be under selection outside the transition area, no evidence was detected to support the speculation that European mtDNA interacts sub-optimally with African nuclear DNA.

Natural selection against feral European maternal descendants is a reasonable assumption in tropical climates[7,20,21] given the known fitness and reproductive advantages of the Africanized population[10,22] and, together with population size disparities[6], may best explain the predominance of African mtDNA in Neotropical honey bees[3,4]. Further studies using markers to detect both maternal and paternal genetic contributions[23] may

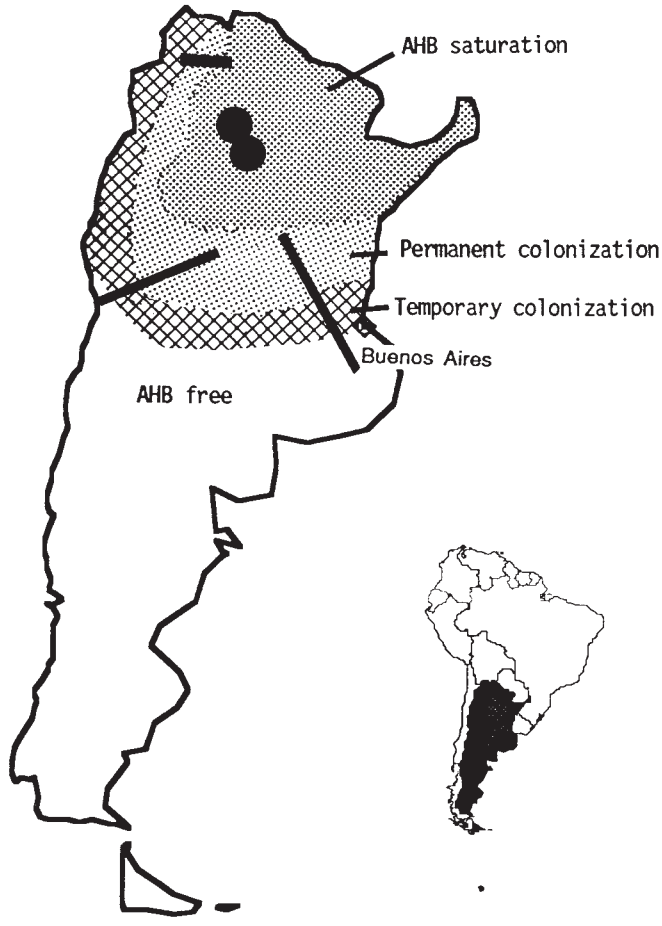

FIG. 1 Map of the collecting transects and published distribution of racial types in Argentina. Transects consisted of a northern Andean transect from Tucuman–Salta–Cachi, a southern Andean transect from Tucuman–San Juan–Uspallata and a southern transect from Tucuman–Cordoba–General Villejas–Chascamus. The major collections of African-derived populations were made near Tucuman, and are represented by the black circles. Honey bees taken from the 'permanent' and 'temporary' colonization regions constitute our transition zone samples. Samples of adult workers from 171 colonies and 44 locations were collected in liquid nitrogen from mtDNA analysis and ethanol for morphological analysis. Samples consisted entirely of feral honey bees to best reflect a measure of adaptation to local ecological conditions[27]. We defined as feral, colonies known to be free from requeening and other management techniques directly affecting the proportion of racial genotypes and included colonies living in bridges, trees, buildings, electric utility poles, fruit boxes and unmanaged beehives. Taken from ref. 17.

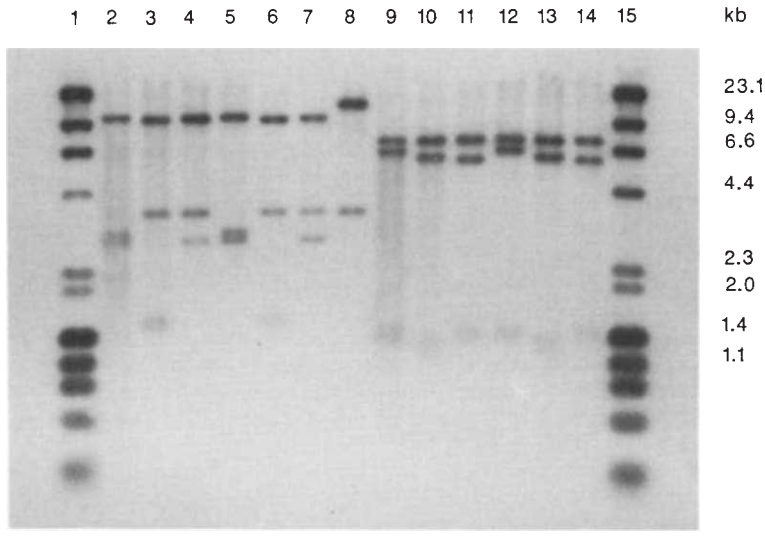

FIG. 2 Autoradiograph of 1% agarose gel showing honey bee mtDNA digested with *Eco*RI (lanes 2–8) and *Bcl*I (lanes 9–14). Lanes 2, 9 are Norwegian *A. m. mellifera*, lanes 3, 10 are Italian *A. m. ligustica* and lanes 4, 11 are Kenyan *A. m. scutellata*. Lanes 5–8 and 12–14 are feral Argentine honeybee samples. The 'carnica/ligustica' pattern (lanes 3, 10; also reported for *A. m. carnica*[3]) constituted 67% of the feral Argentine colonies exhibiting 'European' mtDNA haplotypes. Lane 8 illustrates a previously unreported *Eco*RI mtDNA pattern found in six colonies. *Eco*RI digests of these latter colonies yielded two fragments of approximately 14.0 and 3.8 kilobases. When digested with other restriction enzymes, these samples produced 'typical' African patterns. Lanes 1 and 15 each contain λ/*Hind*III and ϕX174/*Hae*III standards. METHODS. Mitochondrial analysis consisted of an extraction procedure for total nucleic acids[28] followed by digestion with several restriction enzymes (*Eco*RI, *Xba*I, *Bcl*I) considered diagnostic for separating African and European racial groups[3,4,29]. After electrophoresis, the DNA was transferred to nitrocellulose and the blots were hybridized (50 °C, 25% formamide) with ^{32}P-nick-translated probe made from honey bee mtDNA purified on a CsCl gradient. The mitochondrial bands were visualized by autoradiography.

resolve the issue of mitochondrial-nuclear genotype interactions. But the possibility that Africanized populations originally dispersed in the Neotropics by occupying a virtually *Apis mellifera*-free niche, necessitates caution in interpreting putative changes in allele (marker) frequencies in the Neotropics, unless relative sizes of the interacting populations can be estimated.

These results demonstrate that a zone of complex hybridization exists between European- and African-derived racial types of honey bees in temperate Argentina. Gene flow between the racial types occurs with sufficient frequency in this zone for both mtDNA genotypes to be associated with a range of nuclear genotypes. Through backcrossing, mtDNA genotypes move with the 'opposite' morphology (nuclear genotype) into the latter's geographic region. These results are reminiscent of other subspecies and species hybrid zones, insofar as both mtDNA genotypes occur within geographically structured classes of nuclear genotype[24,25], although analysis of additional samples from the transition zone is required to determine the structure of the cline and classify genotype fitness relationships[26]. Further data from this established zone of hybridization in temperate Argentina may help predict the spread of Africanization in temperate North America. □

TABLE 1 Mitochondrial and morphological classification of Argentine honey bee colonies

Geographical zone cf. racial type*	Mitochondrial pattern		Morphology† African-ized	Inter-mediate‡	European
Northern	African	59	58	1	—
'AHB concentration area'	European	8	5	—	3
Transition	African	46	31	13	2
	European	19	14	4	1
Southern	African	6	—	—	6
'AHB-free'	European	33	1	8	24

Twenty-eight colonies where mtDNA and morphological indications were contradictory were assayed also for variation in *Mdh* allele frequencies (20 workers per colony) using starch gel electrophoresis[27]. Colonies were classified as Africanized or European based on morphology, and the distribution of Mdh^{100} was tested by the Mann-Whitney *U*-test. Analysis of the 12 colonies from the AHB concentration area and AHB-free area revealed a significantly higher Mdh^{100} frequency in colonies with Africanized morphology (AHB Mdh^{100} frequency = 0.69, European Mdh^{100} frequency = 0.36; $P = 0.015$). However, there was no significant association of Mdh^{100} frequency with morphology when all 28 colonies were tested.

* From ref. 17.

† Morphological analysis was preceded by dissection, staining and slide-mounting 10 bees from each sample, according to the methods of Daly and Balling[8]. Slides were then digitized and the data analysed using two different programs written for the morphological determination of Africanization[8,30]. These programs use discriminant analysis, with functions derived from (1) South American Africanized populations; (2) 'European' populations from US apiaries; and (3) F_1 hybrids of African- and European-derived populations produced in Venezuela. Colonies were scored Africanized or European on the basis of a 95% probability of group membership as ascertained by both programs. In cases of less than 95% probability or discordant results among the programs, samples were scored as Intermediate, indicating noninclusion in the discriminated groups.

‡ Nondiscriminated, see †.

Received 10 October 1990; accepted 3 January 1991.

1. Ruttner, F. *Biogeography and Taxonomy of Honey Bees* (Springer, Berlin, 1988).
2. Sheppard, W. S. *Am. Bee J.* **129,** 617–619, 664–667 (1989).
3. Smith, D. R., Brown, W. M. & Taylor, O. R. *Nature* **339,** 213–215 (1989).
4. Hall, G. H. & Muralidharan, K. *Nature* **339,** 211–213 (1989).
5. Taylor, O. R. *Bull. ent Soc. Am.* **31,** 14–24 (1985).
6. Page, R. E. Jr *Nature* **339,** 181–182 (1989).
7. Rinderer, T. E. in *Africanized Honey Bees and Bee Mites* (eds Needham, G. R., Page, R. E. Jr, Delfinado-Baker, M. & Bowman, C.) 13–28 (Ellis Horwood, Chichester, 1988).
8. Daly, H. & Balling, S. S. *J. Kans. Entomol. Soc.* **51,** 857–869 (1978).
9. Kerr, W. E. & Bueno, D. *Evolution* **24,** 145–148 (1970).
10. Rinderer, T. E., Hellmich, R. L. III, Danka, R. G. & Collins, A. M. *Science* **228,** 1119–1121 (1985).
11. Roubik, D. W., *Ecology* **61,** 836–845 (1980).
12. Sheppard, W. S & Huettel, M. D. in *Africanized Honey Bees and Bee Mites* (eds Needham, G. R., Page, R. E. Jr, Delfinado-Baker, M. & Bowman, C.) 281–286 (Ellis Horwood, Chichester, 1988).
13. Sylvester, H. A. *J. Apic. Res.* **21,** 93–97 (1982).
14. Lobo, J. A., Del Lama, M. A. & Mestriner, M. A. *Evolution* **43,** 794–802 (1989).
15. Del Lama, M. A., Lobo, J. A., Soares, A. E. E. & Del Lama, S. N. *Apidologie* **21,** 271–280 (1990).
16. Ruttner, F. in *The Hive and the Honey Bee* (eds Dadant & Sons) 19–38 (Dadant, Hamilton, Illinois, 1975).
17. Kerr, W. E., de Leon del Rio, S. & Barrionuevo, M. D. *Am. Bee J.* **122,** 196–197 (1982).
18. Dietz, A. & Krell, R. *Apidologie* **16,** 99–108 (1985).
19. Barton, N. H. & Hewitt, G. M. *A. Rev. ecol. Syst.* **16,** 113–148 (1985).
20. Michener, C. D. *A. Rev. Ent.* **20,** 339–416 (1975).
21. Taylor, O. R. in *Africanized Honey Bees and Bee Mites* (eds Needham, G. R., Page, R. E. Jr, Delfinado-Baker, M. & Bowman, C.) 29–41 (Ellis Horwood, Chichester, 1988).
22. Winston, M. L., Otis, G. W. & Taylor, O. R. Jr *J. Apic. Res.* **18,** 85–94 (1979).
23. Hall, G. H. *Genetics* **125,** 611–621 (1990).
24. Powell, J. R. *Proc. natn. Acad. Sci. U.S.A.* **80,** 492–495 (1983).
25. Marchant, A. D., Arnold, M. L. & Wilkinson, P. *Heredity* **61,** 321–328 (1988).
26. Hewitt, G. M. *Trends Ecol. Evol.* **3,** 158–167 (1988).
27. Sheppard, W. S. *Ann. Ent. Soc. Am.* **81,** 886–889 (1988).
28. Sheppard, W. S. & McPheron, B. A. in *Diversity in* Apis (ed. Smith, D. R.) (Westview, Colorado, in the press).
29. Sheppard, W. S. & Huettel, M. D. *Am. Bee J.* **127,** 851 (1987).
30. Rinderer, T. E. *et al. Ann. Ent. Soc. Am.* **83,** 346–351 (1990).

ACKNOWLEDGEMENTS. We thank the following for assistance in collecting or analysing honey bee samples: Sr Barrera, E. Castro, H. Cordo, R. Glass, Sr Maglioni, B. McPheron, R. Riggio, P. Sapoval, Sr Seghezzo, P. Sianbom, A. Suarez, and M. Zapater. We also thank M. Berenbaum, S. Berlocher, N. Calderone, B. McPheron, B. Oldroyd, C. Sheppard, G. Steck, and J. Villa for valuable discussion and comments on the manuscript.

Ancient *HLA* genes from 7,500-year-old archaeological remains

David A. Lawlor*, Cynthia D. Dickel†, William W. Hauswirth† & Peter Parham*‡

* Departments of Cell Biology, and Microbiology and Immunology, Stanford University, Stanford, California 94305, USA
† Departments of Immunology and Medical Microbiology, and Ophthamology, University of Florida College of Medicine, Gainesville, Florida 32610, USA
‡ To whom correspondence should be addressed

IN the past decade there has been increasing interest in cloning DNA from ancient and preserved tissues[1–6]. Most studies, however, have focused on mitochondrial or chloroplast genes, present at hundreds to thousands of copies per cell compared with one or two for each nuclear gene[7–9]. With a probe containing *Alu* repeat sequences, Pääbo isolated a 3.4-kilobase DNA fragment from a 2,400-year-old Egyptian mummy[10] which was subsequently shown to contain an intron of the nuclear gene *HLA-DQA* (ref. 11). Here we report a more targeted approach to the characterization of nuclear genes from archaeological specimens. The Windover pond of central Florida has provided skeletal and soft tissue remains from 165 humans, radiocarbon-dated to be 6,990–8,130 years old[12–14]. Using DNA obtained from one individual we have characterized segments from six nuclear genes: that for β_2-microglobulin and five members of the class I HLA heavy chain gene family. Distinctive patterns of nucleotide substitution in the cloned heavy chain gene segments permit tentative assignment of the *HLA-A,B* type of the ancient individual.

Brain DNA from male SS325 of the Windover population provided the substrate for polymerase chain reaction amplifications[15]. This used oligonucleotide primers designed to amplify one segment of the β_2-microglobulin (β2m) gene and three segments of class I HLA heavy chain genes (Fig. 1). Although all four primer pairs amplified modern human DNA, only one pair of heavy chain primers and the β2m primers amplified the ancient DNA. The products were heterogeneous as assessed by both agarose gel electrophoresis and sequence analysis after cloning into M13 phage. Of 35 independent clones from the β2m amplification, 11 gave inserts of appropriate size with nucleotide sequences identical to the modern human β2m gene[16]. Initial amplifications with class I heavy chain primer pair 3 resulted in 2–20% of clones having the targeted sequence. Subsequent experiments used a secondary amplification using the indented pair of primers 3′ (Fig. 1). This increased the frequency of clones containing the targeted gene segment to >90%.

Analysis of 89 heavy chain clones from five amplifications using two independent DNA extractions yielded 14 different sequences (Table 1; Fig. 2). Nine of the sequences correspond exactly or closely to class I HLA genes characterized from modern DNA and five appear to be chimaeras with segments derived from more than one gene. Clones with sequences identical to *HLA-G* (ref. 17), *HLA-B*3701* (ref. 18) and to members of the *HLA-A19* family[19] (*HLA-A*2901*, *A*3101* or *A*3201*) were found (Table 1). Segments characteristic of *HLA-A*0201*, *HLA-B*1501* and a pseudogene *HLA-AR* (refs 20–22) are present in the chimaeric products. Clone 325-6 has a sequence the same as that of the chimpanzee B locus allele *PatrB2* (ref. 23) and differs from *HLA-B*1801* (ref. 24) by only two nucleotide substitutions. It may therefore represent a new subtype of *HLA-B18*. Clone 325-5 similarly represented a novel sequence when first determined and at that time we assumed it corresponded to an undiscovered class I HLA gene. This proved to be true as Hansen and colleagues recently obtained a clone, *DAN4*, corresponding to this gene from modern DNA[25]. Over the amplified segment the sequences of *DAN4* and clone 325-5 are identical

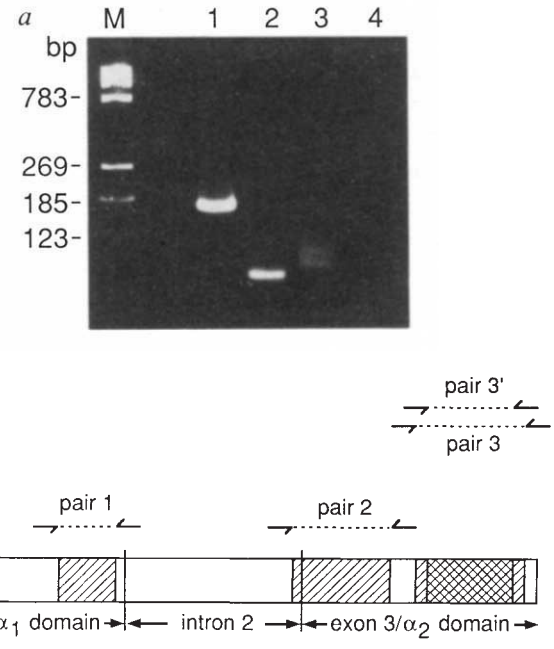

FIG. 1 *a*, Agarose gel stained with ethidium bromide showing the 179-base-pair (bp) amplified class I gene fragments obtained from ancient DNA. Primary amplification was performed with primer pair 3 and secondary amplification with primer pair 3′. Products resulting from DNA extracted from Windover brain tissue (lane 1), mock extraction control (lane 2), reagent control (no DNA) from the secondary amplification (lane 3) and the same reagent control following primary amplification (lane 4). Markers are *Hae*II-digested ΦX174 fragments. The band in lane 2 is a size expected for primer dimers. *b*, Schematic of exon 2, intron 2 and exon 3 of class I HLA genes, indicating hybridization sites for the pairs of amplification primers. Sequences of the HLA primers are: pair 1, 5′-GGGCGTCGACGAGCAGGAGGGGCCGGAGTATT-GGGA-3′ and 5′-CCGCAAGCTTACCGGCCTCGCTCTGGTTGTAGTAGC-3′; pair 2, 5′-GGGCGTCGACCTCGGGGGACTGGGCTGACCGCGGGG-3′ and 5′-CCGC-AAGCTTGCGATGTAATCCTTGCCGTCGTAGGGC-3; pair 3, 5′-GGGCGTCGAC-CCTACGACGGCAAGGATTACATCGCC-3′ and 5′-CCGCAAGCTTCCCGTTC-TCCAGGTATCTGCGGAGC-3′;pair3′,5′-ATCGAAGCTTAAGGATTACATCGCCCTG-AACGAGGA-3′ and 5′-AGTCGTCGACCTCCAGGTATCTGCGGAGCCACTCCA-3′. *Sal*I or *Hind*III restriction sites (underlined) are included in the primers. The regions of the HLA class I genes targeted for amplification are shaded and the predicted size fragments resulting from primer pairs 1, 2, 3 and 3′ are, respectively, 68, 87, 125 and 107 bp (excluding primers).

METHODS. Windover-brain (SS325) cerebral-cortex tissue was extracted by shaking with 0.3 M NaCl, 0.03 M sodium citrate, pH 7.4, 2% SDS for 1 h at 42 °C, extracted twice with phenol:chloroform:isoamyl alcohol (25:24:1), and once with chloroform. The aqueous phase was precipitated with 2.5 volumes of ethanol (20 °C). The precipitate was redissolved in water. Caesium chloride (1 g ml^{-1}) and ethidium bromide (0.5 mg ml^{-1}) were added and the solution centrifuged to equilibrium in a type 50 Ti rotor for 48 h at 40,000 r.p.m. Visible ethidium bromide-stained bands were collected, *n*-butanol-extracted and ethanol-precipitated. Polymerase chain reactions (PCR) were performed in 50-μl reaction volumes containing 10 ng DNA in 10 mM Tris–HCl, pH 8.3 (at 25 °C), 50 mM KCl, 1.5 mM $MgCl_2$, 200 μl each of dATP, dCTP, TTP and dGTP and 0.2 μM each of the 5′ and 3′ oligonucleotide primers. *Thermus aquaticus* DNA polymerase (2 units) was added and an initial denaturation of 94 °C for 10 min was followed by 40 PCR cycles performed as follows: 94 °C for 1 min, 2-min ramp time, 37 °C for 1 min, 30-s ramp time, 72 °C for 3 min and a 30-s ramp time. Secondary amplification was performed by removing a 1-μl aliquot of the completed reaction and adding it to a fresh PCR reaction volume containing primer pair 3′. Amplification parameters were the same but only 25 cycles were performed. Amplified products were sequentially digested with *Sal*I and *Hind*III and ligated into doubly cut M13mp18 and mp19 before transformation of *Escherichia coli* JM109. Transformants were sequenced by the dideoxy chain termination method with both dGTP and dITP termination mixes.

including the base-pair deletion that demonstrates that *DAN4* represents a pseudogene (Fig. 2).

Of concern in analysis of ancient DNA is potential contamination with modern DNA, and we therefore adopted the precautions and quality controls recommended by Pääbo and colleagues[26]. The sequences from SS325 are clearly of human origin and finding that only one of three pairs of class I heavy chain primers amplified ancient DNA, whereas all three amplified modern DNA, provides good evidence for the absence of contamination with modern human DNA. Trivial tissue contaminations are further ruled out by the dissimilarity between the *HLA-A,B* sequences obtained from SS325 and the *HLA-A,B* alleles of the individuals performing the experiments (D.A.L. and C.D.D.). Neither can contamination with modern class I DNA clones explain the data as no class I major histocompatibility complex clones have ever been handled in the Florida laboratory where all amplifications were performed, and clones having the *DAN4, PatrB2* and *HLA-G* sequences have never been introduced into either laboratory. Further evidence for amplification of ancient DNA comes from the distribution of sequences in the amplified products.

One feature is the presence, in three of four amplifications, of a predominant sequence, which differed between amplifications (Table 1). This was most extreme in amplification D for which all 45 clones analysed had the *HLA-A19* sequence. The 'Poisson-like' distribution of amplification targets indicates

a

```
           1                                                  50                                                 100                                                 125
Consensus  CTGAACGAGG ACCTGCGCTC CTGGACCGCG GCGGACACGG CGGCTCAGAT CACCCAGCGC AAGTGGGAGG CGGCCCGTGT GGCGGAGCAG CTGAGAGCCT ACCTGGAGGG CACGTGCGTG CAGTG
    HLA-G  ---------- ---------- ---------a --------t- ---------- -t--a----- -----t---- -----aa--- ---t--a--a ag-------- ---------- ---------- -----
    325-1  ---------- ---------- ---------a --------t- ---------- -t--a----- -----t---- -----aa--- ---t--a--a ag-------- ---------- ---------- -----
    325-2  ---------- ---------- ---------a --------t- --a------- -t--a----- ----at---- -----aa--- ---t-----a ag-------- ---------- ---------- -----
    325-3  ---------- ---------- ---------a --------t- ---------- ---------- ---------- --------tg ---------- ---------- ---------- ---------- -----
   PatrB2  ---------- -----a---- ---------- --------c- ---------- ---------- ---------- --------tg ---------- ---------- ---------- ---------- -----
    325-6  .......... .----a---- ---------- --------c- ---------- ---------- ---------- --------tg ---------- ---------- ---------- --------.. .....
    325-7  .......... .----a---- ---------- --------c- ---------- -g-------- ---------- --------tg ---------- ---------- ---------- --------.. .....
   B*1801  ---------- -----a---- ---------- --------c- ---------- ---------- ---------- ---------- ---------- ---------- ---------- ---------- -----
    AR(bb) ----c----- ---------- ---------- -------t-- -a-------- ----a----- ---------- --------ca ---------- ---------- ---------- -ga--t---- -----
   AR(lbf) ---------- ---------- ---------- -------t-- -a-------- ----a----- ---------- --------cg ---------- -g-----t-- ---------- -ga--t---- -----
    325-4  ---------- ---------- ---------- -------t-- -a-------- ----a----- ---------- ---------a ---------- tg-------- ---------- -ct------- -----
   B*1501  ---------- -----a---- ---------- --------- ---------- ---------- ---------- ---------a ---------- tg-------- ---------- -ct------- -----
     DAN4  ---------- ------a--- ---------c ---a----a- ---------- -t------a- --------a- ---a-aaata ct-a------ g-c--g---- ----*----- --a----a-- -----
    325-5  ---------- ------a--- ---------c ---a----a- ---------- -t------a- --------a- ---a-aaata ct-a------ g-c--g---- ----*----- --a----a-- -----
    325-8  .......... .-----a--- ---------c ---a----a- ---------- -t------a- --------a- ---a-aaata ct-a------ g-c--g---- ----*----- --a----a.. .....
   B*3701  ---------- -----a---- ---------- --------c- ---------- ---------- ---------- ---------- ---------- gac------- ---------- ---------- -----
    325-9  ---------- -----a---- ---------- --------c- ---------- ---------- ---------- ---------- ---------- gac------- ---------- -g-------- -----
   325-10  .......... .----a---- ---------- --------c- ---------- ---------- ---------- ---------- ---------- gac------- ---------- --------.. .....
   325-11  .......... .----a---- ---------- --------c- --c------- --------a- ---------- ------a--- ---------- t--------- ---------- --------.. .....
   325-12  .......... .----a---- ---------- -------t-- -a-------c ----a---a- ---------- ---------- ---------- gac------- ---------- --------.. .....
   325-13  -----a---- ---------- t--------- -------t-- -a-------c ----a---a- ---------- ---------- ---------- gac------- ---------- ---------- -----
   A*0201  -----a---- ---------- t--------- -------t-- -a-------c ----a---a- ---------- ------a--- ---------- t--------- ---------- ---------- -----
   A*0202  -----a---- ---------- t--------- -------t-- -a-------c ----a---a- ---------- ------a--- ---------- tg-------- ---------- ---------- -----
   A*0203  -----a---- ---------- t--------- -------t-- -a-------c ----a---a- ---------a ------a--a ---------- tg-------- ---------- ---------- -----
   A*2901  t--------- ---------- t--------- -------t-- ---------- ---------- ---------- ---------- ---------- t--------- ---------- ---------- -----
   325-14  .......... .--------- t--------- -------t-- ---------- ---------- ---------- ---------- ---------- t--------- ---------- --------.. .....
   A*3101  t--------- ---------- t--------- -------t-- ---------- ---------- ---------- ---------- ---------- t--------- ---------- ---------- -----
   A*3201  t--------- ---------- t--------- -------t-- ---------- ---------- ---------- ---------- ---------- t--------- ---------- ---------- -----
    HLA-F  ---------- ---------- ---------- --------c- t--------- ---------- ttc-at---- -a-aggaata t--a---g-- t-c--ga--- ---------- -ga----c-- ----t
    HLA-E  -----t---- ---------- ---------- -t-------- ---------- -t--g---aa ----caa-t- at---tc--a ---------c -a-------- -------a-a ---a------ -----
   A*0101  ---------- ---------- t--------- -------t-- -a-------- ----a----- ---------- ---t--a--c ---------- -g-----t-- ---------- -cg------- --cg-
   A*1101  ---------- ---------- t--------- -------t-- -a-------- ----a----- ---------- ------a--c ---------- -a-------- ---------- -cg------- -----
   A*0301  ---------- ---------- t--------- -------t-- ---------- ----a----- ---------- ------a--a ---------- t--------- -------t-- ---------- -----
   A*0302  ---------- ---------- t--------- -------t-- ---------- ----a----- ---------- ------a--- ---------- -a-------- -------t-- ---------- -----
   A*2401  -----a---- ---------- t--------- -------t-- ---------- ----a----- ---------- ------a--- ---------- -a-------- ---------- ---------- --cg-
   A*2501  ---------- ---------- t--------- -------t-- ---------- ---------- ---------a ------a--a ---------- tg-------- ---------- -cg------- -----
   A*3001  ---------- ---------- t--------- -------t-- ---------- ---------- ---------- --------tg ---------- t--------- ---------- ---------- -----
   A*3301  t--------- ---------- t--------- -------t-- ---------- ---------- ---------- ------cg-- ---------- t--------- ---------- ---------- -----
   B*1301  ---------- -----a---- ---------- --------c- ---------- --------t- ---------- ---------- ---------- ---------- ---------- -ga------- -----
   B*4901  ---------- -----a---- ---------- --------c- ---------- ---------- ---------- ---------a ---------- ---------- ---------- -ct------- -----
   B*5801  ---------- -----a---- ---------- --------c- ---------- ---------- ---------- ---------- ---------- ---------- ---------- -ct------- -----
   B*5701  ---------- -----a---- ---------- --------- ---------- ---------- ---------- ---------- ---------- ---------- ---------- -ct------- -----
   B*4201  ---------- ---------- ---------- --------c- ---------- ---------- ---------- ---------- ---------- gac------- ---------- ---------- -----
   B*0702  ---------- ---------- ---------c --------c- ---------- ---------- ---------- ---------a ---------- -g-------- ---------- -ga------- -----
   B*1401  ---------- -----a---- ---------- --------c- ---------- ---------- ---------- ---------a ---------- ---------- ---------- ---------- -----
   B*3801  ---------- -----a---- ---------c --------c- ---------- ---------- ---------- ---------- ---------- ------a--- ---------- ---------- -----
   B*2701  ---------- -----a---- ---------c --------c- ---------- ---------- ---------- ---------- ---------- ---------- ---------- -ga------- -----
   B*4402  ---------- -----a---- ---------- --------c- -c-------- ---------- ---------- ---------- ---------- gac------- ---------- -ct------- ----c
   B*4002  ---------- ---------- ---------c --------c- ---------- ---------- ---------- ---------- ---------- ---------- ---------- -ga------- -----
   B*4001  ---------- ---------- ---------c --------- ---------- -t-------- ----t----- ---------- ---------- ---------- ---------- -ga------- -----
  Cw*0101  ---------- ---------- ---------c --------c- ---------- ---------- ---------- ---------a ---------- -g-------- ---------- ---------- -----
  Cw*1101  -----t---- ---------- ---------c --------- ---------- ---------- ---------- --------ac ---------- ---------- ---------- ---------- -----
  Cw*0201  ---------- ---------- ---------c --------a- ---------- ---------- ---------- ---------a ---------- tg-------- ---------- -ga------- -----
  Cw*0301  ---------- -t-------- ---------c ---a------ ---------- ---------- ---------- ---------a ---------- ---------- --t------- -ct------- -----
  Cw*0601  ---------- ---------- ---------c --------- ---------- ---------- ---------- ---------a ---------- tg-------- ---------- ---------- -----
  Cw*0701  ---------- ---------- ---------c --------c- ---------- ---------- ----t----- ---------c ---------- ---------- ---------- ---------- -----
```

FIG. 2 *a*, Comparison of the nucleotide sequences of 14 ancient and 42 modern class I HLA heavy chain gene fragments. The target sequence comprises positions 105–229 of exon 3. The consensus is derived from 113 human and ape class I major histocompatibility complex (MHC) sequences; dashes indicate agreement with consensus; dots, undetermined sequence; *, gap inserted for alignment. Primary references for the sequences are reviewed in ref. 30. *b*, Predicted protein sequences for the ancient gene fragments and the HLA class I consensus. Positions which interact with peptide (▼), T cell receptor (▲) or both (◆) are indicated and secondary structure features are shown by arrows for β-strands and coils for α helix[30]. Numbering corresponds to position of the mature class I heavy chain. Certain pairs of highly related sequences were obtained from the ancient DNA. Thus clones 325-6 and 325-7 differ by a single base substitution, as do 325-9 and 325-10. Although it is possible that these pairs represent different alleles, it seems unlikely. More probable origins for the substitutions are base modifications in the ancient DNA and/or PCR-derived misincorporations. Sequence 325-10 was a predominant product compared to 325-9, which was found only once, results favouring 325-10 as the actual sequence. The two *HLA-G* sequences differ by three scattered nucleotide substitutions with 325-1 corresponding exactly to the *HLA-G* allele described by Orr and colleagues[17]. Whether 325-2 represents another allele of *HLA-G* or an artefact is difficult to judge as little is known of polymorphism at this locus.

b

```
           126                                                                                                                                                                                                                                                                                                                                                                                                                                                                                                                                                                                                                                                                                                                                                                                                                                                                                                                                                                                                                                                                                                                                                                                                                                                                                                                                                                                                                                                                                                                                                                                                                                                                                                                                                                                                                                                                                                                                                                                                                                                                                                                                                                                                                                                                                                                                                                                                                                                                                                                                                                                                                                                                                                                                                                                                                                                                                                                                                                                                                                                                                                                                                                                                                                                                                                                                                                                                                                                                                                                                                                                                                                                                                                                                                                                                                                                                                                                                                                                                                                                                                                                                                                                                                                                                                                                                                                                                                                                                                                                                                                                                                                                                                                                                                                                                                                                                                                                                                                                                                                                                                                                                                                                                                                                                                                                                                                                                                                                                                                                                                                                                                                                                                                                                                                                                                                                                                                                                                                                                                                                                                                                                                                                                                                                                                                                                                                                                                                                                                                                                                                                                                                                                                                                                                                                                                                                                                                                                                                                                                                                                                                                                                                                                                                                                                                
Consensus  LNEDLRSWTAADTAAQITQRKWEAARVAEQLRAYLEGTCVE
    325-1  ------------------sk------n----r-----------
    325-2  ---------------t--sk------n----r-----------
    325-3  ------------------------------w--------------
    325-6  ....-s---------------------w-------------..
    325-7  ....-s------------a--------w-------------..
    325-4  -------------m-----k-------e---w-------l---
    325-5  -----h-----n-----s-h----dkys--v---x--k-m-
    325-8  ....-h-----n-----s-h----dkys--v---x--k-..
    325-9  -----s-------------------------d------a---
   325-10  ....-s-------------------------d--------..
   325-11  ....-s--------p----h-----h--------------..
   325-12  ....-s------m---t-kh-----------d--------..
   325-13  -k----------m---t-kh----------d-----------
   325-14  ....---------m-------------------------..
```

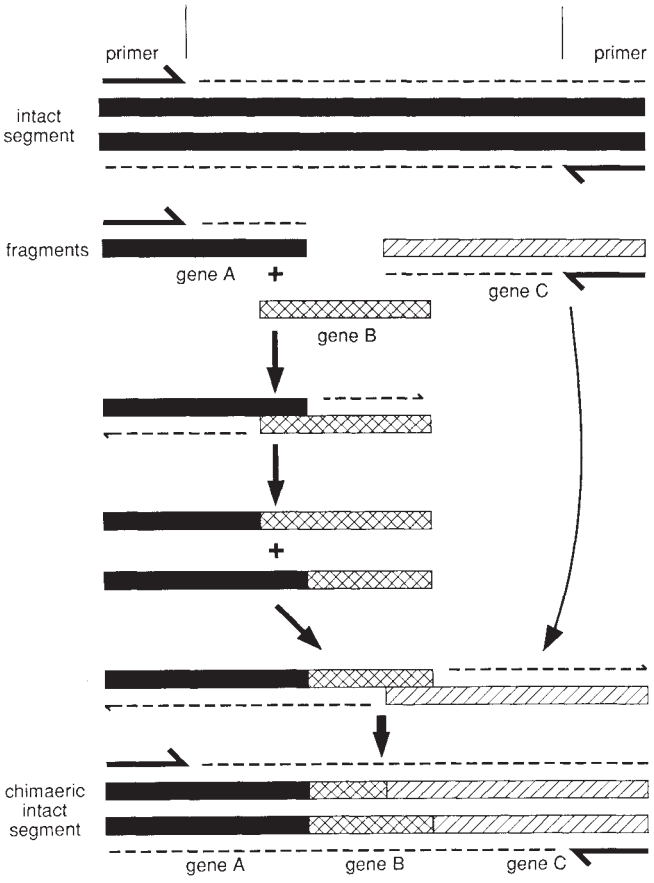

FIG. 3 Schematic representation of the postulated synthesis *in vitro* of chimaeric class I MHC gene fragments during polymerase chain reaction amplification. The intact target, shown at top, possesses priming sites for both amplification primers and the PCR proceeds in an exponential fashion. In contrast, the amplification of truncated segments of three homologous class I genes (A, B and C) is inefficient during initial cycles. Genes A and C possess only one of the two required priming sites and would be amplified arithmetically as single strand products; gene B is not a suitable substrate for amplification as it lacks both priming sites. An increase in length of gene A product occurs if it pairs with an overlapping section of gene B. It is only after the A–B product hybridizes to an overlapping stretch of gene C, thereby spanning both priming sites, that the amplification proceeds in an exponential fashion.

TABLE 1 SS325 class I MHC clones

Clone	Protocol†	Abundance‡	Assignment
325-1	A	1	*HLA-G*
325-2	A	1	*HLA-G*
325-3	A	1	*HLA-G + PatrB2*
325-4	A	1	*HLA-AR + B*1501*
325-5	A	19	*DAN4*
325-6	B	1	*PatrB2*
325-7	B	1	*PatrB2*
325-8	B	3	*DAN4*
325-9	C	1	*B*3701*
325-10	B	12	*B*3701*
325-11	B	1	*B*3701 + A*0201*
325-12	B	1	*B*3701 + A*0201 + B*3701*
325-13	C	1	*A*0201 + B*3701*
325-14	D	45	*A19 (A*2901, A3101* or *A*3201)*
325-β_2m	E	11	β_2m

† Protocol A, DNA extraction (May 1988); primary and secondary amplifications performed with pair 3. B, DNA extraction (November 1989); primary amplification (23 March 1990) with pair 3 and secondary amplification with pair 3′. C, DNA extraction (November 1989); primary (26 March 1990) and secondary amplifications performed with pair 3. D, DNA extraction (November 1989); primary amplification (23 August 1990) with pair 3 and secondary amplification with pair 3′. E, DNA extraction (May 1988); primary and secondary amplifications performed with the β_2m primer pair.

‡ The number of independent clones characterized with the respective sequence.

that most class I genes in the substrate DNA were not suitable targets for amplification. Thus the samples appear highly damaged as expected for ancient DNA[27].

A second feature is for the predominating sequences to be identical to genes found in modern DNA, whereas sequences corresponding to chimaeras of different HLA class I genes were repeatedly found only in the minority products. This phenomenon, in which a product is built up by 'jumping' from one gene to another in sequential amplification cycles (Fig. 3), occurs for modern DNA which was deliberately damaged to mimic ancient DNA[28]. Our finding of similar chimaeras is thus consistent with the amplification substrate being ancient DNA. We interpret the small number of intact class I HLA sequences obtained from any one amplification to reflect a small number (perhaps only one) of intact target molecules in the samples of ancient DNA. These intact targets give rise to the major products, as they provide an appropriate target from the very first cycle of amplification. In contrast, amplification of the chimaeric sequences will not proceed until all segments required to span the primers have been assembled, a relatively slow process requiring multiple cycles of amplification (Fig. 3). In conclusion the chimaeric sequences of clones 325-3, -4, -11, -12 and -13 are likely to be *in vitro* artefacts for which each segment derives from a different ancient class I gene.

The gene segment amplified by primer pairs 3 and 3′ is particularly rich in polymorphic motifs (Fig. 2) which allow many class I HLA alleles to be distinguished[24]. Thus a tentative assignment of an *HLA-A,B* type for SS325 can be made. At the *HLA-A* locus this individual probably expressed an *HLA-A2* allele combined with either *HLA-A*2901, A*3101* or *A*3201*. (This latter allele is most likely to be *A*3101* which is observed at high frequency in the modern Amerindian population[29].) At the *HLA-B* locus he expressed *HLA-B*3701* in combination either with an allele related to *HLA-B*1801* or to *HLA-B*1501*. Further 'HLA typing' may determine familial relationships between Windover individuals and further define the relationship between this ancient population and modern Amerindian populations[12–14]. □

Received 29 October 1990; accepted 10 January 1991.

1. Higuchi, R., Bowman, B., Freiberger, M., Ryder, O. A. & Wilson, A. C. *Nature* **312,** 282–284 (1984).
2. Thomas, R. H., Schaffner, W., Wilson, A. C. & Pääbo, S. *Nature* **340,** 465–467 (1989).
3. Hagelberg, E., Sykes, B. & Hedges, R. *Nature* **342,** 485 (1989).
4. Golenberg, E. M. *et al. Nature* **344,** 656–658 (1990).
5. Thomas, W. K., Pääbo, S., Villablanca, F. X. & Wilson, A. C. *J. molec. Evol.* **31,** 101–112 (1990).
6. Pääbo, S., Gifford, J. A. & Wilson, A. C. *Nucleic Acids Res.* **16,** 9775–9787 (1988).
7. Bogenhagen, D. & Clayton, D. A. *J. biol. Chem.* **249,** 7991–7995 (1974).
8. Michaels, G. S., Hauswirth, W. W. & Laipis, P. J. *Devl Biol.* **94,** 246–256 (1982).
9. Lamppa, G. K., Elliot, L. V. & Bendich, A. J. *Planta* **148,** 437–443 (1980).
10. Pääbo, S. *Nature* **314,** 644–645 (1985).
11. Del Pozzo, G. & Guardiola, J. *Nature* **339,** 431–432 (1989).
12. Doran, G. H. *et al. Nature* **323,** 803–806 (1986).
13. Doran, G. H. & Dickel, D. N. in *Wet Site Archaeology* (ed. Purdy, B.) 263–289 (Telford, Caldwell, New Jersey, 1988).
14. Doran, G. H. & Dickel, D. N. *The Florida Anthropologist* **41,** 365–380 (1988).
15. Mullis, K. B. & Faloona, F. A. *Meth. Enzym.* **155,** 335–350 (1987).
16. Suggs, S. V., Wallace, R. B., Hirose, T., Kawashima, E. H. & Itakura, K. *Proc. natn. Acad. Sci. U.S.A.* **78,** 6613–6617 (1981).
17. Geraghty, D. E., Koller, B. H. & Orr, H. T. *Proc. natn. Acad. Sci. U.S.A.* **84,** 9145–9149 (1987).
18. Ennis, P. D., Zemmour, J., Salter, R. D. & Parham, P. *Proc. natn. Acad. Sci. U.S.A.* **87,** 2833–2837 (1990).
19. Kato, K., Trapani, J. A., Allopena, J., Dupont, B. & Yang, S. Y. *J. Immun.* **143,** 3371–3378 (1989).
20. Koller, B. H. & Orr, H. T. *J. Immun.* **134,** 2727–2733 (1985).
21. Pohla, H., Kuon, W., Tabaczewski, P., Doerner, C. & Weiss, E. H. *Immunogenetics* **29,** 297–307 (1989).
22. Zemmour, J. *et al. J. Immun.* **144,** 3619–3629 (1990).
23. Mayer, W. E. *et al. EMBO J.* **7,** 2765–2774 (1988).
24. Parham, P., Lawlor, D. A., Lomen, C. E. & Ennis, P. D. *J. Immun.* **142,** 3937–3950 (1989).
25. Hansen, T., Markussen, G., Paulsen, G. & Thorsby, E. *Tissue Antigens* (in the press).
26. Pääbo, S., Higuchi, R. G. & Wilson, A. C. *J. biol. Chem.* **264,** 9709–9712 (1989).
27. Pääbo, S. *Proc. natn. Acad. Sci. U.S.A.* **86,** 1939–1943 (1989).

28. Pääbo, S., Irwin, D. M. & Wilson, A. C. *J. biol. Chem.* **265**, 4718–4721 (1990).
29. Chiewsilp, P. & Sujirachato, K. in *HLA in Asia-Oceania 1986* (ed. Aizawa, M.) 40–47 (Hokkaido University Press, Sapporo, Japan, 1986).
30. Bjorkman, P. J. & Parham, P. *A. Rev. Biochem.* **59**, 253–288 (1990).

ACKNOWLEDGEMENTS. We thank Frances E. Ward of Duke University for tissue typing and Patricia Massard for preparation of the manuscript; D. N. Dickel and G. H. Doran, the Florida State legislature and Windover Farms, Inc. for their efforts and support for the Windover archaeological site. This research was supported by the National Institutes of Health and Research to Prevent Blindness, Inc. P.P. was a Scholar of the Leukemia Society.

Lexical organization of nouns and verbs in the brain

Alfonso Caramazza* & Argye E. Hillis†

* Department of Cognitive Science, The Johns Hopkins University, Baltimore, Maryland 21218
† HealthSouth Rehabilitation Corporation, 9512 Harford Road, Baltimore, Maryland, 21234, USA

THE analysis of neuropsychological disorders of lexical processing has provided important clues about the general organization of the lexical system and the internal structure of the processing components[1–3]. Reports of patients with selective dysfunction of specific semantic categories such as abstract versus concrete words[4–6], living things versus inanimate objects[7–11], animals[12–14], fruits and vegetables[15], proper names[16,17] and so forth, support the hypothesis that the neural organization of the semantic processing component is organized in these categories. There are reports of selective dysfunction of the grammatical categories noun and verb[18–21], suggesting that a dimension of lexical organization is the grammatical class of words. But the results reported in these studies have not provided unambiguous evidence concerning two fundamental questions about the nature and the locus of this organization within the lexical system. Is the noun–verb distinction represented in the semantic or in the phonological and orthographic lexicons? Is grammatical-class knowledge represented independently of lexical forms or is it represented separately and redundantly within each modality-specific lexicon? Here we report the performance of two brain-damaged subjects with modality-specific deficits restricted principally (H.W.) or virtually only (S.J.D) to verbs in oral and written production, respectively. The contrasting performance suggests that grammatical-class distinctions are redundantly represented in the phonological and orthographic output lexical components.

H.W. became aphasic due to a stroke (1985) in the parietal region of the left hemisphere (she had earlier suffered a stroke in 1982 in the occipital area). She presented with fluent but paraphasic speech with normal phrase length and intonation. Her selective impairment in comprehending aurally but not visually presented sentences was probably due to a deficit of auditory-verbal short-term memory (repetition span, 3). H.W. showed normal comprehension of both spoken and written words (Peabody Picture Vocabulary Test, PPVT[22]: 153) but oral naming (Boston Naming Test, BNT[23]: 14) and reading were severely impaired. On the Johns Hopkins University Dyslexia and Dysgraphia Batteries (JHU-DDB), her oral reading performance was significantly affected by grammatical word class and frequency, but not by spelling-to-sound regularity or by concreteness or abstractness. Nearly all of her errors were semantically related responses (for example, *dollar* → 'money') or omissions. She wrote all types of words relatively well; her written responses were nearly all legible, although she made many spelling errors (for example, *shake* → 'shaek'); she did not produce semantic paragraphias. H.W. failed to read or write correctly any nonhomophonic nonword (for example, hannee). An earlier analysis of her lexical processing performance confirmed a striking dissociation between oral and written production of words: she produced semantic paraphasias in oral but not written production; and her ability to comprehend the very same words was entirely normal in both modalities[24].

S.J.D. became aphasic in 1985 following a stroke in the left frontotemporal region. Her spontaneous language production and repetition, and her comprehension of spoken and written sentences were very similar to H.W.'s. S.J.D. showed normal comprehension of printed and spoken single words (PPVT: 166). On the JHU-DDB, her writing-to-dictation was significantly affected by grammatical word class and frequency but not by sound-to-spelling regularity or by concreteness or abstractness. Her ability to read (28% correct) and spell (7% correct) nonhomophonic nonwords was severely impaired. Most of S.J.D.'s errors in writing were semantically related responses or omissions; she made no semantic errors in reading. Her relatively infrequent errors in reading were morphological (suffix insertions, deletions or substitutions such as *bowled* → 'bowling') or phonological paraphasias. An earlier analysis of S.J.D.'s lexical processing performance documented a selective deficit in the oral production of morphologically complex words (she read *darken* as 'darkness')[25].

In order to document the double dissociation of disproportionate production of semantic errors in oral and written output, the patients were asked to read aloud and to write-to-dictation a set of 296 words. H.W. made semantic errors only in reading; S.J.D. made semantic errors only in writing. The same type of dissociation was observed for oral and written naming of 60 pictured objects and actions: here, too, H.W. made semantic errors only in the oral naming task, and S.J.D. made semantic errors only in the written naming task (Table 1).

The patients' difficulties in oral and written production were not distributed uniformly across nouns and verbs. As may be seen in Table 2, H.W. performed significantly worse in the oral production of verbs than of nouns, but performed equally well in written production of both types of words. By contrast, S.J.D. performed much worse in the written production of verbs than nouns, but performed equally well in the spoken production of both types of words.

Although the reported greater difficulty in brain-damaged subjects to read verbs in comparison to nouns[26] could reflect greater difficulty in processing abstract words[27], this possibility does not apply to all forms of grammatical-class effects. Thus, there are reports of greater difficulty in naming objects than actions[18], ruling out the possibility that grammatical-class effects are always merely the consequence of greater difficulty in processing abstract words. This possibility can also be ruled out in the present case. As reported, neither H.W. nor S.J.D. showed a concreteness or abstractness effect on controlled lists on the JHU-DDB. Additional tests with concrete and abstract nouns

TABLE 1 Performance across lexical production tasks

		H.W.		S.J.D.	
	N	Total errors (%)	Semantic errors (%)	Total errors (%)	Semantic errors (%)
Spoken output					
Reading	296	53	73	2	0
Naming	60	63	81	2	0
Written output					
Dictation	296	0	0	13	64
Naming	60	0	0	50	100

Column 1 reports the total number of stimuli (*N*). The percentage of lexical or omission errors in each task (columns 3 and 5) and the percentage of erroneous responses that resulted in semantic errors are reported for each patient. It may be noted that H.W. produced semantic errors only in oral production tasks and S.J.D. produced semantic errors only in written production tasks. Both patients also produced some morphologically related responses (*hurry* → 'hurried') for which it could not be established whether they represent true morphological or semantic errors. These responses were not scored as semantic errors. H.W. is a 62-year-old right-handed former salesperson; S.J.D. is a 48-year-old, right-handed librarian; strokes were confirmed by CT scan.

TABLE 2 Percentage correct performance combined for all oral and written production tasks

	H.W.		S.J.D.	
	Nouns	Verbs	Nouns	Verbs
Oral production	56	22	99	97
Written production	99	99	99	70

H.W. performed worse in oral production of verbs than of nouns ($\chi^2=34.3$; $P<0.001$), and S.J.D. performed worse in written production of verbs than nouns ($\chi^2=40.7$; $P<0.001$). H.W.'s written production and S.J.D's oral production of verbs and nouns were virtually flawless. The performance reported here was obtained by collapsing across several tasks described below. In reading and writing sets of nouns and verbs matched in frequency and length ($N=98$, in each set) a dissociation was observed between grammatical classes: H.W. read correctly 46/98 (47%) nouns and 19/98 (18%) verbs, and, ignoring spelling errors (*moose* → 'mosse'; *sneeze* → 'snezze'), she wrote correctly all nouns and verbs; S.J.D. wrote correctly all 98 nouns and 74/98 (76%) verbs, whereas, ignoring pronunciation and morphological errors (*sleeve* → 'sleeves'; *dangle* → 'dangly'), she read correctly 96/98 (98%) nouns and 93/98 (95%) verbs. A similar pattern of performance was obtained for the two patients in oral and written naming of pictures depicting objects (nouns) and actions (verbs; $N=30$ in each word class) whose names were matched in frequency and length: H.W. named correctly 16/30 (53%) objects and 6/30 (20%) actions and, ignoring spelling errors, she wrote correctly all but one noun and one verb; S.J.D. wrote correctly 29/30 (97%) objects and 16/30 (53%) actions, and she named correctly all objects and all but one action. Although relatively few observations are available for sentence production tasks, the results are perfectly consistent with those obtained with single-word processing tasks: H.W. correctly produced 7/12 (58%) verbs in comparison with 23/24 (96%) nouns in oral production; S.J.D. correctly produced 4/6 verbs in comparison with 19/19 nouns. Both patients performed flawlessly for both verbs and nouns in their unimpaired modality (H.W. writing: 3/3 and 6/6 for verbs and nouns, respectively; S.J.D. speaking: 8/8 and 21/21 for verbs and nouns, respectively).

matched in frequency and length showed that neither patient had greater difficulty with abstract than concrete words (H.W. reading: 24/38 and 25/38 correct for concrete and abstract nouns, respectively; S.J.D. writing: 36/38 and 35/38 correct for concrete and abstract nouns, respectively). Also, the mean concreteness values of H.W.'s correctly and incorrectly read nouns were 4.94 (s.d. = 1.05) and 5.12 (s.d. = 1.02), respectively (S.J.D made too few errors to support this type of analysis for her performance). Thus, the reported effects for H.W. and S.J.D. are true grammatical-class effects and cannot be attributed to the differential abstractness of these two classes of words.

It is possible that H.W.'s and S.J.D.'s modality-specific deficit in producing verbs might simply reflect an impairment in producing particular phonological or orthographic forms, and not a deficit in processing words of a particular grammatical category. That is, it could be that S.J.D. has difficulties accessing the specific orthographic representation for the word 'deny' independently of the fact that it is a verb. This possibility can be evaluated by comparing the patients' performance in processing homonyms: words that have the same phonological and orthographic forms (such as crack) but different meanings and grammatical class: a crack, noun; to crack, verb. If the patients' deficit concerned the ability to process specific phonological forms (in the case of H.W.) of specific orthographic forms (in the case of S.J.D.), then we would expect their performance in producing homonyms to be equally impaired independent of the grammatical context in which they are used. By contrast, if the patients' deficit concerned the ability to process words of a specific grammatical class (verbs), then we would expect their performance with homonyms to be poor only when used as verbs despite the fact that they have the same phonological or orthographic form in noun and verb production contexts. The two patients' performance in reading and writing homonyms in noun and verb contexts are shown in Table 3, upper panel: H.W. was selectively impaired in producing the verb form of a homonym only in the reading task, and S.J.D. was selectively impaired in producing the verb form of a homonym only in the writing task. The selective difficulty in producing the verb form of homonyms could not be attributed to a frequency effect since the grammatical class-specific impairment persisted even when the verb form of a homonym is more frequent than the noun form (Table 3, lower panel).

The contrasting patterns of modality-specific and grammatical category-specific impairments reported for H.W. and S.J.D. severely constrain plausible hypotheses about the loci of functional damage to the lexical processing system that may be responsible for these patients' word production impairments, and they provide clear evidence for the hypothesis that knowledge of the phonological and orthographic forms of words is organized by grammatical category.

(1) The fact that the two patients produced semantic errors only in one modality of output (speaking or writing), independent of whether the input was a word or a picture, and the fact that both patients showed normal comprehension of single words rule out the possibility that the lexical impairment in these patients results from a deficit to input lexical representations or to the semantic component. Instead, these facts suggest that the locus of functional deficit is at a level where lexical phonological representations (for H.W.) and lexical orthographic representations (for S.J.D.) are specified for output, either because of damage directly to modality-specific lexical representations or because of damage to access of those representations. This conclusion implies the seemingly counterintuitive possibility that semantic errors can arise from damage to processes at the level of phonological and orthographic output representations[24,28].

(2) The facts in (1), which establish that the locus of functional deficit in H.W. and S.J.D. is respectively at the level where phonological and orthographic lexical forms are computed for output, and the fact that verbs were selectively impaired in a single modality of output in each patient together rule out the possibility that the deficit in these patients concerns a specific grammatical category in a modality-independent lexical component. These results suggest, instead, that the deficit concerns the activation of the category verb in modality-specific lexical

TABLE 3 Oral and written production of homonyms in sentence contexts

	H.W.		S.J.D.	
	Oral reading	Writing	Oral reading	Writing
Nouns	44/50 (88)	49/50 (98)	50/50 (100)	49/50 (98)
Verbs	23/50 (46)	48/50 (96)	50/50 (100)	28/50 (56)
Nouns	19/20 (95)	19/20 (95)	20/20 (100)	20/20 (100)
Verbs	8/20 (40)	19/20 (95)	20/20 (100)	17/20 (85)

In the written version of this task, the patients were dictated a sentence and asked to write the emphasized (and subsequently repeated) word in the blank space in a typed sentence. For example, for the noun form of *crack*, the stimulus was: "There's a *crack* in the mirror; write 'crack'"), and the patient was required to write the word crack in the sentence frame *There's a* _____ *in the mirror*; for the verb form, the stimulus was: "Don't *crack* the nuts in here; write 'crack'", and she was required to write the word crack in the frame *Don't* _____ *the nuts in here*. The reading version of the task simply required the patients to pronounce the underlined word in a sentence (*There's a* <u>*crack*</u> *in the mirror*; *Don't* <u>*crack*</u> *the nuts in here*) after reading the sentence silently. The upper panel reports the number and percentage (in parentheses) for correct responses in oral reading (columns 1 and 3) and writing to dictation (columns 2 and 4) for the noun and verb forms of homonyms (for example, a crack or to crack). It is clear that the two patients are selectively impaired in producing the verb form of homonyms in only one modality of output, oral and written for H.W. and S.J.D., respectively. The lower panel reports performance only for the subset of stimuli in which the verb form is more frequent than the noun form, ruling out the possibility of a frequency effect as the basis for the selective deficit of the verb form of homonyms.

components, again either because of damage directly to modality-specific lexical representations or because of damage to access of these representations. The implication of this conclusion is that phonological and orthographic output representations are organized by grammatical category.

(3) Finally, the facts in (1) and (2) and the fact that H.W. and S.J.D. were impaired in processing only the verb form of homonymic words imply that the deficit does not concern specific lexical forms (for example, the orthographic form *crack*) but the grammatical category verb (of which *crack* is an instance) for modality-specific lexical forms. One implication of this latter conclusion is that we should give serious consideration to the possibility that grammatical category information is represented separately and redundantly in each modality-specific lexical system.

In summary, taken together with recent results of category-specific deficits, the results we have reported suggest a remarkably specific organization of lexical knowledge in the brain, both at the semantic[8] and at the lexical form levels. Although at this time we do not have clear hypotheses about the nature of the brain mechanisms that compute lexical structure, it is clear that the information computed by these mechanisms must represent not only the phonological and orthographic form of words but also their grammatical class. The results reported for H.W. and S.J.D. pose a serious challenge for those models of lexical processing that would dispense with linguistic level information in the representation of lexical knowledge[29]. □

Received 13 September; accepted 31 December 1990.

1. Caramazza, A. *A. Rev. Neurosci.* **11,** 395-421 (1988).
2. Shallice, T. *From Neuropsychology to Mental Structure* (Cambridge University Press, 1988).
3. Ellis, A. & Young, A. *Human Cognitive Neuropsychology* (Lawrence Erlbaum, 1988).
4. Warrington, E. K. *Q. J. exp. Psych.* **27,** 635-657 (1975).
5. Warrington, E. K. *Phil. Trans. R. Soc.* B**295,** 411-423 (1981).
6. Warrington, E. K. & Shallice, T. *Brain* **107,** 829-853 (1984).
7. Warrington, E. K. & McCarthy, R. A. *Brain* **106,** 859-878 (1983).
8. Warrington, E. K. & McCarthy, R. A. *Brain* **110,** 1273-1296 (1987).
9. McCarthy, R. A. & Warrington, E. K. *Nature* **334,** 428-430 (1989).
10. Basso, A., Capitani, E. & Laiacona, M. *J. Neurol. Neurosurg. Psychiat.* **51,** 1201-1207 (1988).
11. Goodglass, H. & Budin, C. *Neuropsychologia* **26,** 67-78 (1988).
12. Sartori, G. & Job, R. *Cognitive Neuropsych.* **5,** 105-132 (1988).
13. Silveri, M. C. & Gainotti, G. *Cognitive Neuropsych.* **5,** 677-709 (1988).
14. Hillis, A. & Caramazza, A. *Brain* (in the press).
15. Hart, J., Berndt, R. & Caramazza, A. *Nature* **316,** 338 (1985).
16. Semenza, C. & Zettin, M. *Nature* **342,** 678-679 (1989).
17. McKenna, P. & Warrington, E. K. *J. Neurol. Neurosurg. Psychiat.* **41,** 571-573 (1978).
18. Miceli, G., Silveri, M. C., Villa, G. & Caramazza, A. *Cortex* **20,** 217-220 (1984).
19. Baxter, D. & Warrington, E. K. *Neuropsychologia* **23,** 653-666 (1985).
20. McCarthy, R. A. & Warrington, E. K. *Neuropsychologia* **23,** 709-723 (1985).
21. Zingeser, L. B. & Berndt, R. S. *Cognitive Neuropsych.* **5,** 473-516 (1988).
22. Dunn, L. M. & Dunn, L. M. *Peabody Picture Vocabulary Test-Revised* (American Guidance Service, 1981).
23. Goodglass, H., Kaplan, E. & Weintraub, S. *The Revised Boston Naming Test* (Lea & Febiger, 1983).
24. Caramazza, A. & Hillis, A. *Cortex* **26,** 95-122 (1990).
25. Badecker, W. & Caramazza, A. *Cognitive Neuropsych.* (in the press).
26. Coltheart, M., Patterson, K. E., & Marshall, J. C. *Deep Dyslexia* (Routledge, 1980).
27. Allport, D. A. & Funnell, E. *Phil. Trans. R. Soc.* B**295,** 397-410 (1981).
28. Patterson, K. E. *Q. J. exp. Psych.* **30,** 587-601 (1978).
29. McClelland, J. L., Rumelhart, D. M. & Hinton, G. E. in *Parallel Distributed Processing: Explorations in the Microstructure of Cognition* Vol. 1 (eds McClelland J. J. & Rumelhart D. E.) 3-44 (MIT, 1986).

ACKNOWLEDGEMENTS. We thank H.W. and S.J.D. for their participation, and B. Badecker, H. Egeth, M. McCloskey and B. Rapp for comments on this paper. The work was supported by NIH, the Seaver Institute, and the McDonnell/Pew Program in Cognitive Neuroscience.

Odorant signal termination by olfactory UDP glucuronosyl transferase

Daniel Lazard, Karin Zupko, Yitzhak Poria, Patrick Nef, Janette Lazarovits, Shirley Horn, Miriam Khen & Doron Lancet*

Department of Membrane Research, The Weizmann Institute of Science, Rehovot, 76100 Israel

THE onset of olfactory transduction has been extensively studied[1–7], but considerably less is known about the molecular basis of olfactory signal termination[6,8,9]. It has been suggested that the highly active cytochrome P_{450} monooxygenases of olfactory neuroepithelium[10–12] are termination enzymes[5,8,11,12], a notion supported by the identification and molecular cloning of olfactory-specific cytochrome P_{450}s (refs. 13–16). But as reactions catalysed by cytochrome P_{450} (refs 17, 18) often do not significantly alter volatility, lipophilicity or odour properties[9,11], cytochrome P_{450} may not be solely responsible for olfactory signal termination. In liver and other tissues, drug hydroxylation by cytochrome P_{450} is frequently followed by phase II biotransformation, for example by UDP glucuronosyl transferase (UGT), resulting in a major change of solubility and chemical properties[19]. We report here the molecular cloning and expression of an olfactory-specific UGT. The olfactory enzyme, but not the one in liver microsomes, shows preference for odorants over standard UGT substrates. Furthermore, glucuronic acid conjugation abolishes the ability of odorants[1,20] to stimulate olfactory adenylyl cyclase. This, together with the known broad spectrum of drug-detoxification enzymes[17,19], supports a role for olfactory UGT in terminating diverse odorant signals.

We previously obtained peptide sequences of bovine gp56, an olfactory epithelial-specific transmembrane glycoprotein which is similar to UGT enzymes[16]. Based on the sequence information, a partial bovine complementary DNA clone (no. 21) encoding this protein was isolated. Using clone 21 as a probe, we isolated a full-length rat olfactory UGT clone (RO1) from a rat olfactory cDNA library (Fig. 1). The UGT clone shares several structural features with other UGT sequences (Fig. 1*b*). It is 87% identical to the partial bovine sequence (a possible orthologue), but only 44–60% identical to other rat liver UGT sequences (Fig. 1*b*). This, together with the expression results below, shows that a novel functional form, termed UGT_{olf}, has been identified which defines a new subfamily within the UGT superfamily[21].

As several olfactory signal-processing enzymes are tissue-specific[4,7,22], we examined the tissue specificity of clone RO1. Figure 2 shows that cross-hybridizing messenger RNA is exclusively expressed in olfactory epithelium, with no reactivity seen in liver or other UGT-containing tissues. A similar tissue specificity has been observed for protein gp56 using immunoblot analysis[16].

The tissue-specific expression of UGT_{olf} points to a possible role in olfaction. By analogy with UGT function in liver[19], olfactory UGT could help clear lipophilic odorant molecules from the chemosensory epithelium. We therefore asked whether olfactory UGT could glucuronidate odorants. When transiently expressed in COS-7 cells, rat UGT_{olf} catalysed the glucuronidation of numerous, chemically diverse substrates, with several odorants showing particularly high efficiency (Fig. 3*a*). In parallel, we measured the enzyme activity in microsomal membranes from olfactory epithelium. Several established[23] (hydroxyl-containing) odorants were efficient UGT substrates (10–70 nmol per mg protein per min) in preparations from cow[24] (Fig. 3*b*) and rat (data not shown). The activity profile of UGT_{olf} expressed in COS cells (Fig. 3*a*) is similar to that of the olfactory microsomal enzyme (Fig. 3*b*). Thus, UGT_{olf} is probably a dominant component of the overall UGT activity in the olfactory epithelium. For all five odorants shown, the olfactory enzyme was two- to fivefold more active than the liver enzyme. In contrast, glucuronation of classical UGT substrates was comparable in both tissues (Fig. 3*b*).

* To whom correspondence should be addressed.

To find out whether odorant glucuronidation could underlie olfactory signal termination, we compared the ability of odorants and their respective glucuronates to activate olfactory adenylyl cyclase, a reaction widely used as an *in vitro* assay for olfactory transduction activity[1-4,6]. Figure 3*c* shows that preincubation of odorants with olfactory microsomes under conditions leading to highly efficient glucuronidation results in a practically complete abolition of their ability to stimulate cyclic AMP generation. This does not occur if UDP-glucuronic acid or microsomes are omitted (Fig. 3*c*), or when heat-inactivated microsomes are used (data not shown).

Finally, UGT_{olf} was immunolocalized with an antiserum to a synthetic peptide. Labelling in bovine tissue (Fig. 4) and in rat (data not shown) was mainly in subepithelial Bowman's glands. Some labelling was seen in a superficial epithelial layer, probably corresponding to the apical cytoplasm regions of the secretory supporting cells[8]. Practically no immunoreactivity was observed in respiratory epithelium (not shown). Similar immunolabelling was previously observed for cytochrome P_{450} and cytochrome P_{450} reductase[25,26].

UGT_{olf} has several properties that make it an excellent candidate for a chemosensory signal termination enzyme. First, it can act on hydroxylated products of mixed function monooxygenases (such as cytochromes P_{450})[11-13,16], as well as on carboxylic acids, amines and thiols[19], allowing modification of a multitude of odorants. Second, its active site inside the endoplasmic reticulum lumen[19,27] can be easily reached by the lipophilic, membrane-penetrable odorants. The resulting membrane-impenetrable glucuronates may be secreted by vesicular traffic and removed by blood or mucus flow[8]. This hypothetical pathway is consistent with the localization of UGT_{olf} in secretory cells, and is similar to a mechanism suggested for the excretion of bilirubin glucuronates in the liver[28]. Third, in contrast to mere hydroxylation by cytochrome P_{450}, UGT-catalysed glucuronation results in a pronounced increase in hydrophilicity, preventing odorant repartition into cells. This will shorten tissue residence times and prevent continuous stimulation. Furthermore, as glucuronation abolishes the ability of odorants to activate adenylyl cyclase, odorants secreted into the mucus bathing the sensory cilia will not interfere with receptor responses to new stimuli. Finally, the high UGT activity in olfactory epithelial membranes (along with the high concentration of cytochrome P_{450} and NADPH-dependent cytochrome P_{450} reductase activity[11-13,25,26]) may compensate for possible slow kinetics[29], potentially allowing odorant removal within 0.1-10 seconds[8,9].

In addition to a role in rapid signal termination, olfactory

b

```
                   ---------------------                                  ###
r-UGTolf     1     MLKNILLWSLQLSLLGMSLGGNVLIWPMEGSHWLNVKIIIDELLRKEHNVTVLVASGALFITPSVSPSLTFEIYPVPFGKEKIESVIKDFVLTWLENRPSPSTIWTF  107
c-UGTolf     1                                                                                   .S.G.....I...M.H....L...R.   26
UDPGTr-2     1 MSMKQTSVF.LIQLICYFRPGAC.K..V..T.Y...I.I...LN..AQRG.E.....S.ASIL.E.TKES.IN....S..LS.SDL.YSFAKWIDE.TRDFETL.-...Y  109
UDPGTr-4     1 MPRKWISA.FLLQISYCFKSGHC.K..V...DF...M.I...L...VQRG.E....KP.AYF.LD.KK.SD.K...FSTSIS.DELQNHFIKLLDV.TYEL.-RD.CLSY  109

r-UGTolf   108 YKEMAKVIEEFHLVSRGICDGVLKNEKLMTKLQRGKFEVLLSDPVFPCGDIVALKLGIPFIYSLRFSPASTVEKHCGKVPFPPSYVPAILSELTDQMSFADRVRNFISYR  217
c-UGTolf    27 .Q.....KD..M...E...S..Q.....E..KKS.....V..........I.............................Y.................T..I......H  136
UDPGTr-2   110 .SK.Q..FN.YSD.VENL.KALIW.KS..K...GSQ.D.I.A.A.G...ELL.EL.KT.LV.....C.GYRC..FS.GL.L......VV....S.R.T.VE..K.MLQML  219
UDPGTr-4   110 SPILQNLVY..SYFYLS..KDAVS.KQ......ES..D..FA...AS...LI.EL.H...L...S...GHKL..SI..FIL......V...G.AGK.T.I...K.M.CML  219
                                                                                                                      ###
r-UGTolf   218 MQDYMFETLW-KQWDSYYSKALGRPTTLCETMGKAEIWLMRTYWDFEFPRPYLPNFEFVGGLHCKPAKPLPKEMEEFVQTSGEHGVVVFSLGSMVKNLTEEKANLIASAL  326
c-UGTolf   137 L.....N.....S.........................I.......................................S...D.I.......R.....  245
UDPGTr-2   220 YF.FW.QPFKE.S.SQF..DV.......T.M....D...I..F..L...H.F....D.............R.....S.........................VV....  329
UDPGTr-4   220 YF.FW..R.RH.E..TF..EI......VD...S.V....I.S...LK..H.T...VDYI.............D......S................S.M......A..W..  329

r-UGTolf   327 AQIPQKVLWRYKGKIPATLGSNTRLFDWIPQNDLLGHPKTRAFITHGGTNGIYEAIYHGIPMVGVPMFADQPDNIAHMKAKGAAVEVNMNTMTSADLLSAVRAVINEPFY  436
c-UGTolf   246 ...........K.....A....Y.............AK..................V.............................I.........N.L.T.....S.  355
UDPGTr-2   330 .......V..FD..K.D........YK.............K..VA................I..I.L........N..V......R.DFSILSTTG..T.LKI.M.D.S.  439
UDPGTr-4   330 .........KFD..T.....P...VYK.L...........K..V....A..L..........I.I.L.G.........V......SL.IR..SKL.F...LEE..DN...  439
                                                                  ++++++++++++++++
r-UGTolf   437 KENAMRLSRIHHDQPVKPLDRAVFWIEFVMRHKGAKHLRVAAHDLSWFQYHSLDVIGFLLACMASAILLVIKCCLFVFQKIGKTGKKNKRD                  527
c-UGTolf   356 .......K.............................P...N.T.Y.............V.T.VF..TR....SCR.F......K..E                  446
UDPGTr-2   440 ............................Y...........STL..................L.VVGVVFIIT.F...CCR.TANM...K.E                  529
UDPGTr-4   440 .K.V.L..T......M............I..........PLG.N.P.Y............T.F.VIAA.TV..L..MYRFFV.KE..M.NE                  530
```

FIG. 1 Nucleotide and deduced amino-acid sequence of rat UGT_{olf}. *a*, The nucleotide sequence of the rat UGT_{olf} (r-UGT_{olf}, clone R01) includes a 1,581-bp coding region (capitals) preceded by 63 bp non-coding sequence (lower case) and followed by 857 bp of non-coding sequence (lower case, 187 bp shown) ending in a polyadenylation signal (AATAAA) and a poly (A) stretch (not shown). The first ATG triplet in clone R01 defines the open reading frame of 527 amino acids (relative molecular weight 62,881), in close agreement with the length of other UGTs. *b*, Deduced amino-acid sequence of rat UGT_{olf} (r-UGT_{olf}, clone R01) and alignment[32] (gap weight, 5.0; length weight, 0.3, University of Wisconsin package) with the partial bovine UGT_{olf} (c-UGT_{olf}, clone 21) and two rat liver UGTs[33,34] (UDPGTr-2 and UDPGTr-4). Identities in the amino-acid sequences are indicated by dots. The following structural features are shared between UGT_{olf} and other known UGTs: (1) an N-terminal hydrophobic signal peptide (-----); (2) two consensus sequences for *N*-linked glycosylation at position 49 and 313 (###), the latter conserved in several other UGTs; (3) a 17 residue long hydrophobic region near the carboxy-terminus (+++), most probably a single transmembrane anchor domain; (4) a cluster of positively-charged residues at the extreme carboxy terminus that appears to be a stop transfer signal; (5) conserved cysteines at positions 126, 157, 280, 498 and 510. The sequences of the three gp56 peptides previously reported[16] are underlined in the bovine sequence. Overall identities between the rat UGT_{olf} amino-acid sequence and other sequences are: bovine UGT_{olf}, 87%; UDPGTr-2, 60%; UDPGTr-4, 59%. The most conserved region is the C-terminal half of the protein. The highest diversity is found in the N-terminal 250 residues and in the 30-residue carboxy-terminal stretch. METHODS. A bovine olfactory epithelial cDNA library in λ-gt11 (Clontech, Palo Alto) was constructed using poly(A)$^+$-enriched RNA isolated from olfactory epithelium of three-month old calves. 350,000 plaques were screened with the following ^{32}P-labelled oligonucleotide mixtures (I is inosine): 5′-CCAIGT$^A/_G$TG$^A/_G$AA$^A/_G$TC$^C/_T$TTIATIAC$^C/_T$TTIG-CCAT-3′ and 5′-TTIGC$^C/_T$TT$^C/_T$TC$^C/_T$TCIGTIA$^A/_G$IGT$^C/_T$TTIACCAT-3′, corresponding to peptides 201 and 202 of gp56, respectively[16]. Three partial clones hybridizing with both oligonucleotides were purified and the 1,393-bp insert of one of them (14) was used for rescreening the cDNA library. This yielded a longer partial-length clone (21). Both clones included all the three reported gp56 peptides[16] in their deduced amino-acid sequence. A fragment of clone 21 (including most of the coding sequence) was used to screen a rat olfactory λgt11 cDNA library[13] with medium stringency washes (52 °C, 0.5 × SSC). Positive signals were observed at a frequency of 1 in 3,000. Fifteen clones were isolated and one (R01) subcloned in M13mpl8 and sequenced on both strands of the coding region.

a

```
   1 gaggactggaaagtagagaaatttgtttgttccacattttcagaagtttacatcaaacca
  61 gtcATGTTGAAGAACATTCTACTGTGGTCTCTTCAGCTAAGTCTCCTAGGAATGAGTCTT
 121 GGCGGGAATGTTCTCATCTGGCCAATGGAAGGCAGTCACTGGCTAAATGTTAAGATCATA
 181 ATAGACGAACTCCTAAGGAAAGAGCATAACGTGACTGTCCTTGTTGCATCCGGGGCCCTT
 241 TTCATCACACCGTCGGTCAGCCCATCTCTGACATTCGAAATATATCCAGTGCCCTTCGGC
 301 AAGGAAAAAATCGAAAGCGTGATCAAGGACTTTGTTTTGACGTGGCTGGAAAACAGGCCG
 361 TCTCCTTCAACTATCTGGACTTTCTATAAGGAAATGGCCAAAGTCATCGAGGAGTTCCAC
 421 TTGGTGTCCAGAGGGATCTGTGATGGCGTTCTTAAGAATGAAAAGCTGATGACCAAGCTG
 481 CAGAGAGGAAAGTTTGAAGTACTGTTGTCAGACCCAGTATTTCCGTGTGGCGATATCGTA
 541 GCTTTAAAACTGGGGATTCCATTTATCTATTCCTTGCGGTTTTCTCCTGCCTCCACAGTG
 601 GAAAAGCACTGTGGAAAAGTCCCGTTTCCTCCTTCCTATGTTCCTGCAATCTTGTCAGAA
 661 CTCACAGACCAGATGTCCTTCGCTGACCGAGTAAGGAACTTTATCTCCTACCGAATGCAG
 721 GACTACATGTTTGAAACTCTTTGGAAGCAATGGGATTCCTATTACAGTAAAGCCTTAGGA
 781 AGACCCACCACACTGTGCGAGACTATGGGGAAAGCTGAGATTTGGCTAATGCGAACATAT
 841 TGGGATTTTGAATTTCCTCGTCCATATTTGCCTAATTTTGAGTTTGTGGGAGGACTGCAC
 901 TGCAAACCTGCCAAGCCTTTGCCTAAGGAAATGGAAGAGTTTGTCCAGACCTCAGGGGAA
 961 CATGGTGTTGTGGTGTTTTCTTTGGGGTCAATGGTCAAAAACCTGACAGAAGAAAAGGCC
1021 AATCTCATTGCCTCAGCCCTTGCCCAGATTCCTCAGAAGGTTTTGTGGCGATACAAAGGA
1081 AAGATACCAGCCACATTAGGATCCAATACGAGATTGTTTGACTGGATTCCTCAGAATGAT
1141 CTTCTTGGACATCCCAAAACCAGAGCTTTTATCACCCATGGTGGAACAAATGGAATCTAT
1201 GAGGCCATTTACCACGGGATCCCGATGGTGGGAGTTCCCATGTTCGCTGATCAGCCTGAC
1261 AACATAGCTCACATGAAGGCTAAAGGAGCAGCTGTGGAGGTGAACATGAACACGATGACG
1321 AGTGCAGATCTGCTCAGTGCTGTGAGAGCAGTCATCAATGAGCCATTTTATAAAGAGAAT
1381 GCCATGAGACTATCAAGAATTCACCACGATCAGCCAGTGAAGCCCCTGGACAGAGCCGTC
1441 TTCTGGATTGAGTTTGTCATGCGTCACAAAGGAGCCAAGCACCTTCGTGTGGCAGCGCAT
1501 GACCTCAGCTGGTTTCAGTACCACTCTCTAGATGTGATTGGGTTCCTGCTGGCTTGTATG
1561 GCATCTGCCATATTATTGGTTATAAAATGTTGTTTATTTGTATTTCAAAAAATTGGTAAG
1621 ACA[illegible]AAGAAGAATAAAAGGGACtagatgaaggaaagacatctcaggtctctgggttg
1681 gtca[illegible]cacaactggagtagcaatagtacttagaaacccagggagttgccagtcaccta
1741 tcctcatcccattttcaatcattccattcctgtcttagcttgaggtaaattggaggatcg
1801 aacatactttctttgctatttcaatgacggt
```

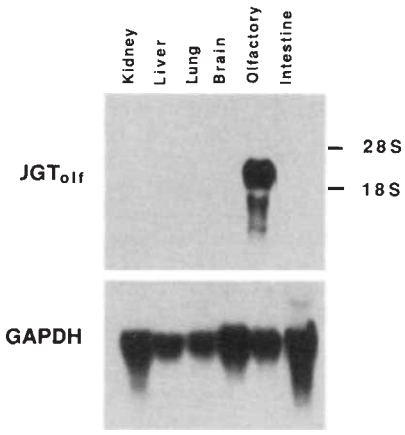

FIG. 2 Distribution of UGT_{olf} mRNA. Messenger RNAs from several rat tissues were probed with rat UGT_{olf}, and with a control glyceraldehyde phosphate dehydrogenase (GAPDH) probe. No detectable signal is seen in tissues other than olfactory epithelium, even with long exposure times. The apparent length of the mRNA is ~2.5 kb. A similar analysis for the bovine UGT clone (not shown) corroborates this observation, except that respiratory epithelium (an adjacent, non-sensory nasal tissue) is also positive, but has a 3-4-fold lower reactivity. Positions of 28S and 18S rRNA are marked.
METHODS. Rat tissues were dissected in the laboratory immediately after death and frozen in liquid nitrogen. Total RNA (20 μg) prepared as described[13] was electrophoresed on 1% agarose gels and blotted onto nylon membranes (Genescreen, DuPont). Membranes were hybridized with ^{32}P-labelled cDNA of clone RO1 (top) or mouse GAPDH (gift of Dr I. Ginsburg, the Weizmann Institute) (bottom). Hybridization was performed in Denhardt's solution with 1 M NaCl at 42 °C for 18 h, followed by two washes at 60 °C, 0.1 × SSC, for 30 min. Autoradiography was for 12 h at −70 °C.

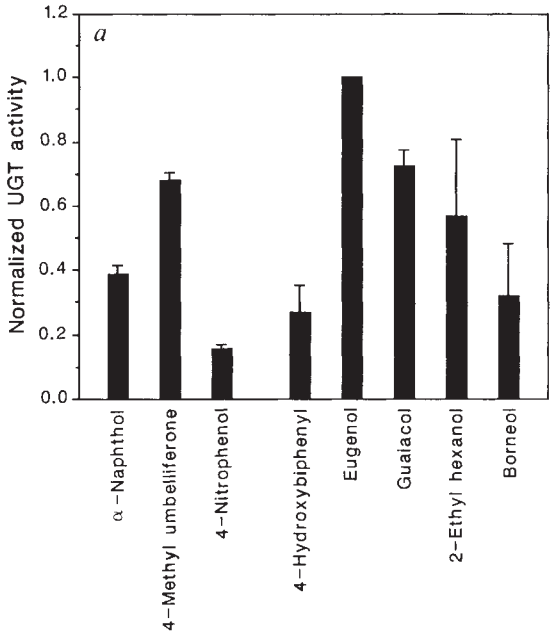

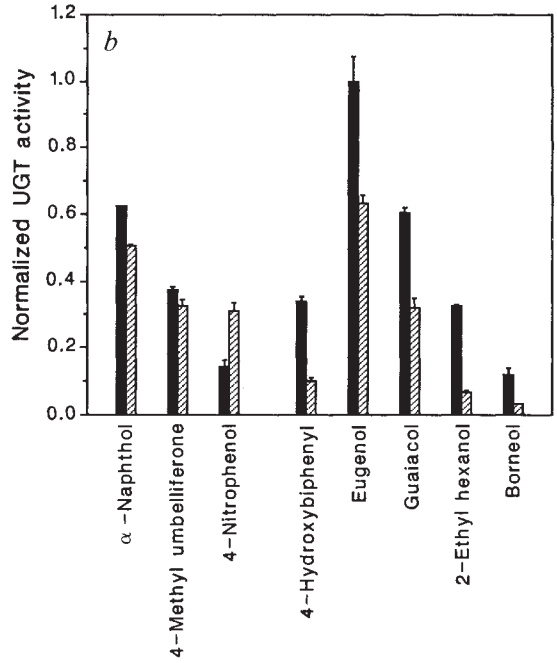

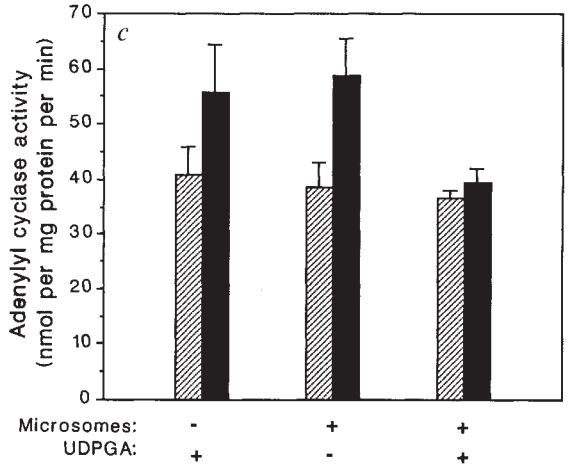

FIG. 3 Action and specificity of UGT_{olf}. *a*, expression of rat UGT_{olf} in COS-7 cells. UGT activity towards standard substrates (three left-hand bars) and hydroxyl-containing odorants (five right-hand bars) was measured in homogenates of COS-7 cells transiently transfected with clone RO1 cDNA. No glucuronidation could be detected in membranes from untransfected cells or from cells transfected with the cDNA in the wrong orientation. Values are normalized relative to eugenol, and represent the mean ± difference of two experiments with two batches of transfected cells. Specific activities towards eugenol were 1.33 and 0.29 nmol per mg protein per min, and in untransfected cells were less than 0.008 nmol per mg protein per min. *b*, UGT activity towards the same substrates in bovine olfactory epithelial (dark) and liver (hatched) microsomes. Values (normalized as in *a*) are representative of two experiments, and each is the mean ± difference of two replicates. Specific activity towards eugenol was 72.7 ± 5.5 nmol per mg protein per min. *c*, Glucuronation abolishes odorant activation of olfactory adenylyl cyclase (mean ± s.d. of triplicates; $P < 0.02$). Odorants (or the vehicle alone for measurement of basal activity) were preincubated with or without bovine olfactory epithelial microsomes or UDP-glucuronic acid as indicated and subsequently used in the odorant-sensitive adenylyl cyclase assay[1]. ▧, Basal; ■, odorants.
METHODS. *a*, The RO1 cDNA was inserted in two possible orientations in the mammalian expression vector pSVL-RS (provided by Dr C. Kahana, the Weizmann Institute), a modified pSVL vector (Pharmacia) in which an *Eco*R1 site was introduced into the multiple cloning site. Subconfluent cultures of COS-7 cells were transfected with 0.24 μg recombinant plasmid per cm^2 as described[35,36]. After 72 h cells were ground-glass hand-homogenized and UGT activity assayed as described[37] with modifications: incubation was with 0.1 M Tris-HCl, pH 7.4, 10 mM $MgCl_2$, 0.05% Triton X-100, 1 mM aglycone, 50 μM UDP-glucuronic acid, 0.1 μCi ^{14}C-labelled UDP-glucuronic acid (304 mCi mmol^{-1}, Dupont), and 10-60 μg homogenate protein in a total volume of 50 μl. After 2 h at 37 °C, the reaction was stopped with 150 μl ethanol, and samples analysed by thin-layer chromatography on silica gel as described[37]. *b*, Microsomes from bovine olfactory epithelium and liver were prepared as described[16]. UGT activity was assayed as described in *a*, except that the incubation mixture contained 1 mM UDP-glucuronic acid, 0.05 μCi ^{14}C-labelled UDP-glucuronic acid and 25 μg microsomal protein, incubation time was 10 min and the reaction stopped with 3% SDS. Measurements were carried out in the excess substrate regimen, and glucuronates identified with β-glucuronidase[37]. *c*, A mixture of the four hydroxyl-containing odorants, eugenol, guaiacol, geraniol and 2-ethyl-1-hexanol (Aldrich, 62.5 μM each), was subjected to glucuronidation as in *b*, with the following modifications: 100 μl reaction volume, 12 mM $MgCl_2$, no Triton X-100, 100 μg microsomal protein, 3 mM UDP-glucuronic acid, and 30 min incubation time, selected to maximize odorant glucuronidation. The reaction mixture was centrifuged (5 min, 12,000*g*) and 20 μl supernatant together with the adenylyl cyclase reaction mix and rat olfactory cilia (0.5-1.0 μg) protein) were analysed for cAMP generation as described[1,38].

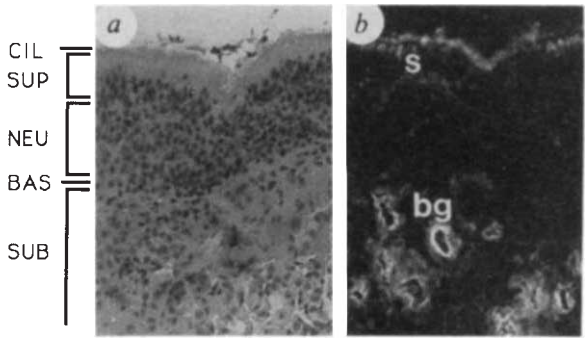

FIG. 4 Tissue localization of UGT_{olf}. Serial frozen sections of bovine olfactory epithelium were stained with *a*, haematoxylin-eosin or *b*, with an antiserum against UGT_{olf}. CIL, ciliary layer; SUP, supporting cells' apical cytoplasm and nuclei; NEU, sensory neuron nuclear layer; BAS, basal cell layer; SUB, subepithelial layers containing the Bowman's glands. *b*, Label is seen in the Bowman's glands (bg) and in a superficial layer (s). Labelling in the latter was more variable in location and intensity. No reactivity with olfactory epithelium was observed using non-specific rabbit serum, or an antiserum against an unrelated synthetic peptide, both purified as described below for the specific antiserum. The bar labelled SUP is 20 μm.

METHODS. Bovine olfactory epithelia were collected as in Fig. 3 and stored in isopentane at −80 °C. Sections (8–10 μm) were prepared on a Reichert-Jung Frigocut 2800 cryostat at −20 °C, dried overnight at 23 °C, fixed for 20 min in acetone at −20 °C and washed in sodium phosphate buffer, pH 7.4, containing 0.15 M NaCl. Immunolabelling was performed with antiserum 11, prepared as described[16], against a BSA-conjugated synthetic peptide corresponding to residues 229–244 of bovine UGT_{olf}. An immunoglobulin fraction was obtained through DEAE-cellulose (Whatman) ion-exchange chromatography, and anti-BSA reactivity was removed by three passes of affinity chromatography on a BSA-Sepharose column (Pharmacia), following which radioimmunoassays for BSA were negative. Sections were incubated with concentrated purified antiserum 11 (0.4 mg protein ml^{-1}), and stained with tetramethylrhodamine-labelled goat anti-rabbit immunoglobulin antibody (gift of Dr B. Geiger, the Weizmann Institute).

cytochrome P_{450} and UGT may be long-term detoxification devices. Olfactory epithelium is the region of the nervous system most exposed to airborne hazardous chemicals, and is only a few millimetres from the brain. Olfactory epithelium has been proposed to be a direct route of pathological agents into the brain[30] and is related to early changes associated with Alzheimer's disease[31]. The study of olfactory cytochrome P_{450}s and UGT could shed light on a potentially relevant toxin inactivation mechanism. In cases where cytochrome P_{450} action leads to cytotoxin bioactivation[17,18], a highly active UGT may be the main detoxification barrier. □

Received 4 October; accepted 27 November 1990.

1. Pace, U., Hanski, E., Salomon, Y. & Lancet, D. *Nature* **316**, 255–258 (1985).
2. Sklar, P. B., Anholt, R. R. & Snyder, S. H. *J. biol. Chem.* **261**, 15538–15543 (1986).
3. Shirley, S. G., Robinson, C. J., Dickinson, K., Aujla, R. & Dodd, G. H. *Biochem. J.* **240**, 605–607 (1986).
4. Lancet, D. & Pace, U. *Trends biochem. Sci.* **12**, 63–66 (1987).
5. Lancet, D., Lazard, D., Heldman, J., Khen, M. & Nef, P. *Cold Spring Harbor Symp. quant. Biol.* **53**, 343–348 (1988).
6. Snyder, S. H., Sklar, P. B., Hwang, P. M. & Pevsner, J. *Trends Neurosci.* **12**, 35–38 (1989).
7. Reed, R. R. *Cell* **60**, 1–2 (1990).
8. Getchell, T. V., Margolis, F. L. & Getchell, M. L. *Prog. Neurobiol.* **23**, 317–345 (1984).
9. Lancet, D. *A. Rev. Neurosci.* **9**, 329–355 (1986).
10. Dahl, A. R., Hadley, W. M., Hahn, F. F., Benson, J. M. & McClellan, R. O. *Science* **216**, 57–59 (1982).
11. Dahl, A. R. in *Molecular Neurobiology of the Olfactory System* (eds Margolis, F. L. & Getchell, T. V.) (Plenum, New York, 1988).
12. Jenner, J. & Dodd, G. H. *Drug Metabol. Drug Interact.* **6**, 123–148 (1988).
13. Nef, P. *et al. J. biol. Chem.* **264**, 6780–6785 (1989).
14. Ding, X. X. & Coon, M. J. *Biochemistry* **27**, 8330–8337 (1988).
15. Nef, P., Larabee, T. M., Kagimoto, K. & Meyer, U. A. *J. biol. Chem.* **265**, 2903–2907 (1990).
16. Lazard, D. *et al. Biochemistry* **29**, 7433–7440 (1990).
17. Black, S. D. & Coon, M. J. *Adv. Enzym.* **60**, 35–87 (1987).
18. Nebert, D. W. & Gonzalez, F. J. *A. Rev. Biochem.* **56**, 945–993 (1987).
19. Burchell, B. & Coughtrie, M. W. *Pharmac. Ther.* **43**, 261–289 (1989).
20. Pace, U. & Lancet, D. *Proc. natn. Acad. Sci. U.S.A.* **83**, 4947–4951 (1986).
21. Mackenzie, P. I., Chowdhury, N. R. & Chowdhury, J. R. *Clin. exp. pharmacol. Physiol.* **16**, 501–504 (1989).
22. Pfeuffer, E., Mollner, S., Lancet, D. & Pfeuffer, T. *J. biol. Chem.* **264**, 18803–18807 (1989).
23. Fenaroli, G. *Fenaroli's Handbook of Flavor Ingredients* (eds Furia, E. T. & Bellanca, N.) (CRC, Cleveland, 1975).
24. Lazard, D., Barak, Y. & Lancet, D. *Biochim. biophys. Acta* **1013**, 68–72 (1989).
25. Voigt, J. M., Guengerich, F. P. & Baron, J. *Cancer Lett.* **27**, 241–247 (1985).
26. Foster, J. R. *et al. Biochem. Pharmacol.* **35**, 4543–4554 (1986).
27. Shepherd, S. R., Baird, S. J., Hallinan, T. & Burchell, B. *Biochem. J.* **259**, 617–620 (1989).
28. Crawford, J. M. & Gollan, J. L. *Am. J. Physiol.* **255**, 121–131 (1988).
29. Gander, J. E. & Mannering, G. J. *Pharmac. Ther.* **10**, 191–221 (1980).
30. Shipley, M. T. *Brain Res. Bull.* **15**, 129–142 (1985).
31. Talamo, B. R. *et al. Nature* **337**, 736–739 (1989).
32. Wilbur, W. & Lipman, D. *Proc. natn. Acad. Sci. U.S.A.* **80**, 726–730 (1983).
33. Mackenzie, P. I. *J. biol. Chem.* **261**, 6119–6125 (1986).
34. Mackenzie, P. I. *J. biol. Chem.* **262**, 9744–9749 (1987).
35. Sompayrac, L. M. & Danna, K. *J. Proc. natn. Acad. Sci. U.S.A.* **78**, 7575–7578 (1981).
36. Graham, F. L. & Van der Eb, A. J. *Virology* **52**, 456–467 (1973).
37. Bansal, S. K. & Gessner, T. *Analyt. Biochem.* **109**, 321–329 (1980).
38. Salomon, Y., Londos, C. & Rodbell, M. *Analyt. Biochem.* **58**, 541–548 (1974).

ACKNOWLEDGEMENTS. We thank Drs D. W. Nebert, C. Kahana, Y. Rosenberg-Hasson and Y. Barak for help and advice. This work was supported by the National Institutes of Health, the United States Army Research Office, the Fund for Basic Research of the Israeli Academy of Sciences, the Heinemann and Minerva Foundations, Munich, Germany, and the Forchheimer Center for Molecular Genetics.

Activation of chloride channels in normal and cystic fibrosis airway epithelial cells by multifunctional calcium/calmodulin-dependent protein kinase

John A. Wagner*†, Alison L. Cozens‡, Howard Schulman§, Dieter C. Gruenert‡, Lubert Stryer† & Phyllis Gardner*||

* Department of Medicine, Falk CVRC, Stanford University School of Medicine, Stanford, California 94305, USA
† Department of Cell Biology, Stanford University School of Medicine, Stanford, California 94305, USA
‡ Cardiovascular Research Institute, University of California, San Francisco, California 94143, USA
§ Department of Pharmacology, Stanford University School of Medicine, Stanford, California 94305, USA

CYSTIC fibrosis is associated with defective regulation of apical membrane chloride channels in airway epithelial cells. These channels in normal cells are activated by cyclic AMP-dependent protein kinase[1,2] and protein kinase C[3,4]. In cystic fibrosis these kinases fail to activate otherwise normal Cl^- channels[1–4]. But Cl^- flux in cystic fibrosis cells, as in normal cells, can be activated by raising intracellular Ca^{2+} (refs 5–10). We report here whole-cell patch clamp studies of normal and cystic fibrosis-derived airway epithelial cells showing that Cl^- channel activation by Ca^{2+} is mediated by multifunctional Ca^{2+}/calmodulin-dependent protein kinase. We find that intracellular application of activated kinase and ATP activates a Cl^- current similar to that activated by a Ca^{2+} ionophore, that peptide inhibitors of either the kinase or calmodulin block Ca^{2+}-dependent activation of Cl^- channels, and that a peptide inhibitor of protein kinase C does not block Ca^{2+}-dependent activation. Ca^{2+}/calmodulin activation of Cl^- channels presents a pathway with therapeutic potential for circumventing defective regulation of Cl^- channels in cystic fibrosis.

To delineate the molecular mechanism by which Ca^{2+} activates Cl^- channels, we used three simian virus 40 (SV40)-transformed cell lines from normal and cystic fibrosis (CF) airway epithelia[3,11–13]. All three contain messenger RNA for the cystic fibrosis transmembrane regulator (CFTR)[14]. One of the CF cell lines (2CFSMEo-; CF-1) was positive for the ΔF508 mutation, the deletion in 70% of CF chromosomes[15], whereas the other (CFNPE-9o-; CF-2) was not[13].

Whole-cell patch clamp recording revealed that only the normal fetal cell line (56FHTE-8o-; refs 3, 20) showed increased Cl^- conductance in response to bath application of 400 μM

|| To whom correspondence should be addressed.

8-(4-chlorophenylthio)-adenosine 3′-5′ cyclic monophosphate (CPTcAMP), a membrane-soluble cAMP analogue (Fig. 1*a*, *b*, *e*). The voltage clamp record displayed little time dependence and the whole-cell *I*-*V* relation was slightly outwardly rectifying. A CPTcAMP-induced current observed in the T84 intestinal adenocarcinoma cell displayed no time-dependence and had a linear whole-cell *I*-*V* relation[16]. The reversal potential in our experiments was -7.5 ± 6.1 mV ($n = 5$), in close agreement with that calculated for Cl^- according to the Nernst equation (-5.4 mV at 30 °C). Current was carried predominantly by Cl^- ions in these conditions because K^+ was absent from the internal buffer (pipette) and Cs^+, used to replace K^+, is known to block K^+ channels[27]; and because reduction of external Cl^- shifted the reversal potential to $+82 \pm 11$ mV ($n = 3$) as predicted by the Nernst equation assuming a Cl^--selective conductance. As expected, CPTcAMP treatment did not markedly increase Cl^- current in either CF cell line.

In contrast, all three cell types showed large increases in whole-cell Cl^- current in response to 500 nM ionomycin, a Ca^{2+} ionophore (Fig. 1*a*, *c*, *e*). Greater outward rectification was observed than for the cAMP response. The maximal outward current was normalized by dividing by cell capacitance, a measure of plasma membrane area, to facilitate comparison between cells. The ratio of the ionomycin-induced current at +100 mV to the cell capacitance was 75.2 ± 45.0 ($n = 6$; $P < 0.002$), 58.0 ± 36.2 ($n = 7$; $P < 0.001$), and 31.0 ± 26.5 ($n = 7$; $P < 0.02$) pA pF^{-1} for the normal, CF-1, and CF-2 cells, respectively, compared with a baseline value of about 2 pA pF^{-1}. Reversal potentials for the whole-cell ionomycin-induced Cl^- conductance for normal, CF-1, and CF-2 cells were -12 ± 16 ($n = 6$),

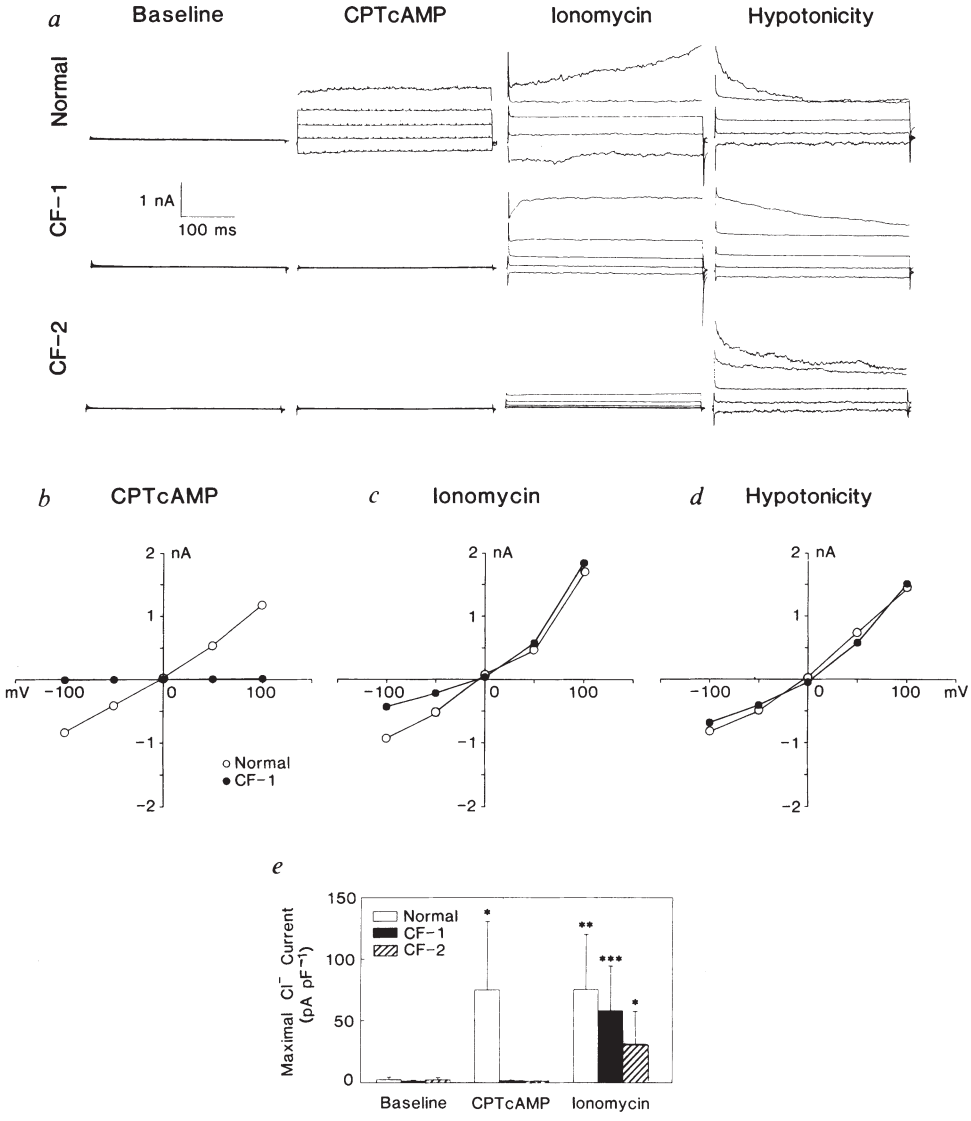

FIG. 1 Whole-cell patch clamp experiments demonstrate that ionomycin-induced and hypotonicity-induced Cl^- currents were present in CF cells, whereas CPTcAMP-induced currents were absent. *a*, Representative whole-cell patch clamp records of epithelial cells. A voltage clamp protocol stepped the membrane potential from a holding potential of −70 mV to voltages between −100 and +100 mV in 50 mV steps. Voltage steps were of 360-ms duration with 640-ms intervals between the end of one step and the start of another. Row 1, normal airway cell; row 2, CF-1 airway cell; row 3, CF-2 airway cell. Column 1, baseline Cl^- currents recorded 1–5 min after obtaining whole-cell configuration; column 2, maximum Cl^- current recorded 2–15 min after addition of 400 μM CPTcAMP (Sigma); column 3, maximum Cl^- current recorded 2–15 min after addition of 500 nM ionomycin (Calbiochem); column 4, maximum Cl^- current recorded 2–10 min after perfusion of the bath with a hypotonic solution (108 mosm kg^{-1}). Inset, scale. *b*, Whole-cell *I*-*V* relation after treatment of epithelial cells with CPTcAMP. ○, Normal airway cells; ●, CF-1 airway cells. Data are from the cells shown in *a* and represent the current averaged over the final 108 ms of the pulses. *c*, Whole-cell *I*-*V* relation after treatment with ionomycin. Data are averaged over the final 108 ms of the pulses. *d*, Whole-cell *I*-*V* relation after hypotonic bath treatment. Data are averaged over the initial 50 ms of the pulses. *e*, Maximal outward Cl^- current at +100 mV (mean ± s.d.). Open bar, normal airway cells (*n* for baseline, CPTcAMP, and ionomycin = 11, 5, 6 cells). Filled bar, CF-1 airway cells (*n* = 14, 7, 7). Hatched bar, CF-2 (*n* = 14, 7, 7). * $P < 0.02$, ** $P < 0.002$ and *** $P < 0.001$, compared to respective baseline values, by *t*-test.

METHODS. Cells were transformed and cultured as described[3,18-20]. Cells were studied 1–3 days after plating on glass coverslips. All experiments were conducted at 30 °C. Coverslips were placed in a 1 ml acrylic chamber on the stage of a Nikon Diaphot inverted microscope and washed six times with bath solution (in mM): 170 Tris-Cl, 1 $MgCl_2$, 2.5 $CaCl_2$, 5 HEPES, 10 glucose, pH 7.4, 325 mosm kg^{-1}). Reduction of Cl^- in the external solution was achieved by replacement of Tris-Cl with Tris aspartate (external Cl^- 7 mM). Reduction of osmolarity was achieved by 1:3 dilution of the bath solution with distilled H_2O. Micropipettes for whole-cell patch clamp recordings were made by the method of Hamill *et al.*[24] and had a tip resistance of 3–4 mΩ when filled with pipette solution (in mM: 140 CsCl, 2 $MgCl_2$, 0.5 EGTA, 2 MgATP, 5 HEPES, 10 glucose, pH 7.35 adjusted with CsOH, 298 mosm kg^{-1}). The difference in osmolarities between bath and pipette solutions was required to prevent a volume-induced Cl^- current[19]. Whole-cell voltage clamp recordings were made using a model 1B Axopatch amplifier (Axon Instruments). The membrane was voltage clamped to a holding potential of −70 mV and stepped to levels between −100 and +100 mV in 50 mV increments using a Tecmar 12-bit A/D-D/A converter (Scientific Solutions), and an IBM-AT computer. Signals were filtered at 1 KHz and stored on a strip chart recorder and a floppy disk.

-13 ± 14 ($n = 7$), and -15 ± 12 ($n = 7$) mV. Ionomycin-induced current was specific for Cl^- because reduction of external Cl^- shifted the reversal potential in normal cells to $+94 \pm 15$ mV ($n = 3$), in accordance with that calculated for Cl^- by the Nernst equation. Ionomycin increased intracellular Ca^{2+} from 129 ± 12.1 to 842 ± 231 nM in normal cells ($n = 3$, measured at 30 °C), as monitored spectrofluorimetrically using indo-1 as the calcium indicator[18]. The Cl^- current induced by exposure of cells to hypotonic solutions was also not defective in CF cells (Fig. 1*a* and *d*). This current was slowly inactivating and slightly outwardly rectifying, similar to that seen with T84 epithelial cells[19].

Excised patch clamp experiments demonstrated that exposure of epithelial membranes to high Ca^{2+} does not activate Cl^- channel[6,7], suggesting that Ca^{2+} acts through a cytosolic protein or one that is loosely bound to the plasma membrane. Purified protein kinase C (PKC) activates a Cl^- channel in inside-out excised patches from normal cells, but not CF cells[3,4], ruling out a role for PKC in the Ca^{2+}-dependent activation observed here in normal and CF epithelia. We tested the hypothesis that the Ca^{2+}-dependent activation of Cl^- current is mediated by a Ca^{2+}/calmodulin-dependent protein kinase (CaMK) by exposing the cytosol of cells in whole-cell patch clamp to peptide inhibitors of CaMK and calmodulin. CaMK inhibitory peptide, a synthetic peptide containing the autoinhibitory region of CaMK (residues 273–302 of the α subunit of CaMK) inhibits brain CaMK activity at 1 μM, and does not bind calmodulin[20]. CaMK control peptide (residues 284–302) is a truncated version of the inhibitory peptide and does not inhibit brain CaMK activity[20]. Calmodulin inhibitory peptide (residues 291–317 of CaMK) binds calmodulin and potently inhibits CaMK and other calmodulin-dependent enzymes[20]. Figure 2 shows that 20 μM CaMK control peptide in the pipette does not affect the amount of ionomycin-induced Cl^- current in normal cells or CF-1 cells. In contrast, 20 μM CaMK inhibitory peptide reduced maximal outward current by 71% ($P < 0.01$) in normal cells and by 87% ($P < 0.001$) in CF-1 cells. Also, calmodulin inhibitory peptide at 2 μM reduced maximal outward current by 93% ($P < 0.002$) and 95% ($P < 0.001$), respectively. Inhibition by CaMK inhibitory peptide and calmodulin inhibitory peptide was specific because neither peptide decreased CPTcAMP-induced current in normal cells (data not shown) and 5 μM PKC control peptide ([Glu[27]]PKC-α 19–31) or PKC inhibitory peptide (PKC-α 19–36)[21] did not decrease the ionomycin-stimulated outward Cl^- current (Fig. 2*b* and *c*). In contrast, PKC inhibitory peptide but not PKC control peptide increased the baseline outward Cl^- current 4.8-fold ($P < 0.05$) in normal cells and 2.8-fold ($P < 0.01$) in CF-1 cells. Baseline Cl^- conductance may be constitutively inhibited by PKC in epithelial cells. Inhibition of Cl^- channels by PKC is preserved in CF epithelial cells[4].

Because both the CaMK and calmodulin inhibitory peptides reduced ionomycin-induced whole-cell Cl^- current, we reasoned that addition of CaMK and ATP would activate Cl^- current. To avoid a complicating effect of added Ca^{2+}, we used purified CaMK[22], which had previously been autophosphorylated to render it autonomous of Ca^{2+} and calmodulin[23]. Addition of autonomous CaMK to the pipette buffer markedly activated Cl^- current both in normal and CF-1 cells (Fig. 3). The ratio of autonomous CaMK-induced whole-cell Cl^- current at +100 mV to cell capacitance gradually increased from 2.50 ± 2.57 to 73.0 ± 29.0 ($n = 6$; $P < 0.01$) and 1.65 ± 0.931 to 71.0 ± 35.5 ($n = 6$; $P < 0.02$) pA pF^{-1} in normal and CF-1 cells, respectively, over the course of 10–15 min. Reversal potentials for whole-cell autonomous CaMK-induced current in normal and CF-1 cells were -4.5 ± 6.3 ($n = 6$) and -1.2 ± 2.8 ($n = 6$) mV, respectively. The CaMK-induced current was specific for Cl^- because reduction of external Cl^- shifted the reversal potential in normal cells to 87 ± 6.4 mV ($n = 2$) in accordance with that calculated for Cl^- by the Nernst equation. In contrast, addition of heat-inactivated, autophosphorylated CaMK to the pipette buffer resulted in a small, variable increase in whole-cell Cl^- current in normal or CF-1 cells. The ratio of whole-cell current at +100 mV to cell capacitance went from 3.08 ± 1.08 to 16.4 ± 19.2 ($n = 5$; not significant (NS) and 2.39 ± 2.02 to 18.6 ± 18.7 ($n = 5$; NS) pA pF^{-1} for normal and CF-1 cells, respectively. A small increase in whole-cell Cl^- current was also observed after addition of 60 μM calmodulin to the pipette buffer. The ratio of whole-cell current to capacitance increased from 2.55 ± 2.26 in the first 2 min to 16.0 ± 16.2 ($n = 5$; NS) pA pF^{-1} after 10–15 min in normal cells. These variable increases, 20% of that observed on addition of autonomous CaMK, may reflect recruitment of endogenous

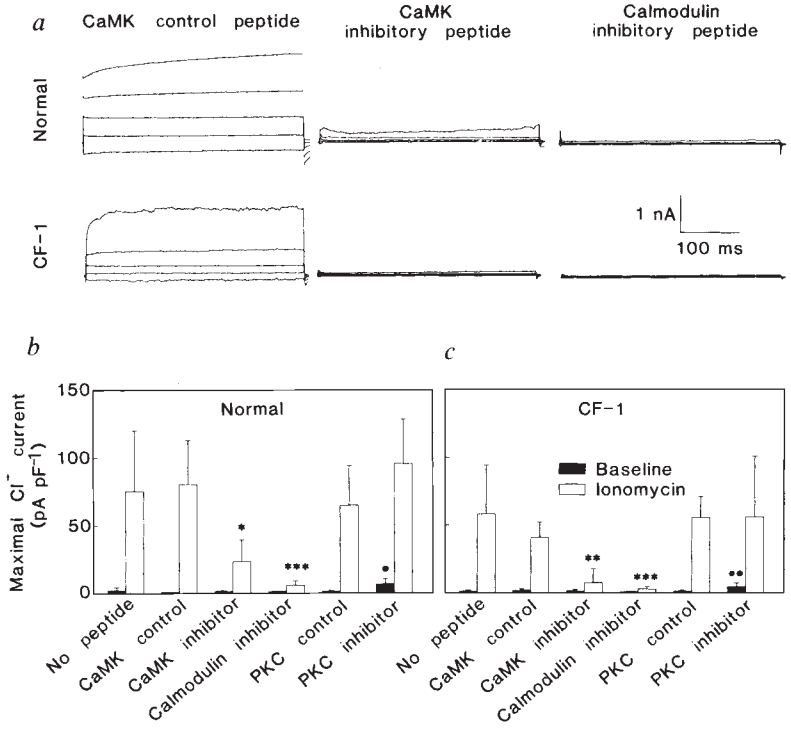

FIG. 2 CaMK inhibitor peptide and calmodulin inhibitor peptide inhibit the ionomycin-induced Cl^- current, whereas CaMK control peptide, PKC inhibitor peptide, and PKC control peptide did not. *a*, Representative patch clamp records showing the effects of exposing the cytosol of epithelial cells to peptide inhibitors of CaMK and calmodulin. Row 1, normal airway cell; row 2, CF-1 airway cell. Additions to the internal pipette solution were: column 1, internal pipette solution plus 20 μM CaMK control peptide; column 2, internal pipette solution plus 20 μM CaMK inhibitor peptide; column 3, internal pipette solution plus 2 μM calmodulin inhibitor peptide. *b*, Maximal outward Cl^- current at +100 mV in normal airway cells exposed to CaMK control and inhibitor peptide, calmodulin inhibitor peptide, 5 μM PKC control peptide, and 5 μM PKC inhibitor peptide, respectively. Current expressed as pA pF^{-1} (mean ± s.d.). The filled bars show peak currents before addition of ionomycin and the unfilled bars show current after addition. *c*, Maximal outward Cl^- current at +100 mV in CF-1 cells exposed to the peptides. * $P < 0.01$, ** $P < 0.002$, and *** $P < 0.001$, compared to respective CaMK control peptide ionomycin-stimulated values. •, $P < 0.05$ and ••, $P < 0.01$, compared to PKC control peptide baseline values. Comparisons are by *t*-test.

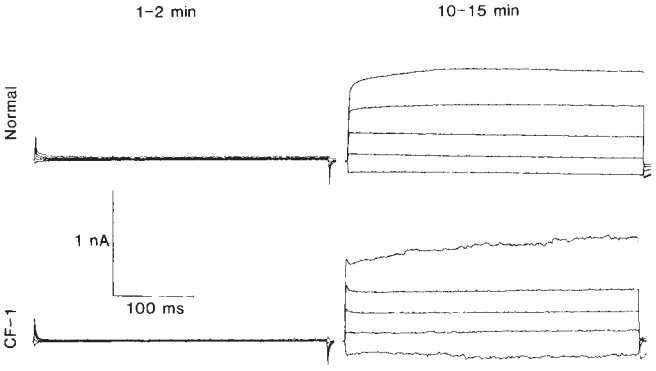

FIG. 3 Exogenous, autonomous CaMK (10 $\mu g\ ml^{-1}$) activated Cl^- current when added to the whole-cell pipette buffer in normal and CF-1 airway cells. A gradual increase in current was observed after obtaining whole-cell patch clamp configuration. The maximal current was observed between 10 and 15 min.

METHODS. Purified CaMK[22] was made autonomous[23] by incubation of 100 $\mu g\ ml^{-1}$ CaMK with 600 μM calmodulin, 500 μM ATP-γ-S, and 100 $\mu M\ CaCl_2$ for 10 min at 4 °C. This reaction was terminated by a 10-fold dilution of the reaction mix with pipette buffer and kept on ice for 20 min or less. Whole-cell patch clamp was done as in Fig. 1. Initial, baseline voltage pulse protocols were collected 1-2 min after obtaining whole-cell patch clamp. Subsequently, a gradual increase was observed in Cl^- current which reached a maximum 10-15 min after obtaining whole-cell patch clamp. Final pipette buffer was: 131 mM CsCl, 1.8 mM Mg-ATP, 0.9 mM $MgCl_2$, 9 mM glucose, 0.485 mM EGTA, 35 $\mu M\ CaCl_2$, 6 mM PIPES, 4.5 mM HEPES, 2.5 mM NaCl, 60 μM calmodulin, 50 μM ATP-γ-S, 27 mM glycerol, 10 $\mu g\ ml^{-1}$ CaMK, pH 7.35 with CsOH, 312 mosm kg^{-1}, and less than 20 nM free Ca^{2+} (calculated). Bath buffer was identical to that in Fig. 1 except that it was supplemented with 15 mM sucrose to 340 mosm kg^{-1} to prevent the volume-induced Cl^- current[19]. CaMK was heat-inactivated at 80 °C for 15 min and then autophosphorylated as above.

CaMK or the involvement of another Cl^- permeability pathway.

Our experiments show that Ca^{2+}-activation of Cl^- channels in normal and CF cells is mediated by stimulation of CaMK by Ca^{2+}-calmodulin. Thus, epithelial Cl^- channels are the target of all three multifunctional protein kinases, PKA, PKC and CaMK. It will be important to learn whether CaMK, PKC and PKA phosphorylate the same regulatory protein or different ones and whether the relationship between the regulatory protein(s) and the Cl^- conduction pathway. It is significant that CF airway cells retain CaMK regulation of Cl^- current even though they lack PKA activation. This difference may be exploited to develop agents that specifically stimulate phosphorylation of the Cl^- channel regulator by CaMK in epithelial cells. Activation of this alternative pathway for regulation of Cl^- conductance could be used to circumvent the defect in CF. □

Received 17 September; accepted 20 December 1990.

1. Schoumacher, R. A. *et al. Nature* **330,** 752-754 (1987).
2. Li, M. *et al. Nature* **331,** 358-360 (1988).
3. Hwang, T.-C. *et al. Science* **244,** 1351-1353 (1989).
4. Li, M. *et al. Science* **244,** 1353-1356 (1989).
5. Welsh, M. J. *Science* **232,** 1648-1650 (1986).
6. Welsh, M. J. & Liedtke, C. M. *Nature* **322,** 467-470 (1986).
7. Frizzell, R. A., Rechkemmer, G. & Shoemaker, R. L. *Science* **233,** 558-560 (1986).
8. Sato, K. & Sato, F. *J. Clin. Invest.* **73,** 1763-1771 (1984).
9. Willumsen, N. J. & Boucher, R. C. *Am. J. Physiol.* **256,** C226-C233 (1989).
10. Schoumacher, R. A. *et al. Proc. natn. Acad. Sci. U.S.A.* **87,** 4012-4016 (1990).
11. Gruenert, D. C., Basbaum, C. B., Welsh, M. J., Finkbeiner, W. E. & Nadel, J. A. *Proc. natn. Acad. Sci. U.S.A.* **85,** 5951-5955 (1988).
12. Gruenert, D. C. *et al. Pediatr. Pulmonol.* **17** (Suppl. 2), 100 (1988).
13. Cozens, A. L., Yezzi, M. J., Simon, E. M., Friend, D. S. & Gruenert, D. C. In *Identification of the CF (Cystic Fibrosis) Gene: Recent Progress and New Research Strategies* (Plenum, New York, in the press).
14. Riordan, J. R. *et al. Science* **245,** 1066-1073 (1989).
15. Kerem, B.-S. *et al. Science* **245,** 1073-1080 (1989).
16. Cliff, W. H. & Frizzell, R. A. *Proc. natn. Acad. Sci. U.S.A.* **87,** 4956-4960 (1990).
17. Gorman, A. L. F., Woolum, J. C. & Cornwall, M. C. *Biophys. J.* **38,** 319-322 (1982).
18. Grynkiewicz, G., Poenie, M. & Tsien, R. Y. *J. biol. Chem.* **260,** 3440-3450 (1985).
19. Worrell, R. T., Butt, A. G., Cliff, W. H. & Frizzell, R. A. *Am. J. Physiol.* **256,** C1111-C1119 (1989).
20. Malinow, R., Schulman, H. & Tsien, R. W. *Science* **245,** 862-866 (1989).
21. House, C. & Kemp, B. E. *Science* **238,** 1726-1729 (1987).
22. Schulman, H. *J. Cell Biol.* **99,** 11-19 (1984).
23. Nichols, R. A., Sihra, T. S., Czernik, A. J., Nairn, A. C. & Greengard, P. *Nature* **343,** 647-651 (1990).
24. Hamill, O. P., Marty, A., Neher, E., Sakmann, B. & Sigworth, F. J. *Pflügers Arch. Eur. J. Physiol.* **391,** 85-100 (1981).

ACKNOWLEDGEMENTS. We thank T. McDonald, P. Nghiem, T. Meyer, B. Premack, R. Aldrich and P. Hanson for advice and stimulating discussions, and J. Horne and E. Simon for tissue culture assistance. This research was supported by the National Institutes of Health, the Cystic Fibrosis Foundation and the Burroughs Wellcome Fund (to P.G.).

ELAM-1 is an adhesion molecule for skin-homing T cells

Louis J. Picker*†, Takashi K. Kishimoto*, C. Wayne Smith‡, R. Aaron Warnock* & Eugene C. Butcher*

* Laboratory of Immunology and Vascular Biology, Department of Pathology and the Digestive Disease Center, Stanford University School of Medicine, Stanford, California 94305, USA and Center for Molecular Medicine, Veterans Administration Medical Center, Palo Alto, California 94304, USA
‡ Section of Leukocyte Biology, Department of Pediatrics, Baylor College of Medicine, Houston, Texas 77030, USA

ENDOTHELIAL cell leukocyte adhesion molecule-1 (ELAM-1) has been described as an inducible endothelial cell-adhesion molecule for neutrophils, and is believed to have a key role in the extravasation of these cells at sites of acute inflammation[1-3]. Here we report that ELAM-1-transfected COS cells also bind a unique skin-associated subset of circulating memory T cells defined by the expression of the cutaneous lymphocyte-associated antigen[4,5]. T cells expressing this antigen bind at least as well as neutrophils to expressed ELAM-1, whereas other lymphocytes in the peripheral blood bind poorly, or not at all. Immunohistological survey of chronically inflamed tissue specimens revealed that vascular expression of ELAM-1 occurs at cutaneous sites in preference to noncutaneous sites. We conclude that at sites of chronic inflammation, ELAM-1 may function as a skin vascular addressin, a tissue-selective endothelial cell-adhesion molecule for skin-homing memory T lymphocytes.

To investigate whether ELAM-1 binds monocytes or lymphocytes, we incubated peripheral blood mononuclear cells (PBMC) on COS cells transfected with ELAM-1 complementary DNA. Although PBMC as a population bound less well than neutrophils[3], many mononuclear cells adhered to the ELAM-1 transfectants, but not to control 'mock'-transfected COS cells (Fig. 1). Confirming the specificity of this interaction, anti-ELAM-1 monoclonal antibodies inhibited PBMC binding by $79 \pm 1.3\%$ (mean ± s.e.m.; $n = 3$). To determine whether ELAM-1 binding was a specific property of a particular PBMC subset, we used flow cytometry to examine the ability of adherence to ELAM-1-transfected COS cells to enrich or deplete the following PBMC subpopulations: monocytes ($CD14^+$, high forward and orthogonal light scatter); B cells ($CD19^+$ or $CD22^+$); whole T cells ($CD2^+$ or $CD3^+$); $CD8^+$ and $CD4^+$ T cells; whole memory (previously activated) T cells (LFA-3/$CD58^{high}$ (ref. 6)); T cells bearing the LECAM-1/peripheral lymph node homing receptor[5,7]; and the unique skin-associated and mucosa-associated memory T-cell populations defined by expression of the cutaneous lymphocyte-associated antigen (CLA, monoclonal antibody HECA-452 (refs 4, 5)), and the mucosal lymphocyte-associated antigen (MLA, monoclonal antibodies HML-1 and Ber ACT 8 (refs 5, 8)), respectively.

Only the CLA^+ T-cell population was significantly affected by this procedure (Fig. 2). The percentage of CLA^+ T cells,

† To whom correspondence should be addressed at Department of Pathology, University of Texas Southwestern Medical Center, 5323 Harry Hines Boulevard, Dallas, Texas 75235-9072, USA.

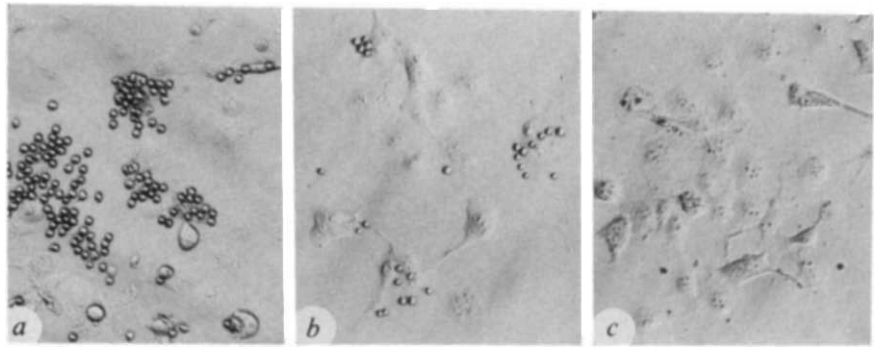

FIG. 1 Adherence of peripheral blood polymorphonuclear leukocytes (PMN) to ELAM-1-transfected COS cells (*a*), peripheral blood mononuclear cells (PBMC) to ELAM-1-transfected COS cells (*b*), or PBMC to control tranfected COS cells (*c*).
METHODS. COS cells were transfected by DEAE-dextran, as previously described[21]. ELAM-1 cDNA in the cDM8 expression vector was provided by B. Seed (Harvard University) and was also derived by polymerase-chain-reaction amplification from a stimulated HUVEC cDNA library using appropriate oligonucleotides based on the published ELAM-1 cDNA sequence[3]. COS cells transfected with either clone stained specifically with anti-ELAM-1 monoclonal antibody and gave similar results in adhesion assays. Typically, more than 40% of the cells were transfected, as judged by immunofluorescence with the appropriate monoclonal. As a control, COS cells were 'mock'-transfected under the same conditions as above, except no DNA was added. After transfection, the COS cells were incubated for 24–48 h, collected, pooled and replated (to ensure an even distribution of transfectants among different plates), and were used for adhesion assays 24 h later. PBMC or PMN were freshly isolated by ficoll-hypaque density centrifugation and dextran sedimentation, respectively[4,7], and suspended at in HEPES-buffered DMEM medium with no serum. Cell suspension (1 ml) with $3-5\times10^5$ cells was added to each 3.5-cm plate (in triplicate) containing control or ELAM-1-transfected COS cells. The plates were gently rotated (60 r.p.m.) on a gyrotory shaker for 30 min at 25 °C, washed four times by aspirating and then gently filling each plate with 2 ml DMEM, and then fixed with 1% glutaraldehyde in Hanks Balanced Salt Solution. Fields shown are representative of the triplicate plates. For antibody blocking experiments, ELAM-transfected COS cells were pretreated with 30 μg ml^{-1} each of the anti-ELAM monoclonal antibodies CL2 (see Fig. 4 legend for description of this antibody) and 1.2B6 (ref. 22) before the binding assay.

which averaged 12% in the starting population, was typically reduced by >50% after one round of adherence to ELAM-1 transfectants, and almost completely depleted after three rounds. Correspondingly, there was a fourfold enrichment in the frequency of CLA$^+$ cells in the pooled bound fractions, and incubation of eluted ELAM-1 adherent cells to ELAM-1-transfected COS cells a second time (that is, a re-adherence) resulted in further enrichment of the CLA$^+$ population (Fig. 2). None of the other antigenically defined lymphocyte subsets studied were substantially or reproducibly enriched or depleted by the incubations, although there was a slight increase in MLA$^+$ cells in the nonbound fraction, and in LFA-3^{high} cells in the adherent population, consistent with CLA$^+$ T cells being LFA-3^{high} and MLA$^-$ (ref. 5). Furthermore, purified CLA$^+$ lymphocytes bound almost quantitatively to the ELAM-1 transfected cells, whereas the isolated CLA$^-$ population bound poorly (Fig. 3). Indeed, the CLA$^+$ population bound at least as efficiently as isolated neutrophils examined in parallel (Fig. 3*c*).

These results indicate that the CLA$^+$ memory T cell subset is the predominant ELAM-1-binding population among circulating lymphocytes. *In vivo*, this subset constitutes 80–90% of T cells in chronic dermotoses, but less than 5% of T cells in extracutaneous sites of chronic inflammation[4]. The selective skin location of CLA$^+$ T cells could be explained if, at sites of chronic inflammation, ELAM-1 were preferentially expressed on venules in the skin. Indeed, immunohistological analysis of 20 biopsies of chronically inflamed skin from patients with a variety of dermatologic disorders revealed moderate to intense ELAM-1 expression by venules in 19 cases, all of which had an associated, predominantly CLA$^+$ T cell infiltrate (Fig. 4). Among the 26

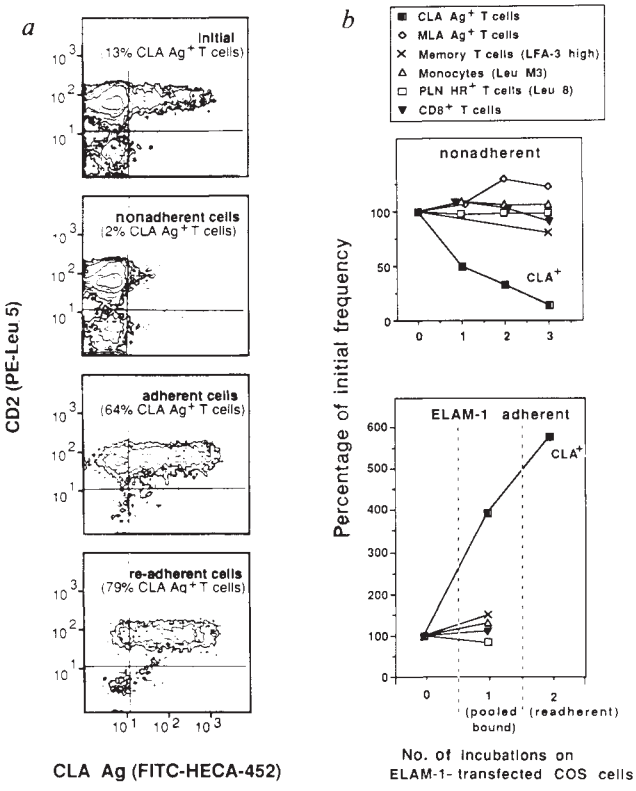

FIG. 2 Adhesion of PBMC subsets to ELAM-1-transfected COS cells: CLA-bearing T cells selectively bind ELAM-1. *a*, Two-colour flow cytometric contour plots (CD2 versus CLA) of input cells (initial PBMC), nonadherent cells (after three rounds of adherence to ELAM-1 transfectants), ELAM-1 adherent cells after a single adherence, and ELAM-1 re-adherent cells (ELAM-1 adherent cells that were eluted, re-adhered, and re-eluted). *b*, Mean size of various PBMC subsets within initial, nonadherent, pooled adherent and re-adherent populations ($n=2-6$). Results for CD4$^+$ T cells and for CD19$^+$ or CD22$^+$ B cells were similar to those of the CD8$^+$ T cell subset (data not shown).
METHODS. Adhesion assays were performed as described in Fig. 1, except that 4×10^6 PBMC in 2 ml HEPES-buffered DMEM were added to 6-cm plates containing the ELAM-1-transfected COS cells. Non-adherent cells were exposed to three cycles of incubation on ELAM-1 transfectants with aliquots from each cycle being saved for analysis. The adherent cells from each round were examined visually and then collected by addition of Ca^{2+}/Mg^{2+}-free HBSS containing 5 mM EDTA and 5 mM EGTA (recovery ≥ 90%). Binding mononuclear cells to plastic under the conditions of this assay was negligible. In some experiments, an aliquot of the collected adherent cells from a single round of adherence was subjected to a second round of adherence to transfected COS cells to further enrich for ELAM-binding mononuclear cells. Input, non-adherent and adherent cells were stained for single- or two-colour immunofluorescence (FITC versus phycoerythrin) and analysed by flow cytometry, as previously described[4,5]. The monoclonal antibodies used included T/S2.9 (anti-LFA-3/CD58; ref. 6), HECA-452 (anti-CLA; refs 4, 5), Ber ACT8 (anti-MLA; ref. 5), Leu 2 (CD8; all Leu monoclonal antibodies from Becton-Dickinson Immunocytometry Systems, San Jose, California), Leu 3 (CD4), Leu 4 (CD3), Leu 5 (CD2), Leu 8 (anti-LECAM-1, the peripheral lymph node homing receptor; refs, 5, 7), Leu 12 (CD19), Leu 14 (CD22) and Leu M3 (CD14).

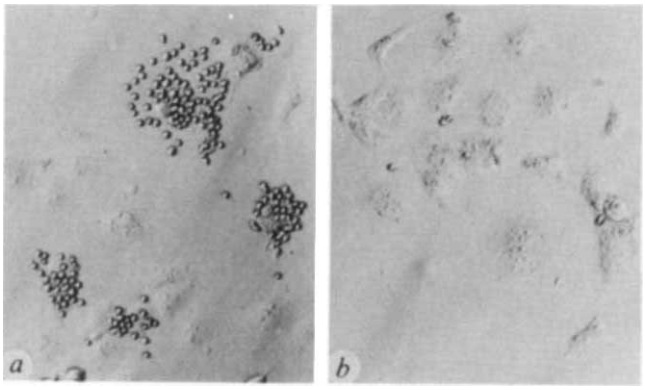

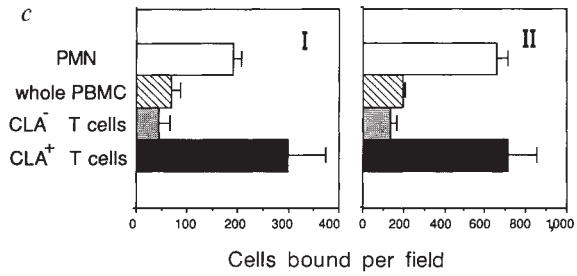

FIG. 3 The CLA$^+$ T cell subset contains most of the ELAM-1 binding activity of PBMC, and binds to ELAM-1-transfected COS cells as efficiently as PMN. *a*, *b*, Representative fields of CLA$^+$ and CLA$^-$ T cells, respectively, bound to ELAM-transfected COS cells. *c*, Data for two separate experiments comparing the cell populations indicated (mean ± s.e.m. for triplicate plates).
METHODS. The ELAM-1 adhesion assay was performed as described in Fig. 1, comparing identical numbers of PMN, PBMC, CLA$^+$ T cells and CLA$^-$ T cells (3–5 × 10^5 cells per 3.5-cm plate of subconfluent ELAM-1-transfected COS cells). Highly purified CLA$^+$ and CLA$^-$ T cells were obtained using a FACSTAR fluorescence activated cell sorter (Becton–Dickinson Immunocytometry Systems), using techniques previously described (ref. 23; preliminary studies indicated the HECA-452 monoclonal antibody did not block ELAM-1 binding in this assay). Binding was quantitated by the counting of bound cells per ×200 field; 10 random fields were counted per plate and triplicate plates were analysed for each cell type. Examination of the plates before washing revealed that more than 90% of added PMN and CLA$^+$ T cells bound to the ELAM-1-transfected COS cells during the assay, compared with less than 10% binding by CLA$^-$ T cells. In a separate experiment, the binding of sorted CLA$^+$ T cells to ELAM-1 transfectants was inhibited by the anti-ELAM monoclonal antibodies CL2 and 1.2B6 (30 μg ml^{-1} each; 84% inhibition relative to a class-matched control monoclonal antibody).

non-skin chronic inflammatory lesions examined (all with few or no CLA$^+$ T cells), 69% of the biopsies contained no venules expressing detectable ELAM-1. Weak to moderate ELAM-1 reactivity was detected on some venules in extracutaneous sites, but the degree of vascular ELAM-1 expression in these cases was considerably less than that in most of the skin lesions.

The results suggest that ELAM-1 is a tissue-selective endothelial cell-adhesion molecule involved in the homing of CLA$^+$ memory T cells to cutaneous sites of chronic inflammation, and so is a skin vascular addressin. Two other vascular addressins—the mucosal vascular addressin (MAd) and the peripheral lymph node vascular addressin (PNAd)—selectively target lymphocytes to peripheral lymph node and mucosal tissues, respectively[9–11]. PNAd and MAd are constitutively expressed on lymphoid organ high endothelial venules (HEV), and seem to be able to recruit both virgin lymphocytes and major memory lymphocyte subsets to their respective lymphoid tissues. By contrast, ELAM-1 is usually absent on HEV in normal lymphoid tissues (see Fig. 4 legend), is preferentially induced at sites of chronic inflammation in skin, and specifically binds a unique subset of of memory T cells. These observations are consistent with previous studies demonstrating that lymphocyte

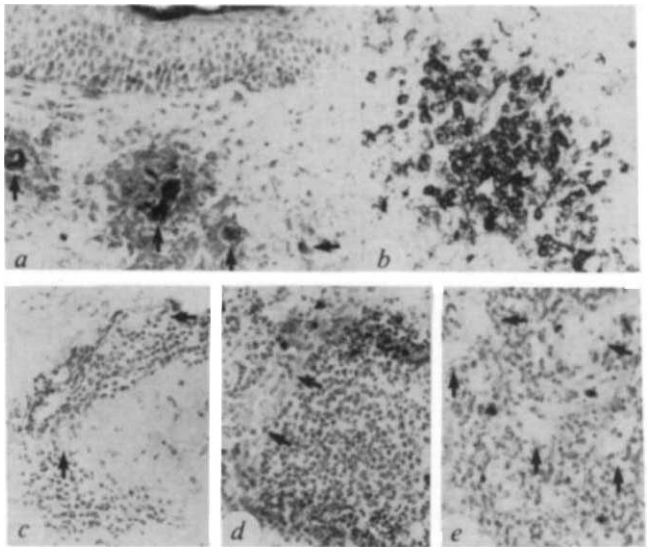

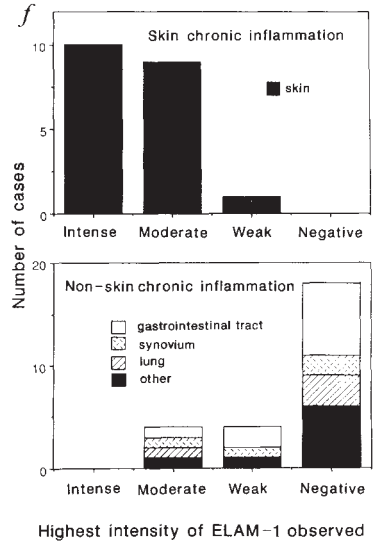

FIG. 4 Venules in cutaneous inflammatory lesions (a contact hypersensitivity lesion is shown) were generally intensely positive for ELAM-1 (*a*, arrows), and were associated with a predominantly CLA$^+$ T cell infiltrate (*b*; same lesion as *a*, shown at higher magnification). Venules (arrows) in extra-cutaneous inflammatory lesions such as myocarditis (*c*), inflammatory bowel disease (*d*) and hepatitis (*e*) were generally negative for ELAM-1, and were associated with CLA$^-$ T cell infiltrates (not shown, see ref. 4). *f*, Data for all the 46 cases examined. ELAM-1 was also not expressed or only poorly expressed on HEV in an additional series of normal or hyperplastic secondary lymphoid tissues (four lymph node, four appendix, two tonsil; data not shown).
METHODS. The distribution of ELAM-1 reactivity on vessels in these chronic inflammatory lesions was analysed using a three-stage immunoperoxidase technique, as described previously[4]. The skin lesions studied included five cases of psoriasis, four of allergic contact dermatitis, three of lichen planus, two of lymphoid hyperplasia in the skin, two of nonspecific chronic dermatitis, and one each of pityriasis lichenoides et varioliformis acuta, granuloma annulare, cutaneous drug eruption, and pityriasis rubra pilaris. Non-cutaneous chronic inflammatory lesions included ten from the gastrointestinal tract (five from the stomach, small bowel or colon, three from salivary glands, and two from liver), four inflamed synovia (rheumatoid arthritis), four from the lung, two each of mycocardium and nasopharynx, and one each of the kidney, bladder, thyroid and subcutaeous soft tissues. ELAM-1 reactivity was defined by monoclonal antibodies CL2 and CL3, and compared with a class-matched negative control on two to six levels through the tissue block for each specimen. Reactivity for each specimen was graded on the most-positive vessels identified, if any, as intense, moderate or weak (barely detectable). The CL2 and CL3 antibodies were raised against interleukin-1-activated human umbilical vein endothelial cells, and have similar patterns of staining reactivity and anti-adhesion activity as previously reported anti-ELAM-1 monoclonal antibodies[1,2], including the recognition of COS cells transfected with ELAM-1 cDNA but not control cDNA (C.W.S., unpublished observations).

binding to venules in inflammed skin involves mechanism(s) distinct from those mediating lymphocyte binding to peripheral lymph node and mucosal HEV (ref. 12); that this binding involves memory T cells in preference to virgin T cells[13]; and that in animal models, lymphocytes in afferent lymph draining normal or inflamed skin are tissue-selective in their homing properties, and show a memory phenotype[14-16].

Whether ELAM-1 is a sole or dominant skin addressin remains to be determined. In man, PNAd can be induced on some venules at sites of chronic inflammation in the skin and elsewhere (L.J.P., unpublished results). Although PNAd was seen in some of the skin lesions studied here, preliminary kinetic studies indicate that this addressin is expressed later than ELAM-1 in the normal course of cutaneous chronic inflammation. Also, general adhesion molecules are probably important in recruiting lymphocytes to inflamed skin[13,17]. For example, the widely expressed adhesion molecule ICAM-1 can be markedly up-regulated on cutaneous venules during inflammation[18], and it and other ligands for the leukocyte integrins may function to cement adhesive interactions initiated by ELAM-1.

We and others[19] have observed high levels of ELAM-1 expression on venules in extracutaneous sites of acute inflammation, implying that, as predicted from studies with cultured endothelial cells[1,2], ELAM-1 is an adhesion molecule for neutrophils that is not tissue-selective. This proposed dual role for ELAM-1 in promoting both general neutrophil and tissue-selective T cell extravasation would suggest that additional factors are important in controlling extravasation specificity. We have proposed that the extravasation of leukocytes requires not only specific adhesion to endothelium, but also secondary leukocyte activation that can trigger leukocyte integrins and subsequent diapedesis[20]. So it is possible that neutrophils and CLA^+ T cells can adhere to $ELAM\text{-}1^+$ venules whether in acute inflammation or in chronically inflamed skin, but that extravasation is dependent also on the local production of neutrophil- or T cell-specific activation/chemoattractant factors.

Note added in proof: Since submission of this manuscript, B. Nickoloff (University of Michigan Medical Center, Ann Arbor) has informed us that his immunohistologic studies of ELAM-1 expression in human inflammatory sites using a different ELAM-1-reactive monoclonal antibody (BB11) revealed strong, diffuse venular ELAM-1 expression in 26/26 varied inflammatory lesions of the skin but only focal expression in 4 of 35 extracutaneous sites of inflammation. □

Received 8 August; accepted 7 December 1990.

1. Bevilacqua, M. P., Pober, J. S., Mendrick, D. L., Cotran, R. S. & Gimbrone, M. A. Jr *Proc. natn. Acad. Sci. U.S.A.* **84**, 9238–9242 (1987).
2. Luscinskas, F. W., Brock, A. F., Arnaout, M. A. & Gimbrone, M. A. Jr *J. Immun.* **142**, 2257–2263 (1989).
3. Bevilacqua, M. P., Stengelin, S., Gimbrone, M. A. Jr & Seed, B. *Science* **243**, 1160–1165 (1989).
4. Picker, L. J., Michie, S. A., Rott, L. S. & Butcher, E. C. *Am. J. Pathol.* **136**, 1053–1068 (1990).
5. Picker, L. J. *et al. J. Immun.* **145**, 3247–3255 (1990).
6. Sanders, M. E. *et al. J. Immun.* **140**, 1401–1407 (1988).
7. Kishimoto, T. K., Jutila, M. A. & Butcher, E. C. *Proc. natn. Acad. Sci. U.S.A.* **87**, 2244–2248 (1990).
8. Cerf-Bensussan, N. *et al. Eur. J. Immun.* **17**, 1279–1285 (1987).
9. Streeter, P. R., Berg, E. L., Rouse, B. T. N., Bargatze, R. F. & Nutcher, E. C. *Nature* **331**, 41–46 (1988).
10. Nakache, M., Berg, E. L., Streeter, P. R. & Butcher, E. C. *Nature* **337**, 179–181 (1988).
11. Streeter, P. R., Rouse, B. T. N. & Butcher, E. C. *J. Cell Biol.* **107**, 1853–1862 (1988).
12. Sakstein, R., Falanga, V., Streilein, J. W. & Chin, Y.-H. *J. invest. Derm.* **91**, 423–428 (1988).
13. Chin, Y.-H., Falanga, V., Taylor, J. R., Cai, J.-P. & Bax, J. *J. invest. Derm.* **94**, 413–417 (1990).
14. Chin, W. & Hay, J. B. *Gastroenterology* **79**, 1231–1242 (1980).
15. Issekutz, T. B., Chin, W. & Hay, J. B. *Cell. Immun.* **54**, 79–86 (1980).
16. Mackay, C. R., Marston, W. L. & Dudler, L. *J. exp. Med.* **171**, 801–817 (1990).
17. Springer, T. A. *Nature* **346**, 425–434 (1990).
18. Munro, J. M., Pober, J. S. & Cotran, R. S. *Am. J. Path.* **135**, 121–133 (1989).
19. Cotran, R. S., Gimbrone, M. A., Jr, Bevilacqua, M. P., Mendrick, D. L. & Pober, J. S. *J. exp. Med.* **164**, 661–666 (1986).
20. Kishimoto, T. K., Jutila, M. A., Berg, E. L. & Butcher, E. C. *Science* **245**, 1238–1241 (1989).
21. Seed, B., and Aruffo, A. *Proc. natn. Acad. Sci. U.S.A.* **84**, 3365–3369 (1987).
22. Wellicome, S. M. *et al. J. Immun.* **144**, 2558–2565 (1990).
23. Terstappen, W. M. M., Hollander, Z., Meiners, H. & Loken, M. R. *J. Leuk. Biol.* **48**, 138–148 (1990).

ACKNOWLEDGEMENTS. We thank H. Stein (Klinikum Steglitz, Free University, Berlin) and D. Haskard (Hammersmith Hospital, London) for providing monoclonal antibodies; B. Seed (Harvard University) for providing an ELAM-1 cDNA clone; L. Rott for assistance with our flow cytometric studies; R. Warnke for help in obtaining human tissues, and E. Berg for comments on the manuscript. This work was supported by the NIH, the tobacco-related disease research program of the University of California and the Veterans Administration. L.J.P is a career Development Awardee of the Veterans Administration. T.K.K is a fellow of the Damon Runyon–Walter Winchell Cancer Foundation. E.C.B is an Established Investigator of the American Heart Association. The contributions of L.J.P. and T.K.K. to this paper should be considered equal.

Activation-independent binding of human memory T cells to adhesion molecule ELAM-1

Yoji Shimizu, Stephen Shaw, Norma Graber*, T. Venkat Gopal*, Kevin J. Horgan, Gijs A. Van Seventer & Walter Newman*

The Experimental Immunology Branch, National Cancer Institute, National Institutes of Health, Bethesda, Maryland 20892, USA
* Departments of Immunology and Molecular Biology, Otsuka America Pharmaceutical Inc., Rockville, Maryland 20850, USA

THE induction of an ensemble of adhesion molecules on endothelial cells by inflammatory cytokines is likely to be crucial to the differential migration of T-lymphocyte subsets into inflammatory sites. Two molecular pathways involving the VLA-4 and LFA-1 integrins are known to mediate T-cell adhesion to activated endothelium[1–4]. Here we show that a third pathway involving the rapidly inducible endothelial cell-surface adhesion molecule ELAM-1 (refs 5, 6) contributes to the binding of resting $CD4^+$ T cells to IL-1-induced human endothelial cells. All three pathways contribute to the greater adhesion to endothelium of memory T cells than naive T cells. There are two unique features of T-cell adhesion to purified ELAM-1: first, ELAM-1 exclusively mediates adhesion of memory T cells; second, memory T-cell binding to ELAM-1 is independent of acute activation events that regulate integrin-mediated adhesion [7,8]. Thus, ELAM-1 may be of primary importance in the initial attachment of memory T cells to inflamed endothelium *in vivo* and to the preferential migration of memory T cells into tissue and inflammatory sites.

Monoclonal antibody blocking studies reveal the involvement of three molecular pathways that mediate adhesion of resting human peripheral $CD4^+$ T cells to IL-1-induced cultured human umbilical-vein endothelial cells (HUVEC). Antibodies specific for both the LFA-1 integrin and the inducible endothelial cell surface protein VCAM-1 weakly but reproducibly inhibit adhesion of resting $CD4^+$ T cells to induced HUVEC (Fig. 1). Inhibition of binding by the combination of LFA-1- and VCAM-1-specific antibodies is greater than that by either antibody alone, as would be expected from earlier studies demonstrating that LFA-1-mediated adhesion to ICAM-1 and other ligands and VLA-4-mediated adhesion to VCAM-1 are both involved in T/HUVEC interaction (refs 1–4, and 9; Y.S. *et al.*, manuscript in preparation). But the combination of LFA-1- and VCAM-1-specific antibodies fails to inhibit T/HUVEC adhesion completely, implying the involvement of additional adhesion molecules. A role for ELAM-1 in T/HUVEC adhesion is suggested by (1) the partial inhibition by monoclonal ELAM-1-specific antibody alone that is at least equal to that seen with either an LFA-1- or a VCAM-1-specific antibody alone; and (2) a marked inhibition of binding by the addition of an ELAM-1-specific antibody (but not a control antibody) in the presence of monoclonal LFA-1- and VCAM-1-specific antibodies (Fig. 1). The interaction of resting $CD4^+$ T cells with induced HUVEC thus involves at least three independent adhesion pathways mediated by LFA-1, VCAM-1 and ELAM-1.

The ability of ELAM-1 to mediate $CD4^+$ T-cell adhesion was confirmed in cell-adhesion assays showing specific T-cell binding to purified ELAM-1 immobilized on plastic. ELAM-1 was affinity-purified from the culture supernatant of Chinese hamster ovary cells transfected with an ELAM-1 complementary DNA encoding a truncated form of the molecule, designated 'ELAM-1-420' (Fig. 2*a*). Studies such as those shown in Fig. 2*b* show that resting $CD4^+$ T cells adhere in a dose-dependent manner to purified ELAM-1 immobilized on plastic. The interaction is specific because an ELAM-1-specific antibody completely

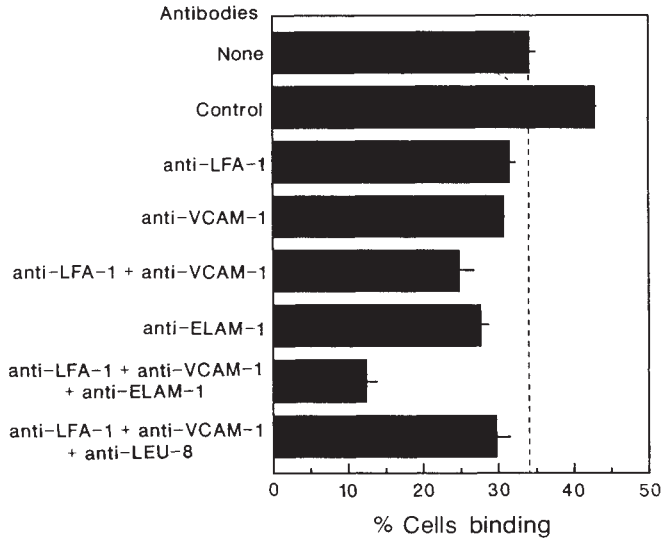

FIG. 1 Multiple molecular pathways mediate adhesion of resting $CD4^+$ T cells to interleukin-1 (IL-1)-induced cultured human umbilical vein endothelial cells (HUVEC). Adhesion of ^{51}Cr-labelled resting $CD4^+$ T cells to HUVEC pre-exposed for 4 h with IL-1β was assessed in the presence of monoclonal antibodies specific for LFA-1, VCAM-1 and ELAM-1.

METHODS. Purified $CD4^+$ T cells were prepared by exhaustive negative selection from peripheral blood mononuclear cells of normal donors using immunomagnetic beads[27]; cells were >98% $CD3^+CD4^+$. The selection cocktail of monoclonal antibodies included the anti-HLA-DR antibody IVA12 to exclude the normal low percentage of circulating activated T cells. HUVEC were prepared from umbilical cords as previously described[5]. Endothelial cells at passage 2 or less were plated onto gelatin-precoated 24-well plates (Costar) and cultured for 48 h or until confluent. HUVEC were exposed to 1 ng ml^{-1} IL-1β in medium (RPMI 1640, 10% FCS) for 4 h at 37 °C before the addition of T cells. HUVEC were then washed once with medium, then 300,000 ^{51}Cr-labelled $CD4^+$ T cells in a final volume of 300 μl were added to each well and the plates incubated for 30 min at 37 °C. Plates were washed twice with medium (RPMI, 10% FCS), the contents of each well were lysed with 300 μl 1% Triton X-100, and γ emissions counted. Wells were inspected before lysis to confirm the integrity of the HUVEC monolayer. Where indicated, binding was assessed in the continuous presence of the following antibodies: the CD45-specific monoclonal antibody NIH45-2 (control), the monoclonal LFA-1 α-chain antibody MHM24 (ref. 28), the monoclonal VCAM-1 antibody 2G7 (ref. 5), the monoclonal ELAM-1 antibody 7A9 (ref. 5) and the monoclonal Leu-8 antibody (L. Lanier). All antibodies were used as purified IgG at a saturating concentration of 10 μg ml^{-1}; previous studies have shown that this concentration maximally inhibits the relevant adhesive function[5,29]. The control antibody NIH45-2 was used at 20 μg ml^{-1}. Data are expressed as the mean percentage of cells binding from duplicate wells. Binding of resting $CD4^+$ T cells to uninduced HUVEC was 15%. No differences in adhesion were observed between freshly isolated $CD4^+$ T cells and purified $CD4^+$ T cells that had been cryopreserved in liquid nitrogen and thawed immediately before use.

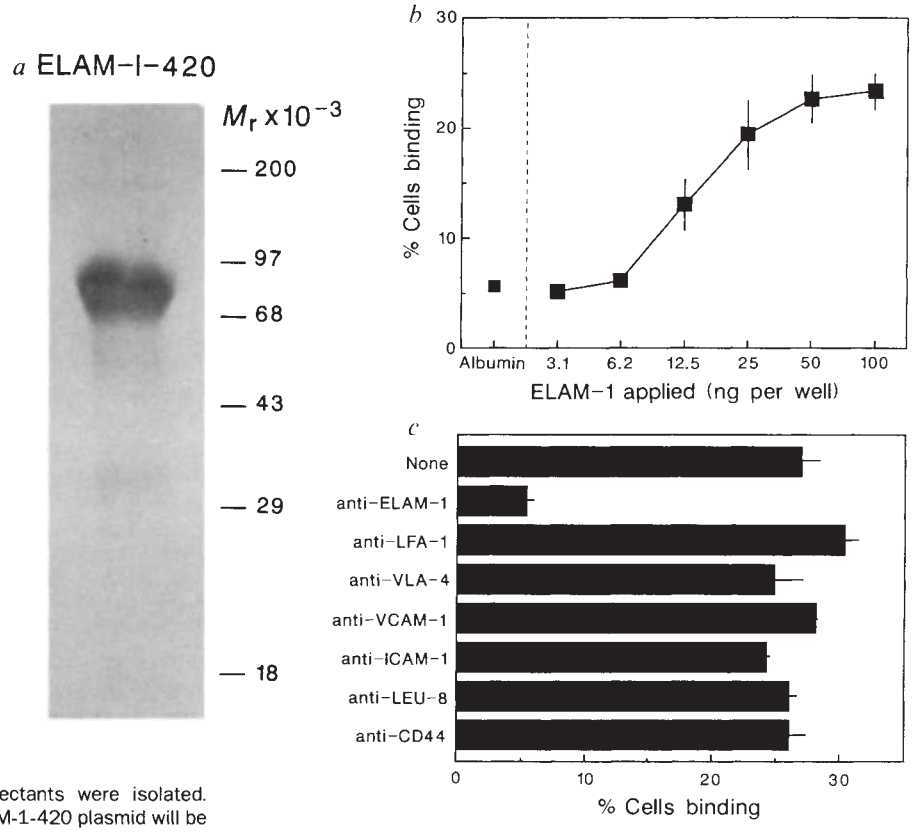

FIG. 2 Resting $CD4^+$ T cells adhere to purified ELAM-1. *a*, Reducing SDS-PAGE analysis of purified ELAM-1-420. Fifteen μg of material was loaded onto a reducing 10% SDS gel. Relative molecular mass (M_r) standards are indicated. *b*, Binding of resting $CD4^+$ T cells to purified ELAM-1 immobilized on plastic. Binding of resting $CD4^+$ T cells to wells coated with BSA ('Albumin') is indicated to the left of the dotted line. *c*, Determination of the specificity of $CD4^+$ T-cell adhesion to purified ELAM-1 (50 ng per well) with antibody blocking.

METHODS. $CD4^+$ T cells were purified as described in the legend to Fig. 1. *a*, A truncated version of ELAM-1 containing 420 amino acids (ELAM-1-420) of the N-terminal end of the mature form, along with the signal sequence, was constructed by the polymerase chain reaction (PCR) using appropriate oligonucleotide primers. ELAM-1-420 contains the lectin and epidermal growth factor domains and a portion of the complement regulatory domain. The PCR-amplified product was cloned into an expression vector containing the Rous sarcoma virus long terminal repeat promoter driving ELAM-1-420, and simian virus SV40 t splice and poly (A) addition sequences from pMSG (Pharmacia, Piscataway, New Jersey) at the 3′ end of the ELAM-1-420 coding sequence. The expression plasmid also contained the human wild-type dihydrofolate reductase (DHFR) transcription unit with the SV40 early promoter and the SV40 mRNA processing sequences at the 3′ end of the DHFR gene. This plasmid was transfected into the $DHFR^-$ CHO cell line, and methotrexate-resistant (600 nM) transfectants were isolated. Details of the construction and isolation of the ELAM-1-420 plasmid will be published elsewhere. The ELAM-1-420 molecule was purified from culture supernatants of transfected cells by sequential affinity chromatography on conconavilin A-Sepharose and ELAM-1 antibody 7A9-coupled Affigel. As a final purification step, the material was eluted as a homogeneous peak from C-18 reversed phase chromatography. Protein concentration was established from amino-acid analysis. Amino-acid sequencing showed tryptophan at the N terminus in accordance with the published sequence[6]; purity was estimated as at least 90%. *b*, and *c*, Adhesion assays were performed essentially as described[8,30]. Purified ELAM-1 was applied to 96-well enzyme-linked immunosorbent assay plates (Nunc) at the indicated concentrations in PBS at 4 °C overnight; plastic was subsequently blocked with PBS, 2.5% BSA for 2–3 h at 37 °C to prevent nonspecific attachment. Plates were washed three times with PBS before the addition of 50,000 ^{51}Cr-labelled $CD4^+$ T cells to each well in a final volume of 100 μl PBS, 0.5% human serum albumin. After 1 h settling at 4 °C, plates were rapidly warmed to 37 °C for 15 min, and non-adherent cells washed off. Well contents were lysed with 1% Triton X-100, and γ emissions of well contents determined. *c*, $CD4^+$ T cell adhesion to ELAM-1 (applied at 50 ng per well) was assessed in the continuous presence of the following monoclonal antibodies: the anti-ELAM-1 antibody 7A9, the anti-LFA-1 α chain antibody MHM24, the anti-VLA-4 antibody L25 (refs 31, 32; E. Evans), the anti-VCAM-1 antibody 2G7, the anti-ICAM-1 antibody 84H10 (ref. 33), the anti-Leu-8 antibody, and the anti-CD44 antibody NIH44-1 (ref. 34). All antibodies were added as purified IgG at a saturating concentration of 10 μg ml^{-1}; at this concentration they inhibit the relevant cell adhesion interactions maximally[5,8,29,34]. Binding of $CD4^+$ T cells to a control protein (type III collagen) in *c*, was 5%, and has not been subtracted from the data shown. Data are expressed as mean percentage of cells binding from triplicate wells.

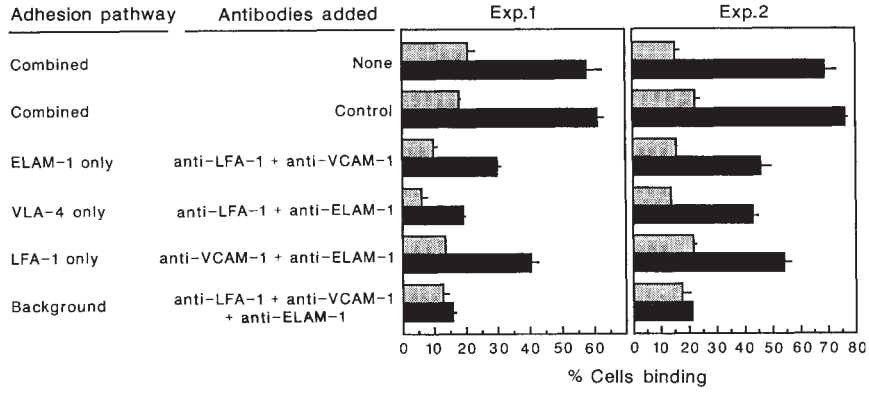

FIG. 3 Differential binding of purified naive and memory $CD4^+$ T cells to IL-1-induced HUVEC. Binding of resting $CD4^+CD45RA^+$ naive T cells (shaded bars) and resting $CD4^+CD45RA^-$ memory T cells (solid bars) from a representative donor was assessed in the presence of the indicated combinations of antibodies in order to restrict the binding to a single adhesion pathway (as indicated). METHODS. Purified $CD4^+CD45RA^+$ ('naive') and $CD4^+CD45RA^-$ ('memory') T cells from the same donor were prepared by exhaustive negative immunoselection[27]. Purity of naive and memory subsets was greater than 95% by flow cytometric analysis. Binding to IL-1-induced HUVEC was assessed as described in the legend to Fig. 1 in the presence of the antibodies indicated at the concentrations used for Fig. 1. Results from two independent experiments using cells isolated from different donors are presented.

inhibits binding, whereas other monoclonal antibodies (including antibodies against LFA-1, ICAM-1 and VCAM-1) fail to inhibit this interaction (Fig. 2*c*).

Various adhesion molecules, including VLA-4 and LFA-1, are differentially expressed on two distinct reciprocal subsets of $CD4^+$ T cells functionally defined as naive and memory T cells[8,10-13]. The higher expression of adhesion molecules on memory T cells is associated with greater memory-cell adhesion to HUVEC[14-16] and preferential memory-cell migration into tissue and inflammatory sites[14,17-19]. Figure 3 shows that purified resting memory $CD4^+$ T cells bind much more strongly to induced HUVEC than do naive cells. T-cell adhesion to endothelium can be restricted to a single adhesion pathway by adding monoclonal antibodies that block each of the other two pathways; such studies show that each pathway in isolation mediates stronger adhesion of memory T cells to HUVEC (Fig. 3). The greater binding of memory T cells to HUVEC through VLA-4 and LFA-1 is consistent with previous studies using purified ligands for VLA-4 (fibronectin) and LFA-1 (ICAM-1)[8,13]. The data in Fig. 3 suggest that memory T cells also use the ELAM-1 pathway more than naive cells.

The greater binding of memory $CD4^+$ T cells to ELAM-1 is demonstrated by studies with purified ELAM-1 (Fig. 4). There are two important distinctions between memory T-cell binding to ELAM-1 and to integrin ligands such as fibronectin (Fig. 4). First, although both naive and memory T cells are able to adhere to fibronectin, T-cell binding to ELAM-1 is completely memory-cell specific. Second, the strength of many adhesion pathways is dramatically regulated by acute activation of the T cell[7,8,20]; integrin-mediated adhesion of both naive and memory T cells to ligands such as fibronectin is rapidly and dramatically increased by 12-*O*-tetradecanoylphorbol-13-acetate (TPA) activation (ref. 8; and Fig. 4). In contrast, memory T cells adhere well to purified ELAM-1 without activation, and binding is not augmented by TPA activation. Thus ELAM-1 mediates activation-independent adhesion of memory $CD4^+$ T cells.

Although ELAM-1 mediates the adhesion of granulocytes[6,21] and monocytes (P. DiCorleto, C. A. de la Motte, T.V.G. and W.N., manuscript submitted) to induced HUVEC, its importance in T-cell/HUVEC adhesion has not been fully appreciated. Our previous studies suggested the involvement of ELAM-1 in T/HUVEC adhesion[5], but the multiple pathways mediating T/HUVEC interaction (Fig. 1) made it difficult to analyse ELAM-1-dependent T-cell binding to endothelium. Using purified ELAM-1, we show that T cells bind specifically to ELAM-1, and that T-cell adhesion to ELAM-1 is distinct from adhesion mediated by integrins such as VLA-4 and LFA-1. The specific binding of memory but not naive T cells to ELAM-1 is striking; there is greater binding of memory T cells to integrin ligands such as fibronectin and ICAM-1[8,13], but naive T cells are still able to bind after acute activation (refs 8, 13; and Fig. 4). The activation-independence of T-cell adhesion to ELAM-1 (Fig. 4) also distinguishes this adhesion pathway from others in which activation is important in regulating either augmentation[7,8,13,20] or abrogation[22,23] of adhesion.

Although the nature of the ELAM-1 ligand on T cells is undefined, the presence of a lectin-binding domain on ELAM-1 (ref. 6) and other members of the 'LEC-CAM' family of cell adhesion molecules[24,25] indicates that it could be a carbohydrate. Furthermore, as memory but not naive T cells bind to ELAM-1 (Fig. 4), the T-cell ELAM-1 ligand may be preferentially, if not exclusively, expressed on memory T cells.

The induction of adhesion molecules such as ELAM-1 and VCAM-1 on HUVEC by inflammatory cytokines provides a

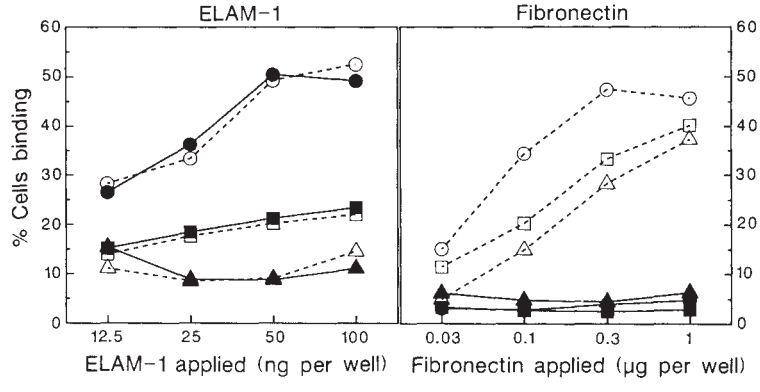

FIG. 4 Purified memory $CD4^+$ T cells but not naive $CD4^+$ T cells adhere to purified ELAM-1 in an activation-independent fashion. Binding of $CD4^+$ T cells (squares), and the $CD4^+CD45RA^+$ naive (triangles) and $CD4^+CD45RA^-$ memory (circles) T-cell subsets from a representative donor to the indicated concentrations of purified ELAM-1 (left panel) or fibronectin (right panel) was assessed. Binding of both resting T cells (solid figures) and T cells activated for 15 min at 37 °C with 10 ng ml^{-1} TPA (open figures) was measured.
METHODS. Purified $CD4^+$, $CD4^+CD45RA^+$ naive and $CD4^+CD45RA^-$ memory T cells were prepared from one donor as previously described[27]. Purified ELAM-1 was prepared and used in cell-adhesion assays as described in Fig. 2. ELAM-1 and fibronectin (New York Blood Center) were applied to microtitre wells at the indicated concentrations in PBS at 4 °C overnight. For the TPA activation conditions, T cells were added to coated microtitre wells containing a final concentration of 10 ng ml^{-1} TPA as described[8]. Binding of $CD4^+$ T cells to the control protein type III collagen was $<6\%$, and has not been subtracted from the data shown. Data are expressed as mean percentages of cells binding from triplicate wells.

mechanism for the selective attachment of lymphocytes to endothelium and their subsequent migration into the site of tissue injury[21]. As there are few activated T cells in the circulation, adhesion pathways must exist that allow inflamed endothelium to 'capture' circulating resting T cells. Our results show such activation-independent binding of resting T cells to purified ELAM-1 and indicate that the ELAM-1 pathway may be critical to the initial attachment of T cells to inflamed endothelium *in vivo*. In addition, the binding of memory but not naive T cells to ELAM-1 suggests that the ELAM-1 pathway not only plays a part in the preferential migration of memory cells into inflammatory sites[14,17-19] but also may contribute to the differential recirculation patterns of naive and memory T cells[26]. In conclusion, we have identified ELAM-1 as a molecule involved in the activation-independent binding of resting memory T cells to endothelium. Thus, T-cell binding to endothelium is mediated by multiple adhesion pathways with distinct modes of regulation that permit the differential attachment and subsequent migration of specific lymphocyte subsets into tissue. □

Received 1 October; accepted 27 November 1990.

1. Dustin, M. L. & Springer, T. A. *J. Cell Biol.* **107,** 321-331 (1988).
2. Elices, M. J. *et al. Cell* **60,** 577-584 (1990).
3. Rice, G. E., Munro, J. M. & Bevilacqua, M. P. *J. exp. Med.* **171,** 1369-1374 (1990).
4. Schwartz, B. R., Wayner, E. A., Carlos, T. M., Ochs, H. D. & Harlan, J. M. *J. clin. Invest.* **85,** 2019-2022 (1990).
5. Graber, N. *et al. J. Immunol.* **145,** 819-830 (1990).
6. Bevilacqua, M. P., Stengelin, S., Gimbrone, M. A. Jr & Seed, B. *Science* **243,** 1160-1164 (1989).
7. Dustin, M. L. & Springer, T. A. *Nature* **341,** 619-624 (1989).
8. Shimizu, Y., van Seventer, G. A., Horgan, K. J. & Shaw, S. *Nature* **345,** 250-253 (1990).
9. Oppenheimer-Marks, N., Davis, L. S. & Lipsky, P. E. *J. Immun.* **145,** 140-148 (1990).
10. Sanders, M. E., *et al. J. Immun.* **140,** 1401-1407 (1988).
11. Tedder, T. F., Cooper, M. D. & Clement, L. T. *J. Immun.* **134,** 2989-2994 (1985).
12. Sanders, M. E., Makgoba, M. W. & Shaw, S. *Immun. Today* **9,** 195-199 (1988).
13. Shimizu, Y., van Seventer, G. A., Horgan, K. J. & Shaw, S. *Immunol. Rev.* **114,** 109-143 (1990).
14. Pitzalis, C., Kingsley, G., Haskard, D. & Panayi, G. *Eur. J. Immun.* **18,** 1397-1404 (1988).
15. Cavender, D. E., Haskard, D. O., Maliakkai, D. & Ziff, M. *Cell. Immun.* **117,** 111-126 (1988).
16. Damle, N. K. & Doyle, L. V. *J. Immun.* **144,** 1233-1240 (1990).
17. James, S. P., Fiocchi, C., Graeff, A. S. & Strober, W. *Gastroenterology* **91,** 1483-1489 (1986).
18. Janossy, G., Bofill, M., Rowe, D., Muir, J. & Beverley, P. C. *Immunology* **66,** 517-525 (1989).
19. Kingsley, G., Pitzalis, C., Kyriazis, N. & Panayi, G. S. *Scand. J. Immun.* **28,** 225-232 (1988).
20. Springer, T. A. *Nature* **346,** 425-434 (1990).
21. Osborn, L. *Cell* **62,** 3-6 (1990).
22. Jung, T. M. & Dailey, M. O. *J. Immun.* **144,** 3130-3136 (1990).
23. Kishimoto, T. K., Jutila, M. A., Berg, E. L. & Butcher, E. C. *Science* **245,** 1238-1241 (1989).
24. Siegelman, M. H., van de Rojn, M. & Weissman, I. L. *Science* **243,** 1165-1172 (1989).
25. Johnston, G. I., Cook, R. G. & McEver, R. P. *Cell* **56,** 1033-1044 (1989).
26. Mackay, C. R., Marston, W. L. & Dudler, L. *J. exp. Med.* **171,** 801-817 (1990).
27. Horgan, K. J., van Seventer, G. A., Shimizu, Y. & Shaw, S. *Eur. J. Immun.* **20,** 1111-1118 (1990).
28. Hildreth, J. E., Gotch, F. M., Hildreth, P. D. & McMichael, A. J. *Eur. J. Immun.* **13,** 202-208 (1983).
29. van Seventer, G. A., Shimizu, Y., Horgan, K. J. & Shaw, S. *J. Immun.* **144,** 4579-4586 (1990).
30. Shimizu, Y., van Seventer, G. A., Horgan, K. J. & Shaw, S. *J. Immun.* **145,** 59-67 (1990).
31. Clayberger, C. *et al. J. Immun.* **138,** 1510-1514 (1987).
32. Takada, Y., Elices, M. J., Crouse, C. & Hemler, M. E. *EMBO J.* **8,** 1361-1368 (1989).
33. Makgoba, M. W. *et al. Nature* **331,** 86-88 (1988).
34. Shimizu, Y., van Seventer, G. A., Siraganian, R., Wahl, L. & Shaw, S. *J. Immun.* **143,** 2457-2463 (1989).

ACKNOWLEDGEMENTS. We thank Z. Randhawa for amino-acid analysis and sequencing of ELAM-1-420, L. D. Beall for assistance with purification of ELAM-1-420, the NIH Blood Bank donors, D. Roberts and R. Hodes for review of the manuscript, and E. Evans and L. Lanier for monoclonal antibodies. Y.S. is supported by a Damon Runyon-Walter Winchell Cancer Research Fund Postdoctoral Fellowship. G.A.v.S. and K.J.H. are Visiting Associates supported by the Fogarty Exchange Program.

Protein synthesis required to anchor a mutant p53 protein which is temperature-sensitive for nuclear transport

Julian V. Gannon & David P. Lane*

Imperial Cancer Research Fund, Clare Hall Laboratories, South Mimms, Potters Bar, Herts EN6 3LD, UK

THE p53 protein is rendered temperature-sensitive by a point mutation[1]. Rat cells transformed by this mutant p53 and an activated *ras* oncogene grow well at 37 °C but cease DNA synthesis and cell division when shifted to 32 °C (ref. 1). Immunostaining demonstrates that the mutant p53 protein is in the nucleus of the arrested cells at 32 °C but in the cytoplasm of the growing cells at 37 °C. This is the first example of a protein which is temperature-sensitive for nuclear transport. The translocation from cytoplasm to nucleus and vice versa occurs 6 h after temperature shift and is coincident with the inhibition of DNA synthesis; transport from cytoplasm to nucleus does not require protein synthesis. Remarkably, inhibition of protein synthesis at 37 °C also results in the rapid appearance of mutant p53 in the cell nucleus. These results suggest the presence of a short-lived protein responsible for holding p53 in the cytoplasm at 37 °C but not at 32 °C. Analysis of a non-temperature-sensitive mutant p53 protein shows that its cytoplasmic location is sensitive to protein synthesis inhibitors but not to temperature.

Clone 6 cells, a line of rat embryo fibroblasts transformed by a temperature-sensitive mutant p53 gene and an activated *ras* gene[1] were stained with four different anti-p53 monoclonal antibodies[2,3] at 37 °C and 32 °C. All four antibodies used independently showed the same result. At 37 °C the p53 protein was predominantly in the cytoplasm, whereas at 32 °C it was located in the cell nucleus (Fig. 1*a*, *b*). p53 first became apparent in the cell nucleus 6 h after shift down to 32 °C and translocation was complete by 12 h. The effect was reversible, with cytoplasmic staining for p53 reappearing 6 to 12 h after shift up to 37 °C. There was a striking correlation between p53 location, cell division and DNA synthesis. Autoradiography of [^{3}H]-thymidine-labelled cultures demonstrates that the three phenomena occur with similar kinetics as DNA synthesis also ceases within 12 h of shift down and returns 12 h after shift up (Table 1). Analysis of cell division by fluorescence-activated cell sorting showed that 24 h after temperature shift the fraction of cells in S phase has fallen from 29% at 37 °C to 7.5% at 32 °C (a fall of 76%) and there was an increase in cells with both G2/M and G1 DNA content. Because there is no detectable DNA synthesis at this time as determined by [^{3}H]thymidine incorporation, this suggests that the temperature shift leads to arrest throughout the cell cycle in accordance with the results of Michalovitz *et al.*[1].

The effect is specific to the temperature-sensitive mutant p53. Rat embryo fibroblasts (RKT101-Y cells) transformed by another mutant p53 grew at both temperatures (Table 1) and showed cytoplasmic staining with anti-p53 antibodies at both temperatures, whereas another independent cell line (p53A1; ref. 4) transformed by the temperature-sensitive mutant p53 showed the same results as the clone 6 cells. The effect is specific to p53 protein as other nuclear antigens, for example proliferating cell nuclear antigen (PCNA)[5] and eukaryotic single-stranded binding protein (SSB)[6], remain in the nucleus of clone 6 cells at both temperatures (not shown).

To determine whether the translocation requires active protein synthesis, we treated the cells with a range of concentrations of the protein synthesis inhibitors cycloheximide or emetine at 37 °C at the time of temperature shift. Although [^{35}S]methionine labelling experiments indicated that the drugs prevented at least 99% of protein synthesis, p53 was still found to have moved to the nucleus after shift down. Thus protein synthesis is not required for the translocation. Unexpectedly, mutant p53 in control cells treated with cycloheximide or emetine but maintained at 37 °C also moved to the nucleus within 6 h of

* Present address: Cancer Research Campaign Laboratories, Department of Biochemistry, Dundee University, Dundee DD1 4HN, UK.

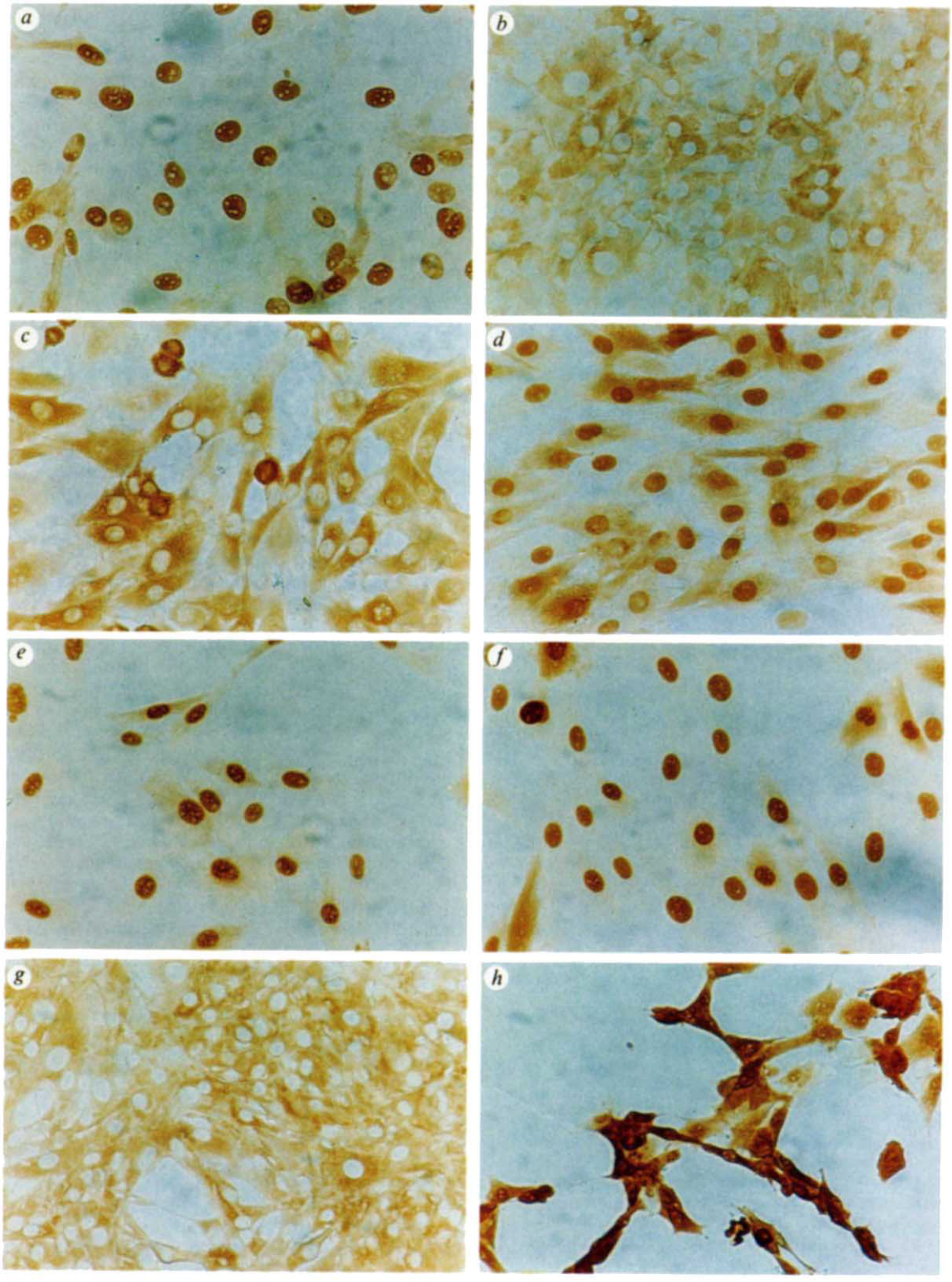

FIG. 1 Immunohistochemistry of mutant p53 translocation in response to temperature and protein synthesis inhibitors. Clone 6 cells grown at 32 °C (*a*) and shifted to 37 °C for 24 h (*b*), then stained. Clone 6 cells grown at 37 °C in the presence of: *c*, 0 $\mu g\ ml^{-1}$ (mock treated); *d*, 0.1 $\mu g\ ml^{-1}$; *e*, 1 $\mu g\ ml^{-1}$; *f*, 10 $\mu g\ ml^{-1}$ cycloheximide. RKT101-Y cells grown at 37 °C for 24 h in the absence (*g*) or presence (*h*) of 10 $\mu g\ ml^{-1}$ cycloheximide.

METHODS. Cells were fixed in 50% acetone, 50% methanol for 2 min. p53 was detected with PAb421, PAb246, PAb240 and PAb248 (ref. 2) monoclonal anti-p53 antibodies used as hybridoma supernatants and HRP-conjugated rabbit anti-mouse immunoglobulin and the diaminobenzidine hydrogen peroxide substrate[26]. All illustrations show results with PAb421.

adding the drug. The effect of the drugs is dose-dependent (Fig. 1*c*-*f*) and reversible. Cytoplasmic p53 is first seen 6 h after removal of the inhibitor. These results argue strongly for the existence of a labile protein that retains p53 in the cytoplasm at 37 °C. The correlation between the effect of temperature and inhibition of protein synthesis on the location of p53 suggests that the cytoplasmic anchor can distinguish between wild-type and mutant p53. The protein must be continually synthesized to maintain p53 in the cytoplasm.

RKT101-Y cells contain a cytoplasmic mutant p53. Although p53 protein is virtually undetectable in the nuclei of these cells at all temperatures tested, a significant amount enters the nuclei of cells treated with protein synthesis inhibitors (Fig. 1*g*, *h*).

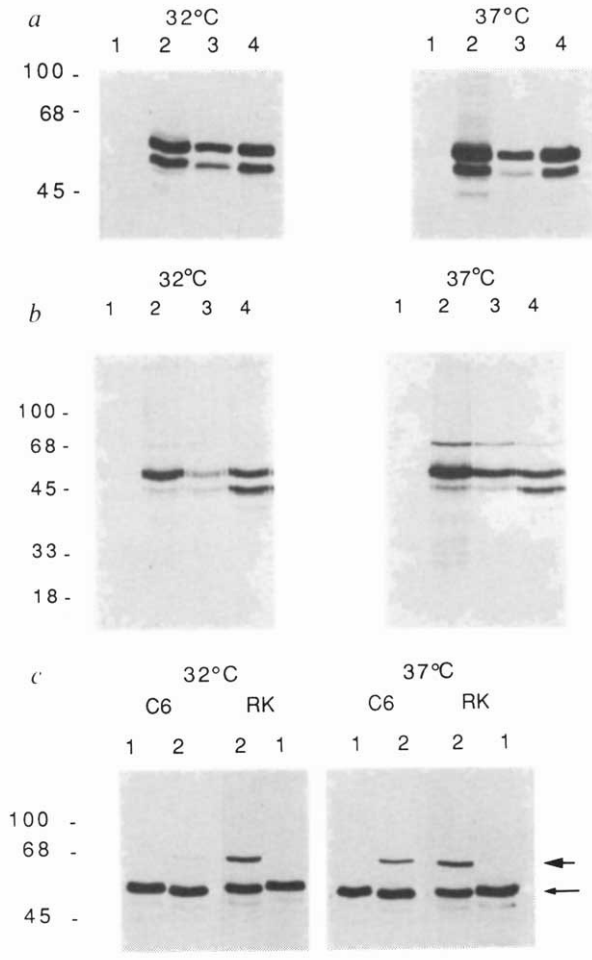

FIG. 2 The effect of temperature on p53 levels, epitope display and HSP70 binding. *a*, Steady-state levels of different immunological subtypes of p53 measured by immunoprecipitation and western blotting of extracts of clone 6 cells grown at 32 and 37 °C. Lane 1, control immunoprecipitation with the anti-T antibody PAb419; lane 2, immunoprecipitation with the anti-p53 antibody PAb421; lane 3, PAb246; lane 4, PAb240. Immunoprecipitated p53 was detected with a polyclonal rabbit anti-p53 antibody[3]. *b*, Synthesis of p53 and the p53-HSC70 complex using a 3-h pulse of [^{35}S]methionine. Lane 1, control immunoprecipitation with the anti-T antibody PAb419; lane 2, immunoprecipitation with the anti-p53 antibody PAb421; lane 3, PAb240; lane 4, PAb246 (ref. 3). *c*, Steady-state level of the p53-HSC70 complex in clone 6 (C6) and RKT101-Y (RK) cells. p53 was measured by immunoprecipitation with anti-p53 antibodies and western blotting of the immunoprecipitated proteins with a murine polyclonal antibody to HSC70. Lane 1, immunoprecipitated with control antibody PAb419; lane 2, immunoprecipitated with anti-p53 antibody PAb421. The heavy arrow marks the HSC70 band; the light arrow marks the immunoglobulin heavy chain present in the immunoprecipitates and reactive with the rabbit anti-mouse immunoglobulin conjugate used in this detection system.

The effect is reversible and much less complete than that seen in clone 6 cells, suggesting that the cytoplasmic anchor mechanism can distinguish between different p53 mutants with different conformations[2]. Further support for the specificity of the effect of cycloheximide on nuclear transport comes from observations on the subcellular location of a cytoplasmic mutant of SV40 large T antigen[7]. This T mutant was able to retain p53 in the cytoplasm even after treatment with protein synthesis inhibitors.

The entry of proteins into the cell nucleus is controlled by at least two mechanisms. The first consists of an active transport process whereby proteins whose relative molecular mass exceeds about 50,000 are specifically transported through the nuclear pores. The process is ATP dependent and requires the recognition of a defined basic amino-acid motif on the target protein[8]. Such a motif has been found in p53, but neither of the mutations in p53 analysed here involves this sequence[9,27]. A second level of control of subcellular location is provided by cytoplasmic anchor proteins[10-15]. Our results argue that p53 is regulated by both mechanisms. In transfected cells p53 may function as a dominant oncoprotein by virtue of its cytoplasmic location, perhaps by sequestering endogenous normal p53 in the cytoplasm.

Mutation of p53 is associated with increased half-life, binding of the heat-shock proteins HSP/HSC70 and the appearance of the PAb240 epitope on a variable proportion of p53 molecules[3]. An extensive immunochemical analysis of the p53 protein at the two temperatures and in the presence and absence of protein synthesis inhibitors was conducted. It showed that none of these three properties of the mutant state were needed for nuclear translation to occur, implying that a novel mechanism is involved. The steady-state level of total p53 and of the PAb240 and PAb246 forms measured by immunoprecipitation, quantitative two-site ELISA assay[3] and western blotting of cell extracts was not greatly affected by temperature shift (Fig. 2*a*). A significant reduction in the level of p53 immunoprecipitated by PAb240 at 32 °C compared to 37 °C is seen when newly synthesized p53 is examined (see Fig. 2*b*, lane 3), though such a clear-cut effect of temperature is not seen with the PAb246 form of p53. This must mean that some of the PAb240-negative p53 molecules mature into a PAb240-positive form. This result in clone 6 cells contrasts with the results in clone 2 cells described by Michalovitz[1], but variation in the amount of p53 in the PAb246 conformation in different lines of REF cells transformed by the *ts* mutant of p53 has been noted before[4]. Significant loss of bound HSC70 (although the cellular overall level of HSC70 did not change) was seen on shift down from 37 °C to 32 °C both when looking at steady-state levels (Fig. 2*c*) and at newly synthesized p53 (Fig. 2*b*). This latter observation was also noted by Michalovitz[1]. But this loss of HSC70 binding is not a prerequisite for nuclear translocation as p53-HSC70 complexes are readily detected in cells treated with cycloheximide where p53 is clearly

TABLE 1 Inhibition and recovery of cellular DNA synthesis in clone 6 cells compared with RKT101-Y on temperature shift

Time after shift (h)	% Labelled nuclei: Clone 6 cells 32 °C > 37 °C	Clone 6 cells 37 °C > 32 °C	RKT101-Y cells 32 °C > 37 °C	RKT101-Y cells 37 °C > 32 °C
0	0	25	13	25
6	0	23	23	23
12	10	4	34	23
18	22	0	40	32
24	26	0	42	35
48	25	0	40	23

DNA synthesis was measured by autoradiography. The cells were labelled by a pulse with [^{3}H]thymidine for 3 h then chased for the times indicated. Over 100 nuclei were counted and the fraction of labelled nuclei is given as a % value.

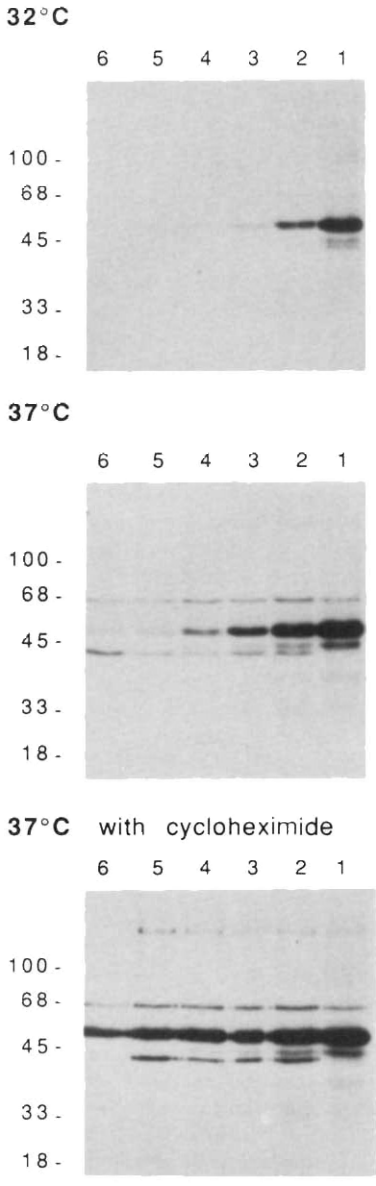

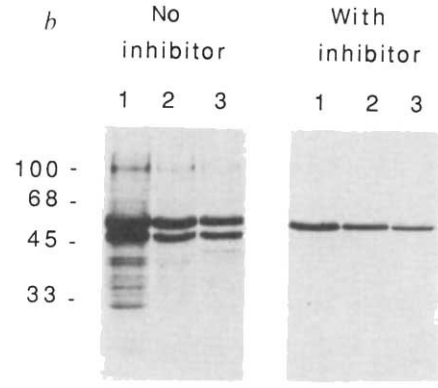

FIG. 3 Effect of protein synthesis inhibitors on the half-life of p53 and its degradative fragments. *a*, Measurement of p53 half-life by pulse-chase at 32 °C, 37 °C and at 37 °C in the presence of 10 μg ml^{-1} cycloheximide. Clone 6 cells were labelled for 3 h with [^{35}S]methionine, the label removed and then chased with excess unlabelled methionine for: lane 1, 0 h; lane 2, 3 h; lane 3, 9 h; lane 4, 15 h; lane 5, 24 h; lane 6, 36 h; All immunoprecipitations shown were with PAb421. *b*, Effect of cycloheximide on the steady-state level of p53 and its degradative fragments analysed by immunoprecipitation and western blotting. Clone 6 cells were grown in the presence and absence of 10 μg ml^{-1} cycloheximide for 24 h. Extracts were immunoprecipitated with: lane 1, PAb421; lane 2, PAb240; lane 3, PAb246. p53 immunoprecipitates were separated on a 10% SDS-polyacrylamide minigel and western blotted with the polyclonal rabbit anti-p53 serum.

in the nucleus (Figs 1 and 3*a*). This suggests that HSC70 is not directly or solely responsible for anchoring p53 in the cytoplasm.

The mutant p53 has a shorter half-life as measured by pulse chase, immunoprecipitation and laser scanning densitometry at 32 °C ($t_{1/2}$ = 3 h) than at 37 °C ($t_{1/2}$ = 8 h), consistent with acquisition of wild-type p53 properties at the lower temperature (Fig. 3*a*); however, the rapid degradation of p53 at 32 °C is not absolutely required for transport as treatment with cycloheximide or emetine increases the half-life dramatically ($t_{1/2}$ > 24 h) (Fig. 3*a*), despite transport of p53 to the nucleus (Fig. 1). The stabilization we have observed principally affects the full-length protein, as smaller fragments are chased away during the cycloheximide block (Fig. 3*a*, *b*) (stabilization of p53 by cycloheximide was noted some years ago[16]). Thus two labile proteins control p53 protein expression. One is part of a short half-life degradative pathway and the other is part of a short half-life cytoplasmic retention pathway. As relatively rapid turnover of p53 occurs at both 37 °C (cytoplasm) and at 32 °C (nucleus), the degradation of p53 occurs in both locations and these two control pathways are probably discrete. Their specificity for p53 and their ability to detect differences between the temperature-sensitive mutant at 32 °C and 37 °C argues strongly that they function in normal cells to control p53 function.

Unravelling the systems that control the p53 protein is now a primary goal in the search for new cancer chemotherapeutics as the majority of malignant human tumours accumulate high levels of the p53 protein and contain mutations in the p53 gene[17-25].

Note added in proof: While this paper was in press, D. Ginsberg *et al.*[28] also reported the change in cellular location of the temperature-sensitive mutant p53 on temperature shift, and G. Shauslky *et al.*[29] reported that p53 moves from the cytoplasm to the nucleus of 3T3 cells on serum stimulation. □

Received 29 October 1990; accepted 10 January 1991.

1. Michalovitz, D., Halvey, O. & Oren, M. *Cell* **62,** 671-680 (1990).
2. Yewdell, J. W., Gannon, J. V. & Lane, D. P. *J. Virol.* **59,** 444-452 (1986).
3. Gannon, J. V., Greaves, R., Iggo, R. & Lane, D.P. *EMBO J.* **9,** 1595-1602 (1990).
4. Finlay, C. A. *et al. Molec. cell Biol.* **8,** 531-539 (1988).
5. Waseem, N. H. & Lane, D. P. *J. Cell Sci.* **96,** 121-129 (1990).
6. Kenny, M. K., Schlegel, U., Furneaux, H. & Hurwitz, J. *J. biol. Chem.* **265,** 7693-7700 (1990).
7. Kalderon, D., Richardson, W. D., Markham, A. F. & Smith, A. E. *Nature* **311,** 33-38 (1984).
8. Dingwall, C. & Lasky, R. A. *A. Rev. Cell. Biol.* **2,** 367-390 (1986).
9. Dang, C. V. & Lee, W. M. F. *J. biol. Chem.* **264,** 18,019-18,023 (1989).
10. Nasmyth, K., Adolf, G., Lydall, D. & Seddon, A. *Cell* **62,** 631-647 (1990).
11. Steward, R. *Cell* **59,** 1179-1188 (1989).
12. Rushlow, C. A., Han, K., Manley, J. & Levine, M. *Cell* **59,** 1165-1177 (1989).
13. Roth, S., Stein, D. & Nusslein-Volhard, C. *Cell* **59,** 1189-1202 (1989).
14. Lenardo, M. J. & Baltimore, D. *Cell* **58,** 227-229 (1989).

15. Van Etten, R. A., Jackson, P. & Baltimore, D. *Cell* **58**, 669-678 (1989).
16. Oren, M., Maltzman, W. & Levine, A. J. *Molec. cell Biol.* **1**, 101-110 (1981).
17. Crawford, L. V., Pim, D. C. & Lamb, P. *Molec. biol. Med.* **2**, 261-272 (1984).
18. Cattoretti, G., Rilke, F., Andreola, S., D'Amato, L. & Delia, D. *Int. J. Cancer* **41**, 178-183 (1988).
19. Van Den Berg, F. M. *et al. J. Path.* **157**, 193-199 (1989).
20. Takahashi, T. *et al. Science* **246**, 491-494 (1989).
21. Baker, J. S. *et al. Science* **244**, 217-221 (1989).
22. Nigro, J. M. *et al. Nature* **342**, 705-708 (1989).
23. Bartek, J., Iggo, R., Gannon, J. & Lane, D. P. *Oncogene* **5**, 893-899 (1990).
24. Iggo, R., Gatter, K., Bartek, J., Lane, D. & Harris, A. L. *Lancet*, 675-679 (1990).
25. Rodrigues, N. R. *et al. Proc. natn. Acad. Sci. U.S.A.* **87**, 7555-7559 (1990).
26. Harlow, E. & Lane, D. *Antibodies: A Laboratory Manual* (Cold Spring Harbor Laboratory, New York, 1988).
27. Shaulsky, G., Goldfinger, N., Ben-Ze'ev, A. & Rotter, V. *Molec. cell Biol.* **10**, 6565-6577 (1990).
28. Ginsberg, D., Michael-Michalovitz, D., Ginsberg, D. & Oren, M. *Molec. cell. Biol.* **11**, 582-585 (1991).
29. Shaulsky, G., Ben-Ze'ev, A. & Rotter, V. *Oncogene* **5**, 1707-1711 (1990).

ACKNOWLEDGEMENTS. We thank M. Oren for the clone 6 cells, A. Levine for the RKT101-Y and p53 A-1 cells, R. Campeljohn for the FACS analysis and P. Rigby for the cell line transformed by the cytoplasmic mutant SV40 large T antigen.

Assembly of yeast Sec proteins involved in translocation into the endoplasmic reticulum into a membrane-bound multisubunit complex

Raymond J. Deshaies*, Sylvia L. Sanders, David A. Feldheim & Randy Schekman

Division of Biochemistry and Molecular Biology, University of California, Berkeley, 401 Barker Hall, Berkeley, California 94720, USA

SECRETORY-protein translocation into the endoplasmic reticulum (ER) is thought to be catalysed by integral membrane proteins. Genetic selections uncovered three *Saccharomyces cerevisiae* genes (*SEC61*, *SEC62* and *SEC63*), mutations in which block import of precursor proteins into the ER lumen *in vivo*[1-3] and *in vitro*[2-4]. The DNA sequences of *SEC62* (ref. 4) and *SEC63* (ref. 5) predict multispanning membrane proteins, and biochemical characterization of the *SEC62* protein (Sec62) confirms that it is an integral ER membrane protein[6]. Here we show that Sec61, Sec62 and Sec63 are assembled with two additional proteins into a multisubunit membrane-associated complex. These results confirm previous predictions, based upon genetic interactions between the *SEC* genes, that Sec61, Sec62 and Sec63 act together to facilitate protein translocation into the ER.

To test whether Sec62 is physically associated with other components of the ER membrane, we devised conditions for the efficient extraction of Sec62 from crude membrane fractions by monitoring the solubilization of invertase activity with a bifunctional Sec62-invertase hybrid protein[6] (data now shown). Solubilization conditions that reproducibly extracted Sec62-invertase (see Fig. 1 legend) were also effective for wild-type Sec62. Detergent-solubilized membrane fractions prepared from radiolabelled cells were treated with the thiol-reversible cross-linking agent dithio-*bis*-(succinimidylpropionate) (DSP) and immunoprecipitated under denaturing conditions with either of two distinct anti-Sec62 IgG preparations, then the crosslinker was cleaved with dithiothreitol and the proteins evaluated by SDS-PAGE. As expected, samples treated with inactivated DSP contained a polypeptide of relative molecular mass 30,000 (M_r 30K) corresponding to Sec62 (Fig. 1*a*). When active DSP was added, Sec62 and four additional polypeptides (73K, 31.5K, 23K and 41K) were reproducibly precipitated by either antibody. The 73K and 41K polypeptides comigrated exactly with Sec63 and Sec61 immunoprecipitated from non-crosslinked, SDS-denatured membranes. The 41K polypeptide was identified as Sec61 as it migrated as a ~39K species in complexes isolated from cells expressing a functional, truncated version of Sec61 lacking the C-terminal 17 amino acids (data not shown).

A similar cohort of polypeptides (minus Sec61) was co-immunoprecipitated with Sec62 under native, but not under denaturing, conditions (Fig. 1*b*). The absence of Sec61 from native immunoprecipitates suggests that its association with the complex is labile. As association of Sec61 with the complex was found to be variable, the stable 73K, 31.5K, 30K, 23K aggregate is referred to as the Sec62/Sec63 complex. A 50K species precipitated by anti-LacZ-Sec62 IgG (lane 10) was probably an irrelevant contaminant, as it was absent from immunoprecipitates prepared with anti-protein A-Sec62 IgG (lane 8), and was detected in precipitates prepared from *sec62-1* membranes, even though the other components of the complex were absent (data not shown). The 73K species that co-immunoprecipitated with Sec62 was directly identified as Sec63 by sequential immunoprecipitation with anti-Sec62 IgG followed by anti-Sec63 serum (Fig. 1*c*).

The physical state of the Sec proteins in detergent-solubilized membrane extracts reflects the behaviour of these proteins in the ER membrane, as similar multisubunit complexes containing Sec61, Sec62 and Sec63 were detected by treating intact membranes with DSP followed by immunoprecipitation with either anti-Sec62 IgG (data not shown) or anti-Sec63 IgG (Fig. 2, lanes 1 and 2). Compared with results obtained with anti-Sec62 IgG, complexes immunoprecipitated with anti-Sec63 IgG contained more Sec63 and more of the 31.5K and 23K proteins. This difference may arise from the relative abundance of the Sec proteins. Quantitative immunoprecipitation of Sec61, Sec62 and Sec63 from radiolabelled membranes indicated that Sec62, Sec63 and Sec61 exist in the membrane in the molar ratio of 1:5:14 (Fig. 2, lanes 3-5). Quantitation of radioactivity precipitated by anti-Sec62 antibodies indicated that Sec62 comprises ~0.015% of newly synthesized membrane protein. The relative paucity of Sec62 in complexes detected with anti-Sec63 IgG, and the presence of Sec61 in solubilized preparations treated with either antibody suggest that Sec63 and the 31.5K and 23K proteins can exist as a stable subcomplex lacking both Sec61 and Sec62. The dynamic assembly states of these Sec proteins may reflect cycles of subunit association and dissociation during the actual translocation event.

Digestion of immunopurified complexes with endoglycosidase H indicated that the 31.5K subunit is N-glycosylated, suggesting that it is either a transmembrane or lumenal polypeptide of the ER (Fig. 3). The molecular weights of gp31.5 and the 23K polypeptide (p23) are reminiscent of those reported for the two subunits (34K and 23K (refs 7-9)) of the dog pancreas microsomal membrane signal-sequence receptor[7]. Like glycoprotein 31.5, the 34K subunit of this receptor contains asparagine-linked oligosaccharide[7].

The observation that yeast Sec proteins required for translocation are assembled into a complex is consistent with the view that a multisubunit protein 'machine' catalyses the transfer of secretory precursor proteins across the ER membrane[10]. Complexes containing the Sec proteins may constitute the bulk of the membrane-associated portion of the yeast translocon, or may be subcomplexes of the translocon holoenzyme. We previously suggested that *SEC61*, *SEC62* and *SEC63* encode interacting proteins on the basis of genetic interactions observed between these loci[2,6]. The observations documented here validate the usefulness of synthetic lethality and high copy-number suppression in identifying genes encoding affiliated polypeptides.

A subdomain of Sec63 is homologous to an amino-terminal segment of the *Escherichia coli* DnaJ protein, which collaborates with the HSP70-like DnaK protein to promote activation of bacteriophage lambda DNA replication[11-14]. Certain alleles of the yeast *KAR2* gene, which encodes an ER lumenal HSP70

* Present address: Department of Biochemistry and Biophysics, University of California School of Medicine, San Francisco, California 94143-0448, USA.

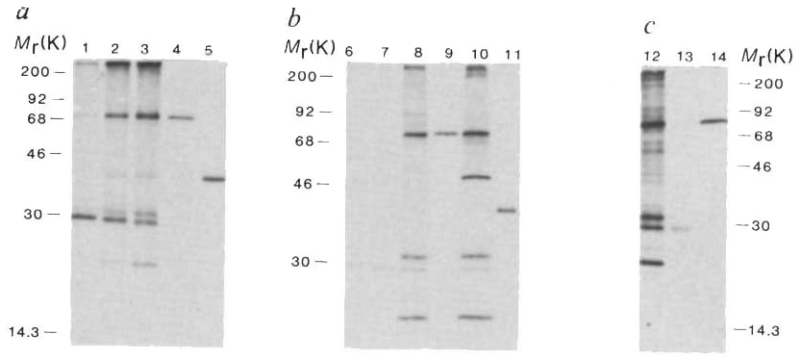

FIG. 1 Identification of a membrane-associated multisubunit Sec protein complex. *a*, Detergent-solubilized membranes from radiolabelled cells were incubated for 20 min with the crosslinking reagent DSP. Lane 1, samples were treated with previously inactivated DSP at 4 °C; lanes 2 and 3, crosslinking reactions were conducted with active DSP at 4 °C and 20 °C, respectively. Crosslinking reactions were quenched, subjected to immunoprecipitation with affinity-purified anti-Sec62 IgG and analysed by SDS–PAGE as described below. Lanes 4 and 5, Sec63 and Sec61 immunoprecipitated from SDS-denatured membranes with anti-Sec63 (D.F., J. Rothblatt and R.S., submitted) and anti-Sec61 (prepared by immunization with the C-terminal peptide CLVPGFSDLM; provided by C. Stirling) serum. *b*, The same material used in part *a* was either denatured with SDS before immunoprecipitation (+SDS, lanes 6 and 7), or immunoprecipitated under native conditions (lanes 8 and 10) with affinity-purified IgG elicited against a protein A-Sec62 (lanes 6 and 8) or a LacZ-Sec62 (lanes 7 and 10) hybrid protein[6]. Lanes 9 and 11, aliquots of the same samples as lanes 4 and 5. Asterisk refers to a contaminant precipitated by the anti-LacZ-Sec62 IgG. *c*, Immune complexes formed under native conditions with anti-protein A-Sec62 antibodies were directly analysed by SDS-PAGE (lane 12), or subjected to secondary precipitation with anti-sec62 (lane 13) and anti-Sec63 (lane 14) sera.

METHODS. Wild-type strain BF-1 (ref. 6) was radiolabelled with Tran-^{35}S-label (30 μCi per 10^7 cells) for 60 min at 30 °C and spheroplast homogenates were prepared by agitation with glass beads in lysis buffer (0.2 M mannitol, 0.1 M NaCl, 25 mM sodium phosphates, pH 7.4, 1 mM $MgCl_2$, 1 mM PMSF, 10 μM leupeptin and pepstatin) as described[21]. The homogenate was centrifuged for 4 min at 370*g* followed by 12 min at 50,500*g*. The final pellet was washed with lysis buffer, resuspended in lysis buffer (minus leupeptin and pepstatin) containing 10% glycerol (GLB), and adjusted to 1% Triton X-100. After 25 min at 4 °C, unsolubilized material was sedimented for 30 min at 148,400*g*. For crosslinking, the 148,400*g* supernatant was supplemented with 0.02 volumes 10 mg ml^{-1} DSP (Pierce) in dimethylsulphoxide. Reactions were terminated by adding 1 volume 0.2 M ammonium acetate, incubated on ice for 10 min, adjusted to 1% SDS, heated at 65 °C for 10 min and processed for immunoprecipitation with anti-LacZ-Sec62 IgG (ref. 6) as described[2]. For native immunoprecipitation, 6–10 × 10^6 c.p.m. of the 148,400*g* supernatant was diluted tenfold with GLBT (GLB containing 1% Triton X-100), supplemented with 40 μl of a 10% suspension of fixed *Staphylococcus aureus* cells and centrifuged 5 min at 10,000*g*. The supernatant was treated with antibodies, incubated 2–4 h at 4 °C and centrifuged for 5 min at 10,000*g* to remove denatured proteins. Immune complexes were collected on protein A–Sepharose CL-4B beads (1–2 h at 4 °C) and washed six times with ice-cold GLBT. Washed precipitates (of crosslinked and native samples) were resuspended in SDS–PAGE sample buffer supplemented with 50 mM DTT, heated for 10 min at 65 °C and subjected to SDS–PAGE on 12.5% polyacrylamide gels followed by autoradiography.

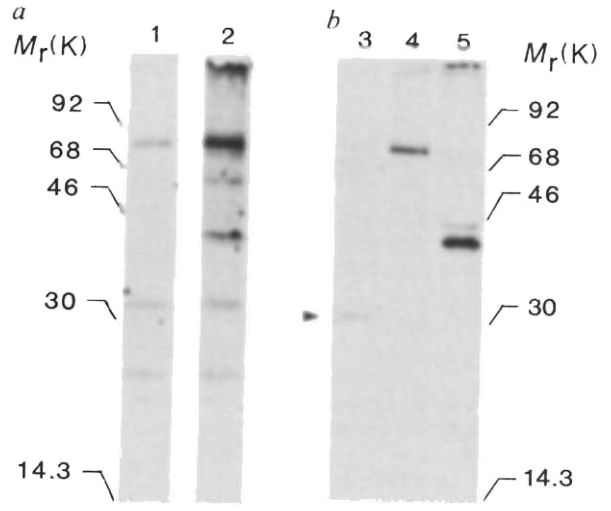

FIG. 2 Detection of the Sec62/Sec63 complex in whole membranes. Membrane fractions prepared from wild-type (RSY32) cells radiolabelled for 60 min at 30 °C were assayed for the presence of the Sec62/Sec63 complex. Samples were crosslinked with DSP either after the membranes were solubilized with Triton X-100 (lane 2) as described in the legend to Fig. 1, or before solubilization with Triton X-100 (lane 1), followed by immunoprecipitation with affinity-purified Sec63 IgG. Lanes 3, 4 and 5 depict Sec62, Sec63 and Sec61, respectively, quantitatively immunoprecipitated from non-crosslinked, SDS-denatured membranes with their respective antibodies. The arrow denotes Sec62.

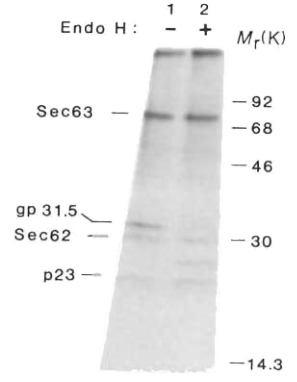

FIG. 3 The 31.5K subunit of the Sec62/Sec63 complex is a glycoprotein. An aliquot of the sample depicted in Fig. 1, lane 12 was either mock-treated (lane 1) or digested[22] with the enzyme endoglycosidase H (lane 2) before SDS–PAGE.

homologut[15,16] (known as BiP) involved in translocation[17], display synthetic lethality with *sec63-1* (M. Rose, personal communication). We propose that Kar2 acts reversibly through Sec63 to modify the composition of the Sec62/Sec63 complex, or to catalyse the association-dissociation of the complex with other factors, including Sec61, cytoplasmic HSP70 (refs 18, 19) and components of a putative cytoplasmic signal sequence receptor[20]. The identification of a complex of Sec proteins involved in translocation provides a focus for future biochemical reconstitution. □

Received 17 September; accepted 14 December 1990.

1. Deshaies, R. J. & Schekman, R. *J. Cell Biol.* **105,** 633-645 (1987).
2. Rothblatt, J. A., Deshaies, R. J., Sanders, S. L., Daum, G. & Schekman, R. *J. Cell Biol.* **109,** 2641-2652 (1989).
3. Toyn, J., Hibbs, A. R., Sanz, P., Crowe, J. & Meyer, D. I. *EMBO J.* **7,** 4347-4353 (1988).
4. Deshaies, R. J. & Schekman, R. *J. Cell Biol.* **109,** 2653-2664 (1989).
5. Sadler, I. *et al. J. Cell Biol.* **109,** 2665-2675 (1989).
6. Deshaies, R. J. & Schekman, R. *Molec. cell. Biol.* **10,** 6024-6035 (1990).
7. Wiedmann, M., Kurzchalia, T. V., Hartmann, E. & Rapoport, T. *Nature* **328,** 830-833 (1987).
8. Hartmann, E., Wiedmann, M. & Rapoport, T. A. *EMBO J.* **8,** 2225-2229 (1989).
9. Rapoport, T. A. in *Dynamics and Biogenesis of Membranes* 231-245 (Springer, Berlin, 1990).
10. Blobel, G. & Dobberstein, B. *J. Cell Biol.* **67,** 835-851 (1975).
11. Alfano, C. & McMacken, R. *J. biol. Chem.* **264,** 10699-10708 (1989).
12. Alfano, C. & McMacken, R. *J. biol. Chem.* **264,** 10709-10718 (1989).
13. Dodson, M., McMacken, R. & Echols, H. *J. biol. Chem.* **264,** 10719-10725 (1989).
14. Zylicz, M., Ang, D., Liberek, K. & Georgopoulos, C. *EMBO J.* **8,** 1601-1608 (1989).
15. Normington, K., Kohno, Kozutsumi, Y., Gething, M.-J. & Sambrook, J. *Cell* **57,** 1223-1236 (1989).
16. Rose, M. D., Misra, L. M. & Vogel, J. P. *Cell* **57,** 1211-1221 (1989).
17. Vogel, J. P., Misra, L. M. & Rose, M. D. *J. Cell Biol.* **110,** 1885-1896 (1990).
18. Deshaies, R. J., Koch, B. D., Werner-Washburne, M., Craig, E. A. & Schekman, R. *Nature* **332,** 800-805 (1988).
19. Chirico, W. J., Waters, M. G. & Blobel, G. *Nature* **332,** 805-810 (1988).
20. Hann, B. C., Poritz, M. A. & Walter, P. *J. Cell Biol.* **109,** 3223-3230 (1989).
21. Bernstein, M., Hoffmann, W., Ammerer, G. & Schekman, R. *J. Cell Biol.* **101,** 2374-2382 (1985).
22. Böhni, P. C., Deshaies, R. J. & Schekman, R. *J. Cell Biol.* **106,** 1035-1042 (1988).

ACKNOWLEDGEMENTS. We thank A. Nakano for advising us on the use of DSP for the cross-linking studies, C. Stirling for the anti-Sec61 serum and the truncated *SEC61* clone, and J. Rothblatt for anti-Sec63 serum. This work has been supported by an NSF Graduate Minority Fellowship (S.L.S.), a Merck Foundation fellowship (D.A.F.) and NIH grants (R.S.).

Fission yeast p107^{wee1} mitotic inhibitor is a tyrosine/serine kinase

Carol Featherstone & Paul Russell*

Department of Molecular Biology, Research Institute of Scripps Clinic, La Jolla, California 92037, USA

THE fission yeast *wee1*$^+$ gene product is a dose-dependent, negative regulator of entry into mitosis[1,2]. *wee1*$^+$ encodes a protein of relative molecular mass 107,000 (M_r 107K), the C-terminal third of which has strong similarities with the serine/threonine protein kinase family[2,3]. Here we report that p107^{wee1} immune complexes phosphorylate p107^{wee1} equally on serine and tyrosine residues, and also phosphorylate an exogenous substrate, angiotensin II, on tyrosine. Both kinase activities are attributable to p107^{wee1} because they are also observed when *wee1*$^+$ is expressed in heterologous systems; both are abolished by a point mutation in the ATP-binding domain, and both behave like an asymmetric monomer of M_r 114K on gel filtration and density-gradient centrifugation. Thus the *wee1*$^+$ gene product is representative of a novel class of protein kinase that phosphorylates both serine and tyrosine residues.

The *wee1*$^+$ product is detected as a protein of M_r 107K in immunoblots (Fig. 1). p107^{wee1} is a phosphoprotein *in vivo*, as shown by gel electrophoresis of immunoadsorbed protein after metabolic labelling with [^{32}P]inorganic phosphate (Fig. 1*b*, lane2). Only phosphoserine was detected on two-dimensional phosphoamino-acid analysis (2D-PAA) of the labelled protein (Fig. 1*b*, lower panel). To test directly if p107^{wee1} acts as a protein kinase, we used immunoadsorbed p107^{wee1} washed under stringent conditions, in kinase assays with several protein substrates including histone H1, casein, enolase and p34^{cdc2}. No phosphorylation of these substrates was detected (data not shown), but p107^{wee1} itself readily became phosphorylated when incubated with [γ-^{32}P]ATP (Fig. 1*c*). Surprisingly, p107^{wee1} phosphorylated *in vitro* contains both phosphoserine and phosphotyrosine in approximately equal proportions (Fig. 1*c*, lower panel). Incorporation was linear throughout the course of the assay (Fig. 1*e*), and assays using higher ATP concentrations (10 μM) produced identical results (data not shown). The

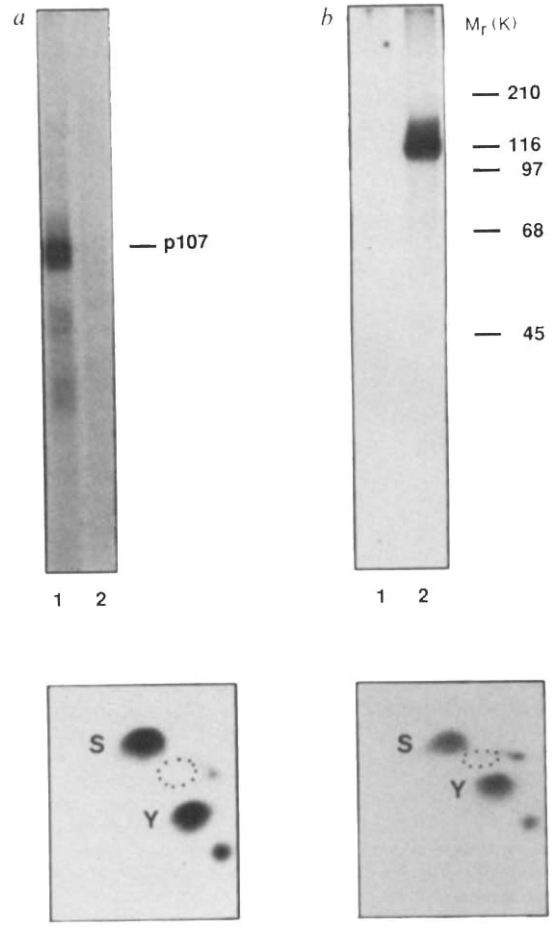

FIG. 2 Kinase activity of p107^{wee1} expressed in heterologous systems. *a*, The *wee1*$^+$ gene was expressed in the *S. cerevisiae* strain J16D (J16D-WG) under the control of the galactose-inducible *GAL1* promoter[4]. Kinase assays were performed on immunoadsorbed p107^{wee1} as described in Fig. 1. Upper panel: p107^{wee1} kinase activity was detected in cells grown in inducing conditions (lane 1) but was not detected in a *wee1*-K596L mutant expressed from the same promoter (lane 2). Lower panel: The p107^{wee1} phosphoprotein contained phosphoserine and phosphotyrosine by 2D-PAA. *b*, Wild-type *wee1* was expressed in Sf9 cells using the baculovirus expression system. Upper panel: p107^{wee1} kinase activity was assayed as described in Fig. 1, using immunoadsorbed material from cells expressing the wild-type virus (lane 1) and the *wee1*$^+$ recombinant virus (lane 2). Lower panel: p107^{wee1} contained phosphoserine and phosphotyrosine as observed by 2D-PAA.
METHODS. *S. cerevisiae* J16D-WG and J16D-WGK596L cells[4] were grown in YP-Raf (2% yeast extract, 1% peptone, 2% raffinose) to an OD_{600} of 1.0, then *wee1* expression was induced with galactose for 3 h. p107^{wee1} kinase assays were performed on immunoadsorbed material and detected by autoradiography of SDS gels, and the PAA content was determined as described in Fig. 1. Full-length *wee1*$^+$ was cloned as a *Bam*H1 fragment into the pVL941 vector[12], transfected into Sf9 cells together with viral DNA by lipofection for 4-5 h as described by BRL, and recombinant virus cloned[13]. Cells infected with wild-type or recombinant virus were grown for 3 days then extracted with lysis buffer and p107^{wee1} kinase activity was assayed as described in Fig. 1.

* To whom correspondence should be addressed.

finding that p107^{wee1} was phosphorylated on tyrosine *in vitro* was unexpected because sequence comparisons have placed p107^{wee1} in the serine/threonine family of protein kinases[2,3], and because tyrosine phosphorylation is exceedingly rare in yeast. Controls using pre-immune serum, affinity-purified antibodies and antisera raised against different fragments of the p107^{wee1} molecule showed that the tyrosine and serine phosphorylation was dependent on immunoadsorption with antibodies specific for p107^{wee1} (data not shown). Two explanations could account for the phosphorylation of p107^{wee1} on serine and tyrosine *in vitro*: either p107^{wee1} is tightly associated with an unidentified yeast tyrosine kinase, or it is a new type of kinase having both activities.

To test these possibilities, we assayed a *wee1* null mutation, created by mutating lys 596 to leucine (*wee1*-K596L)[4]. This lysine is required for binding ATP in the active site and is absolutely conserved in protein kinases[3]. The *wee1*-K596L mutant is inactive as an M-phase inhibitor *in vivo*[4]. When expressed in *Schizosaccharomyces pombe* the *wee1*-K596L gene product was detected as a 107K protein by immunoblotting (data not shown), but it had no detectable protein kinase activity (Fig. 1*d*), showing that the activity and/or immunoadsorption of both kinase activities is abolished by the *wee1*-K596L mutation.

To extend our findings, we asked whether p107^{wee1} retained tyrosine kinase activity when expressed in cells of two divergent

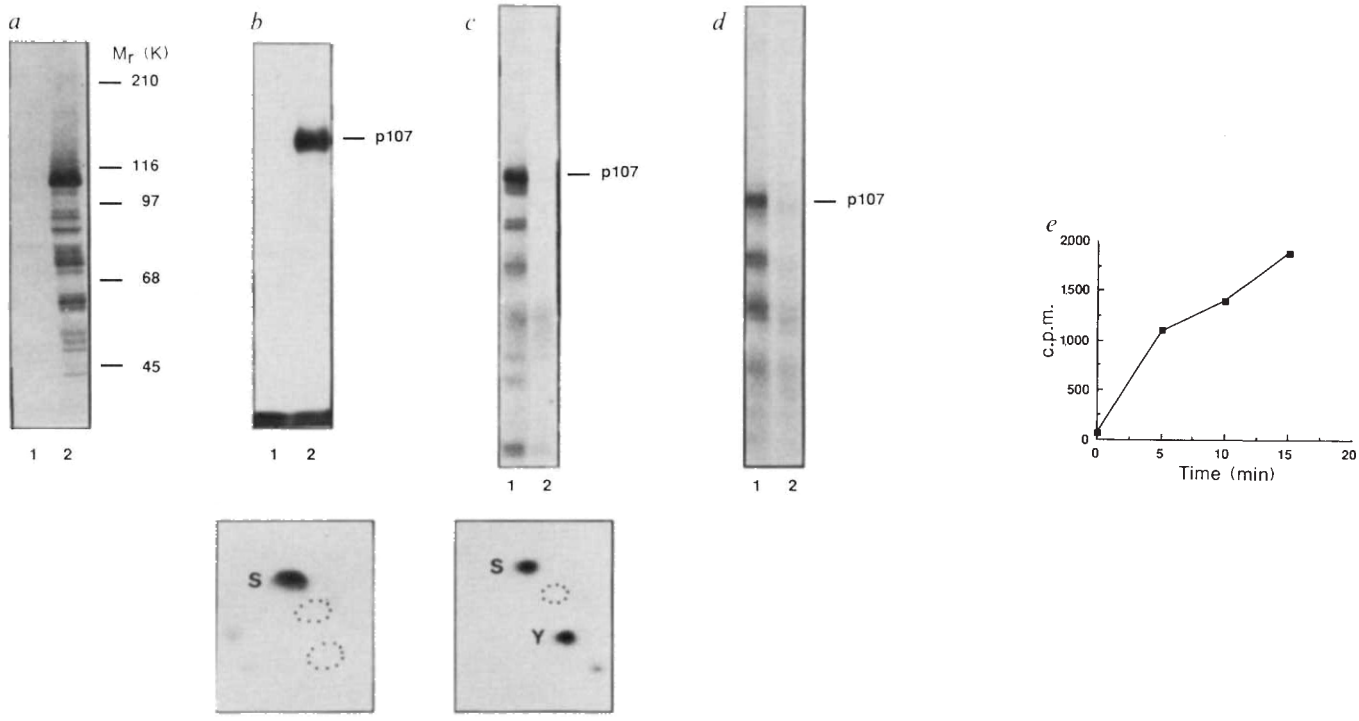

FIG. 1 Phosphorylation of p107^{wee1} *in vivo* and *in vitro*. p107^{wee1} was overexpressed in *S. pombe* as a temperature-sensitive mutant, *wee1*-50 as described[2]. *a*, p107^{wee1} is detected on immunoblots of the overproducer as a major species of M_r 107 K and a number of fragments (lane 2). No protein is detected in a *wee1* deletion mutant (lane 1). *b*, upper panel: immunoadsorption of p107^{wee1}, metabolically-labelled with ^{32}P, shows that it is a phosphoprotein (lane 2). No phosphoprotein is immunoadsorbed from a *wee1* deletion mutant (lane 1); lower panel: Only phosphoserine was detected by 2D-PAA of ^{32}P-p107^{wee1} labelled *in vivo*. *c*, Upper panel: kinase assays of immunoadsorbed p107^{wee1} from p107^{wee1} overproducer (lane 1) and deletion mutant (lane 2); lower panel: 2D-PAA of full-length p107^{wee1} labelled *in vitro* shows both serine- and tyrosine-kinase activity in the immunoadsorbed material. *d*, Kinase assays of immunoadsorbed p107^{wee1} from overproducers of *wee1-50* (lane 1) and *wee1*-K596L (lane 2) show that a mutation in the ATP-binding site abolishes activity. The very faint band at the position of p107^{wee1} in the mutant was probably due to a small amount of transcription from the copy of *wee1-50* that is not under the control of the *adh* promoter in this strain. *e*, Time-course of accumulation of [^{32}P]p107^{wee1} labelled *in vitro* using fission yeast *wee1-50* overproducer, assayed at 25 °C, showing approximately linear rate of incorporation.

METHODS. *S. pombe* overexpressing *wee1-50* were grown in YES (ref. 8) medium at 35 °C to an optical density at 600 nm (OD_{600}) of 1.0, then grown at 25 °C for 3 h. Cells were collected by filtration, washed with ice-cold STOP (150 mM NaCl, 50 mM NaF, 10 mM EDTA, 1 mM NaN_3, pH 8) buffer[8], flash-frozen on dry-ice/ethanol as cell pellets of 40 OD_{600} then stored at −70 °C. Cell pellets were extracted with 300 ml lysis buffer (50 mM Tris-HCl, pH 7.4, 0.1% NP-40, 50 mM NaF, 10 mM sodium pyrophosphate, 250 mM NaCl, 10% glycerol, 0.5 mM sodium *o*-vanadate, 0.5 mM phenylmethylsulphonyl fluoride (PMSF), 5 mg ml^{-1} leupeptin, 5 mg ml^{-1} pepstatin, 5 mg ml^{-1} aprotinin) using glass beads on a vortex at 4 °C for 5 min. Whole cell extracts were boiled in SDS gel sample buffer and centrifuged at 15,000 r.p.m. in a microfuge for 5 min. The supernatants were separated by SDS gel electrophoresis[9] in 8% polyacrylamide and transferred to nitrocellulose membranes using a semi-dry blotter. Blots were processed with a rabbit antiserum (raised against the C-terminal third of p107^{wee1} expressed in *E. coli* and purified from inclusion bodies), using 10% powdered milk in 0.5% Triton X-100, PBS as blocking solution as described[10], and a goat anti-rabbit IgG antibody conjugated to alkaline phosphatase. Production and characterization of antibodies will be described in detail elsewhere (Featherstone and Russell, in preparation). For ^{32}P-labelling, cells were grown in EMM (ref. 8) medium with 100 mM inorganic phosphate. Mid log-phase cells were resuspended at a density of 0.4 OD_{600} per ml in EMM with no added phosphate, and labelled with 0.25 mCi ml^{-1} carrier-free [^{32}P]inorganic phosphate at 25 °C for 3 h. Extracts were prepared essentially as above but using the buffers described[8], and p107^{wee1} was immunoadsorbed with anti-*wee1* serum and protein A–Sepharose. The bound proteins were eluted by boiling with SDS sample buffer and separated on 8% polyacrylamide gels. Radioactive proteins were detected by autoradiography. *wee1*-K596L was expressed in *S. pombe* by gene conversion of the *adh:wee1-50* strain with the *wee1*-K596L gene to produce an *adh:wee1*-K596L strain. Protein kinase reactions were performed on p107^{wee1} immunoadsorbed as described above. The beads were washed twice with 0.5 M LiCl, 20 mM Tris-HCl, pH 7.5 and twice with kinase assay buffer (50 mM Tris-HCl, pH 7.5, 10 mM $MgCl_2$, 10 mM $MnCl_2$, 1 mM DTT), resuspended in 40 ml of the same buffer and assayed with 10 μCi [γ ^{32}P]ATP for 15 min at 25 °C. Time-course experiments showed that the rate of ^{32}P incorporation into p107^{wee1} was linear throughout the course of the incubation. The reaction was stopped with an equal volume of SDS sample buffer and boiled. The soluble fraction was separated by SDS gel electrophoresis and exposed for autoradiography as above. The phosphoamino-acid content of ^{32}P-labelled p107^{wee1} was determined by elution of the proteins from the gel slice and 2D-PAA as described[11].

species, *Saccharomyces cerevisiae*[4] and insect *Spodoptera frugiperda* (Sf9 cells)[5]. Immunoadsorbed p107^{wee1} expressed in these species became phosphorylated *in vitro* on serine and tyrosine residues in similar proportions to those seen in assays with p107^{wee1} expressed in *S. pombe* (Fig. 2). No activity was seen with the *wee1*-K596L mutant expressed in *S. cerevisiae* (Fig. 2*a*, lane 2). These data are consistent with the idea that p107^{wee1} is both the serine and tyrosine kinase, or that association with a tyrosine kinase is highly conserved through evolution.

p107^{wee1} comprised ~1% of total cellular protein when expressed in Sf9 cells. Therefore if p107^{wee1} interacts with a tyrosine kinase, one would expect to find at least two populations of p107^{wee1}, a minor one bound to the less abundant tyrosine kinase, and a major, unbound population. To determine whether this is so, we fractionated the extract by gel filtration (Fig. 3). The p107^{wee1} protein (Fig. 3*a* upper panel) and kinase activity (Fig. 3*a*, middle panel) eluted together as a single, symmetrical peak indicative of one species with an apparent M_r of 400 K and a Stoke's radius of 62 Å (Fig. 3*a*, bottom panel). 2D-PAA analysis of p107^{wee1} phosphorylated *in vitro* showed that the leading and trailing edge fractions contained phosphoserine and phosphotyrosine in similar proportions (data not shown). These observations suggest strongly that p107^{wee1} is both a serine and tyrosine kinase. If the tyrosine kinase activity was due to a tightly-bound host cell enzyme, this must be both highly conserved across species and present in sufficiently large quantities to saturate binding to the very large amounts of p107^{wee1} expressed in the insect cells.

The apparent M_r of 400K suggested that p107^{wee1} could be oligomeric, for example a homotetramer, or could be an asymmetric monomer. The latter was most likely because p107^{wee1} eluted in the same position when the column was run in 4M LiCl (data not shown). To confirm this interpretation, we used sucrose velocity-gradient centrifugation to determine the sedimentation coefficient of p107^{wee1}. Fractions from the sucrose gradient were assayed by immunoblotting (Fig. 3*b*). p107^{wee1} was found in a single peak centred in fraction 3, with a sedimentation coefficient of 4.4 S, approximately equal to that of BSA, which is a 66 K globular monomer. We repeated the experiment using glycerol to form the velocity gradients, in which we were able to measure p107^{wee1} autophosphorylation as well as detecting the protein by immunoblotting (Fig. 3*c*). The p107^{wee1} polypeptide and kinase activity comigrated, forming a peak between fractions 5 and 6, with a sedimentation coefficient of 4.5 S. The ratio of phosphoserine to phosphotyrosine was similar in the leading and trailing edges of the peak. Assuming a partial specific volume for p107^{wee1} of 0.73, we used the Stokes radius (62 Å) and the sedimentation coefficient (4.4 S) to calculate a molecular weight for p107^{wee1} of M_r 114 K (ref. 6). This strongly suggests that p107^{wee1} is an asymmetric monomer when expressed in Sf9 cells.

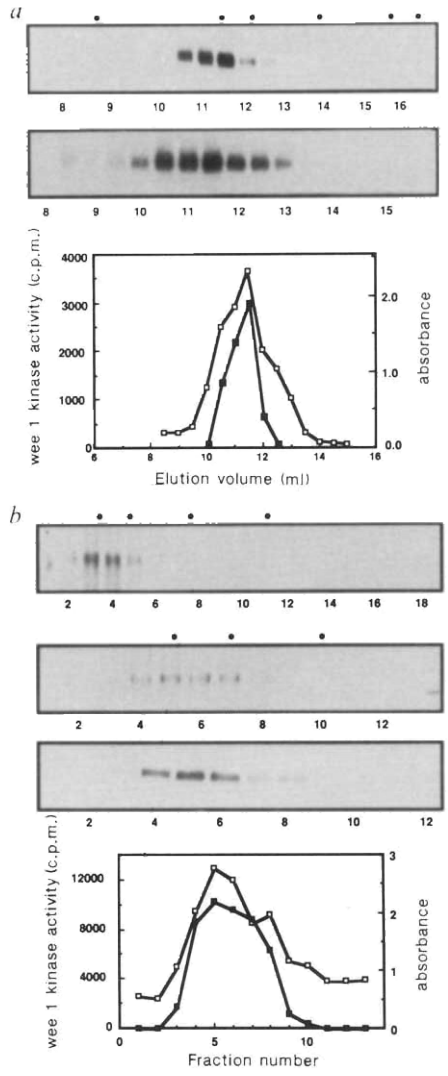

FIG. 3 Fractionation of p107^{wee1} in Sf9 cell extracts by gel filtration and velocity-gradient centrifugation. *a*, top panel: immunoblot of p107^{wee1} in fractions from gel filtration on Superose 12. p107^{wee1} behaves as a single species of M_r 400 K. The dots represent the elution volumes of molecular mass standards, from left to right: thyroglobulin (667 K), apoferritin (443 K), β-amylase (200 K), BSA (66 K), carbonic anhydrase (29 K) and cytochrome *c* (12.4 K). The numbers along the bottom indicate the elution volume. Middle panel: the p107^{wee1} protein phosphorylated in kinase assays of the fractions from gel filtration, as detected by autoradiography of SDS gels. Numbers indicate elution volume. Bottom panel: the radioactive bands were cut out and quantitated by scintillation counting. p107^{wee1} kinase activity eluted as a single, symmetrical peak, coincident with the peak of protein detected by immunoblotting. Open squares represent kinase activity, closed squares denote protein level. *b*, Immunoblot of p107^{wee1} from fraction 11.5 of the gel-filtration column above, after separation by sucrose velocity-gradient centrifugation. p107^{wee1} migrates as a peak in fraction 3. Dots represent peaks of standards, from left to right: BSA (4.5S), human IgG (7.2S), catalase (11.3S) and β-galactosidase (16S). Numbers indicate fractions. *c*, Top panel: immunoblot of p107^{wee1} from total protein extract of Sf9 cells expressing *wee1* after separation by glycerol velocity-gradient centrifugation. Dots represent peaks of standards, from left to right: BSA (4.5S), human IgG (7.2S) and catalase (11.3S). Middle panel: p107^{wee1} protein phosphorylated in kinase assays of the fractions from glycerol gradient. Bottom panel: quantitation of p107^{wee1} immunoblot and kinase activity of fractions from glycerol gradient which co-migrate with a peak centred in fractions 5 and 6. METHODS. Sf9 cells in suspension were infected with *wee1*$^+$ recombinant baculovirus for 3 days[13]. Approximately 1.3×10^8 cells were extracted with lysis buffer as described in Fig. 1, and centrifuged at 45,000 r.p.m. for 45 min at 4 °C in a Beckman TLA45 rotor. Supernatant (0.5 ml) was loaded onto a Pharmacia Superose 12 FPLC column equilibrated in lysis buffer and eluted at 0.5 ml min^{-1}. Fractions of 0.5 ml were collected from 6 to 25 ml. The fractions were divided in half. One half was assayed for kinase activity after immunoadsorption as in Fig. 1. The other half was precipitated with 20% TCA on ice for 60 min, the pellets were washed with 90% acetone, 0.1 M HCl and dissolved in SDS gel sample buffer. The precipitates were analysed for p107^{wee1} by immunoblotting as described in Fig. 1. Immunoblots were quantitated by laser scanning densitometry. Radioactive p107^{wee1} was quantitated by scintillation counting of the gel slices after autoradiography. Linear 11.5 ml, 5–25% sucrose gradients were prepared in lysis buffer without glycerol. Fraction 11.5 from the gel filtration column was layered onto the top of the gradient and centrifuged for 16 h at 35,000 r.p.m. and 4 °C in a Beckman SW41 rotor. Gradients were fractionated into 0.5 ml fractions from top to bottom and processed for immunoblotting as above. Linear 5–30% glycerol gradients were prepared in lysis buffer. Total protein extracts (0.1 ml) from Sf9 cells were layered onto gradients and centrifuged in a Beckman VTi65.1 rotor at 64,000 r.p.m. for 130 min at 4 °C. The gradients were fractionated into 1-ml fractions and assayed for kinase activity and p107^{wee1} protein as above.

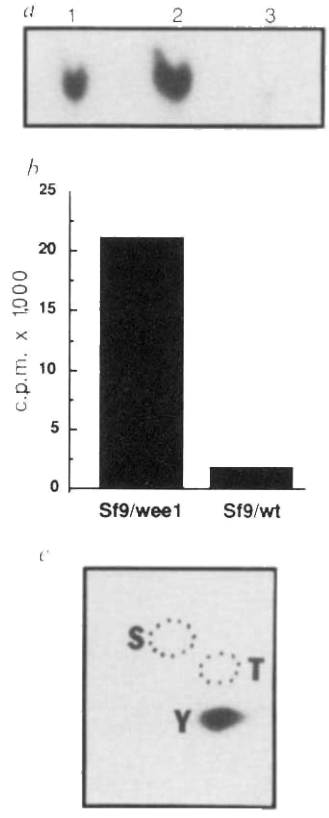

FIG. 4 Phosphorylation of angiotensin II on tyrosine by p107^{wee1} immunoprecipitates. The ability of p107^{wee1} kinase to phosphorylate angiotensin II was assayed using immunoadsorbed material from Sf9 cells expressing the wild-type virus (Sf9/wt) and the *wee1*$^{+}$ recombinant virus (Sf9/wee1). *a*, Angiotensin II was resolved by thin-layer electrophoresis. Lanes 1 and 2 are Sf9/wee1 immunoprecipitates assayed at angiotensin II concentrations of 1.0 and 2.0 mM, respectively; lane 3 is Sf9/wt assayed at 1.0 mM angiotensin II. *b*, Quantitation of angiotensin phosphorylation shows a > tenfold increase in kinase activity in immunoadsorbed material from Sf9/wee1 cells compared to that from Sf9/wt cells, when assayed at 1.0 mM concentration. *c*, 2D-PAA determination of angiotensin II phosphorylated by Sf9/wee1 shows that all phosphorylation occured on tyrosine.
METHODS. Kinase assays were performed as described in Fig. 1 using human (Val^{5})-angiotensin II (Calbiochem, La Jolla) at the indicated concentrations. Assays were performed at 25 °C for 20 min and terminated by freezing in a dry-ice/ethanol bath. Thin-layer electrophoresis was performed at pH 1.9 as described[11].

Given the evidence that both serine and tyrosine autophosphorylation activities were intrinsic to p107^{wee1}, we re-examined whether p107^{wee1} was able to phosphorylate tyrosyl residues in exogenous substrates, including angiotensin II, myelin basic protein, and poly (Glu-Tyr). Angiotensin II proved an excellent substrate (Fig. 4). As angiotensin II has the sequence Asp-Arg-Val-Tyr-Val-His-Pro-Phe, it seemed very probable that phosphorylation was on tyrosine. This was confirmed by phosphoamino-acid analysis (Fig. 4*c*), showing that p107^{wee1} is an authentic tyrosine kinase.

All protein kinases thus far characterized are specific either for serine and threonine or for tyrosine residues. Although the relationship between structure and substrate specificity is not well understood, the phylogeny of protein kinase catalytic domains indicates that the two types of protein kinase have evolved from a common precursor[3]. Thus it is perhaps not surprising that there is a protein kinase such as p107^{wee1} with properties of both classes. The finding that p107^{wee1} is a functional mosaic, with properties of both tyrosine and serine kinases, has important implications for structural and evolutionary studies of these enzymes.

In fission yeast, p107^{wee1} phosphorylation *in vivo* was only detected on serine residues. Likewise, anti-phosphotyrosine antibodies failed to detect p107^{wee1} in yeast or Sf9 cells overproducing *wee1* (unpublished data), suggesting that autophosphorylation of p107^{wee1} on tyrosine residues *in vivo*, if it exists, must occur at a very low level and may not be the important physiological function of the p107^{wee1} kinase. It has been shown that the p34^{cdc2} M-phase induction function is subject to negative regulation by tyrosine phosphorylation[7], and the proposal that p107^{wee1} is directly responsible for this phosphorylation provides an appealing model for the inhibition of mitosis by p107^{wee1}. We have been unable to demonstrate phosphorylation of p34^{cdc2} purified after expression in *E. coli*, or purified as the active histone H1 kinase complex from mitotic HeLa cells. This suggests either that p107^{wee1} is extremely specific for a particular conformation or complex of p34^{cdc2} or that p34^{cdc2} is not the physiological substrate and another protein mediates the negative regulation of p34^{cdc2}. □

Received 14 November 1990; accepted 7 January 1991.

1. Nurse, P. *Nature* **334,** 503-508 (1990).
2. Russell, P. & Nurse, P. *Cell* **49,** 559-567 (1987).
3. Hanks, S. K., Quinn, A. M., & Hunter, T. *Science* **241,** 42-52 (1988).
4. Russell, P., Moreno, S. & Reed, S. I. *Cell* **57,** 295-303 (1989).
5. Smith, G. E., Summers, M. D. & Frazer, M. J. *Molec. cell. Biol.* **3,** 2156-2165 (1983).
6. Siegel, L. M. & Monty, K. J. *Biochim. biophys. Acta* **112,** 346-362 (1966).
7. Gould, K. L. & Nurse, P. *Nature* **342,** 39-45 (1989).
8. Moreno, S., Klar, A. & Nurse, P. *Meth. Enzym.* **56,** 795-823 (1991).
9. Maizel, J. V. in *Fundamental Techniques in Virology* (eds Habel, K. H. & Salzman, N. P. 334-362 (Academic, New York, 1969).
10. Burnette, W. N. *Analyt. Biochem* **112,** 195-203 (1981).
11. Cooper, J. A., Sefton, B. M. & Hunter, T. *Meth. Enzym.* **99,** 387-402 (1983).
12. Luckow, V. A. & Summers, M. D. *Virology* **170,** 31-39 (1989).
13. Summers, M. & Smith G. *A Manual of Methods for Baculovirus Vectors and Insect Cell Culture Procedures* (Texas Agricultural Experiment Station Bulletin No. 1555, College Station, Texas, 1987).

ACKNOWLEDGEMENTS. We thank P. Dixon, K. Gould, T. Hunter, R. Lindberg, C. McGowan, H. Piwnica-Worms, S. Reed, P. Turmel and C. Wittenberg for technical advice and discussions, and the NIH for funding.

ERRATUM

The extended sodium nebula of Jupiter

Michael Mendillo, Jeffrey Baumgardner, Brian Flynn & W. Jeffrey Hughes

Nature **348,** 312-314 (1990)

IN the above Letter, the sentence in the first paragraph starting "Sodium emission has been reported..." should have read "Sodium emission has been reported at greater distances[5], even as far as $60R_J$ (ref. 6), but these observations have been controversial in view of suggestions[7] that the detection of sodium beyond $\sim 10R_J$...". The two references to the radius of Jupiter (R_J) were incorrectly ascribed to the radius of Io(R_{Io}), owing to an error in the *Nature* office.

High-speed DNA sequencing by capillary gel electrophoresis

L.M. Smith

Capillary gel electrophoresis with fluorescence detection is a new technique for rapid DNA sequence analysis. The state of this technology and the potential for its future use are discussed.

THE tremendous demands of the Human Genome Initiative for improved DNA sequencing methodologies has spurred a multitude of innovative new approaches to high-speed DNA sequence analysis. One of the most promising of these new techniques is capillary gel electrophoresis (CGE). This method is a variant of capillary zone electrophoresis (CZE), discussed in an earlier product review[1].

As in CZE, electrophoretic separations are performed in extremely thin (1 to 100-microns i.d.) fused silica capillaries; the difference is that in CGE the capillary is filled with a polyacrylamide gel matrix to permit separation on the basis of molecular weight, as in conventional gel electrophoretic separations. The principal advantage of the method is its speed — the electrical resistance of these thin capillaries is sufficiently great that electric fields as large as 400 V cm^{-1} (compared to the 30 or so volts per cm used in conventional DNA sequencing gels) can be applied to them without excessive Joule heating. These large fields result in a corresponding increase in the migration velocity of the DNA fragments, with a concomitant reduction in analysis time[2-4] (Fig. 1).

Resolution

The resolutions obtained in these CGE separations are also extremely high, in the range of 10 to 30 million theoretical plates per metre[2,4,5]. There is, as yet, a lack of consensus on whether these results differ materially from those obtained under similar conditions in conventional slab gel electrophoresis. Data from our group have shown roughly similar resolving power in the two methods[4], whereas results reported elsewhere showed a greater difference[2]. The apparent discrepancy seems to be due primarily to variations in the conditions of the conventional electrophoresis, as both groups obtained similar results using CGE. In any case, band broadening is clearly not diffusive in nature, as turning off the electrophoresis mid-run, even for several hours, has no effect on band widths. The relative importance of other broadening mechanisms, such as random variations in the path lengths taken by DNA molecules through the gel or sample injection effects, is not yet clear. The potential for preparing capillary gels several metres in length may eventually turn out to be the best method for extending the length of sequence obtained in a single analysis, although clearly this will be at the expense of separation speed.

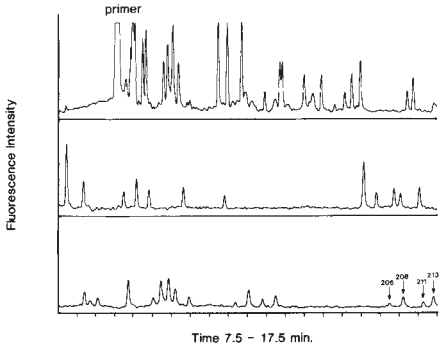

FIG. 1 Separation of fluorescein-labelled G reaction of M13mp19 DNA by capillary electrophoresis using an electric field of 400 V cm^{-1} on a 50-cm capillary gel. (Reproduced from ref. 3.)

Detection limits

Another interesting aspect of DNA sequencing by CGE is the extreme sensitivity of the fluorescence detection methods used.

Detection limits from 6,000 to 60,000 molecules of fluorescein have been reported [2-4] (see Fig. 2 for a schematic of the fluorescence detection system used in our laboratory), and the potential exists for reducing this to as low as the single-molecule level[6,7]. This level of sensitivity suggests that it may be possible to simplify greatly another aspect of the DNA sequencing process, the production of DNA templates[8]. A single bacteriophage M13 plaque commonly obtained on a lawn of *Escherichia coli* cells contains up to 10^{10} viral particles. If methods can be developed to isolate efficiently the DNA molecules from the plaque and perform the enzymatic extension reactions upon them, it should be possible to analyse directly the plaque DNA by CGE, eliminating the template amplification step entirely. The enzyme *Bst* DNA polymerase (Bio-Rad, Richmond, California) appears to be well suited for the performance of sequencing reactions at these low template concentrations (D.A. Mead *et al.*, submitted). Working with such small amounts of material would also greatly reduce the cost of other sequencing reagents, and could lead to a scaling down of the entire sequencing process.

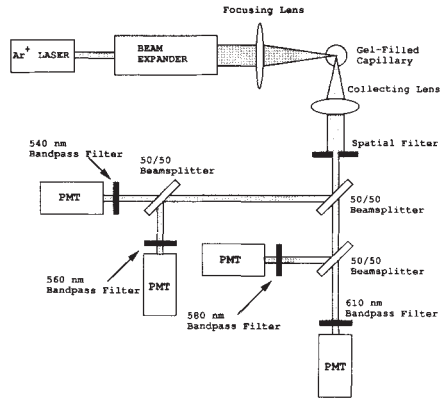

FIG. 2 Optical system used for multiple wavelength fluorescence detection in capillary electrophoresis. (Reproduced from ref. 4.)

Throughput

The high-speed of these capillary separations does not automatically lead to an increased throughput in automated DNA sequence analysis. Commercially available automated sequencers can analyse up to 24 samples simultaneously and, hence, an instrument that can run only one sample, but 24 times as fast, will not necessarily give a better overall performance. In order to obtain increased throughput, it is necessary to extend the high-speed capability to the simultaneous analysis of multiple samples. There are two approaches to the problem: use multiple capillaries set up in parallel or, alternatively, export the basic principle of CGE, its minute dimensions, back to the slab- gel format that is commonly used in DNA sequencing. Most of our efforts are concentrated on the latter.

The concept of ultrathin slab gels is not new[9,10], but such gels have not been widely used for DNA sequencing, probably in large part because of difficulties in their preparation and in sample loading. We have recently developed an ultrathin gel system that overcomes some of these difficulties (B. Brumley & L.M. Smith, in preparation). When used in conjunction with a suitable fluorescence detection scheme, the system appears to show considerable promise for the parallel analysis of multiple samples. If such a system was capable of analysing 500 bases from 50 samples every hour, its theoretical

throughput would be 600,000 bases of raw data per day, a major jump over existing technology.

Limitations

Least an unduly rosy picture of CGE be painted, it should be noted that there are both fundamental and practical limitations to the method. The most serious fundamental limitation may stem from the deleterious effect that an increased electric field strength can have upon resolution. Experimental and theoretical studies have demonstrated a decrease in resolution with increased field strength in the agarose gel electrophoresis of DNA fragments[11-13]. A similar effect in acrylamide gel electrophoresis was reported recently by Ulanovsky and colleagues[14].

Although the practical consequences of this effect upon performance in CGE have not as yet been determined, experiments to do so are underway in several laboratories. The primary practical barrier to the widespread dissemination of CGE-based sequencing has thus far been the difficulty of producing capillary gels of adequate quality on a commercial scale. The denaturing polyacrylamide gels used in conventional DNA sequencing are themselves not yet amenable to large-scale production primarily because of problems with their chemical stability. The denaturants used in sequencing gels to minimise the formation of secondary structures (compressions) in the DNA strands during separation seem to be the primary culprits. For example, the most widely used denaturant is 8 M urea, which is both hydrolytically unstable at the alkaline pH of these gels, and also tends to crystallize out of solution rather readily. Capillary gels face these and additional issues such as bubble formation caused by contraction of the gel matrix during polymerization[3]. Indeed, the procedures for preparing such gels even in research laboratories remain something of a black art. The first commercial capillary gel columns have recently become available from Applied Biosystems (San Jose, California), and two other companies, Beckman Instruments (Fullerton, California) and J & W Scientific (Folsom, California), plan to introduce such columns early this year. Although the suitability of these columns for DNA sequencing remains to be demonstrated, the considerable commercial interest in this area does provide hope that solutions to some of the problems described above may be found.

In summary, CGE is an exciting new technique that has already demonstrated its potential for increasing performance in automated DNA sequencing. The minute samples that can be analysed with this technique, the promise of methods for the simultaneous analysis of multiple samples, and the tremendous sensitivities of the fluorescence detection methods used all tend to suggest an active future for the technology. □

Lloyd M. Smith is assistant professor in the Chemistry Department, University of Wisconsin, Madison, Wisconsin 53706, USA. For more information, fill in reader service number 100.

1. Karger, B.L. *Nature* **339**, 641–642 (1990).
2. Swerdlow, H. & Gesteland, R. *Nucleic Acids Res.* **18** (6), 1415–1419 (1990).
3. Drossman, H., Luckey, J.A., Kostichka, A.J., D'Cunha, J. & Smith, L.M. *Analyt. Chem.* **62**, 900–903 (1990).
4. Luckey, J.A. *et al. Nucleic Acids Res.* **18** (15), 4417–4421 (1990).
5. Guttman, A., Cohen, A.S., Heiger, D.N. & Karger, B.L. *Analyt. Chem.* **62**, 137–141 (1990).
6. Peck, K., Stryer, L., Glazer, A.N. & Mathies, R.A. *Proc. natn. Acad. Sci. U.S.A.* **86**, 4087–4091 (1989).
7. Shera, E.B., Seitzinger, N.K., Davis, L.M., Keller, R.A. & Soper, S.A. *Chem. Phys. Lett* **174**, 553–557 (1990).
8. Mead, J.A., Luckey, J.A., Uzgiris, J. & Smith, L.M. Abstr. 99 *Human Genome II*, San Diego, California, 22–24 October 1990.
9. Radola, B.J. *Electrophoresis* **1**, 43–56 (1980).
10. Ansorge, W. & De Maeyer, L. *J. Chromatog.* **202**, 45–53 (1980).
11. Lumpkin, O.J., Dejardin, P. & Zimm, B.H. *Biopolymers* **24**, 1573–1593 (1985).
12. Hervet, H. & Bean, C.P. *Biopolymers* **26**, 727–742 (1987).
13. Holmes, D.L. & Stellwagen, N.C. *Electrophoresis* **11**, 5–15 (1990).
14. Ulanovsky, L., Drouin, G. & Gilbert, W. *Nature* **343**, 190–192. (1990).

Analytical aids

Over 850 companies will be exhibiting their wares at the Pittsburgh Conference on analytical chemistry and applied spectroscopy, to be held next week in Chicago, Illinois, USA.

THE Model DNA 100 **dedicated DNA concentrator** from Savant, which is based on earlier SpeedVac models, is designed for drying low volume ethanol precipitates or methanol/water precipitates of DNA and RNA (*Reader Service No. 101*). The dedicated system uses a combination of vacuum, radiant heat and evaporative cooling, in addition to centrifugal force, to localize DNA at the bottom of the tube for easy recovery. The new Model DNA 100 can accommodate 24 1.5-ml or 48 0.5-ml tubes. Other design features include three drying rates; an integral automatic bleeder valve and oil-free, Teflon-coated vacuum pump; and a corrosion-resistant, Teflon-coated concentration chamber. A chemical trap or refrigerated vapour trap, which can be connected to the DNA concentrator for solvent disposal, are optional extras. See the latest SpeedVac model in booth 3009.

Multiple cell facilities, extraction pressures of up to 10,000 p.s.i., flow measurement and a plug-free resistant collection technique are design features of the new SE-703 **supercritical fluid extractor** from the Lee Scientific Division of Dionex (*Reader Service No. 102*). The oven of the SE-703, which can be heated to 150 °C, can accommodate up to eight cells. The cells can be extracted simultaneously using supercritical carbon dioxide and other system-compatible fluids. According to Dionex, the problem of plugging — a common problem of supercritical fluid extractors — has virtually been eliminated by the development of a temperature-controlled restrictor. Control of the collection temperature and the design of the collection vials ensure uniform recovery of both light and heavy analytes, says Dionex. By monitoring the flow through each cell, the SE-703 provides real time as well as cumulative flow data. Visit Dionex on booth 4637.

Chemical computing

Molecular Design will be launching ISIS/Draw, a new windowed **chemical drawing package**, at Pittcon — see booth 3567 (*Reader Service No. 103*). ISIS/Draw will be available on several computing platforms and will be fully compatible across those platforms. The drawing tools of ISIS/Draw approach structures and reactions in the same way that a chemist does, says the company. For example, the

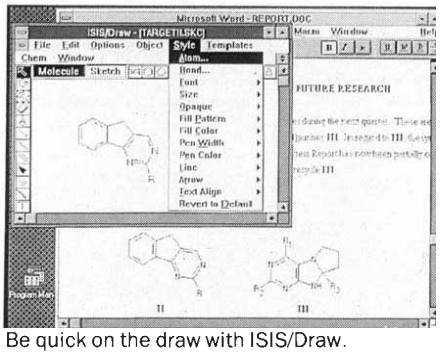

Be quick on the draw with ISIS/Draw.

program 'sprouts' new chemical bonds in a chemically logical direction, 'understands' aromaticity and places double bonds accordingly, automatically places hydrogen atoms, recognizes valence limits and warns the chemist when the limit is exceeded. As ISIS/Draw operates in windowed environments, users can insert structures using cut-and-paste techniques into word processing, graphics or spreadsheet programs. ISIS/Draw will be the first in a series of programs that will make up ISIS — the Integrated Scientific Information System. The complete ISIS product, which will include programs for managing scientific information at the

workstation and host computer level, will be available in April. Microsoft Windows and Macintosh versions of ISIS/Draw, the structure drawing component of the full system, will be the first releases; the remainder will be available by autumn 1991. The cost of a single-user licence for ISIS/Draw is $500 (US).

In booth 3757, Molecular Simulations will be announcing the launch of a new version of its NMRgraf **structure prediction software** program, which uses molecular modelling techniques to predict molecular structures from NMR spectroscopy data (*Reader Service No. 104*).

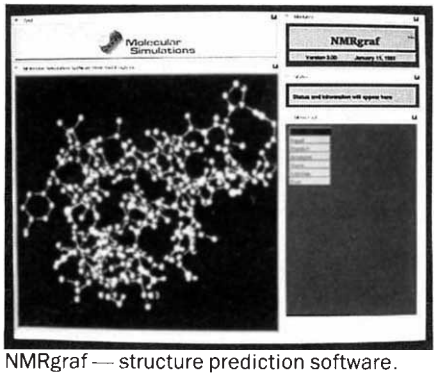

NMRgraf — structure prediction software.

NMRgraf is a stand-alone software package that uses Nuclear Overhauser Effect and J- Coupling data, in conjunction with molecular mechanics and molecular dynamics simulations, to predict the structure of unknown molecules. The new look NMRgraf package now has the capability to predict the structures of small molecules and polymers, as well as proteins; a direct interface to Hare Research's FELIX spectral analysis software; and a new X-windows-type interface with pull-down menus, prompt and dialogue boxes, and full support of the MOTIF graphical user interface.

Time savers

As an alternative to manual counting, Dynatech has developed the 982B Image Analyser/Counter, which can be used with Petri dishes, microplates and microscope slides (*Reader Service No. 105*). The basic **image analysis and colony counting system** includes an image monitor, an image camera and electronically-controlled object detection, particle size discrimination and data functions. The user is provided with a choice of three operating modes: fully automatic, semi-automatic and normal. The system can be interfaced with an IBM PC, XT, AT or compatible computer for full data handling capabilities. An automated computer-controlled X,Y stage mover and Auto-Accustat software are optional extras. See booth 2743.

Manual colony counting is outmoded with Dynatech's image analyser.

Digiflex is the new **automatic diluting/dispensing device** from ICN Flow that can be fitted with interchangeable sample syringes from 40 μl to 2,000 μl for pipetting volumes from 2 μl to 2,000 μl (*Reader Service No. 106*). The £2,500 (UK) Digiflex device can be interfaced with a PC via the RS232 port to allow for simplified programming of complex dispensing sequences. Multimode operation is offered using pre-programmed options, including sample/dispense mode, reagent/sample transfer mode and sample/transfer mode. Internal surfaces of the liquid pathway are either Teflon-coated or glass to ensure minimal carryover and allow the use of corrosive substances. The Digiflex is accurate to within ±1 per cent or ±1 μl across a range of 5–100 per cent of the syringe's capacity; with a variation of 0.5 per cent on multiple dispenses, says ICN. An optional handheld computer provides the user with programming flexibility using Digiflex-TP Developmment Software. The Digiflex-TP with hand-held computer costs £2,900 (UK).

Digiflex liquid dispenser from ICN Flow.

Modes of separation

The Model 3140 Electropherograph from Isco is a fully **automated capillary electrophoresis system** that supports a wide range of methods, including separations in surface-modified capillaries and micellar and electrofocusing techniques, in addition to conventional free-solution capillary electrphoresis columns (*Reader Service No. 107*). The system features a 40-position autosampler, 30-kV reversible-polarity power supply, computer-based method and data handling capability, variable UV detection, programmable buffer switching and software-selectable vacuum and electromigration sample injection. Temperature control to within ±0.5 °C and pressure-time integral control of vacuum injection ensure reproducible results, says Isco. The Model 3140 can make multiple injections from 5 μl of sample. The detection sensitivity of absorbing species is in the low-femtomole range. See booth 3821.

Automated CE with the Model 3140.

Beckman has introduced the new GS-6 Series of **tabletop and kneewell centrifuges**, which are available with or without refrigeration for operation down to −10 °C (*Reader Service No. 108*). The GS-6 Series offers speeds of up to 6,400 r.p.m. (5642 *g*) with fixed-angle rotors, and a sample capacity of three litres with the swinging-bucket rotor, says Beckman. The Accuset speed control provides adjustment of speed in 10-r.p.m. increments. The centrifuges can accommodate two fixed-angle rotors, and the workhorse swinging-bucket rotor that can be used to spin a wide range of tubes and bottles when using adapters and spacers. The swinging-bucket rotor can also take microplate carriers and blood bags. For added protection of the user against hazardous biological materials and aerosols, Beckman offers Aerosolve cannisters. Using these O-ring-sealed transparent cannisters, the user can spot breakages and take appropriate action before breaking the seal. Beckman's booth is 3300.

FMC BioSupport Materials has expanded its ACTI-DISK **separation/purification cartridge line** to include a handy 25-mm diameter minicartridge size in addition to the 50-mm diameter size (*Reader Service No. 109*). ACTI-DISK cartridges are available with Protein A, Protein G or glutaraldehyde (GTA) activation and are intended for sample preparation or screening applications, says FMC. The ACTI-DISK line also includes ion exchange DEAE, QUAT, PEI, SP and CM, as well as affinity Protein A, Protein G, GTA, hydrazide and amino chemistries. See booth 3140.

Accessories to HPLC

Bio-Rad's new line of HRLC MA7 **columns** are designed for applications in which milligram quantities or less of a

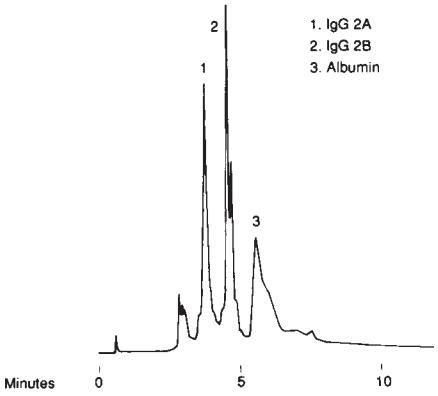

For rapid separations — see booth 5167.

protein mixture need to be analysed or purified rapidly (*Reader Service No. 110*). A full range of MA7 ion exchangers is offered, including a carboxymethyl weak cation exchanger, a PEI weak anion exchanger, a sulphopropyl strong cation exchanger and a quaternary amine strong anion exchanger. As the nonporous beads that make up the packing allow no mass transfer into and out of the pores of the beads, chromatographic speed is increased and high recovery rates of proteins are possible, says Bio-Rad. The 7 μm polymer spheres that form the HRLC column packing can withstand harsh chromatographic conditions: pH 2 to 12, flow rates of up to 5 ml min^{-1} and washing with acid (20% acetic) or base (0.1 M NaOH). The maximum loading capacity is about 5 mg per column injection and the recommended injection volume is 100 μl. Bio-Rad's booth will be 5167.

For both analytical and preparative HPLC applications, Rainin Instruments recommends its Dynamax Model UV-1 **UV/visible absorbance detector** (*Reader Service No. 111*). The Model UV-1 features a xenon flashlamp for detection in the 190–700-nm range. The xenon lamp provides rapid stabilisation and, in order to minimise lamp replacement, can be switched to standby during idle periods. This dual-beam instrument provides low noise and drift, and refractive index effects are virtually eliminated, says Rainin. An 'extended range' feature allows both analytical and preparative separations to be performed with one flow cell, without any loss of sensitivity or accuracy. Rainin will be in booth 4438.

Collect samples by time, number of drops, fraction volume or external signal with the latest **fraction collector** to come off the Water's production line (*Reader Service No. 112*). The fraction collector is designed to collect up to 120 fractions of microlitre-to-litre volumes in virtually any size of container or test tube, says Waters. The fraction collector arm can be varied for collection vessels that measure between 90 mm to 180 mm in height and for tubes from 12 mm to 18 mm in diameter. The fraction collector's internal peak separator can be programmed to activate the fraction collector based on threshold or peak slope. Users can programme the fraction collector to start and stop collection at specified times during the run. In addition the time window and peak sensing functions can be combined so that only certain peaks for a given part of the run are collected. Waters Chromatography Division of Millipore will be in booth 5300

A microscopic view

By applying modern design principles to the whole optical transmission system and not just the objectives, that is to the zoom optics, the binocular tube and the eyepieces, Leica has come up with the Wild M10 **zoom stereomicroscope**, which

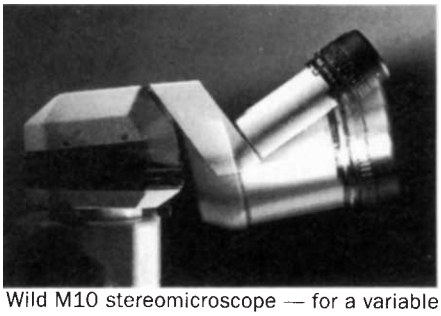
Wild M10 stereomicroscope — for a variable angle of observation and large zoom range.

the company hopes will have broad applicability in fields as diverse as the biological sciences to the semiconductor industry (*Reader Service No. 113*). The unusually large zoom range of 1:10 allows studies to be carried out at magnifications from 5× to 410× at the same workstation, if optical accessories are used. The Wild M10 is fitted with a binocular tube, which has an angle of observation that can be varied between 10° and 50°. The zoom stereomicroscope is suitable for photography, drawing, video, dual-station viewing, or measuring applications — whether in incident or transmitted light. Leica will be in booth 5432.

The computer-controlled 'Hiper' specimen stage, a design feature of the newly introduced H-7100 **electron microscope** offers improved stability over conventional side-entry stages, says Hitachi (*Reader Service No. 114*). In addition, the Hiper stage permits autotracking, autore-

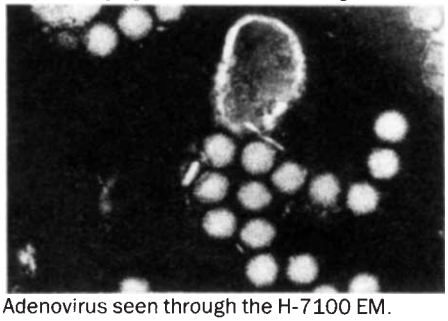
Adenovirus seen through the H-7100 EM.

ADVERTISEMENTS

Customs DNA-Synthesis

Probes and Primers	Germany	EEC
Price per coupling 0,2 μmol	9,00 DM	9,00 DM
1,0 μmol Synthesis	+1,50 DM	+1,50 DM
Customs duty		
Freight	no charge	25,00 DM
SETUP Costs	no charge	no charge
Poly Pak Purification	40,00 DM	40,00 DM
Delivery Time	3-4 days	3-5 days

Price does not include tax, freight and customs duty for non EEC countries.

Order per Telefax or Telephone

MWG-BIOTECH
Gesellschaft für angewandte Biotechnologie
Sportparkstr. 7 · D-8017 Ebersberg
Tel. (08092) 2 40 71 · Fax (08092) 2 10 84

Reader Service No.18

O2/CO2 RESPIROMETER
measures bacterial and fungal growth

* IBM-PC based.
* Fully automatic 24hour measurements.
* Periodic air refresh.
* 1-20 measuring chambers (50ml-20 L).
* Sensitivity 0.2μL/h.

For more information please contact:
Columbus Instruments
P.O. Box 44049 Columbus, Ohio 43204 USA
PH: (614) 488-6176; 1-800-669-5011
TLX: 246514 FAX: (614) 276-0529

Reader Service No.10

Custom DNA
Purified and Shipped in 48 hours, Worldwide.
100 ug, $10.00 a base for the first 15 bases, $7.50 for each additional base. Delivered.
Research Genetics
1-800-533-4363
In the United Kingdom 0-800-89-1393
In Canada 1-800-533-4363
FAX 205-536-9016

Reader Service No.26

Synthetic Oligonucleotides
Custom made Probes and Primers, Synthesised, purified and shipped in 3 days
£4.00 per base
(All inclusive)
0.2 μM scale (approx. 500 μg)
Modified bases, aminoalkylation, data base analysis and full design facilities
Molecular Medicine Unit,
King's College School of Medicine & Dentistry,
Denmark Hill, London SE5 8RX
Tel. XX-44-(0)71 - 326 3126
FAX XX-44-(0)71 - 733 3877

Reader Service No.56

setting and montaging, with the specimen stage movements being linked to magnification steps via the computer. High-resolution images can be obtained with the high-contrast electron column operating at acceleration voltages of between 25 kV and 125 kV (10 kV for SEM and STEM), which absorbs scattered electrons and prevents image distortion, says Hitachi. With the ultra zoom magnification system, rapid changes in magnification are possible from 1,000× to 600,000× without the need for image rotation or inversion.

The new 125 μm × 125 μm **scanners** for Digital Instruments' NanoScope STM and AFM (atomic force microscope) now combine large scan areas with a three-dimensional capability (*Reader Service No. 115*). They can scan up to 100 $\mu\ s^{-1}$ and can operate in both air and liquids. Tips for STM and cantilevers for AFM are available. The NanoScope AFM/STM offers considerable advantages over electron microscopy and optical interferometry: surfaces can be imaged with nanometre resolution in all three dimensions and, typically, the AFM/STM system is faster and easier to use than electron microscopes, which can require extensive sample preparation, says Digital. The 125 μm × 125 μm scanners are interchangeable with other NanoScope scanners. See booth 2133.

125μm X 125μm AFM/STM scanners.

Analytical instrumentation

The Model 2000 **laser desorption time-of-flight mass spectrometer**, which has been developed by Vestec, will be making its debut appearance at Pittcon (*Reader Service No. 116*). This linear TOF instrument is intended for applications that require accurate molecular weight determinations on trace amounts of high molecular weight materials. For example, the instrument is designed to make accurate molecular weight determinations on sub-picomolar quantities of proteins, peptides, oligonucleotides and other biological polymers present in complex biological samples. The integrated system consists of a linear TOF mass spectrometer with a two-metre flight path, two-stage 40-kV acceleration, and a 20-stage focused mesh electron multiplier detector. Matrix-assisted laser desorption ionization, coupled with up-to-date data acquisition allow molecular weights to be determined to within 0.1 per cent up to at least 20,000 Da and to within 0.01 per cent up to 200,000 Da, says Vestec. The instrument can be interfaced to HPLC and capillary zone electrophoresis set ups. See booth 3356.

Building upon the double-beam, double monochromator system of the Lambda 9, the new Lambda 19 **UV/visible/NIR spectrometer** from Perkin-Elmer offers detection in the wavelength range of 175–3,200 nm and linearity up to 6 A (*Reader Service No.117*). Lambda 19 is PC-controlled and is supplied with UV Computerized Spectroscopy Software as standard to provide increased flexibility in data handling and spectrum manipulation. The standard PPLOT routine provides the user with flexibility with printouts and can be used with a variety of plotters and printers. Perkin-Elmer's line of spectrometers will be in booth 4162.

The fully computerized J-710/720 **spectropolarimeter** system can be adapted for every aspect of chiroptical spectroscopy, says Jasco (*Reader Service No. 118*). Two models are available: the basic J-710 model, which has a compact sample compartment and air-cooled 150 W xenon arc light source; and Jasco's top-of-the-line model with a large sample compartment and water-cooled 450 W arc light source. The design of the J-700 series monochromator allows circular dichroism measurement down to the VUV range of 170 nm. The J-710 model measures in the wavelength range of 175–700 nm; the J-720 has an extended range of 170–800 nm. The signal-to-noise ratio over the entire far UV range has been increased by a factor of five over previously available systems, says Jasco. Baseline stability with temperature change has also been increased and the internal nitrogen purging efficiency has been improved. Data processing software includes full functions for arithmetic calculations, peak picking, derivatives and calculation of optical constants. A new fast Fourier transform smoothing function allows enhancement of spectra without sacrificing peaks. See Jacso in booth 4554. □

These notes are compiled by Diane Gershon from information provided by the manufacturers. To obtain further details, use the reader service card bound inside the journal. Prices quoted are sometimes nominal, and apply only within the country indicated.

ADVERTISEMENTS

SINGER INSTRUMENTS

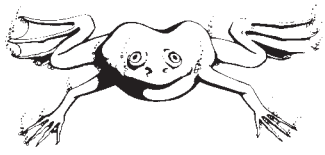

COMPLETE SYSTEMS FOR
XENOPUS
OOCYTE INJECTION

INT. SALES: +44. 984. 40226.
FAX: + 44. 984. 41166
Singer Instrument Co. Ltd.
Roadwater, Watchet, Somerset, England, TA23 0QL. Tel: Washford (0984) 40226.
Telex: 337492 Comcab G

Reader Service No.50

METABOLITES analysed
rapidly, enzymatically, using micro-samples

with the

ANALOX GM7 MICRO-STAT

A wide range of biological fluids including whole blood are acceptable for direct injection. Turbidity no problem. Sample size 2.5 - 25ul. Results in 20 seconds.

glucose	lactate	urea
alcohol	pyruvate	creatinine
cholesterol	ammonia	3-OH butyrate
uric acid		acetoacetate

Analox Instruments Ltd
8 Goldhawk Industrial Estate
Brackenbury Road
Hammersmith, London W6 0BQ
Tel: 081-749 7635
Fax: 081-740 6608

Reader Service No.16

LIPOSOMES
NEW
REPRODUCIBLE — HOMOGENEOUS — EXTREMELY RAPID

Our new LIPOSOMAT guarantees rapid (5ml within 60 minutes) preparation of uniformly sized unilamellar liposomes. Liposome size is selectable between 25 and ca. 600 nm diameter Sample volume is normally 5-10ml or up to 200ml if used in combination with an additional instrument. Lipid concentration can be up to 300 mg/ml.

BIANORM
POB 126, D-8000 Munich 65, FRG

Reader Service No.17